A FINITE DIFFERENCE MODEL FOR FREE SURFACE GRAVITY DRAINAGE

A DISSERTATION
SUBMITTED TO THE DEPARTMENT OF PETROLEUM ENGINEERING
AND THE COMMITTEE ON GRADUATE STUDIES
OF STANFORD UNIVERSITY
IN PARTIAL FULFILLMENT OF THE REQUIREMENTS
FOR THE DEGREE OF
DOCTOR OF PHILOSOPHY

By
Francisco Roberto Couri
November 1992

I certify that I have read this thesis and that in my opinion it is fully adequate, in scope and in quality, as a dissertation for the degree of Doctor of Philosophy.

Henry H. Ramey Jr.
(Principal Adviser)

I certify that I have read this thesis and that in my opinion it is fully adequate, in scope and in quality, as a dissertation for the degree of Doctor of Philosophy.

Roland N. Horne

I certify that I have read this thesis and that in my opinion it is fully adequate, in scope and in quality, as a dissertation for the degree of Doctor of Philosophy.

Martin J. Blunt

Approved for the University Committee on Graduate Studies:

TO BE DONE

TO BE DONE

Contents

List of Tables

List of Figures

Chapter 1

Introduction

The main objective of this study is the development of a numerical simulator to study the transient drawdown and buildup behavior of a liquid in a gravity drainage well with a moving free surface boundary. The purpose of this work is to provide a tool to help understanding the flow mechanism in the vicinity of the wellbore where the known methods of interpretation fail to determine the transient pressure behavior or to establish physical grounds for creating a method of interpretation of pumping gravity well tests.

In the last few years, much attention has been dedicated to depleted petroleum reservoirs in the oil industry all over the world. The interdependency of oil and gas reserves, price, demand, and politics is a major factor affecting interest in developing alternative sources of energy, and enhanced oil recovery from abandoned fields, heavy oil reservoirs, tar sands, bitumen shales, etc.

Among the potential targets for enhanced oil recovery projects are many depleted oil reservoirs, some with such a low pressure that the gas cap is at atmospheric pressure. This is the case when gas solubility is low, or for water flooded shallow reservoirs which have produced much of the oil, water and associated gas.

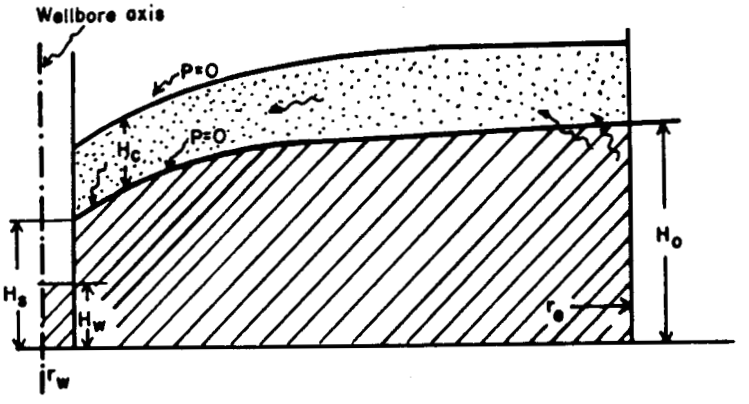

Figure 1.1: Unconfined free surface gravity drainage reservoir producing to a single well - *Muskat* (1937)

A common characteristic of such a reservoir is the lack of detailed information about the formation properties necessary to plan an enhanced oil recovery project. Unfortunately, the present petroleum well testing techniques do not consider the case of a well in a reservoir with a phreatic liquid table. In hydrology, a phreatic aquifer is defined as an unconfined reservoir with an air-water contact at atmospheric pressure. Pumping a well that penetrates a formation with a phreatic gas-liquid contact develops a downward movement of the free surface, under a gravity flow mechanism. Often, no other source of energy is present for driving the liquid into the wellbore. An exception is capillary forces acting in the capillary fringe above the phreatic line. A schematic view of the gravity well problem is presented in the Fig. 1.1, representing a cross section of a fully penetrating open hole well in an unconfined sandstone reservoir.

Until recently, most theory found in the petroleum literature about well test analysis has concerned confined flow of compressed fluid. However, the groundwater literature contains many studies where phreatic aquifers are a common subject. On the other hand, even hydrologists have not focused on pumping wells where the presence of a seepage face along the sandface adds further difficulties to a moving boundary

problem. Since unconfined aquifers are often shallow and the wells are easy and cheap to drill, methods of interpretation often concerned interference tests.

The theory associated with the gravity flow mechanism with a variable free surface started in the last century with the *Dupuit* (1862) approach, generalized by *Forchheimer* (1886) in the so-called Dupuit-Forchheimer partial differential equation, which for radial incompressible flow is:

$$\frac{\partial^2 h^2}{\partial r^2} + \frac{1}{r}\frac{\partial h^2}{\partial r} = 0 \qquad (1.1)$$

Eq. 1.1 concerning saturated flow in an incompressible radial system. Many assumptions were made such as formation isotropy and neglection of vertical flow gradients. The Dupuit-Forchheimer approach has become a standard reference for improved theories and interpretation methods.

The first rigorous attempt to solve the steady-state gravity problem under several different flow geometries using a hodographic transformation was made by *Wyckoff et al.* (1932) and *Muskat* (1937). A hodographic transformation is a representation of the dynamical system by coordinates that are the velocity components. This rather difficult method, although supporting the Dupuit-Forchheimer theory, fails in producing the shape of the free surface, as observed in Chapter 2 of this study.

The classic transient solution for compressed liquid flow *(Theis,* 1935) is often used today to represent the late time drawdown behavior in observation wells by well known Groundwater authors like *Boulton, Neuman, Streltsova,* among many others. Although the hydrology literature is rich concerning this subject, there is a great deal of confusion about the physical principles governing unconfined flow - see Chapter **2.**

Regarding transient drawdown in observation wells near well producing at a constant pumping rate, there are three different flow regimes characterized by the S-shaped curve illustrated by Fig. 1.2 from the Groundwater literature. Observation

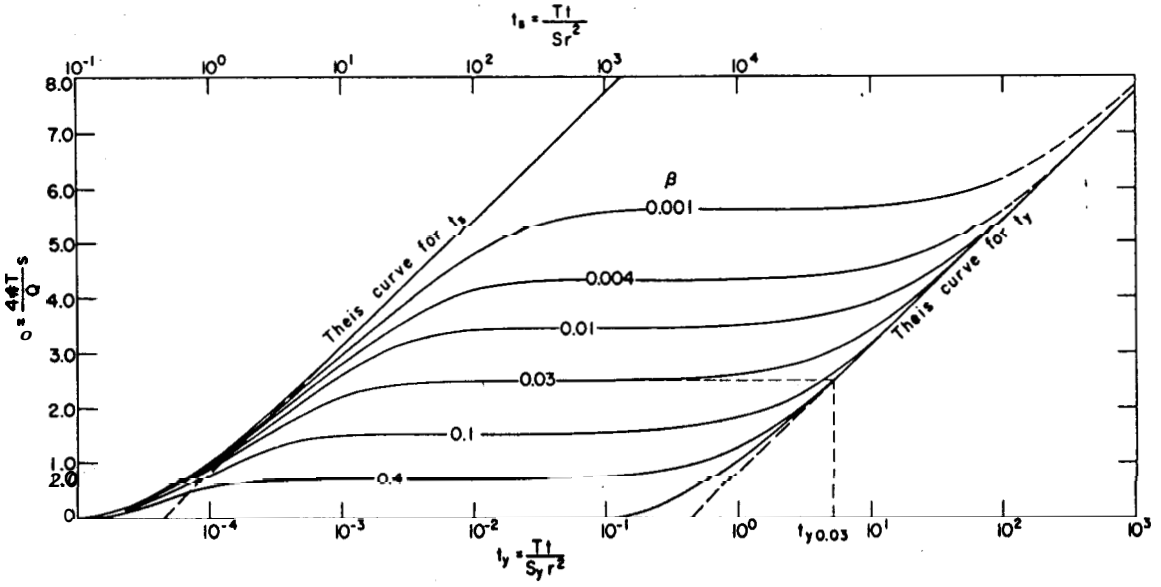

Figure 1.2: Typical type curve for unconfined flow from the groundwater literature - *Neuman* (1975-a).

wells located far from the producing well present a characteristic time-drawdown curve reflecting three stages of flow in the reservoir. The first stage is attributed to a pure radial flow by fluid expansion and compactation of the aquifer before the free surface starts a downward movement. The *Theis* solution applies, according to many hydrologists. **As** the free surface responds to the well pumping,. an intermediate stage is marked by a reduction in the slope of the head drawdown, approaching zero in some circumstances. This is the period of desaturation of the cone around the well. The last stage would again follow radial flow behavior because of stabilization of the free surface changes. The analytical methods presented by *Streltsova* (1972-a, 1972-b, 1973) and *Neurnan* (1972, 1975) considered elastic and formation storage properties lumped into the specific yield parameter. To get the analytical solution for the boundary problem (see Chapter 2), Neuman imposed such conditions as the head drawdown must be much smaller than the initial head, the well was a line-source well, wellbore storage and skin effects were neglected, and the seepage face was neglected. **As** a result, analytical methods were not applicable to a pumping well or its vicinity, and were insufficient to analyze the transient pressure behavior in the produced

wellbore.

Using the *Dupuit-Forchheimer* approach, *Ramey et. al* (1989) derived a partial differential equation for incompressible radial flow into a single well located in an infinite reservoir. In terms of pressure, instead of liquid head, the p.d.e. takes the form of Eq. 1.2, in Darcy units:

$$\frac{\partial^2 p^2}{\partial r^2} + \frac{1}{r}\frac{\partial p^2}{\partial r} = \frac{\phi \mu\ (p^{-1})}{k}\frac{\partial p^2}{\partial t}\ . \qquad (1.2)$$

By analogy with the flow of ideal gas, the *Aronofsky* and *Jenkins* (1953) correlations were applied to obtain the approximate wellbore transient pressure solution, as follows in English petroleum field units:

$$p_o^2 - p_w^2 = 325.2\frac{qB\mu}{k(h/p)}\left\{\log\left(\frac{0.000264kt}{\phi\mu\ (p_o^{-1})r_w^2}\right) + 0.351 + \frac{s}{1.151}\right\} \qquad (1.3)$$

This appears to be the first approach for gravity drainage well test analysis found in the petroleum engineering literature since the classic stydies of *Wyckoff et al* (1932) and *Muskat* (1937).

From the many concepts and ideas related to unconfined flow into a well, it is possible to consider the physical flow mechanism. First, start with the rest condition of an unconfined, single-phase reservoir, like that represented in the Fig. 1.1. Above the phreatic surface, there is a partly-saturated region containing liquid called the capillary fringe where the pressures are negative. **As** a consequence, the static potentials are constant and equal to the potentials anywhere in the saturated region below the phreatic table, defined throughout this report by $\Phi = p + yh$. The degree of liquid saturation in the capillary region and the elevation of liquid above the free surface is dependent on the surface tension between the liquid and the porous medium and the gas and the pore throats related to the shape and grain size distributions.

When the well is pumped at a constant rate in an infinite, unconfined reservoir, the liquid level in the wellbore drops at a velocity that depends on the well storage capacity. Due to the viscous forces in the formation, the potential drop in the well is not immediately transmitted to the reservoir. This causes a discontinuity of potentials at the sandface. With increasing time, the potential drops in the formation causing the liquid to start moving into the well at increased rates as the potential differentials become large, and the pressure drop is transmitted radially and vertically through the formation. During this period, called the wellbore storage period, the withdrawal1 from the well is greater than the flow from the formation.

Vertically along the sandface in the well, there are two different regions of flow: an open face, where the liquid falls, and the liquid filled well region below the liquid level in the hole. The seepage length is the difference between the liquid levels in the sandface and in the well. Thus, at the sandface wall, the potentials vary from a maximum value at the intersection point of the phreatic free surface down to the liquid level in the well, and remain constant from there down to the bottom of the well.

Following an initial period of flow, the potential drawdown in the pumping well deccelerates, due to an increasing contribution of flow from the formation. The withdraw in the neighborhood of the well develops gradients of potential driving the streamlines to bend gradually, with decreasing slopes from the free surface down to the sand base. The produced mass of liquid, considering a low compressibility system, leaves a desaturated region behind the free surface. Neglecting for a while the capillary region, which is discussed in Chapter. 4.7, the desaturated region is a two-phase flow region where the liquid saturations successively drop to an irreducible value. Due to the low velocity of vertical displacements of the free surface, the resistance created to the gas entry into the porous spaces left by the liquid under the gravity flow are of minor importance to create a delay in the process, according to some authors, even around the wellbore. Also, the liquid retained by capillary forces in the desaturated zone, though known to exist in small amounts, is not rigorously considered in the

present study.

After the wellbore storage effects cease and the desaturation cone starts developing in the formation, the pressure in the well stabilizes at a certain level as a result of equilibrium between the rates of pumping and the withdrawal from the surroundings. At this time, the seepage face trends to shrink. The cone of depression develops radially from the wellbore. As the depression of the free surface reaches remote regions, a small free surface displacement corresponds to a large volume of liquid. In other words, the storage capacity becomes large with increased radius.

Since an external boundary is not reached and the free surface presents a fairly stable shape, the potential changes reflect a confined system behavior corresponding to a third cycle of observed pressures in the well. During this period, one expects a slow, uniform downward displacement of the free surface, and the seepage face changes at a much lower rate.

The transmissivity has an important effect on the potentials and free surface profiles. The velocity along stream lines at any radial location, a consequence of the transmissivity and withdraw rates, is of interest. In other words, if we track two single stream flow lines from a remote region to the sandface, vertically spaced by a certain difference in height, we observe a reduction in the distance between them by the stream-line merging process. Since the material balance condition for two consecutive stream flow lines to converge is to double their velocities (case of incompressible flow), the viscous forces are the most responsible for the shape of the free surface, and also for the seepage face length. By itself, the viscous flow theory can explain the formation of the seepage face without invoking surface tension effects. Those capillary end effects, although present in the very top of the seepage face are of minor importance, according to some experimental sandbox models ***(Hull,*** 1955). *Wyckoff et al.* (1932) explained the influence of the resistance forces to the vertical flow in the formation neglecting capillary forces by expressing the potential in the free surface as a function of the average vertical velocity at some radial position:

$$Z_s = Z + \frac{\overline{v}\, Z_s}{k \gamma g}, \qquad (1.4)$$

where:

- Z_s - sandface vertical distance from the sand bottom
- Z - head of liquid at the bottom
- $\overline{v}$ - average vertical velocity of the liquid
- k - equivalent to the transmissivity
- γg - liquid gradient

In App. D Eq. **1.4** is verified against $\Phi = p + \gamma h$, verifying the free surface boundary condition found in the literature.

The buildup process in gravity wells has been overlooked in most studies. Some references in the Groundwater literature takes buildup as a reversible process similar to drawdown, but there has not been a careful investigation of the physical behavior during this period. *Ramey et al.* (1989), analyzing a field case, concluded that the pressure buildup is "essentially different" from the prior drawdown process, leading to a rapid establishment of a semilog straight line. According to *Ramey et al.*, radial flow occurs below the free surface during the buildup, and the free surface is displaced up by radial flow into the cone of depression. After pumping stops, the liquid flows into the wellbore, and starts refilling the well. Chapter 7.1.2 presents considerations of the buildup analysis.

The first attempt to study the gravity well problem was to find a bi-dimensional numerical model that could answer most of the questions related to the real physics of the mechanism. A moving boundary simulator was developed and named *Stream Layer Model.* A *stream layer* is a set of stream flow lines in a vertical section of an axial flow into the well. The next chapter presents a literature survey for gravity drainage well test analysis.

Chapter 2

Literature Review

The mechanism of gravity drainage flow in a porous medium has not been completely studied in either Groundwater research or the oil industry. In this chapter, a review of the main works in gravity drainage well test analysis is presented. Also, studies of two dimensional well model simulators are reviewed both in Groundwater and Petroleum Engineering.

Pumping tests are common in hydrologic evaluations, and gravity drainage evaluation methods have been necessary due to the fact that many shallow aquifers (phreatic) are free surface systems. Hence, the Groundwater literature was the main source of information for the present investigation.

In most studies of unconfined radial flow, water is the only saturating fluid in the porous medium, and the presence of other phases is not considered, except in a few studies dealing with a desaturated region and/or a capillary fringe between the water table and the air-filled pores above it. Generally, most models consisted of a well located in the center of an infinite reservoir where the formation properties were often considered anisotropic, and the presence of a damaged region was neglected. Wellbore effects were some of the major difficulties encountered in this study and

only recent studies of wellbore effects have been made by some authors.

A small difficulty is relating petroleum engineering terms to the reservoir properties and parameters defined by hydrologists. A set of relationships and unit conversions between the definitions employed in both branches of study is given in Appendix B.

2.1 Early History

Apparently, the first important contribution to the gravity flow problem was the *Dupuit* (1863) analytical solution which assumed a radial, steady-state parabolic distribution of head with the distance from the wellbore. **A** simplification of the mathematical steady-state problem was made by assuming that for a small slope of the water table, which is also a streamline, the Darcy law velocity vector is proportional to the tangent of the angle the streamline makes with the horizontal, rather than the sin of the angle. Thus, instead of

$$v_s = -K\frac{\partial \Phi}{\partial s} = -K\frac{\partial z}{\partial s} = -K\sin\theta\,, \tag{2.1}$$

$sin\theta$ was replaced by $tun\theta = \frac{dh}{dx}$, where $h = h(x)$ is the vertical coordinate of the water table position. This assumption permitted a derivation of the steady-state flow equation by Dupuit, which for radial flow is:

$$Q_w = 2\pi\frac{K}{\mu} r\, h\frac{\partial h}{\partial r} = \frac{\pi\, k\,(h_e^2 - h_w^2)}{\mu \log\left(\frac{r_e}{r_w}\right)} \tag{2.2}$$

Forchheimer (1886) applied the *Dupuit* assumption to the continuity equation and produced the partial differential equation for radial flow:

$$\frac{\partial^2 h^2}{\partial r^2} + \frac{1}{r}\frac{\partial h^2}{\partial r} = 0 \qquad (2.3)$$

Equation **2.3** is the well known *Dupuit-Forchheimer* partial differential equation for steady-state gravitational radial flow.

2.2 Experimental and Analytical Models - Steady-State

Wyckoff et al. **(1932)** investigated gravity flow using an experimental 15" sector sand box to simulate the radial flow of a single liquid (water) saturating the reservoir. Their results provided important informations about the free surface and streamline behavior along the reservoir and around the wellbore. The radial sector was laterally bounded by glass walls which permitted visual inspection of the liquid level in the porous medium, and streamlines traced by ink injected at points at the outer boundary. Eighteen complete steady-state experimental runs were presented, varying initial heads and flow rates in order to compare the results with the Dupuit model and other models. The capillary fringe effects were important in the lab scale, and most of the the deviations from the Dupuit model were attributed to the capillary fringe. The tables summarizing the results of each experiment presented the liquid heads taken at the sand bottom, and the liquid level (free surface position) profiles were graphed for runs No. 18 and **19.** There were no direct seepage face length measurements, but visual inspections and the graphs presented in the paper indicated the seepage face existence.

Muskat **(1937)** dedicated an entire chapter to the analysis of gravity flow systems. His study of steady state flow for different configurations *(Muskat,* **1935,1937)** of porous medium included physical experiments such as sandbox and electrical models (by other investigators). He pointed out the weakness of the *Dupuit* assumptions, and

raised the concept of a seepage face along the downstream boundary that introduces a complication to the problem once the water table causes a discontinuity in the wellbore. Since the Dupuit equation depends only on radial distance, this equation fails to determine the head distribution along the vertical coordinate in the vicinity of the wellbore. Far from the well, horizontal flow dominates, and the Dupuit results are reasonable. *Muskat* concluded the Dupuit equation, although based on incorrect assumptions, gives fortuitously accurate results in the calculation of the discharge of a well when the head values are taken at the base of the formation.

Muskat **(1935,1937)** solved the steady gravity flow problem analytically through two methods: an exact solution using the hodograph method, and an approximate solution by Fourier series expansion of the boundary conditions. These solutions are not simple even for an isotropic medium. The method of hodographs, though powerful, is difficult to apply. Analytical and experimental results were compared in several figures in the *Muskat* **(1937)** book.

Babbit and *Caldwell* **(1948)** used one electrical and two sandbox models (small and large scales) to corroborate the observations of *Wyckoff et al.* and *Muskat.* The effect of the capillary fringe was omitted in this **work** which generated an empirical equation to locate the free surface as a function of the distance from the wellbore axis:

$$Q = \frac{\pi k h_e (h_e - h_x)}{2.3 C_x \log r_e/0.1 h_e} \tag{2.4}$$

where h, and h_e are respectively the free surface positions at distances r_x and r_e from the wellbore center, and C_x is an empirical constant obtained as a function of the dimensionless radial distance.

The most valuable experimental work, is a major reference in the Groundwater literature by *Hall* **(1955).** ***Hall*** presented four series of sandbox experiments analyzing capillary effects, the hysteresis due to air invading the desaturating cone, and changes

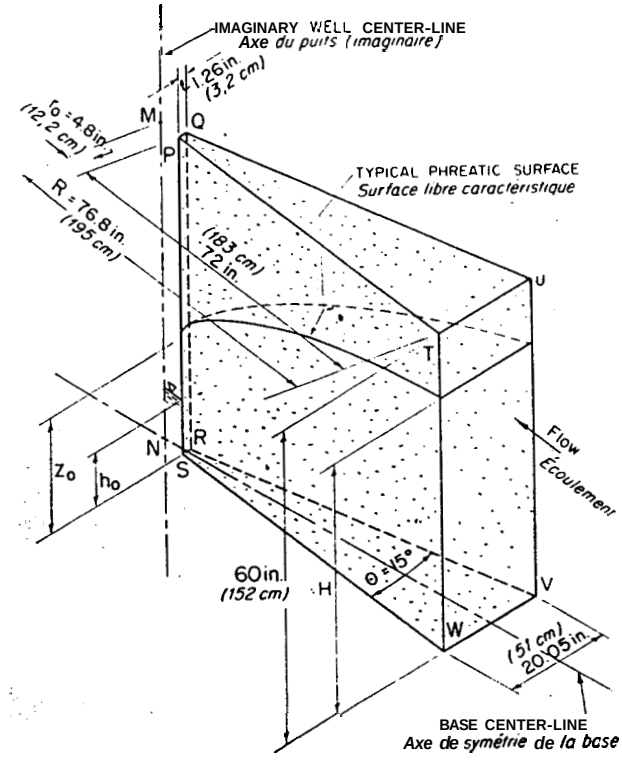

Figure 2.1: Essential dimensions of well model - from *Hall* **(1955).**

in the surface tension in the rock-fluid system. Figure 2.1 from the *Hall* paper shows a 15" sector and the essential sandbox model dimensions. Series **A** of tests performed by *Hall* presented eight steady-state steps of successive flow rates starting from a completely water saturated system with an average capillary fringe height of **3.5** inches. It is remarkable to observe the behavior of the free surface as the flow rate increases. From run **A-4** to **A-8,** the free surface position at the sandface varied only -3.6%, while the wellbore liquid level dropped from half of the initial height to zero, and the production flow rate increased more than **32%.** This result is a difficult mathematical condition to be represented by only a few variables as in the *Dupuit* formula. The streamline traces were qualitatively and quantitatively studied, demonstrating the importance of the vertical position of a streamline related to the time necessary to flow from the outer source to the inner boundary. See Fig. 2.2. The uppermost streamline requires twice as long to reach the wellbore as the lowermost streamline. There are two possible reasons for this phenomenon. First, the uppermost inner boundary potentials are always greater than the lowermost potentials. See Ch. **3.**

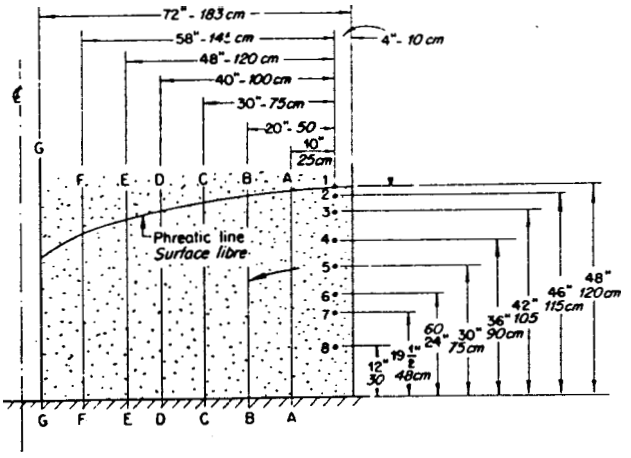

POINT OF INJECTION *Point d'injection*	TIME, IS MINUTES, REQUIRED TO REACH SECTION *Temps, en minutes, nécessaire pour ntleindre la secfion*							REMARKS *Observations*
	A-A	B-B	C-C	D-D	E-E(	F-F	G-G	
1	2.5	6.0	9.0	11.3	13.5	**15.0**	16.0	Capillary layer. *Fcapillairc.*
2	**2.2**	4.5	6.7	8.5	10.1	11.2	12.0	
3	**2.0**	4.2	6.2	8.0	9.3	10.3	11.0	
4	**2.0**	**4.0**	6.2	7.8	9.0	**10.0**	10.5	
5	2.0	3.9	5.8	7.3	8.4	9.3	9.8	
6	1.8	**3.8**	5.5	**7.u**	8.0	8.8	9.2	
7	1.8	**3.6**	5.2	6.8	**7.71**	8.4	9.0	
8	1.8	**3.5**	**5.0**	**6.6**	*7.6*	8.0	8.5	

Figure 2.2: Time for flow along the streamlines - ***Hull*** (1955).

Second, the uppermost streamlines are much longer than the lowermost streamlines.

2.3 Transient Analysis

An early important study of compressible transient flow was presented by *Theis* (1935). Previous groundwater hydraulics had been based on steady flow conditions. *Theis* applied the theory of heat conduction in solids using the line-source solution adapted to the flow of fluids in porous medium. In the paper, the limitations of the use of the exponential integral, $E_i(-x)$, in analyzing unconfined flow were considered. Early time effects due to a finite radius wellbore and gravitational flow around the wellbore were considered. *Theis* presented the technique later used by *Horner* (1951) to analyze the pressure-time behavior in well recovery (buildup) analysis by plotting pressure-drawdown versus the dimensionless time relation $(t_p + \theta)/\theta$.

A paper by *Walton* (1960), written in two parts, considered pumping test analysis for both artesian and unconfined aquifers. The author pointed out that the true behavior of water table models deviates from the line-source solution, mainly at early times. Three different segments of the time-drawdown curve were recognized: a very early one in which the well starts producing under decompression of the water and formation (as short as a few seconds or minutes) followed by a gravity drainage period when vertical flow near the wellbore controls and the free surface changes rapidly, and finally a late period where the rate of change of the water table is no longer important. In the first and last periods, the so-called non-equilibrium formula *(Theis* solution or its logarithmic approximation) could be applied, because the flow is dominantly horizontal. However, when and where gravity drainage is the most important mechanism, solutions like *Bodton* (1954-b) should be used.

In 1954, *Bodton* (1954-a) introduced a new approach to represent unconfined

transient flow behavior. Using ***Darcys*** Law and the continuity equation for flow of incompressible liquids, the following partial differential equation in terms of the liquid potential $\Phi = p/g\gamma_w + z$ was posed in the case of isotropic aquifers:

$$\nabla^2(\Phi) = \frac{\partial^2\Phi}{\partial r^2} + \frac{1}{r}\frac{\partial\Phi}{dr} + \frac{\partial\Phi^2}{\partial z^2} = 0 \qquad (2.5)$$

The water table boundary condition was expressed by:

$$\Phi(r,z,t) - z = 0 \qquad (2.6)$$

The differentiation following the motion of a particle located on the free boundary streamline was defined:

$$\frac{D}{Dt}(@- z) = 0 \qquad (2.7)$$

In Eq. 2.7:

$$\frac{D}{Dt} = \frac{\partial}{\partial t} + \frac{v_r}{S}\frac{\partial}{dr} + \frac{v_z}{S}\frac{\partial}{\partial z} \qquad (2.8)$$

Applying the differential operator as defined, the following non-linear equation was obtained:

$$\frac{\partial\Phi}{\partial t} = \left\{\left(\frac{\partial\Phi}{\partial r}\right)^2 + \left(\frac{\partial\Phi}{\partial z}\right)^2 - \frac{\partial\Phi}{\partial z}\right\} \qquad (2.9)$$

Equation **2.9** was simplified by the assumption that the Φ gradients are small, and when $z = h$:

$$\frac{\partial \Phi}{at} + \frac{k}{S}\frac{\partial \Phi}{\partial z} = 0 \qquad (2.10)$$

The inner boundary condition considered a line sink at a constant pumping rate per unit length:

$$Q = 2\pi k h_e r \frac{\partial \Phi}{\partial r}; \qquad r \to 0; \quad 0 \le z \le h_e \qquad (2.11)$$

A general solution of Eqs. *2.6* to *2.11* and the boundary conditions was reached after simplifying assumptions:

$$h_e - \Phi = \frac{Q}{2\pi k h_e}\int_0^\infty \frac{J_o(\beta r)}{\beta}\left\{1 - \frac{\cosh(\beta z)}{\cosh(\beta h_e)}\exp\left(-\frac{k}{S}t\beta\tanh(\beta h_e)\right)\right\} d\beta \qquad (2.12)$$

Further simplifications were made and a definite integral denoted by $V(r,t)$ was introduced:

$$V(\rho,\tau) = \int_0^\infty \frac{J_o(\lambda\rho)}{\lambda}\{1 - \exp[-\lambda\tau\tanh(\lambda)]\} d\lambda \qquad (2.13)$$

$$s = \frac{Q}{2\pi T} V(\rho,\tau) \qquad (2.14)$$

where ρ and τ are dimensionless radius and time, respectively:

$$\rho = \frac{r}{h_e} \qquad (2.15)$$

and:

$$\tau = \frac{k t}{S h_e} \qquad (2.16)$$

Values of the Eq. 2.13 integral were tabulated, as well as corrections for deviations due to the several simplifications. *Boulton* (1954-a) also handle modifications to consider anisotropy and head recovery (buildup), and a correction for a finite wellbore radius.

The second *Boulton* paper (1954-b) contains a solution that became an most important reference in the Groundwater literature during the subsequent 15 to 20 years, because it introduced a new theory for unsteady radial flow in an unconfined isotropic aquifer. Two different cases were considered, but the one that fitted the gravity drainage model best assumed a delayed yield from storage caused by an idealized bed of fine-grained material overlaying the aquifer with the stabilized water table within this section of low permeability. The rate of delayed yield was empirically represented by:

$$\delta s \quad \propto \quad S' \, e^{-\alpha(t-\tau)} \tag{2.17}$$

where a is an empirical constant. Neglecting the vertical components of flow, the final form of the P.D.E. considering delayed yield is:

$$\frac{\partial^2 s}{\partial r^2} + \frac{1}{r}\frac{\partial s}{\partial r} \quad = \quad \frac{S}{T}\frac{\partial s}{T} + \frac{\alpha S'}{T}\int_0^t \frac{\partial s}{\partial t}_{t=\tau} e^{-\alpha(t-\tau)} dt \tag{2.18}$$

The following solution for Eq. 2.18 was obtained properly using the Laplace transform technique:

$$s \quad = \quad \frac{Q}{4\pi k h_e}\left\{\int_0^{\alpha}\left(1 - e^{-ut}\right) J_o\left[r\sqrt{\frac{u}{a}\frac{\eta\alpha - u}{\alpha - u}}\right]\frac{du}{u} + \right.$$

$$\left.\int_{\eta\alpha}^{\infty}\left(1 - e^{-ut}\right) J_o\left[r\sqrt{\frac{u}{a}\frac{\eta\alpha - u}{\alpha - u}}\right]\frac{du}{u}\right\} \tag{2.19}$$

where:

$$\eta \quad = \quad 1 + \frac{a\,c}{a} \quad - \quad \frac{S + S'}{S}, \qquad a \quad = \quad \frac{T}{S}, \qquad \text{and} \qquad c \quad = \quad \frac{a\,S'}{T}$$

(2.20)

Some approximations of the solutions were prepared by assuming limiting values of η. Tables containing numerical values for different approximations of Eq. 2.19 were provided.

The explanation used to justify the *Boulton* model was weak and had little physical connection with the pure gravity flow mechanism. However, the mathematical formulation was shown to match many sets od field data, and later *Boulton* (1963) presented the same model applied to unconfined aquifer drawdown, and a group of delayed yield type curves generated by a computer program - see Fig. 2.3. The early and late time behaviors were analyzed, and two different sets of curves were plotted on the same graph at two different dimensionless time scales. The shapes of these curves, according to the author, show different flow patterns. Under the consideration of the initial and internal boundary conditions at the very early time of pumping, the time-drawdown curve follows the *Theis* solution for an artesian aquifer. Next, as the yield from the water table becomes effective, the drawdown behavior deviates from the line-source solution due to the contribution by the water table fall, and the curves bend to the right (Type A curves), trending to an asymptotic behavior. After a time, the approximations of the integral show flat curves which start to bend up (type B curves), merging into the *Theis* solution. The dimensionless time at which the departure from *Theis* solution drawdown and the calculated type B curve from the *Boulton* model equals 0.02 generates a new parameter called the delayed index $(\frac{1}{\alpha})$. This delayed index is a characteristic of the formation and is physically related to the gravity vertical flow around the wellbore. As in the previous work *(Boulton,* 1954-b), only isotropic formations were considered.

Prickett (1965) applied the *Boulton* (1963) solution to eighteen pumping tests and found good agreement with the theory. The relationship obtained in the tests between the delay index and the grain size of sand demonstrated a physical correlation. Also, an interesting set of graphs shows the individual variation of different parameters. Theoretical time-drawdown curves indicated the effects of changing only one variable of the basic equation (such as $1/\alpha, S, \mathrm{Sy}, r,$ and T), while all other coefficients

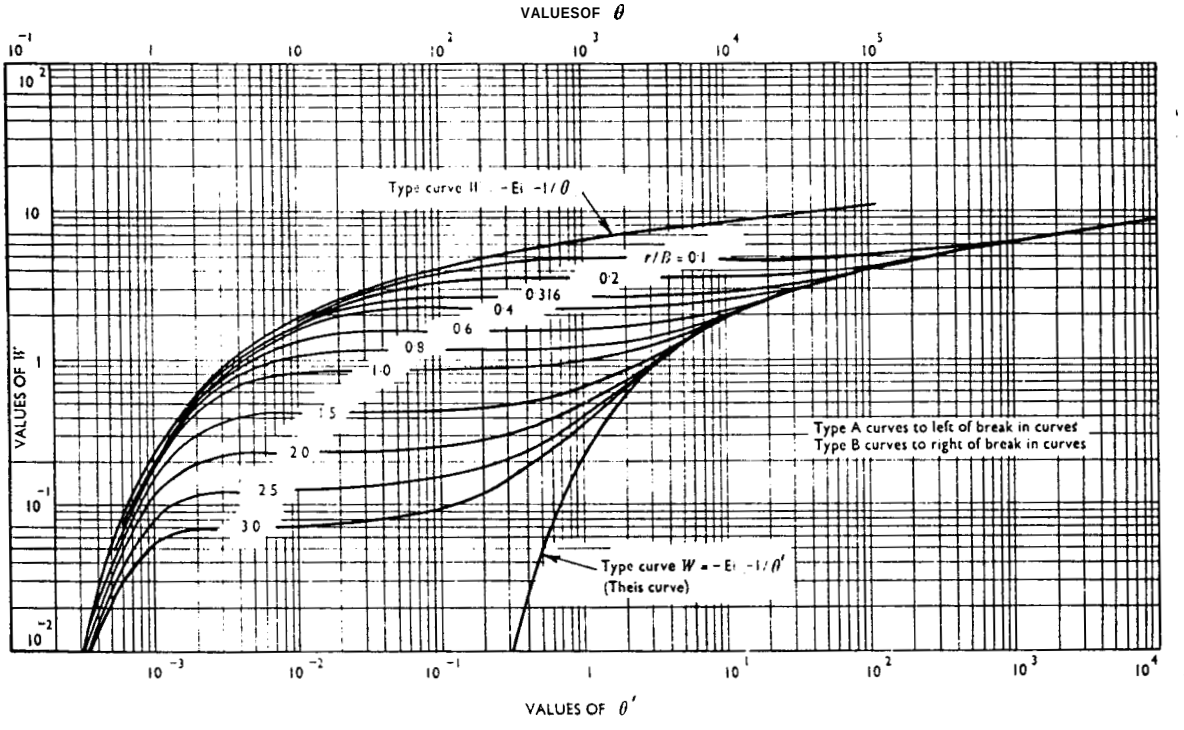

Figure 2.3: From *Boulton* (1963) paper: Delayed yield type curves.

remained fixed.

To consider the vertical flow around a well, *Boulton* (1970) presented, without derivation, an equation based on the delayed yield *(Boulton,* 1954-b and 1963) and the vertical velocity-component of the flow *(Boulton,* 1954-a). However, this equation was not applied in the 1970 study. Instead, some considerations were suggested in order to have "the most reliable method of analyzing pumping test data for **an** unconfined aquifer", using previous theories:

(a) the use of matching distance-drawdown by type-curves based on a constant coefficient of Storage (such as the *Boulton* V-function, *Boulton* 1954-a), and

(b) the application of the delayed yield analysis *(Boulton,* 1963).

A practical example of these methods applied to observation wells was given. There is a comment on page 375, in which *Boulton* 1970 explains the deviation of the early time behavior from the type **A** (early *Theis)* solution, shown in his Fig. 2 by the

need for a "type-curve based on a differential equation which contains an additional term for the short-term delayed yield". He justified the simplification of the problem by stating that the parameters involved in this early period of flow are "of small importance".

In order to enhance the solution *(Boulton,* 1954-a, 1954-b, 1963) for drawdown of an unconfined aquifer, an additional empirical term allowing for early time delayed yield from storage was considered by *Boulton* and *Pontin* (1971). The new solution enabled one to consider anisotropy and partial penetration, as well as to calculate the specific yield with "greater confidence". By considering a second delayed yield term, the new results at early times were not associated with the previous early Type **A** curve. **A** practical example of application was given, using the same pumping test reported in a previous paper *(Bodton,* 1970). The figures presented showed a better match of the theoretical solution with the data, even at early times.

Dagan (1964, 1967) proposed a perturbation technique to linearize-the equations of unsteady flow toward a partially penetrating well in an unconfined aquifer which considered the velocity potential and Darcys Law to describe the motion of the liquid in an anisotropic aquifer of infinite extent. The resulting first and second order linearized equations were solved using Green Functions for different sink configurations, considered as point or line sources. The restrictions requiring small drawdowns and vanishing sinks contained in the *Dagan* solutions restrict use in the neighborhood of the sandface. However, the ***Dagan*** solutions have advantages over the *Boulton* (1963) solution, by the consideration of the vertical component of velocities. At least, better results than the *Theis* approach would be expected in the vicinity of a well. The problem posed by ***Dagan*** neglected compressible effects in the unconfined aquifers, later included by *Neurnan* (1974) by incorporating the aquifer compressibility in the *Dagan* (1967) equations.

Streltsova (1972-a) and (1972-b) considered slow drainage as the delayed process

of vertical transfer, and not a delayed yield as did *Bodton*. She reduced the tri-dimensional problem to a two-dimensional problem by considering an average head along the vertical coordinates, given by the relationship:

$$h = \frac{1}{h^o} \int_0^{h^o} \Phi(r,z)\, dz \qquad (2.21)$$

Therefore, the unsteady radial free surface flow partial differential equation is:

$$T\left(\frac{\partial^2}{\partial r^2} + \frac{1}{r}\frac{\partial h}{\partial r}\right) = S\frac{dh}{\partial t} + S'\frac{dh''}{\partial t} \qquad (2.22)$$

The specific rate of the vertical transfer of flow was assumed to vary linearly with the difference between the average head h and the free surface h'':

$$\frac{\partial h^o}{at} - \bar{\alpha}(h - h'') \qquad (2.23)$$

The relationship between Q and other properties is:

$$\alpha = \frac{1}{S'}\Phi = \frac{k}{S'b} \qquad (2.24)$$

where, k and b are the average value of the permeability coefficient and the thickness of the vertical flow, respectively, and Φ is the specific hydraulic conductivity. A constant rate inner boundary condition given by the following equation was considered, as $r \rightarrow r_w$:

$$Q = 2\pi k H r\left(\frac{\partial h(r,t)}{\partial t}\right) = \text{constant} \qquad (2.25)$$

and the initial condition is:

$$h(r,0) = h''(r,0) = H. \qquad (2.26)$$

The combination of the differential equations permitted the partial differential Equation (Eq. **2.22)** to be represented in terms of h and the radial distance from the well axis r:

$$T\left(\frac{\partial^2 h}{\partial r^2} + \frac{1}{r}\frac{\partial h}{\partial r}\right) = S\frac{\partial h}{\partial t} + S' \int_0^t \frac{\partial h}{\partial \tau}\left[1 - e^{-\alpha(t-\tau)}\right] d\tau \qquad (2.27)$$

Equation **2.27** has a similar solution to the *Boulton* **(1963)** problem for which compressible flow was neglected, i.e., $S = 0$:

$$h = H - \frac{Q}{2\pi T}\int_0^\infty \frac{J_o\left(\frac{r}{B}x\right)}{x}\left\{1 - \frac{1}{x^2+1}\, e^{\left(-\frac{\alpha t x^2}{x^2+1}\right)}\right\} dx \qquad (2.28)$$

A solution for h'', which is the position of the free surface with time, was also obtained by assuming an exponential rate of discharge resulting from the discontinuity in head at a well:

$$Q'' = \boldsymbol{Q}\,(1 - e^{-\alpha t}) \qquad \textbf{(2.29)}$$

and so:

$$h^o = H - \frac{Q}{2\pi kT}\int_0^\infty \frac{J_o\left(\frac{r}{B}x\right)}{x}\left\{1 - \exp\left(-\frac{\alpha t x^2}{x^2+1}\right)\right\} dx \qquad \textbf{(2.30)}$$

In a subsequent paper, *Streltsova* **(1973)** analyzed the contribution of the unsaturated zone (capillary forces and additional retarded flow) above the free surface to the head drawdown response in the wellbore, and concluded that the unsaturated zone contributions were of minor importance compared with the vertical fall of the water table. An important observation in this paper was the conclusion that the specific yield for vertical flow is a constant property of the formation, and the relationship between the unsteady water table heights and the flux at the water table averaged over the area is also constant. However, the free surface and the flux have an exponential change with time. In this same paper, *Streltsova* showed results from an

experimental radial flow model using an analog electrical resistance network for simulating unconfined flow around the well. These results were compared with results of analytical solutions from the *Boulton* **(1963)** type-curves for average drawdown, and with the *Barenblatt et al.*(1960) solution for a similar equation for the free surface drawdown applied to unconfined flow. A good match between experimental and analytical results was used to verify the theory, and to show the degree of reliability of assumptions of neglected flow from the unsaturated region and capillary pressure effects.

Complementing the previous work, *Streltsowa* and *Rushton* **(1973)** presented a table for the definite integral $W_o[r/B, u]$ defined in Eq. **2.30,** and compared the *Streltsova* **(1972-b)** solution based on the previous assumptions and the *Boulton* **(1963)** integral $V[r/H, t]$ given by Eq. **2.13.** The basic difference between the two methods is that the former's main assumption is a finite difference approximation for the free surface condition (see Eq. 2.23), whereas the latter makes an assumption of constant discharge per unit length over the entire depth of the well and establishes an empirical relationship creating the delayed yield parameter. The comparison is presented in both table and graph. **A** computer code for the main part of a program to calculate the position of the free surface according to the *Streltsowa* approach is available.

The elastic properties of the aquifer were considered by *Streltsowa* **(1974)** in solving the gravity drainage flow problem for a partially penetrating line-sink. Different boundary conditions and a more rigorous mathematical approach were used, instead of the finite difference approximation described before. In the conclusions, it was emphasized that the elastic properties of the aquifer were essential during the early periods of pumping before gravity drainage has started.

A new analytical approach was presented by *Neuman* **(1972)** which defined a set of equations, considering formation anisotropy and constant values of specific storage and specific yield with no empirical considerations. According to the author, this method eliminates the conceptual difficulties in the *Boulton* theory of "delayed yield",

and suggested calling the physical process involved in the early time flow behavior of an unconfined aquifer as "delayed response". Also, a comparison with the results from a numerical solution using the Cooley **(1971)** finite difference model showed the unsaturated region flow to be important to the drawdown in a free surface aquifer. The *Neuman* model treated the unconfined aquifer as a compressible system and the free surface as a moving boundary. One common assumption in the *Neuman* theory as well as that of others is the treatment of the well as a line sink. This simplification of the problem, using the author's words, introduces "a certain error in the solution near the well bore" by neglecting the presence of a seepage face. The governing set of equations for the tri-dimensional problem is:

$$(0 < z < \xi) \qquad K_r \frac{\partial^2 s}{\partial r^2} + \frac{K_r}{r}\frac{\partial s}{\partial r} + K_v \frac{\partial^2 s}{\partial z^2} = S_s \frac{\partial h}{\partial t} \qquad (2.31)$$

$$s(r,z,0) = 0 \qquad \textbf{(2.32)}$$

$$\xi(r,0) = 0 \qquad (2.33)$$

$$s(\infty,z,t) = 0 \qquad \textbf{(2.34)}$$

$$K_r \frac{\partial s}{\partial r} n_r + K_z \frac{\partial s}{\partial z} n_z = \left(S_y \frac{\partial \xi}{\partial r} - I\right) n_z \qquad at \qquad (r,\xi,t) \qquad (2.35)$$

$$\xi(r,t) = b - s(r,z,t) \qquad \textbf{(2.36)}$$

$$\lim_{r\to 0} \int_0^{\xi} r \frac{\partial s}{\partial r}\, dz = -\frac{Q}{2\pi k_r} \qquad \textbf{(2.37)}$$

Equations **2.31** and **2.37** were solved using a perturbation technique and Laplace and Hankel transforms. The solution is given in the Appendix of *Neurnan* **(1972)** and is:

$$s(r, z, t) = \frac{Q}{4\pi T} \int_0^\infty 4x J_o\left[x\sqrt{k_D}\right] \left[w_o(x) + \sum_{n=1}^{\infty} w_n(x)\right] dx \qquad (2.38)$$

where, $w_o(x)$ and $w_n(x)$ are expressions given by Eq.15 in the original paper. That solution is **a** function of the coordinate z. In order to find an average solution over the aquifer thickness in an observation well, the following expression was used:

$$s(r, z, t) = \frac{1}{z_2 - z_1} \int_{z_2}^{z_1} s(r, z, t)\, dz \qquad (2.39)$$

where z_1 and z_2 are elevations of the open sandface in the observation well. For a well that completely penetrates the aquifer, the final result for the average drawdown is calculated from Eq. 2.38 after redefining $w_o(x)$ and $w_n(x)$ as Eqs. 20 and 21 in *Neuman* (1972). The influence of each dimensionless parameter was studied and interesting graphs presented. See Figs. **4** and 5 *(Neuman,* 1972, pp. 1037-1038). Figure 4 suggests an approximate linear relationship of the logarithm of water table drawdown with the logarithm of time (curve corresponding to $z_D = 1$), and Fig. **5** presents a dimensionless constant position $z_D \approx 0.57$ for the average drawdown over the entire aquifer. The *Neuman* (1972) solution was supplemented by a subsequent paper *(Neuman,* 1973) whose main purpose was to modify the original **Eq.** 27 (Neuman,1972), allowing for anisotropy. The result presented in Eq. 2.40 is similar to the *Boulton* (1954-b) solution:

$$s(r, z, t) = \frac{Q}{4\pi T} \int_0^\infty 2J_o\left[y\sqrt{\eta}\right] \left\{1 - \exp\left(-t_y \eta y \tan(y)\right) \frac{\cosh(y z_D)}{\cosh(y)}\right\} \frac{dy}{y} \qquad (2.40)$$

The new theory *(Neuman,* 1972,1973,1974) was applied to pumping tests for fully and partially penetrating wells by *Neuman* (1975-a). Besides the general procedure of curve-matching, this paper introduced a method of interpretation based on the semi-logarithmic relationship between drawdown and time. For type-curve analysis,

the methodology follows that previously described by *Prickett* (1965). The semi-log interpretation is based on the linear behavior of drawdown with the logarithm of time at late times when the rate of change in the free surface has become small. However, due to the assumption of a line-sink well, the theoretical early time behavior is also supposed to fall on a semi-log straight line since the initial flow from the formation into the wellbore is essentially horizontal. The practical example of application of this method in analyzing pump test data seems to be conclusive with respect to the late time behavior, but not well fitted to the early time data points for a pumping well. In describing this method, *Neuman* suggests deleting the early time data analysis if the slope of the straight line obtained differs noticeably from the straight line fitted to the late time data points. In this case, the method of interpretation should be complemented by matching of type-curves. Another important consideration made in the paper by *Neuman* (1975-a) concerns recovery (buildup) tests. Because no flow from the unsaturated region is considered in this method, and the unconfined aquifer is treated as a compressible system, no hysteresis is expected. **As** a consequence, the same analytical equations and interpretation methods should applyfor both drawdown and buildup. However, *Ramey et al.* (1989) observed that the semi-log graphs for drawdown and buildup show much different times for the start of the straight line behavior for the same well test data. This and similar physical observations make questionable the reversibility of the process of gravity drainage under the free surface. On this same paper, *Neuman* (1975-a) relates the *Boulton* reciprocal delay index a with aquifer properties by establishing a numerical relationship between *Boulton* type-curves expressed by the dimensionless parameter $(r/B)^2/b$ versus s_D. In semi-logarithmic paper, a linear relationship was obtained by regression analysis:

$$\frac{(r/\beta)^2}{\beta} = 3.063 - 0.567 \log \beta \tag{2.41}$$

Using definitions of r/B, β, and a, Eq. 2.41 becomes:

$$\alpha = \frac{k_z}{s_y b}\left[3.063 - 0.567 \log\left(\frac{k_D r^2}{b^2}\right)\right] \tag{2.42}$$

Equation 2.42 represents a connection between the *Boulton* and *Neuman* theories. *Neuman* also recognized the relationship of the a-parameter and physical properties of the aquifer in the *Streltsova* study, but claims that the relationship exists only as a function of distance r (see Eq. 2.42), and not of time, as is clear from the dependence of s_{w_T} in the following Eq. 2.43 by *Streltsova* (1972-b):

$$\alpha = \frac{3k_z}{s_y (b - s_{w_T})} \tag{2.43}$$

Streltsova (1976) believes that the *Neuman* boundary condition for the free surface *(Neuman,* 1972) leads to a mathematical formulation equivalent to *Boulton* (1954-b, 1963) and *Streltsova* (1972). Therefore, she concludes that the solutions are identical, and claims that once the a-parameter is determined, it is possible to determine the degree of anisotropy by calculating μ from the relationship with a:

$$\alpha = \frac{3k_z}{S' h^o} = \frac{3\mu^2}{h^{o2} S'}, \tag{2.44}$$

where:

$$\mu = \frac{k_z}{k_r}$$

This procedure yields a different k, from the *Neuman* theory due to the approximation in the *Streltsova* model relating the average drawdown and the drawdown of the free surface by a finite difference relationship given by Eq. 2.23. Plots of β and $(r/B)_2$ versus s_D are matched to demonstrate the correlation between the dimensionless parameters. These considerations were denied by *Neuman* (1976), asserting that the matching was "grossly misleading".

The discussions with respect to delayed yield are summarized in a paper *(Neuman,* 1979) which compares the relevant theories on delayed yield. *Neuman* seems to have adopted the term "delayed yield" to characterize the phenomena which he previously suggested *(Neuman,* 1972) should be referred to as "delayed gravity response". **A** brief

speculation about Boulton theory raises the possibility of delayed yield being caused by delayed air entry in the high water saturation porous region above the free surface. However, referring to several authors, and specifically to works by *Kroszynski* and *Dagan* (1975), *Neuman* (1975-b) and *Neuman* et al. (1974), *Neuman* concludes that the unsaturated flow has a minor influence on the time-drawdown response during gravity drainage of liquid. **A** justification for large apparent storage coefficients S in unconfined aquifers compared to artesian aquifers is explained by entrapped air bubbles or dissolved air in the saturated zone. Thus, the fluid compressibility could have large values. Therefore, *Neuman* uses this argument against the idea of *Bouwer* and *Rice* (1978) that the delayed air entry is due to the slow movement of liquid in the unsaturated porous space above the free surface. The liquid in the capillary fringe is drained slowly as a consequence of a negative pressure differential created when the liquid surface moves vertically down. *Neuman* again referred to the rate of head recovery (buildup) as a fully-reversible mirror-image process, and, therefore, incompatible with the theory of the air entry concept of *Bouwer* and *Rice*. *Neuman* criticized the idea that the influence of radial distance on the ***Prickett*** (1965) and *Gambolati* (1976) theories that at a certain time during the desaturating period the region around the wellbore may be divided into three different sub-regions of different flow patterns. *Neuman* stated that "the cone of depression is not distorted, and its slope varies monotonically with radial distance".

The most important theories of gravity drainage flow so far reviewed do not consider the flow in the unsaturated zone rigorously. Even the *Boulton* (1954-b) model does not consider the characteristics of the region above the free surface directly. Instead, the *Boulton* model approximates this effect by creating the delayed yield parameter ***a.*** In the following, flow in the unsaturated zone will be considered in regard to the gravity flow problem.

A complete analytical solution reflecting the flow in the unsaturated region above the free surface, an anisotropic formation, and a partially penetrating line-sink well were considered by *Kroszynski* and *Dagan* (1975). According to *Neuman* (1979), this

is "... the most definitive study about the role of unsaturated flow ..." published so far. Using the same original notation, the following equation is used to represent the flow in the unsaturated zone:

$$\frac{D'}{S_v}\frac{d\theta}{d\Psi'}\frac{d\Phi}{dt} = \nabla\left(k\left(\Psi\right)\nabla\Phi\right) \qquad (2.45)$$

where D' is the initial saturated thickness of the aquifer, θ is the volumetric moisture content, Ψ' is the capillary head, k is the relative hydraulic conductivity (function of **0** or ***8***), and Φ is the total head corresponding to the isolated sink solution. The other equations and the analytical solution will not be presented here. The model was tested by comparing results with numerical solutions from a modified program after *Neuman* (1975-b). The results indicate little influence of the unsaturated flow on the time-drawdown response. Only for special conditions of thin and low permeability aquifers were significant effects observed at early times. Another important consideration is the finite wellbore radius used in the numerical model to simulate wellbore storage effects. Unfortunately, *Kroszynski* and *Dagan* did not apply this model to the producing well, and the closest observation well was located at 4.4 ft from the symmetry axis.

Bouwer and *Rice* (1978) presented a physical basis for delayed yield response as a restriction of the unsaturated zone to air entry due to the fall of the water table. **As** the free surface moves down, air penetration into the rock pores is impeded by the high initial water content of this region reducing the relative permeability to air. The initial specific yield is small, but increases with time as vertical drainage occurs. This process is important if the draining region contains layers of fine-textured materials which have high water retention. In this case, the entry capillary pressure retards the air movement downward. Once started, the pressure directly above the water table varies from vacuum to equilibrium at atmospheric pressure. The time lag is reflected in the variation of the specific yield. *Bouwer* and *Rice* use the explained principles to run laboratory experiments to explore field observations. Apparently, the typical inflection in the time-drawdown curve observed for pumping tests could

not be reproduced in the lab, and, according to *Neurnan* (1979), the results were not conclusive.

Another physical explanation for delayed yield is attributed to the hysteresis effect on the capillary fringe and transition zone above the water-table, and also underneath the free surface *(Bouwer,* 1979). According to *Bouwer,* pumping tests are often done in wells that were previously operated. **As a** consequence, the region of the reservoir around the wellbore, once drained by pumping the well, is not completely re-saturated after the recovery of the initial head after pumping is stopped. Hence, bubbles of air, entrapped in the initial capillary fringe or in the previously saturated zone, will create a more compressible system than the original one, causing a delay in releasing significant amount of water from the pores. Therefore, the fall of the water-table will be retarded by an increase of the compressibility in that region. In *Bouwer* opinion, the air compressing effects could well be a common cause of delayed yield, in addition to the elastic response of the aquifer and the restricted air entry. There was no mention of a reduction in transmissivity caused by the presence of another phase.

Analyzing pumping tests for an unconfined aquifer in Canada, *Nwankwor et al.* (1984) made a comparative study of their determinations of specific yield with results from other methods. The tests were run in a pattern formed by a centered pumping well and observer wells distributed into two perpendicular lines to monitor the drawdown at different levels in the aquifer. Using the *Boulton* (1963) and *Neurnan* (1972) theories, the authors observed that at early times very low results for specific yield were calculated from both methods. As time increased, specific yield increased slightly, but never approached the values calculated from the volume-balance method or determined by laboratory measurements. The volume-balance method consists of calculating the cumulative water produced V_w and dividing it by the volume of the cone of water-table drawdown V_c, obtained from observation well drawdown mapping. Despite that discrepancy, ***Nwankwor et al.*** concluded the various methods of interpretation give similar results for transmissivity. The apparent reasons for the differences in the long-term specific yield were attributed to neglecting the delayed

drainage from above the water table in the *Neuman* (1972) theory, and the downward hydraulic gradients in the Boulton theory. Therefore, a more rigorous model considering flow in the unsaturated zone and vertical flow processes simultaneously should be more appropriate.

The large differences in the specific yield described before caused concerns about the reason for such deviations. A convincing explanation for this problem was given by *Neuman* (1987). A superficial analysis of the *Nwankwor et al.* (1984) study shows an invalid assumption concerning the volume-balance method. The criteria used in performing that balance is that the total volume of water produced by a well comes from the depressed cone in the reservoir. Therefore, applying the ratio of volumes, the specific yield would vary, and reach high values after a long time. Regarding laboratory results, one is supposed to accept the concept of specific yield as the difference between the saturated core and residual water in the pores of the rock. Apparently only a fraction of the produced water comes from the depressed cone. *Nwankwor et al. et al.* (1984) neglected the volume of water that comes from the outer reservoir. Neuman (1987) demonstrated this idea in two different ways: an approximate calculation based on the presented data *(Nwankwor et al.*, 1984), and a theoretical approach. In other words, the water balance was not valid because only a small fraction of the water comes from the observed cone of depression. *Neuman* theoretical analysis was also confirmed by the pumping test data from *Nwankwor et al.*, and substantially supports the idea that the variation of the free surface "in response to pumping is relatively insensitive to residual drainage in the unsaturated zone".

2.4 Inner Boundary Condition

Until the middle sixties, the inner boundary condition had not been treated adequately in hydrology, and only the line source well (*Theis*, **1935)** had been considered in pumping tests. Wellbore storage and finite radius well effects were neglected, mainly in shallow and unconfined aquifers where most of the pressure observations in pumping tests were usually performed in shut-in observation wells, not in the producer. In petroleum engineering, **an** early application of the finite well radius and well storage was presented by *Moore et al.* **(1933).** This was a remarkable early study of transient flow which included an example of field well test data interpretation. Sonic annulus liquid levels were measured and sandface flow rates found by subtracting production from the wellbore storage. **A** variable rate analysis was used to interpret the well test data. One of the authors, *W. Hurst* was a co-author of the classic paper *van Everdingen and Hust* **(1949)** which included both finite-producting well radius solutions and defined wellbore storage and produced a log-log storage type curve which is the basis of modern type curve data interpretation.

Wellbore conditions were completed defined in **1953** by the *van Everdingen* **(1953)** and *Hurst* **(1953)** skin effect concept. The skin effect defined well condition quantitavelly by adding a dimensionless resistance to flow at the sandface. In the following, a brief analysis of selected studies of wellbore condition is presented.

In **1964,** *Hantush* reviewed solutions of the continuity equation for a well of finite radius in a confined aquifer, without storage effects. Consideration of well bore storage in analyzing pumping tests for a confined aquifer was presented by *Papadopulos and Cooper* (1967), who appeared to be unware of the earlier study by *van Everdingen* and *Hurst* **(1949).** The wellbore storage inner boundary condition can be represented by a material balance equation:

$$\boxed{\text{sandface flow rate}} \quad + \quad \boxed{\text{wellbore flow rate}} \quad = \quad \boxed{\text{pumping rate}} \tag{2.46}$$

$$2\pi r_w T \frac{\partial s(r_w t)}{\partial r} \quad - \quad \pi r_c^2 \frac{\partial s(t)}{\partial t} \quad = \quad -Q \tag{2.47}$$

The solution in Laplace space is:

$$\bar{s} \quad = \quad \frac{Q\, K_o(q\, r)}{\pi p \left[r_c^2 p K_o(q\, r_w) + 2 r_w T q K_1(q\, r_w)\right]}\,, \tag{2.48}$$

where, $\bar{s}$ is the Laplace transform of the drawdown, p is the Laplace parameter, and $q = \left(\frac{pS}{T}\right)^{1/2}$. The inversion, obtained from an analogous problem in heat flow (*Carslaw* and *Jaeger*, 1959), gives the drawdown at any distance r from the well bore center:

$$\begin{aligned} s \quad = \quad & \frac{2Q\alpha}{\pi^2 T} \int \left(1 - e^{-b^2/4u_w}\right) \{J_o(\beta r/r_w)\left[\beta Y_o(\beta) - Y_1(\beta)\right] \\ & - Y_o(\beta r/r_w)\left[\beta J_o(\beta) - 2\alpha J_1(\beta)\right]\} \frac{d\beta}{\beta^2 \Delta(\beta)} \end{aligned} \tag{2.49}$$

where, $a = r_s{}^2 S/r_c{}^2$, and $u_w = r_s{}^2 S/4Tt$. When $r = r_w$, Eq. *2.49* simplifies to:

$$s_w \quad = \quad \frac{Q}{4\pi T} F(u_w, \alpha)\,, \tag{2.50}$$

where

$$F(u_w, \alpha) \quad = \quad \frac{32\alpha^2}{\pi^2} \int_0^\infty \frac{\left(1 - e^{-b^2/4u_w}\right)}{\beta^3 \Delta(\beta)}\, d\beta\,. \tag{2.51}$$

In the *Papadopulos* and *Cooper* paper, Fig. *2* shows a set of type curves based on this solution, and compares several results for parameters a (related to the well bore

storage), with the *Theis* and *Huntush* solutions. As an addendum to the previous work ***(Papadopulos*** and ***Cooper*** **,** 1967), ***Papadopulos*** (1967) presented an additional logarithmic plot of $s/Q/4pT$ versus $r^2S/4Tt$ for several dimensionless distances from the well.

Cooper *et al.* (1967) use a procedure similar to ***Papadopulos*** and ***Cooper*** (1967) to study the "slug-test" in a confined aquifer. Equation 2.50 is used as an inner boundary condition, and the final solution for the head in Laplace space has the same format as **Eq.** 2.48, here represented by Eq. 2.53:

$$2\pi r_s T \frac{\partial h\,(r_s + 0, t)}{\partial r} = \pi r_c^2 \frac{\partial H\,(t)}{\partial t}\,, \tag{2.52}$$

$$\bar{h} = \frac{r_s S H_o K_o\,(q r)}{T q\,[r_s q K_o\,(q r_s) + 2\alpha K_1\,(q r_s)]}\,, \tag{2.53}$$

where, q and cy have the same definition as before, and H_o is the initial head increase in the well. Analogously, the solution at the producing well, i.e., when $r = r_s$, is:

$$H = \frac{8H_o\alpha}{\pi^2} \int_0^\infty \frac{e^{-\beta u^2/\alpha}}{u\Delta\,(u)}\,du \tag{2.54}$$

Kipp (1973) presents another theoretical solution for the unconfined flow problem. A homogeneous isotropic aquifer of infinite thickness and infinite lateral extent, partially penetrated by a well of finite radius was assumed. Other important assumptions were single phase flow, an incompressible system and no surface of seepage in the well bore. **A** set of boundary condition equations in terms of velocity potential was solved using a perturbation technique. The approximations made restrict applications of the semi-analytical results to short times after pumping start-up. The line-sink solution by other authors *(Boulton,* 1954-a, and *Dagan,* 1967) was found to have reasonable agreement with the ***Kipp*** solution, at radial positions greater than 15% of the well depth below the initial free surface. Although some graphical comparisons were shown, no attempt to create dimensionless type curves was made. There

are some disadvantages of this solution with respect to analysis of well tests besides limitations imposed by the initial assumptions and the solution method: a "tedious trial and error search is necessary to determine the aquifer parameters".

A simple procedure for calculating aquifer properties by a slug test is shown in a paper by *Bouwer* and *Rice* (1976) using a modified *Thiem* equation and a resistance network analog computer. The method is based on the assumption that the nature of flow around the well is predominantly radial during a pressure recovery after a fixed volume of water is instantaneously removed from the wellbore:

$$Q = 2\pi K L \frac{y}{\ln (r_e/r_w)} \qquad (2.55)$$

where y is the instantaneous position of the water level in the well, with respect to the original water-table and r_e is the effective drainage radius in which the slug volume is dissipated. The drainage radius is obtained by empirical correlations from the electrical model, and is expressed as a function of parameters which depend only on the geometry of the system. The expressions for both a partially and fully penetrating well are given below.

partially Penetrating well:

$$\ln \frac{r_e}{r_w} = \left[\frac{1.1}{\ln (H/r_w)} + \frac{A + B \ln [(D - H)/r_w]}{L/r_w} \right]^{-1} \qquad (2.56)$$

fully penetrating well:

$$\ln \frac{r_e}{r_w} = \left(\frac{1.1}{\ln (H/r_w)} + \frac{C}{L/r_w} \right)^{-1} \qquad (2.57)$$

where A, B and C are empirical functions of L/r_w obtained from Fig. **3** in the *Bouwer* and *Rice* (1976) paper. To estimate the aquifer conductivity, Eq. ***2.58*** was derived from integration of Eq. ***2.55:***

$$t = \frac{r_c^2}{2KL} \ln\left(\frac{r_e}{r_w}\right) \ln\left(\frac{y_o}{y_t}\right) . \qquad (2.58)$$

A semi-log plot of the ratio y_o/y_t was used to determine K. According to *Bouwer* and *Rice,* the approach used to determine $\ln(r_e/r_w)$ yielded values of K *10%* to **25%** in error, depending on the geometric characteristics of the system.

Dagan (1978) presented an approach for interpreting packer, slug and recovery tests in unconfined aquifers in order to determine the permeability of low conductivity aquifers. He did not consider variations of the free surface due to small volumes drained from the system for those type of tests. The method consisted in integrating the source function continuously through the open interval in the well bore:

$$Q = \int_0^L q(z)\, dz , \qquad (2.59)$$

where:

$$q = 2\pi r_w K \frac{\partial \Psi}{\partial \rho} , \qquad r = r_w , \quad 0 < z < L \qquad (2.60)$$

Using a Greens function to define $d\Psi(r, z, \bar{z})$ for an element along $r = 0$ centered at $z = \bar{z}$ with sources of strength $q(\bar{z})$ distributed along the z axis, the solution produces the integral

$$\Psi(r, z) = \int_0^L \frac{q(\bar{z})}{K} G(r, z, \bar{z})\, dz \qquad (2.61)$$

The integral in eq. *2.61* is discretized and a finite sum is used instead:

$$\sum_{i=1}^{N} \frac{q(\bar{z})}{K} A_{ij} = \beta_{ij} \qquad (2.62)$$

The length L is divided in N equal intervals of length AL $= L/N$ and $q(z)$ is replaced by $q_i(i = 1, 2, ..., N)$; $\beta_j(j = 1, 2, ..., N)$ is started from the boundary condition and stands for $\beta[z = (j - 0.5)\Delta L]$ at the middle of the j^{th} interval. The system composed of Eq. 2.62 is solved for q_i/K by a computer program. Therefore, the result from Eq. 2.55 is:

$$\frac{Q}{K} = \Delta L \sum_{i=1}^{N} \frac{q_i}{K} \tag{2.63}$$

The hydraulic conductivity is:

$$K = \frac{r_w^2}{2\bar{Q}\, L\, (t - t_o)} \ln\left[\frac{(2L - y)/(2L - y_o)}{y/y_o}\right] \tag{2.64}$$

where Q is generated from a computer program, and:

$$\bar{Q} = \frac{1}{2\pi L y\,[1 - (y/2L)]} \frac{Q}{K} \tag{2.65}$$

The main limitation of this method is that the length of the sandface open to flow must be much larger than the wellbore radius.

Rushton and *Holt* (1981) compared analytical and numerical solutions for gravity drainage for aquifers and concluded that the numerical solutions were accurate in representing the phenomenon of unconfined flow. *Rushton* and *Holt* developed a finite difference form to solve the partial differential equation, Eq. 2.66, and simulated the wellbore storage effect by including a portion of the aquifer that represents the region within the well in the model .

$$\frac{\partial^2 s}{\partial r^2} + \frac{1}{r}\frac{\partial s}{\partial r} = \frac{S}{T}\frac{\partial s}{\partial t} \tag{2.66}$$

The transmissivity was set to a very high value in the well partly to simulate the

horizontal water level in the well, while the storage coefficient (equivalent to the effective porosity) was set to unity. The authors explained superficially that liquid level variations in the saturated depth was handled by considering the transmissivity equal to the permeability multiplied by the saturated depth, which was a function of the drawdown. Probably an iterative procedure was used if the drawdown was unknown. Figure 4 in *Rushton* and ***Holt*** compared the numerical results with field data, and showed good agreement with the early and late time drawdown. However, the intermediate period was poorly matched.

A kernel approach was used by ***Patel*** and *Mishra* (1983) for unsteady flow to a large diameter well in a confined aquifer taking wellbore storage into consideration. Using $s(r,0) = 0$ for the initial condition and $s(\infty,0) = 0$ for an external boundary condition, the solution of Eq. 2.66 when a unit impulse quantity is withdrawn from the aquifer is given by (*Carslaw* and ***Jaeger***, 1959):

$$s(r,t) = \frac{e^{-[r^2/4\beta t]}}{4\pi T t} \tag{2.67}$$

where $\beta = T/\Phi$. By defining a unit kernel function $k(t)$ as the right hand side of Eq. 2.67, the drawdown for a variable pumping rate $Q_A(t)$ is:

$$s(r,t) = \int_0^t Q_A(c)\, k(t - c)\, dc \tag{2.68}$$

From discretizing and applying Eq. 2.68 to the sandface:

$$s_A(n) = \sum_{z=1}^{n} Q_A(z)\, \delta_{r_w}(n - z + 1) \tag{2.69}$$

where $\delta r_w(m)$ is the discretized kernel coefficient at the sandface. For the wellbore, the discretized drawdown for the time step *n* is:

$$s_w(n) = \frac{1}{\pi r_c^2} \sum_{p=1}^{n} Q_A(p) \tag{2.70}$$

The combination of Eqs. 2.69 and 2.70 through a material balance in the well $Q_p = Q_A(n) + Q_w(n)$ and the continuity of the drawdown through the sandface into the well (no seepage face in the confined flow), $S_A(n) = S_w(n)$, the following solution was obtained in a matrix form:

$$\begin{vmatrix} Q_A(n) \\ \\ Q_w(n) \end{vmatrix} = \begin{vmatrix} \delta_{r_w} - \frac{1}{\pi r_c^2} \end{vmatrix}^{-1} \begin{vmatrix} \frac{1}{\pi r_c^2} \sum_{p=1}^{\cdot\cdot} Q_A(p) - \sum_{z=1}^{\cdot\cdot} Q_A(p)\, \delta_{r_w}\ (n - z + 1) \\ \\ Q_p \end{vmatrix} \tag{2.71}$$

Dimensionless curves were generated after calculating $s(r,t)$ and s_w from Eqs. 2.68 and 2.70. The results match with those from *Papadopulos* and *Cooper* (1967).

A consideration of the seepage face was presented in a method of interpretation of pumping tests by *Rushton* and *Singh* (1987). This method has an important restriction because it assumed that the change in the saturated depth was negligible. Hence, the superposition principle may be applied the same way **as** in the work of *Patel* and *Mishra* (1983). The method also depended on empirical relationships between the height of the seepage face and the withdrawal rate from the aquifer, Q_A. The suggested relationship was of the form:

$$f = G_1 Q_A + G_2 Q_A^2 \tag{2.72}$$

Rushton and *Singh* based their model on an unpublished report by *Sakthivadivel* (1986), (see ref. in the paper) , and the parameters G_1 and G_2 must be deduced from field measurements. Coupling Eq. 2.72 it with a material balance in the well (see Eq. 2.47), the resulting set of discretized equations allowed the iterative calculation of the sandface rates, and, consequently, the determination of the drawdown

distribution. The paper also presented a comparison of two different approaches: one considering the seepage face and the other neglecting the seepage face. The results showed that the resulting transmissivity could be underestimated by 25%, while the storage coefficient value could be of the order of one-fifth of the true value in the simplified model neglecting the seepage face. The example shown in Figs. 5a and 5b in *Rushton* and ***Singh*** shows Cartesian graphs of drawdown and discharge from the aquifer versus time for both field data and computed results. Our observation of the plot of drawdown versus time identifies a linear relationship for the early time drawdown points. The early time recovery points also show the same behavior, although for a different period of time. Such a linear period is analogous to the well bore storage effects in confined systems. However, fitting the calculated curves by a theoretical approach is open to discussion.

2.5 Unconfined Flow in the Petroleum Industry

Although *Muskat* (1949) presented a brief discussion of the free surface gravity flow well problem, there have been only a few works concerning gravity drainage well test analysis in the petroleum literature. In 1956, *Mutthews* and *Lefkovits* published a paper in which were presented some approximate expressions to calculate the production rate decline for homogeneous reservoirs with a free surface pumped at a constant wellbore pressure (liquid level). The flow dynamics were neglected in the derivations which were based on the drainage radius and the *Dupuit* formula to get the following second order hyperbolic expression, not valid in the early stage of production:

$$\frac{q}{q_i} = \frac{1}{(1+\gamma t)^2}, \tag{2.73}$$

where q_i is the rate of oil production at time $t = 0$ ($t = 0$ may be taken arbitrarily), and γ is given by the following expression, translated into the symbology used in the

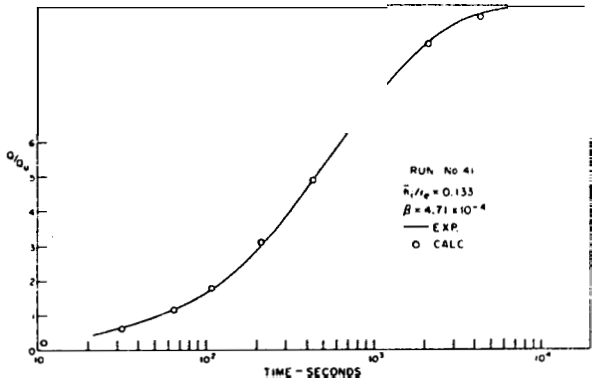

Figure **2.4:** Cumulative Production for Small Values of $\overline{h}_i/r_e$. - from *Mutthews* and *Lefkovits* **(1956).**

present dissertation:

$$\gamma = \frac{k_o \Delta\rho g H_o}{\phi (S_o - S_{o_r}) \mu_o \frac{1}{2} \left[1 + \sqrt{1 - \frac{1}{2 \ln \frac{r_e}{r_w} - 1}}\right] \left[\ln \frac{r_e}{r_w} - \frac{1}{2}\right]} \qquad (2.74)$$

A scaled sandbox model was built to verify particular field data and used to validate the theoretical approach. There were two important conclusions from this work: (a) a completely pumped-off well produces at higher rates than a partially pumped well, and higher flow rates may be obtained in completely pumped-off wells if the rates were reached by small increases rather than through sudden well withdrawal, and (b) as shown in Fig. **2.4,** the time derivative of the cumulative production indicates flow rates increasing to a maximum value in the early seconds of pumping (out of **Eq. 2.73** validity range), probably due to the potential gradient development in the vicinity of the well.

In recent years, there has been interest in evaluating depleted fields for EOR projects. Many of these fields produce under a pure gravity drainage mechanism and available methods of well test interpretation are not appropriate. *Ramey et al.* (1989)

was the first paper in many years to consider this sort of problem. Starting from a material balance on an infinitesimal radial flow element, the *Dupuit-Forchheimer* Partial Differential Equation was obtained:

$$\frac{\partial^2 p^2}{\partial r^2} + \frac{1}{r}\frac{\partial p^2}{\partial r} = \left(\frac{\phi\mu(p^{-1})}{0.000264k}\right)\frac{\partial p^2}{\partial t^2} \qquad (2.75)$$

where p is the pressure at the bottom of the formation. In the formulation, both the system compressibility and vertical velocity variations along the formation thickness were neglected. By inspection, Eq. 2.75 resembles the ideal gas equation of *Aronofsky* and *Jenkins* (1953). Since the simplifying assumptions are more appropriate at late times, the approximate solution for Eq. 2.75 (also shown in Ch. 1 as Eq. 1.3) was presented:

$$p_o^2 - p_w^2 = 325.2\,\frac{qB\mu}{k(h/p)}\left\{\log\left(\frac{0.000264kt}{\phi\mu\,(p_o^{-1})r_w^2}\right) + 0.351 + \frac{s}{1.151}\right\} \qquad (2.76)$$

Because vertical flow in the formulation was neglected, h/p could be considered constant and equal to the liquid gradient for incompressible flow. The *van Everdingen* (1953) skin parameter s was included in the inner boundary condition. From **Eq.** 2.76, a p^2 versus time semilog graph should produce a straight line, with a slope m that may be used to obtain the permeability - see Ch. 7.1. The ***Ramey et al.*** (1989) solution represented an improvement with respect to the *Theis* (1935) approach in that variation in height and the skin effect were considered. Also highlighted in the *Ramey et al.* paper is a discussion of the role of compressible effects in gravity transient flow behavior. Also, the reversibility of the buildup pressure behavior was questioned because a different physical process occurred during buildup, compared to drawdown. Those subjects are further discussed in Chapter 7.

Equations of the type of Eq. 2.75 were solved numerically in a broader context including wellbore storage effects and a skin by *Fligelman* (1980) and is discussed in Ch. 7 and in App. C.2.

2.6 Numerical Solutions

With the development of large, fast computing machines, numerical methods became a powerful source of solutions for non-linear problems, avoiding simplifications that were used in approximate analytical solutions with relaxed constraints. Numerical solutions have been an important tool to verify analytical methods when necessary, and to test correlations in general.

In the groundwater literature, the main references on numerical methods dedicated to the study of unconfined flow started in the 60's. Cooley and *Donohue* **(1969)** developed a numerical simulator to solve a finite-difference equation system for unsteady flow in a radial flow problem using two-phase flow in the desaturating region based on classical methods employed in the petroleum industry. This work was advanced by *Cooley* **(1971)** and presents an axial model converted into a cross-sectional model geometrically divided into cylindrical blocks in the radial direction. In the vertical direction, constant thickness was allocated to each row. The potentials were the unknowns in each equation, and the flow was divided into radial (horizontal) and vertical directions ruled by the continuity equation coupled with ***Darcys*** *Law*. Multiphase air-liquid flow was governed by capillary pressure. The posed problem did not establish a boundary condition for the free surface. Instead, the model had a fixed grid and calculated the potentials at every block, even those located in the desaturated region. The free surface position could be obtained indirectly by interpolation by the relationship of h (head) and z (vertical coordinate of the node points). The model permitted the existence of two different overlaying beds of sediments with different properties. Unfortunately, the inner boundary condition did not consider wellbore storage, and the wellbore liquid level was obtained by an iterative process. LSOR was the most general method used to solve the non-linear system, generating tridiagonal matrixes, and the time interpolation factor used was 0.5. The model was verified using the *Boulton* approach applied to synthetic data of two observation locations far from the pumping well. There were no verification runs for the pumping

well itself.

A similar method was described in a recent work by *Narusimhan* and *Zhu* (in press) who used the *Agarwal et al.* (1970) definition of wellbore storage constant in the inner boundary condition and verified their finite difference model with a series of analytical solutions and numerical experiments. A better verification of the same model applied to radial flow into a gravity drainage well at steady conditions with respect to the inner boundary seepage face was done by *Shamsai* and ***Narasimhan*** (1991), by comparing results with the *Hall* (1955) experiments.

Szabo and *McCaig* (1968) created a general finite difference model to solve the transient gravity flow problem which considered single-phase fluid and a moving boundary free surface whose grid blocks presented adjustable triangular shapes between consecutive time steps. An analogue device was used to compare results with the numerical solutions for a bidimensional linear flow. ***Szabo*** and *McCaig* considerated a constant head inner boundary condition.

Finite element methods have been widely used to simulate steady or unsteady flow conditions such as *Neuman* (1975-b), *Neuman* and *Witherspoon* (1970-a, 1970-b, 1971). In the latter, a general transient gravity drainage model using a variational principle considered wellbore storage and had a Crank-Nicolson time interpolation method. The nodal distribution was variable to adjust to the free surface at the end of each time step. No wellbore solution or verification run was provided in the paper.

Two phase, one-dimensional flow was studied by *Green et al.* (1970) and ***Hornberger*** and *Remson* (1970) who developed finite difference models using relative permeability and capillary pressure relationships with liquid saturations to analyze moisture movement in the porous medium. The results in the *Green et al.* paper were compared with experimental measurements of the local saturations using neutron log devices. The importance of hysteresis caused by residual air saturation was highlighted and caused concerns about reversibility of formation properties in the buildup

analysis.

Special procedures in simulation are important to enhance the capability of numerical solutions. As an example, logarithmic and geometric grid spacing have been used in numerical simulation of radial flow into a centered well of accuracy and stability. **A** handy algorithm to create an adjustable log radial spacing by *Tera'n* and *la Garza* (1988) allows one to specify the ratio between the first and last cylindrical block sizes keeping truncation error in the same magnitude all over the grid. An advantage of this algorithm is to provide control of the inner radial block storage capacity reducing the dependence of the number of blocks in the radial direction, and also to provide different radial node distributions as desired with minor consequences on the computational efforts.

Further techniques of numerical simulation in petroleum engineering are presented in many references, but most of the procedures in the development of the present dissertation are summarized in the classical books by *Peaceman* (1977), *Aziz* and *Setari* (1979) and *Thomas* (1982).

Chapter 3

Mathernatical Model

In the following, a complete finite difference formulation of a well test in a gravity drainage unconfined reservoir is presented. The groundwater literature presents several attempts to develop analytical solutions to this problem, and all attempts produced equations that are applicable under limitations imposed by restrictive assumptions. One common constraint requires the water table gradient and/or the water table fall to be small. Therefore, high flow-rates should be avoided in pumping test analysis due to the resulting steep gradient around the wellbore.

3.1 Basic Assumptions

The present numerical model consists of a discretization in time and space of a cylindrical reservoir producing at constant flow rate under a gravity drainage drive from a centered, open hole wellbore. The model formulates bi-dimensional flow and considers the height variation of the liquid column in the reservoir as a consequence of the free surface position change. Other important effects also considered in this model are wellbore storage, skin effect, and the variation of the direction of the flow

at each position (r, z) in an anisotropic medium.

A single-phase flow model was developed using an adaptive grid based on a *stream-layer* concept described in the following. The following considerations for an unconfined aquifer flow will be assumed until otherwise modified:

- horizontal reservoir of finite, constant thickness
- anisotropy (k_h, k_v)
- Darcys Law
- conservation of mass and energy
- compressible system containing a single liquid phase with constant properties
- uniform undisturbed free-surface as initial condition
- constant outer boundary pressure
- finite wellbore radius

3.2 Partial Differential Equations and Boundary Values

In a two-dimensional gravity flow system, several distinct regions with appropriate characteristics of flow may be defined: a saturated region where the porous space is completely filled by the liquid; a free liquid surface where the liquid table is in contact with gas at atmospheric pressure; a desaturated region left behind the free surface on drainage during production; the finite radius wellbore inner boundary;

an impermeable lower boundary layer; a constant potential outer boundary which is far enough from the producing well to assure an infinite reservoir behavior. Also, a capillary fringe above the free surface is considered in a separate chapter. For each one of these regions, a mathematical representation of the physical conditions are posed in the following.

- Saturated Region:

  The diffusivity equation is applied to a compressible system completly saturated with a single liquid. From the combination of mass conservation and Darcys Law principles:

$$\nabla \cdot \left[\frac{k}{\mu}\right] \nabla \Phi = \phi c_t \frac{\partial \Phi}{\partial t} \tag{3.2.1}$$

  where the potential Φ is:

$$\Phi = p + \left(\frac{\rho g}{g_c}\right) z \tag{3.2.2}$$

- Free surface Boundary:

  The potential at the free surface is proportional to position. This is equivalent to atmospheric pressure everywhere on the free surface:

$$\Phi (r, H) = \left(\rho \tfrac{g}{g_c}\right) H \tag{3.2.3}$$

  If the capillary fringe is to be considered, the following equation is valid:

$$\Phi (r, H_c) = \Phi (r, H) = \left(\rho \tfrac{g}{g_c}\right) H \tag{3.2.4}$$

- Inner Boundary:

  A constant flow rate inner boundary condition considering wellbore storage effects is obtained from a material balance at the well by the following equation:

$$qB_{wb} = -\pi r_w^2 \frac{\partial H_w}{\partial t} + \frac{2\pi}{\mu} \int_0^{H_s} k \frac{\partial \Phi}{\partial r}\bigg|_{r=r_w} dz \tag{3.2.5}$$

A complementary condition at the wellbore sandface must to be defined. The potential at the sandface is specified by the observation of the existence of a seepage surface, characterizing the discontinuity of the positions of the free surface and the wellbore liquid level. At the inner boundary r_{w+} location, it is assumed that the potential is constant and equal to the potential at r_{w-}, when $z_w \leq H_w$. On the seepage surface ($H_s \geq z_w > H_w$), the potential is proportional to the vertical coordinate, since the point is on a stream-flow line at atmospheric pressure. Hence:

$$H_s \geq z_w > H_w \quad \Rightarrow \quad \Phi_w = \left(\rho \frac{g}{g_c}\right) z_w \qquad \textbf{(3.2.6)}$$

$$z_w \leq H_w \quad \Rightarrow \quad \Phi_w = \left(\rho \frac{g}{g_c}\right) H_w \qquad \textbf{(3.2.7)}$$

A detailed numerical treatment of the inner boundary condition is presented in Section 4.8.

- Infinite Reservoir Behavior:

  Infinitely large reservoir behavior is obtained by assuming a large external radius. Therefore, a constant pressure outer boundary condition is used:

$$\Phi = \Phi_o = \left(\rho \frac{g}{g_c}\right) H_o \quad \Rightarrow \quad r \to \infty \qquad (3.2.8)$$

- Lower Boundary:

  A no-flow lower boundary condition is used:

$$\frac{\partial \Phi}{\partial z} = 0 \quad \Rightarrow \quad z = o \qquad \textbf{(3.2.9)}$$

or

$$k_v = 0 \quad \Rightarrow \quad z = o \qquad \textbf{(3.2.10)}$$

According to *Muskat* **(1936)** and several other authors, analytical solution of the system of partial differential equations in this boundary problem is of *insurmountable difficulty.* As seen in Ch. **2,** not one of the analytical solutions surveyed was obtained without restrictive assumptions, and none appeared to represent pumping well

pressure behavior. The numerical solution developed in the next chapter, although possessing the well known limitations of a finite difference method, is intended to present a tool to solve the gravity drainage well problem completely.

3.3 Dimensionless Parameters

Before modeling the numerical problem, a set of dimensionless constants and variables is required. The relationships presented use Darcy units for the reservoir parameters.

(a) Dimensionless length or thickness:

$$z_D = \frac{z}{r_w}, \qquad H_D = \frac{H}{r_w}, \qquad H_{w_D} = \frac{H_w}{r_w}, \qquad H_{o_D} = \frac{H_o}{r_w}$$

$$r_D = \text{—}, \qquad r_{e_D} = \text{—} \tag{3.3.11}$$

(b) Dimensionless pressure and potential:

$$p_D = \frac{p}{\rho \frac{g}{g_c} H_o} \tag{3.3.12}$$

$$\Phi_D = W = \frac{\Phi}{\rho \frac{g}{g_c} H_o} \tag{3.3.13}$$

(c) Dimensionless static liquid gradient:

$$\gamma_o = \frac{1}{H_{o_D}} \tag{3.3.14}$$

(d) Dimensionless production rate:

$$q_D = \frac{q\,\mu}{2\pi r_w\, k_h\, \rho \frac{g}{g_c} H_o} \tag{3.3.15}$$

(e) Dimensionless time:

$$t_D = \frac{k_h\, \rho \frac{g}{g_c} H_o}{\phi\, \mu\, r_w^2}\, t \tag{3.3.16}$$

(f) Dimensionless liquid and total compressibilities:

$$c_{L_D} = \rho \frac{g}{g_c} H_o\, c_L$$

$$c_{t_D} = \rho \frac{g}{g_c} H_o\, c_t \tag{3.3.17}$$

In the next chapter, a finite difference model is considered in detail.

Chapter 4

Finite Difference Model

The partial differential equation that represents radial liquid flow in the reservoir may be generated from a material balance in an infinitesimal element of porous medium, based on the conservation of mass and ***Darcys*** flow law. The complexities of the boundary conditions in the free surface gravity flow problem drive the present solution to a numerical approach, making it possible to linearize the boundary equations. The discretized form of these equations can be formulated from the same material balance criteria using a finite-difference formulation described in this chapter.

Figure **4.1** represents a grid configuration of the problem, depicting a half-cross-section of a cylindrical reservoir with a free-surface developed from the original position H_o. The horizontal dimensions of the grid blocks can be scaled to provide accuracy around the well bore, where the most important flow effects occur. The radial grid spacing used the *Multimodal* method [*Terán* and ***de*** *la* ***Garza,*** 19881, in which logarithmic spacing is a particular case.

In order to simulate the variable free surface position, an adaptive vertical griding was conceived to group a set of streamlines, and referred to **as** the *Stream* ***Layer***

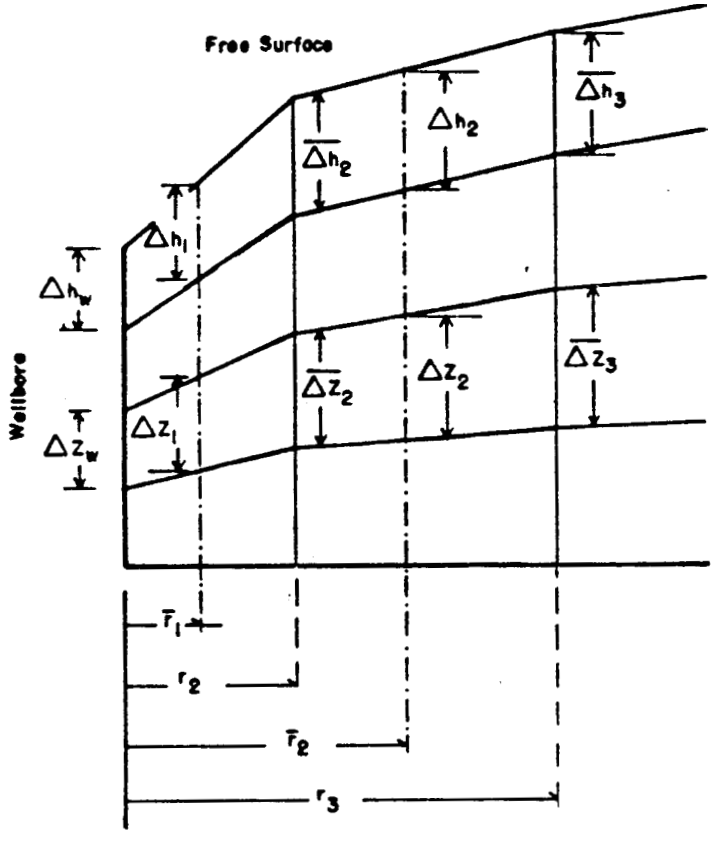

Figure **4.1:** The Stream Layer Modelgrid

Model (SLM) in the following. During a discrete time step, each block but the one containing the free surface will keep its geometrical dimensions unchanged while the liquid flows through the block boundaries in the vertical and axial directions. In this cross sectional model, no angular flow normal to the cross section is allowed, and the axial directions are not necessarily horizontal, as can be seen in Fig. 4.1. The dimensions normal to the axial flow are corrected by the average slopes **of** the block boundaries, according to Fig. **4.2.**

In a separate section of this chapter, the capillary fringe is added to the model

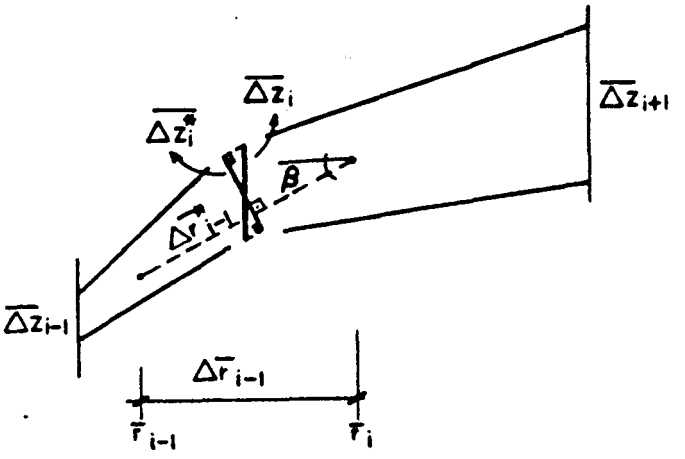

Figure 4.2: Geometric corrections based in the slope of the flow axix.

by incorporating an additional layer with constant height on the top of the free surface layer, or phreatic layer. Capillary flow is important for small scale sand-box experiments where capillarity has a sensitive role in the results.

In the present model, the free surface layer is the only one that changes position during a production or buildup time step period, because the free surface layer contains the movable boundary. In the case of neglecting the capillary region above the free surface, the free surface downward movement leaves behind a liquid saturation in the desaturating zone. In the present model, no later flow from that region is allowed, and the liquid moves entirely within a specific period. The liquid saturation behind the free surface boundary is considered residual. Based on groundwater studies - see *Bouwer and Rice* (1978) and *Neurnan* (1979), the air entry effects in the desaturing region (two-phase flow) are neglected.

The technique used in calculations was the iterative solution of the block potentials, concentrating the non-linearities in the free surface and the wellbore potentials where the boundary values are pre-estimated based on the previous time step. The

X	X	X	X	X	0	0	0	0	0	0	0	0	0	0	0	0	0	0	0
X	X	X	X	0	X	0	0	0	0	0	0	0	0	0	0	0	0	0	0
X	X	X	X	0	0	X	0	0	0	0	0	0	0	0	0	0	0	0	0
X	X	X	X	0	0	0	X	0	0	0	0	0	0	0	0	0	0	0	0
X	0	0	0	X	X	0	0	X	0	0	0	0	0	0	0	0	0	0	0
0	X	0	0	X	X	X	0	0	X	0	0	0	0	0	0	0	0	0	0
0	0	X	0	0	X	X	X	0	0	X	0	0	0	0	0	0	0	0	0
0	0	0	X	0	0	X	X	0	0	0	X	0	0	0	0	0	0	0	0
0	0	0	0	X	0	0	0	X	X	0	0	X	0	0	0	0	0	0	0
0	0	0	0	0	X	0	0	X	X	X	0	0	X	0	0	0	0	0	0
0	0	0	0	0	0	X	0	0	X	X	X	0	0	X	0	0	0	0	0
0	0	0	0	0	0	0	X	0	0	X	X	0	0	0	X	0	0	0	0
0	0	0	0	0	0	0	0	X	0	0	0	X	X	0	0	X	0	0	0
0	0	0	0	0	0	0	0	0	X	0	0	X	X	X	0	0	X	0	0
0	0	0	0	0	0	0	0	0	0	X	0	0	X	X	X	0	0	X	0
0	0	0	0	0	0	0	0	0	0	0	X	0	0	X	X	0	0	0	X
0	0	0	0	0	0	0	0	0	0	0	0	X	0	0	0	X	X	0	0
0	0	0	0	0	0	0	0	0	0	0	0	0	X	0	0	X	X	X	0
0	0	0	0	0	0	0	0	0	0	0	0	0	0	X	0	0	X	X	X
0	0	0	0	0	0	0	0	0	0	0	0	0	0	0	X	0	0	X	X

Figure **4.3:** Matrix representation of a **5x4** cross sectional grid

convergence method was the Newton-Raphson procedure which generates a diagonal Jacobian matrix with special characteristics due to the non-zero coefficients corresponding to the inner boundary blocks, as shown in Fig. **4.3.**

A single step solution follows the sequence:

(a) Calculate the inner boundary potential as a first approach

(b) Calculate the equation coefficients

(c) Calculate the Jacobian matrix elements

(d) Solve the matrix for the potentials

(e) Recalculate the inner boundary potential

(f) Check the results for convergence and iterate if necessary

Since the layer containing the free surface is the only one moving during a discrete time period, the block thicknesses are dependent on the free surface position, or dependent on the block potentials. This loop dependency is responsible for the strong non-linearity of the gravity drainage problem.

Skin effect was considered in the model by assuming a cylindrical damaged region around the well with an altered permeability, using *Hawkins* **(1956)** approach:

$$s = \left(\frac{k}{k_d} - 1\right) \ln\left(\frac{r_d}{r_w}\right) \tag{4.1}$$

The finite difference treatment of the equations and the boundary conditions is presented in the sections that follow. **A** detailed description of the computer model is given in the Sec. **4.9.**

4.1 Grid Distribution

The cross-sectional model is composed of a grid of $M \times N$ radial and vertical blocks, numbered from the left to the right, and from the top to the bottom. The uppermost layer corresponding to the position $j = 1$ contains the liquid-free surface. The inner blocks are set at i = 1. Thus, the number of radial blocks is M, not considering the wellbore and the external outer blocks with constant potential.

The radial grid distribution is a special kind of logarithmic spacing using the *multimodal* method of discretization adopting the the block-centered scheme. In this method, the problems of stability are reduced by controlling the radial size of the

blocks by fixing a ratio R between the inner and the outer blocks. Hence, the critical conditions of potential changes in the inner blocks, those containing the sandface, are decreased, reducing the stability problems that commonly happen in such radial flow models at late times. The usual logarithmic scale is a particular case of the *multimodal* method.

In the cross-sectional view, the blocks embrace sets of streamlines with variable slope depending on the block position and the time. Yet, the vertical flow between consecutive layers allows some flow lines to move from a layer set to an adjacent layer set during a period of time Δt. The stream layer is a geometric location containing the streamlines moving through it. The only moving boundary within that time period will exactly be the top of the first (uppermost) layer which contains the free surface, while all other layers have the same uniform thickness over all time steps.

The time discretization uses a variable parameter θ between 0 and 1, assigning a variable degree of implicitness to the model. The nature of the gravity problem requires analysis of ideal θ values, which is done in the model sensitivity analysis.

The coordinates are named in the following way, according to the figures presented in this chapter:

r_i = radial distance of the inner limit of the block i,j to the wellbore axis

$\bar{r}_i$ = radial distance of the block node to the wellbore axis [1]

$z_{i,j}$ = vertical coordinate of the lower block i,j lower boundary at $\bar{r}_i$, taken from the base of the formation

Δz_i = vertically uniform thickness of the block i,j at position $\bar{r}_i$

$\overline{\Delta z}_i$ = thickness of the block i,j at the position r_i

[1] In the *MULTIMODAL* method, both r_i and $\bar{r}_i$ are calculated implicitly - see [*Terán* and *de la Garza*, 1988]

H_i = height of the free surface at the position $\overline{r}_i$

$Ah;$ = equivalent to Δz_i, referred to the free surface layer blocks

$\overline{Ah};$ = equivalent to $\overline{\Delta z}_i$, referred to the position r_i

H_o = initial position of the free surface at rest, from the impermeable base

H_w = liquid level in the well

H_s = liquid level in the sandface

z_{w_j} = lower inner block boundary position j at the sandface

Δz_{w_j} = inner block boundary thickness at the sandface

$Ah,$ = equivalent to Δz_{w_j} referred to the free surface layer inner block

Figure 4.2 shows a special representation of a grid block (i, j) at a time **t,** containing a set of streamlines and an adjacent block. Due to increased slopes of the streamlines around the well, the geometric projections of the lengths and heights are based on angles calculated on the following basis:

$$\beta_{i,j} = tg^{-1}\left(\frac{z_{i,j} + \frac{1}{2}\Delta z_{i,j} - \left(z_{i-1,j} + \frac{1}{2}\Delta z_{i-1,j}\right)}{\overline{r}_i - \overline{r}_{i-1}}\right), \qquad (4.1.1)$$

and the average slope of an individual block:

$$\overline{\beta}_{i,j} = tg^{-1}\left(\frac{z_{i+1,j} + \frac{1}{2}\Delta z_{i+1,j} - \left(z_{i-1,j} + \frac{1}{2}\Delta z_{i-1,j}\right)}{\overline{r}_{i+1} - \overline{r}_{i-1}}\right). \qquad (4.1.2)$$

The flow domain is divided into two main directions of flow, namely the vertical (subscript v), and the axial (quasi-radial) (subscript x). The mathematical description of such a flow can be formulated through the general finite difference equation for a single liquid phase flowing in a low compressibility system:

$$\Delta_x (T_x \Delta_x \Phi) + \Delta_v (T_v \Delta_v \Phi) = \frac{1}{\Delta t} \Delta_t (\phi V) \qquad \textbf{(4.1.3)}$$

In gravity drainage flow, the direction of the streamlines change continuously, and for that reason, the true transmissivity considers the geometry and also the permeability tensor. In this work where anisotropy is considered, the pseudo-axial permeability (in the streamline direction) is taken as an elliptic function of the horizontal (radial) and vertical permeabilities, according to the rule:

$$k_{x_{i,j}} = \frac{k_h \, k_v}{k_h \, sin\beta_{i,j} + k_v \, cos\beta_{i,j}} \qquad \textbf{(4.1.4)}$$

Each of the boundary conditions will define individual treatment for the transmissivity terms, as well as the storage variation. In the next sections of this chapter, Eq. **4.1.3** will be expanded and applied to the saturated region and the boundaries.

4.2 Balance of Unknowns and Equations

Number of unknowns:

Reservoir block potentials	$M \times N$
Free surface positions	**M**
Position of the fluid level in wellbore	**1**
Total unknowns:	$M(N+1)+1$

Number of equations:

Material balance for the blocks	$M \times N$
Free surface position	M
Wellbore material balance	1
Total equations:	$M(N+1)+1$

4.3 Saturated Region

Equation 4.1.3 can be writen for the saturated region and the inner and outer boundaries.

4.3.1 Discretization of the Saturated Region Equations

Discretization of a block i,j, for $M > i > 1$, and N $> j >$ 2:

$$\Delta_x (T_x \Delta_x \Phi) = T_{x_{i+1,j}} (\Phi_{i+1,j} - \Phi_{i,j}) - T_{x_{i,j}} (\Phi_{i,j} - \Phi_{i-1,j}) , \qquad (4.3.1)$$

$$\Delta_v (T_v \Delta_v \Phi) = T_{v_{i,j-1}} (\Phi_{i,j-1} - \Phi_{i,j}) - T_{v_{i,j}} (\Phi_{i,j} - \Phi_{i,j+1}) , \qquad (4.3.2)$$

and:

$$\frac{1}{\Delta t} \Delta_t (\phi V) = \frac{A_{v_i} \Delta z_i \phi c_t}{\Delta t \cos \overline{\beta}_{i,j}} \Delta_t \Phi_{i,j} \qquad (4.3.3)$$

where the typical transmissivity terms are:

$$T_{x_{i,j}} = \frac{2\pi}{\mu} \frac{k_{x_{i,j}}}{\ln\left(\frac{\bar{r}_i}{\bar{r}_{i-1}}\right)} \overline{\Delta z}_i \cos\beta_{i,j} \quad \textbf{(4.3.4)}$$

$$T_{v_{i,j}} = \frac{A_{v_i}}{\mu} \frac{k_{v_{i,j}}}{\Delta z_i} \quad \textbf{(4.3.5)}$$

The time interpolation used a parameter θ to weight the old unknowns and the unknowns within a time step. Thus, using the dimensionless parameters defined in the Ch. **3.3,** re-organizing, and collecting terms, the resulting equation may be summarized in the following way:

$$A_{i,j}\ W_{i,j} + B_{i,j}\ W_{i,j-1} + C_{i,j}\ W_{i,j+1} + D_{i,j}\ W_{i-1,j} + E_{i,j}\ W_{i+1,j} = F_{i,j} \quad (4.3.6)$$

where the coefficients of the unknown dimensionless potentials and the independent term are:

$$A_{i,j} = -\theta \left[\overline{\Delta z}_{D_{i+1}} + f_{x_{i,j}} f_{r_i} \overline{\Delta z}_{D_i} + \frac{2k_v}{k_{x_{i+1,j}} cos\beta_{i+1,j}} \frac{A_{1_i}}{\Delta z_{D_i}} + \frac{k_h}{k_{x_{i+1,j}} cos\beta_{i+1,j}} \frac{A_{1_i} \Delta z_{D_i}}{\theta\ cos\overline{\beta}_{i,j}\ \Delta t_D} c_{t_D} \right] \quad \textbf{(4.3.7)}$$

$$B_{i,j} = \frac{\theta\ k_v\ A_{1_i}}{k_{x_{i+1,j}}\ cos\beta_{i+1,j}\ \Delta z_{D_i}} \quad (4.3.8)$$

$$C_{i,j} = \frac{\theta\ k_v\ A_{1_i}}{k_{x_{i+1,j}}\ cos\beta_{i+1,j}\ \Delta z_{D_i}} \quad \textbf{(4.3.9)}$$

$$D_{i,j} = \theta\ f_{x_{i,j}}\ f_{r_i}\ \overline{\Delta z}_i \quad \textbf{(4.3.10)}$$

$$E_{i,j} = \theta\ \overline{\Delta z}_{i+1} \quad \textbf{(4.3.11)}$$

$$F_{i,j} = -\frac{k_h}{k_{x_{i+1,j}}\, cos\beta_{i+1,j}} \frac{A_{1_i}\, \Delta z_{D_i}}{cos\overline{\beta}_{i,j} \Delta t_D} c_{t_D}\, W_{i,j}^k - (1-\theta) \times$$

$$\left\{\overline{\Delta z}_{D_i+1} \left[W_{i+1,j}^k - W_{i,j}^k\right] - f_{x_{i,j}}\, f_{r_i} \overline{\Delta z}_{D_i} \left[W_{i,j}^k - W_{i-1,j}^k\right]\right.$$

$$\left. + \frac{k_v\, A_{1_i}^*}{k_{x_{i+1,j}}\, cos\beta_{i+1,j}\, \Delta z_{D_i}} \left[W_{i,j-1}^k - 2W_{i,j}^k + W_{i,j+1}^k\right]\right\} \quad (4.3.12)$$

In these coefficients, the superscript k refers to the beginning of the present time step values. Other parameters are:

$$A_{1_i} = \frac{A_{v_i} \ln\left(\frac{\overline{r}_{i+1}}{\overline{r}_i}\right)}{2\pi\, r_w^2} \quad \textbf{(4.3.13)}$$

$$f_{x_{i,j}} = \frac{k_{x_{i,j}}\, cos\beta_{i,j}}{k_{x_{i+1,j}}\, cos\beta_{i+1,j}} \quad \textbf{(4.3.14)}$$

$$f_{r_i} = \frac{\ln\left(\frac{\overline{r}_{i+1}}{\overline{r}_i}\right)}{\ln\left(\frac{\overline{r}_i}{\overline{r}_{i-1}}\right)} \quad \textbf{(4.3.15)}$$

The values of $\overline{\Delta z}_D$ are estimated by interpolation between nodes.

The Jacobian matrix elements for the block i, j were obtained using a Newton-Raphson procedure.
The residue Ψ is:

$$\Psi_{i,j} = A_{i,j}\, W_{i,j} + B_{i,j}\, W_{i,j-1} + C_{i,j}\, W_{i,j+1} + D_{i,j}\, W_{i-1,j} + E_{i,j}\, W_{i+1,j} - F_{i,j} \quad (4.3.16)$$

Differentiating Eq. 4.3.16 with respect to each variable W :

$$DA_{i,j} = \frac{\partial \Psi_{i,j}}{\partial W_{i,j}} = A_{i,j} + \frac{\partial A_{i,j}}{\partial W_{i,j}} W_{i,j} + \frac{\partial B_{i,j}}{\partial W_{i,j}} W_{i,j-1} + \frac{\partial C_{i,j}}{\partial W_{i,j}} W_{i,j+1}$$
$$\frac{\partial D_{i,j}}{\partial W_{i,j}} W_{i-1,j} + \frac{\partial E_{i,j}}{\partial W_{i,j}} W_{i+1,j} - \frac{\partial F_{i,j}}{\partial W_{i,j}} \quad (4.3.17)$$

Since all the partial differentials are zero:

$$DA_{i,j} = A_{i,j} \quad \textbf{(4.3.18)}$$

Similarly, other Jacobian coefficients are:

$$DB_{i,j} = \frac{\partial \Psi_{i,j}}{\partial W_{i,j-1}} = B_{i,j} \quad \textbf{(4.3.19)}$$

$$DC_{i,j} = \frac{\partial \Psi_{i,j}}{\partial W_{i,j+1}} = C_{i,j} \quad \textbf{(4.3.20)}$$

$$DD_{i,j} = \frac{\partial \Psi_{i,j}}{\partial W_{i-1,j}} = D_{i,j} \quad \textbf{(4.3.21)}$$

$$DE_{i,j} = \frac{\partial \Psi_{i,j}}{\partial W_{i+1,j}} = E_{i,j} \quad \textbf{(4.3.22)}$$

4.3.2 Saturated Region Inner Boundary Equations

The blocks containing the sandface require a special treatment because of their location. The transmissivity connected to the sandface can be estimated by geometric extrapolation of thicknesses and slopes of the layers. The inner boundary potentials are determined by the wellbore condition, as shown in the Section **4.8.** Figure **4.1** presents a schematic of the inner blocks around the wellbore and the extrapolated

thicknesses. The average thickness of a block flowing to the wellbore is taken half-way between the the node and the inner face. If small radial spacing is used near the well, the geometric extrapolation can be relaxed, and a constant thickness can be adopted for the whole block and its inner boundary. To be general, the equations presented below used extrapolated thicknesses.

We now consider discretization of block $1,j$ for $N > j > 2$. Following the same procedures as before and considering the proper symbology for the inner boundary parameters, the resulting equation is:

$$A_{1,j}\ W_{1,j} + B_{1,j}\ W_{1,j-1} + C_{1,j}\ W_{1,j+1} + + E_{1,j}\ W_{2,j} = F_{1,j} \qquad (4.3.23)$$

where the coefficients of the unknown dimensionless potentials and the independent term are:

$$A_{1,j} = -\theta \left[\overline{\Delta z}_{D_2} + f_{x_{1,j}} f_{r_1} \overline{\Delta z}_{D_1} + \frac{2k_v}{k_{x_{2,j}} cos\beta_{2,j}} \frac{A_{1_1}}{\Delta z_{D_1}} + \frac{k_h}{k_{x_{2,j}} cos\beta_{2,j}} \frac{A_{1_1} \Delta z_{D_1}}{\theta\ cos\overline{\beta}_{1,j} \Delta t_D} c_{t_D} \right] \qquad (4.3.24)$$

$$B_{1,j} = \frac{\theta\ k_v\ A_{1_1}}{k_{x_{2,j}}\ cos\beta_{2,j}\ \Delta z_{D_1}} \qquad (4.3.25)$$

$$C_{1,j} = \frac{\theta\ k_v\ A_{1_1}}{k_{x_{2,j}}\ cos\beta_{2,j}\ \Delta z_{D_1}} \qquad (4.3.26)$$

$$D_{1,j} = 0 \qquad (4.3.27)$$

$$E_{1,j} = \theta\ \overline{\Delta z}_2 \qquad (4.3.28)$$

$$F_{1,j} = -f_{x_{1,j}} f_{r_1} \overline{\Delta z}_{D_1} \left\{ \theta W_{w_j} - (1-\theta) \left[W_{1,j}^k - W_{w_j}^k \right] \right\}$$

$$- \frac{k_h}{k_{x_{2,j}} cos\beta_{2,j}} \frac{A_{1_1} \Delta z_{D_1}}{\Delta t_D cos\overline{\beta}_{1,j}} c_{t_D} W_{1,j}^k - (1-\theta) \left\{ \overline{\Delta z}_{D_2} \left(W_{2,j}^k - W_{1,j}^k \right) \right.$$

$$\left. + \frac{k_v}{k_{x_{2,j}} cos\beta_{2,j}} \frac{A_{1_1}}{\Delta z_{D_1}} \left[-2W_{1,j}^k + W_{1,j-1}^k + W_{1,j+1}^k \right] \right\}. \quad \textbf{(4.3.29)}$$

In these coefficients, the superscript k refers to the previous time step value. Other parameters are:

$$A_{1_1} = \frac{A_{v_1} \ln\left(\frac{\overline{r}_2}{\overline{r}_1}\right)}{2\pi r_w^2} \quad \textbf{(4.3.30)}$$

$$f_{x_{1,j}} = \frac{k_{x_{1,j}} cos\beta_{1,j}}{k_{x_{2,j}} cos\beta_{2,j}} \quad \textbf{(4.3.31)}$$

$$f_{r_1} = \frac{\ln\left(\frac{\overline{r}_2}{\overline{r}_1}\right)}{\ln\left(\frac{\overline{r}_1}{\overline{r}_w}\right)} \quad \textbf{(4.3.32)}$$

Determine Jacobian matrix elements for the block $1,j$ using a Newton-Raphson procedure. The residue Ψ is:

$$\Psi_{1,j} = A_{1,j} W_{1,j} + B_{1,j} W_{1,j-1} + C_{1,j} W_{1,j+1} + E_{1,j} W_{2,j} - F_{1,j} \quad (4.3.33)$$

Differentiating **Eq. 4.3.33** with respect to each variable $W_{i,j}$:

$$DA_{1,j} = \frac{\partial \Psi_{1,j}}{\partial W_{1,j}} = A_{1,j} + \frac{\partial A_{1,j}}{\partial W_{1,j}} W_{1,j} + \frac{\partial B_{1,j}}{\partial W_{1,j}} W_{1,j-1} + \frac{\partial C_{1,j}}{\partial W_{1,j}} W_{1,j+1} + \frac{\partial E_{1,j}}{\partial W_{1,j}} W_{2,j} - \frac{\partial F_{1,j}}{\partial W_{1,j}} \quad (4.3.34)$$

Except the last one, all the partial differentials in **Eq. 4.3.34** are zero. Thus:

$$DA_{i,j} = A_{i,j} - \frac{\partial F_{1,j}}{\partial W_{1,j}} = A_{i,j} + \theta f_{x_{1,j}} f_{r_1} \overline{\Delta z}_{D_1} \frac{\partial W_{w_j}}{\partial W_{1,j}} \quad (4.3.35)$$

Similarly, the other Jacobian coefficients are:

$$DB_{1,j} = \frac{\partial \Psi_{1,j}}{\partial W_{1,j-1}} = B_{1,j} + \theta f_{x_{1,j}} f_{r_1} \overline{\Delta z}_{D_1} \frac{\partial W_{w_j}}{\partial W_{1,j-1}} \quad (4.3.36)$$

$$DC_{1,j} = \frac{\partial \Psi_{1,j}}{\partial W_{1,j+1}} = C_{1,j} + \theta f_{x_{1,j}} f_{r_1} \overline{\Delta z}_{D_1} \frac{\partial W_{w_j}}{\partial W_{1,j+1}} \quad (4.3.37)$$

$$DD_{1,j} = 0 \quad (4.3.38)$$

$$DE_{1,j} = \frac{\partial \Psi_{1,j}}{\partial W_{2,j}} = E_{1,j} \quad (4.3.39)$$

The partial differentiations of the inner boundary potentials (see App. A.1), calculated individually, may be substituted above.

4.3.3 Saturated Region Outer Boundary Blocks

The outer boundary condition is a constant potential at the external radius. The index m is used to refer to the M^{th} block, and $m+1$ is a dummy external block with constant potential and geometry.

Now we consider discretization of the block m,j, for $N > j > 2$. Following the same procedures and considering the proper symbology for the outer boundary parameters, the resulting equation is:

$$A_{m,j}\ W_{m,j} + B_{m,j}\ W_{m,j-1} + C_{m,j}\ W_{m,j+1} + + D_{m,j}\ W_{m-1,j} = F_{m,j} \quad (4.3.40)$$

where the coefficients of the unknown dimensionless potentials and the independent term are:

$$A_{m,j} = -\theta \left[\overline{\Delta z}_{D_{m+1}} + f_{x_{m,j}}\, f_{r_m}\, \overline{\Delta z}_{D_m} + \frac{2k_v}{k_h} \frac{A_{1_m}}{\Delta z_{D_m}} + \frac{A_{1_m}\, \Delta z_{D_m}}{\theta\ cos\overline{\beta}_{m,j}\, \Delta t_D}\, c_{t_D} \right] \quad \textbf{(4.3.41)}$$

$$B_{m,j} = \frac{\theta\ k_v\ A_{1_m}}{k_h\ \Delta z_{D_m}} \quad \textbf{(4.3.42)}$$

$$C_{m,j} = \frac{\theta\ k_v\ A_{1_m}}{k_h\ \Delta z_{D_m}} \quad \textbf{(4.3.43)}$$

$$D_{m,j} = \theta\, f_{x_{m,j}}\, f_{r_m}\, \overline{\Delta z}_{D_m} \quad \textbf{(4.3.44)}$$

$$F_{m,j} = -\frac{A_{1_m}\,\Delta z_{D_m}}{\Delta t_D\, cos\overline{\beta}_{m,j}}\, c_{t_D}\, W^k_{m,j} - \overline{\Delta z}_{D_{m+1}}\left[1-(1-\theta)\, W^k_{m,j}\right] - (1-\theta)\left\{-f_{x_{m,j}}\, f_{r_m}\, \overline{\Delta z}_{D_m}\left[W^k_{m,j} - W^k_{m-1,j}\right] + \frac{k_v\, A_{1_m}}{k_h\, \Delta z_{D_m}}\left[W^k_{m,j-1} - 2\, W^k_{m,j} + W^k_{m,j-1}\right]\right\} \quad (4.3.45)$$

At the external boundary, the flux is always normal to the external face, and so, $cos\beta_{m+1,j} = 1$. Thus, other parameters are:

$$A_{1_m} = \frac{A_{v_m}\, \ln\left(\frac{\overline{r}_{m+1}}{\overline{r}_m}\right)}{2\pi\, r_w^2} \quad \textbf{(4.3.46)}$$

$$f_{x_{m,j}} = \frac{k_{x_{m,j}}\, cos\beta_{m,j}}{k_h} \quad \textbf{(4.3.47)}$$

$$f_{r_m} = \frac{\ln\left(\frac{\overline{r}_{m+1}}{\overline{r}_m}\right)}{\ln\left(\frac{\overline{r}_m}{\overline{r}_{m-1}}\right)} \quad \textbf{(4.3.48)}$$

Determine the Jacobian matrix elements for the block m, j using a Newton-Raphson procedure. The residue Ψ is:

$$\Psi_{m,j} = A_{m,j}\, W_{m,j} + B_{m,j}\, W_{m,j-1} + C_{m,j}\, W_{m,j+1} + D_{m,j}\, W_{m-1,j} - F_{m,j} \quad (4.3.49)$$

Differentiating Eq. **4.3.49** with respect to each variable $W_{m,j}$:

$$DA_{m,j} = \frac{\partial \Psi_{m,j}}{\partial W_{m,j}} = A_{m,j} \quad \textbf{(4.3.50)}$$

$$DB_{m,j} = \frac{\partial \Psi_{m,j}}{\partial W_{m,j-1}} = B_{m,j} \quad \textbf{(4.3.51)}$$

$$DC_{m,j} = \frac{\partial \Psi_{m,j}}{\partial W_{m,j+1}} = C_{m,j} \quad \textbf{(4.3.52)}$$

$$DD_{m,j} = \frac{\partial \Psi_{m,j}}{\partial W_{m-1,j+1}} = D_{m,j} \quad \textbf{(4.3.53)}$$

$$DE_{m,j} = 0 \quad \textbf{(4.3.54)}$$

4.4 Free Surface Blocks

The free surface blocks are those containing the free moving boundary on top of them. In the present discretization, the capillary fringe is neglected and the no-flow upper condition is applied. The free surface block thicknesses are the unknowns that cause the non-linearity in the problem and are calculated by an iterative process.

4.4.1 Free Surface Layer Equations

The principle of mass conservation associated with ***Darcys*** law applied to **an** element of reservoir containing the free surface was written in Darcy units according to the conventions adopted in Fig, **4.4,** which shows a representation of a block element containing the free surface. In this study, the directions of flow and the transmissivities are ruled by the streamline slopes, That characteristic of the model enables one to consider the axial transmissivity terms as a function of the the direction of flow normal to the block boundaries, similarly to the saturated region equations.

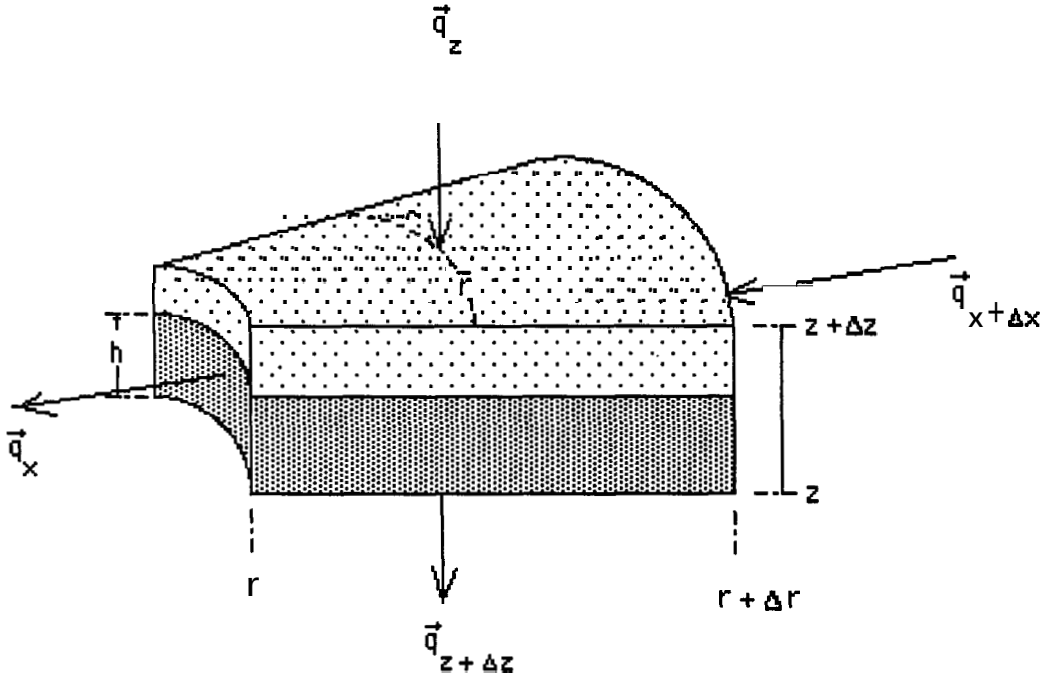

Figure **4.4:** Representation of a block containing the free surface. Convention of flow and coordinate directions.

The condition that the components of velocity normal to the free surface are null means there is no external flow through the free surface, neglecting the unsaturated flow. Taking that observation and the condition given by Eq. **3.2.3,** the expansion of **Eq. 4.1.3** is described in the next sections.

Discretization of a block i, 1, for $M > i > 1$**:**

$$\Delta_x (T_x \Delta_x \Phi) = T_{x_{i+1,1}} (\Phi_{i+1,1} - \Phi_{i,1}) - T_{x_{i,1}} (\Phi_{i,1} - \Phi_{i-1,1}) \quad (4.4.1)$$

$$\Delta_v (T_v \Delta_v \Phi) = - T_{v_{i,1}} (\Phi_{i,1} - \Phi_{i,2}) \quad (4.4.2)$$

$$\frac{1}{\Delta t} \Delta_t (\phi V) = \frac{A_{v_i} \phi}{\Delta t \cos\bar{\beta}_{i,1}} \left[S_g \left(\Delta h_i - \Delta h_i^k \right) + \left(\frac{\Delta h_i + \Delta h_i^k}{2} \right) c_t \Delta_t \Phi \right] \quad (4.4.3)$$

Typical transmissivity terms are:

$$T_{x_{i,1}} = \frac{2\pi}{\mu} \frac{k_{x_{i,1}}}{\ln\left(\frac{\bar{r}_i}{\bar{r}_{i-1}}\right)} \overline{\Delta z_i} \cos\beta_{i,1} \quad \textbf{(4.4.4)}$$

$$T_{v_{i,1}} = \frac{A_{v_i}}{\mu} \frac{2k_v}{\Delta z_i + \Delta h_i} \quad \textbf{(4.4.5)}$$

The usual procedures to develop the discretized equations taking the time relaxation parameter 8 is synthetized by the general equation:

$$A_{i,1}\, W_{i,1} + + C_{i,1}\, W_{i,2} + D_{i,1}\, W_{i-1,1} + E_{i,1}\, W_{i+1,1} = F_{i,1} \quad (4.4.6)$$

where the coefficients of the unknown dimensionless potentials and the independent term are:

$$A_{i,1} = -\theta \left[\overline{\Delta h}_{D_{i+1}} + f_{x_{i,1}} f_{r_i} \overline{\Delta h}_{D_i} + \frac{2k_v}{k_{x_{i+1,1}} \cos\beta_{i+1,1}} \frac{A_{1_i}}{\Delta z_{D_i} + \Delta h_{D_i}} + \frac{k_h A_{1_i}}{k_{x_{i+1,1}} \cos\beta_{i+1,1}} \frac{\Delta h_{D_i} + \Delta z_{D_i}}{2\theta \cos\bar{\beta}_{i,1} \Delta t_D} c_{t_D} \right] \quad \textbf{(4.4.7)}$$

$$B_{i,1} = 0 \quad \textbf{(4.4.8)}$$

$$C_{i,1} = \frac{2\theta\, k_v\, A_{1_i}}{k_{x_{i+1,1}} \cos\beta_{i+1,1} (\Delta z_{D_i} + \Delta h_{D_i})} \quad \textbf{(4.4.9)}$$

$$D_{i,1} = \theta\, f_{x_{i,1}}\, f_{r_i}\, \overline{\Delta h}_{D_i} \quad \textbf{(4.4.10)}$$

$$E_{i,1} = \theta\, \overline{\Delta h}_{D_{i+1}} \quad \textbf{(4.4.11)}$$

$$F_{i,j} = -\frac{k_h}{k_{x_{i+1,1}}\, cos\beta_{i+1,1}} \frac{A_{1_i}}{cos\overline{\beta}_{i,1}\Delta t_D} \left[\left(\Delta h_{D_i} - \Delta h^k_{D_i}\right) S_g - \left(\frac{\Delta h_{D_i} + \Delta h^k_{D_i}}{2}\right) c_{t_D} W^k_{i,1} \right]$$

$$- (1-\theta) \left\{ \overline{\Delta h}^k_{D_{i+1}} \left[W^k_{i+1,1} - W^k_{i,1} \right] - f_{x_{i,1}}\, f_{r_i} \overline{\Delta h}_{D_i} \left[W^k_{i,1} - W^k_{i-1,1} \right] \right.$$

$$\left. + \frac{2\, k_v\, A_{1_i}}{k_{x_{i+1,1}}\, cos\beta_{i+1,1}\, (\Delta z_{D_i} + \Delta h_{D_i})} \left[- W^k_{i,1} + W^k_{i,2} \right] \right\} \qquad (4.4.12)$$

These definitions of A_{1_i}, $f_{x_{i,1}}$, and f_{r_i} are the same as given by Eqs. **4.3.13** through **4.3.15.** Determine the Jacobian matrix elements for the block $i, 1$ using a Newton-Raphson procedure. Let Θ be defined as the residue:

$$\Psi_{i,1} = A_{i,1}\, W_{i,1} + C_{i,1}\, W_{i,2} + D_{i,1}\, W_{i-1,1} + E_{i,1}\, W_{i+1,1} - F_{i,1} \qquad (4.4.13)$$

The Jacobian elements are summarized in the following:

$$DA_{i,1} = \frac{\partial \Psi_{i,1}}{\partial W_{i,2}} = A_{i,1} - \left[\frac{\theta \left(1 - \alpha_{i+1} + \alpha_i f_{x_{i,1}} f_{r_i}\right)}{\overline{\gamma}_i} \right.$$

$$\left. - \frac{C_{i,1}}{(\Delta h_{D_i} + \Delta z_{D_i})\,\overline{\gamma}_i} + \frac{k_h\, A_{1_i}}{k_{x_{i+1,1}}\, cos\beta_{i+1,1}} \frac{c_{t_D}}{2\overline{\gamma}_i \Delta t_D cos\overline{\beta}_{i,1}} \right] W_{i,1}$$

$$- \frac{C_{i,1}}{(\Delta h_{D_i} + \Delta z_{D_i})\,\overline{\gamma}_i} W_{i,2} + \frac{\theta \left(f_{x_{i,1}}\, f_{r_i}\right) \alpha_i}{\overline{\gamma}_i} W_{i-1,1} + \frac{\theta\,(1-\alpha_{i+1})}{\overline{\gamma}_i} W_{i+1,1}$$

$$- \frac{k_h}{k_{x_{i+1,1}}\, cos\beta_{i,1}} \frac{A_{1_i}}{\Delta t_D\, cos\overline{\beta}_{i,1}\, \overline{\gamma}_i} \left[S_g - \frac{c_{t_D}\, W^k_{i,1}}{2} \right] \qquad (4.4.14)$$

$$DB_{i,1} = 0 \qquad \textbf{(4.4.15)}$$

$$DC_{i,1} = \frac{\partial \Psi_{i,1}}{\partial W_{i,2}} = C_{i,1} \qquad (4.4.16)$$

$$DD_{i,1} = \frac{\partial \Psi_{i,1}}{\partial W_{i-1,1}} = D_{i,1} + \frac{\theta\,(1-\alpha_i)\, f_{x_{i,1}}\, f_{r_i}}{\overline{\gamma}_{i-1}} \left[W_{i-1,1} - W_{i,1} \right] \qquad (4.4.17)$$

$$DE_{i,1} = \frac{\partial \Psi_{i,1}}{\partial W_{i+1,1}} = E_{i,1} + \frac{\theta\, \alpha_{i+1}}{\overline{\gamma}_{i+1}} [W_{i+1,1} - W_{i,1}] \qquad (4.4.18)$$

In these expressions, some parameters were introduced such as the dimensionless dynamic average pressure gradient $\overline{\gamma}_i$ which can be approximated by the dimensionless static liquid gradient, since the vertical grid sizes of the blocks are small.

$$\overline{\gamma}_i \cong \gamma_0 = \frac{1}{H_o}. \qquad (4.4.19)$$

The average dimensionless gradient is used to find the dimensionless potential at the free surface, according to the boundary condition expressed by the **Eq. 3.2.2,** discretized below:

$$W_{i,1} = p_{D_{i,1}} + \gamma_o \left(z_{D_{i,1}} + \frac{\Delta h_{D_i}}{2} \right), \qquad (4.4.20)$$

Since $p_{D_{i,1}}$ is the pressure at the block node center, and considering that the free surface is at atmospheric pressure, the above expression can simplified to:

$$W_{i,1} = \frac{h_{D_i}}{H_{oD}}. \qquad (4.4.21)$$

Thus, the uppermost layer properties become congruent to the free surface properties in the discretized process.

Between nodes, the free surface elevation is interpolated by:

$$\overline{h}_{D_i} = (1 - \alpha_i)\, h_{D_{i-1}} + \alpha_i h_{D_i} \qquad (4.4.22)$$

where the parameter $a;$ is a linear function of the radial distance:

$$\alpha_i = \frac{r_{D_i} - \overline{r}_{D_{i-1}}}{\overline{r}_{D_i} - \overline{r}_{D_{i-1}}} \qquad (4.4.23)$$

Since we define:

$$h_{D_i} = z_{D_{i,1}} + \Delta h_{D_i} \quad \textbf{(4.4.24)}$$

$$\overline{h}_{D_i} = \overline{z}_{D_{i,1}} + \overline{\Delta h}_{D_i} \quad \textbf{(4.4.25)}$$

and:

$$\overline{z}_{D_i} = (1-\alpha_i)\, z_{D_{i-1}} + \alpha_i\, z_{D_i} \quad \textbf{(4.4.26)}$$

then:

$$\overline{\Delta h}_{D_i} = (1-\alpha_i)\, \Delta h_{D_{i-1}} + \alpha_i\, \Delta h_{D_i}\,, \quad \textbf{(4.4.27)}$$

the overbar indicating the values taken between two consecutive nodes.

4.4.2 Free Surface Inner Boundary Equation

Similar procedures are used to get the equation for the inner boundary block containing the free surface, and the results are summarized below. A discretization of the continuity equation gives the following material balance residue equation:

$$\Psi_{1,1} = A_{1,1}\, W_{1,1} + C_{1,1}\, W_{1,2} + E_{1,1}\, W_{2,1} - F_{1,1} \quad \textbf{(4.4.28)}$$

where:

$$A_{1,1} = -\theta \left[\overline{\Delta h}_{D_2} + f_{x_{1,1}}\, f_{r_1} \overline{\Delta h}_{D_1} + \frac{2k_v\, A_{1_1}}{k_{x_{2,1}}\, cos\beta_{2,1}\, (\Delta h_{D_1} + \Delta z_{D_1})} + \frac{k_h\, A_{1_1}}{k_{x_{2,1}}\, cos\beta_{2,1}} \frac{\Delta h_{D_1} + \Delta h^k_{D_1}}{2\theta\, \Delta t_D}\, c_{t_D} \right] \quad \textbf{(4.4.29)}$$

$$C_{1,1} = \frac{2\theta\, k_v\, A_{1_1}}{k_{x_{2,1}}\, cos\beta_{2,1}\,(\Delta h_{D_1} + \Delta z_{D_1})} \tag{4.4.30}$$

$$E_{1,1} = \theta\, \overline{\Delta h}_{D_2} \tag{4.4.31}$$

$$F_{1,1} = \frac{k_h}{k_{x_{2,1}} cos\beta_{2,1}} \frac{A_{1_1}}{\Delta t_D cos\overline{\beta}_{1,1}} \left[\left(\Delta h_{D_1} - \Delta h^k_{D_1} \right) S_g - \left(\frac{\Delta h_{D_1} + \Delta h^k_{D_1}}{2} \right) c_{t_D} W^k_{1,1} \right]$$

$$-f_{x_{1,1}}\, f_{r_1} \left[\theta\, \overline{\Delta h}_{D_1} W_{w_1} - (1-\theta)\, \overline{\Delta h}^k_{D_1} \left(W^k_{1,1} - W^k_{w_1} \right) \right] - (1-\theta) \times$$

$$\left\{ \overline{\Delta h}^k_{D_2} \left[W^k_{2,1} - W^k_{1,1} \right] - \frac{2\, k_v\, A_{1_1}}{k_{x_{2,1}} cos\beta_{2,1} \left(\Delta h^k_{D_1} + \Delta z_{D_1} \right)} \left[W^k_{1,1} - W^k_{1,2} \right] \right\} \tag{4.4.32}$$

Consider Δh_{D_w} the extrapolated thickness at the sandface, and the mean thickness:

$$\overline{\Delta} h_{D_1} = \frac{\Delta h_{D_1} + \Delta h_{D_w}}{2} \tag{4.4.33}$$

Also:

$$_{Q2} = \frac{r_{D_2} - \overline{r}_{D_1}}{\overline{r}_{D_2} - \overline{r}_{D_1}}, \tag{4.4.34}$$

$$\alpha_w = \frac{\overline{r}_{D_2} - 1}{\overline{r}_{D_2} - \overline{r}_{D_1}}, \tag{4.4.35}$$

$$\alpha_1 = \frac{1 + \alpha_{D_w}}{2} \tag{4.4.36}$$

The differentiations of the residue equation give the Jacobian elements, as follows:

$$DA_{1,1} = \frac{\partial \Psi_{1,1}}{\partial W_{1,1}} = A_{1,1} + \frac{\partial A_{1,1}}{\partial W_{1,1}} W_{1,1} + \frac{\partial C_{1,1}}{\partial W_{1,1}} W_{1,2} + \frac{\partial E_{1,1}}{\partial W_{1,1}} W_{2,1} - \frac{\partial F_{1,1}}{\partial W_{1,1}} \tag{4.4.37}$$

The resulting differentiation produces:

$$\begin{aligned} DA_{1,1} = A_{1,1} &- \left[\frac{\theta \left(1 - \alpha_2 + \alpha_1 f_{x_{1,1}} f_{r_1}\right)}{\overline{\gamma}_1} - \frac{C_{1,1}}{(\Delta h_{D_1} + \Delta z_{D_1})\overline{\gamma}_1} + \frac{k_h A_{1_1}}{k_{x_{2,1}}} \frac{c_{t_D}}{2\overline{\gamma}_1 \Delta t_D} \right] W_{1,1} \\ &- \frac{C_{1,1}}{(\Delta h_{D_1} + \Delta z_{D_1})\overline{\gamma}_1} W_{1,2} + \frac{\theta(1-\alpha_2)}{\overline{\gamma}_1} W_{2,1} - \frac{k_h}{k_{x_{2,1}}} \frac{A_{1_1}}{\Delta t_D \overline{\gamma}_1} \left[S_g - \frac{c_{t_D} W^k_{1,1}}{2} \right] \\ &+ \frac{\theta\, \alpha_1\, f_{x_{1,1}} f_{r_1}}{\overline{\gamma}_1} W_{w_1} + \theta\, f_{x_{1,1}} f_{r_1} \overline{\Delta h}_1 \frac{\partial W_{w_1}}{\partial W_{1,1}} \end{aligned} \tag{4.4.38}$$

α_1 and α_2 above were obtained from the differentiations of $\overline{\Delta h}_D$. Similarly, the other Jacobian coefficients are:

$$DB_{1,1} = 0 \tag{4.4.39}$$

$$DC_{1,1} = \frac{\partial \Psi_{1,1}}{\partial W_{1,2}} = C_{1,1} + \theta\, f_{x1,1}\, f_{r1} \overline{\Delta h}_1 \frac{\partial W_{w_1}}{\partial W_{1,2}} \tag{4.4.40}$$

$$DD_{1,1} = 0 \tag{4.4.41}$$

$$\begin{aligned} DE_{i,1} = \frac{\partial \Psi_{1,1}}{\partial W_{2,1}} &- E_{1,1} - \frac{\theta \left[\alpha_2 + f_{x_{1,1}} f_{r_1} (1 - \alpha_1)\right]}{\overline{7\,2}} W_{1,1} + \frac{\theta \alpha_2}{\overline{7\,2}} W_{2,1} \\ &+ f_{x_{1,1}} f_{r_1} \theta \left(\frac{1 - \alpha_1}{\angle 2} W_{w_1} + \Delta \overline{h}_{D_1} \frac{\partial W}{\sigma W_{2,1}} \right) \end{aligned} \tag{4.4.42}$$

Values of the derivatives of the inner boundary potentials can be obtained separately, and the equations are presented in App. A.1.

4.4.3 Free Surface Outer Boundary Blocks

Following the same procedures, the final coefficients are:

$$A_{m,1} = -\theta \left[\overline{\Delta h}_{D_{m+1}} + f_{x_{m,1}} f_{r_m} \overline{\Delta h}_{D_m} + \frac{2k_v A_{1_m}}{k_h \left(\Delta h_{D_m} + \Delta z_{D_m}\right)} \right. \tag{4.4.43}$$

$$\left. + \frac{A_{1_m}\left(\Delta h_{D_m} + \Delta h^k_{D_m}\right)}{2\,\theta\, cos\overline{\beta}_{1,m}\,\Delta t_D} c_{t_D} \right] \tag{4.4.44}$$

$$C_{m,1} = + \frac{2\theta\, k_v\, A_{1_m}}{k_h \left(\Delta h_{D_m} + \Delta z_{D_m}\right)} \tag{4.4.45}$$

$$D_{m,1} = \theta\, f_{x_{m,1}}\, f_{r_m} \overline{\Delta h}_{D_m} W_{m-1,1} \tag{4.4.46}$$

$$F_{m,1} = \frac{A_{1_m}}{\Delta t_D\, cos\overline{\beta}_{1,m}} \left[\left(\Delta h_{D_m} - \Delta h^k_{D_m}\right) S_g - \left(\frac{\Delta h_{D_m} + \Delta h^k_{D_m}}{2} \right) c_{t_D} W^k_{m,1} \right]$$

$$- \overline{\Delta h}^k_{D_{m+1}} \left[1 - (1-\theta)\, W^k_{m,1} \right] - (1-\theta) \times$$

$$\left\{ - f_{x_{m,1}} f_{r_m} \overline{\Delta h}^k_{D_m} \left[W^k_{m,1} - W^k_{m-1,1} \right] - \right.$$

$$\left. \frac{2\, k_v\, A_{1_m}}{k_h \left(\Delta h^k_{D_m} + \Delta z_{D_m}\right)} \left[W^k_{m,1} - W^k_{m,2} \right] \right\} \tag{4.4.47}$$

The Jacobian matrix elements for the block $m, 1$ are determined using a Newton-Raphson procedure:

Let:

$$\Psi_{m,1} = A_{m,1}\, W_{m,1} + C_{m,1}\, W_{m,2} + D_{m,1}\, W_{m-1,1} - F_{m,1} \quad (4.4.48)$$

Differentiating Eq. **4.4.48** with respect to each variable $W_{m,n}$:

$$DA_{m,1} = \frac{\partial \Psi_{m,1}}{\partial W_{m,1}} = A_{m,1} + \frac{\partial A_{m,1}}{\partial W_{m,1}} W_{m,1} + \frac{\partial C_{m,1}}{\partial W_{m,1}} W_{m,2} + \frac{\partial D_{m,1}}{\partial W_{m,1}} W_{m-1,1} - \frac{\partial F_{m,1}}{\partial W_{m,1}} . \quad \textbf{(4.4.49)}$$

The resulting differentiation produces:

$$\begin{aligned} DA_{m,1} = A_{m,1} &- \left[\frac{\theta \left(\alpha_m f_{x_{m,1}} f_{rm} \right)}{\overline{\gamma}_m} - \frac{C_{m,1}}{(\Delta h_{D_m} + \Delta z_{D_m})\,\overline{\gamma}_m} + \frac{A_{1_m} c_{t_D}}{2\overline{\gamma}_m\, \Delta t_D \cos\overline{\beta}_{m,1}} \right] W_{m,1} \\ &- \frac{C_{m,1}}{(\Delta h_{D_m} + \Delta z_{D_m})\,\overline{\gamma}_m} W_{m,2} + \frac{\theta\, \alpha_m\, f_{x_{m,1}}\, f_{r_m}}{\overline{\gamma}_m} W_{m-1,1} + \\ &- \frac{A_{1_m}}{\Delta t_D \cos\overline{\beta}_{m,1}\, \overline{\gamma}_m} \left[S_g - \frac{c_{t_D}\, W^k_{m,1}}{2} \right] \end{aligned} \quad \textbf{(4.4.50)}$$

In Eq. **4.4.50** the same definitions as those used so **far** are applied to the parameters. It is helpful to define the outer boundary average thickness:

$$\overline{\Delta h}_{D_{m+1}} = (1 - \alpha_{m+1})\, \Delta h_{D_m} + \alpha_{m+1}\, \Delta h_{D_{m+1}} = (1 - \alpha_{m+1})\, \Delta h_{D_m} + \frac{\alpha_{m+1}}{n}$$

(4.4.51)

where:

$$\alpha_{m+1} = \frac{r_{e_D} - \overline{r}_m}{\overline{r}_{m+1} - \overline{r}_m} . \quad \textbf{(4.4.52)}$$

Similarly, the other Jacobian coefficients are:

$$DB_{m,1} = 0 \quad \textbf{(4.4.53)}$$

$$DC_{m,1} = \frac{\partial \Psi_{m,1}}{\partial W_{m,2}} = C_{m,1} \quad \textbf{(4.4.54)}$$

$$DD_{m,1} = \frac{\partial \Psi_{m,1}}{\partial W_{m-1,1}} = D_{m,1} + \frac{\theta\ (1-\alpha_m)\ f_{x_{m,1}}\ f_{r_m}}{\overline{\gamma}_{m-1}} [W_{m-1,1} - W_{m,1}] \quad (4.4.55)$$

$$DE_{m,1} = \frac{\partial \Psi_{m,1}}{\partial W_{m+1,1}} = 0 \quad \textbf{(4.4.56)}$$

4.5 Lower Boundary Blocks

The lower boundary is defined by the no-flow condition defined by Eq. **3.2.10.** The resulting discretization of Eq. **4.1.3** for each region, namely the inner boundary, the outer boundary, and the main reservoir follows.

4.5.1 Saturated Region Lower Boundary Equations

The residue in the block i,n is:

$$\Psi_{i,n} = A_{i,n}\, W_{i,n} + B_{i,n}\, W_{i,n-1} + D_{i,n}\, W_{i-1,n} + E_{i,n}\, W_{i+1,n} - F_{i,n} \quad (4.5.1)$$

where the coefficients are:

$$A_{i,n} = -\theta \left[\overline{\Delta z}_{D_{i+1}} + f_{x_{i,n}} f_{r_i} \overline{\Delta z}_{D_i} + \frac{k_v}{k_{x_{i+1,n}} cos\beta_{i,n}} \frac{A_{1_i}}{\Delta z_{D_i}} + \frac{k_h}{k_{x_{i+1,n}} cos\beta_{i,n}} \frac{A_{1_i}\, \Delta z_{D_i}}{\theta\, \Delta t_D\, cos\overline{\beta}_{i,n}} c_{t_D} \right] \quad (4.5.2)$$

$$B_{i,n} = \frac{\theta\, k_v\, A_{1_i}}{k_{x_{i+1,n}} cos\beta_{i,n} \Delta z_{D_i}} \quad (4.5.3)$$

$$D_{i,n} = \theta\, f_{x_{i,n}} f_{r_i} \overline{\Delta z}_{D_i} \quad (4.5.4)$$

$$E_{i,n} = \theta\, \overline{\Delta z}_{D_{i+1}} \quad (4.5.5)$$

$$F_{i,n} = -\frac{k_h}{k_{x_{i+1,n}} cos\beta_{i,n}} \frac{A_{i_1}\, \Delta z_{D_i}}{\Delta t_D\, cos\overline{\beta}_{i,n}} c_{t_D}\, W^k_{i,n} - (1-\theta) \left\{ \overline{\Delta z}_{D_{i+1}} \left[W^k_{i+1,n} - W^k_{i,n} \right] - f_{x_{i,n}} f_{r_i} \overline{\Delta z}_{D_i} \left[W^k_{i,n} - W^k_{i-1,n} \right] + \frac{k_v}{k_{x_{i+1,n}} cos\beta_{i,n}} \frac{A_{1_i}}{\Delta z_{D_i}} \left[W^k_{i,n-1} - W^k_{i,n} \right] \right\} . \quad (4.5.6)$$

Jacobian matrix elements for the block i, n were determined using a Newton-Raphson procedure. Differentiating **Eq. 4.5.1** with respect to each variable W:

$$DA_{i,n} = \frac{\partial \Psi_{i,n}}{\partial W_{i,n}} = A_{i,n} \quad (4.5.7)$$

$$DB_{i,n} = \frac{\partial \Psi_{i,n}}{\partial W_{i,n-1}} = B_{i,n} \quad (4.5.8)$$

$$DC_{i,n} = 0 \quad (4.5.9)$$

$$DD_{i,n} = \frac{\partial \Psi_{i,n}}{\partial W_{i-1,n}} = D_{i,n} \quad (4.5.10)$$

$$DE_{i,n} = \frac{\partial \Psi_{i,n}}{\partial W_{i+1,n}} = E_{i,n} \quad (4.5.11)$$

4.5.2 Lower Inner Boundary Equation

The residue in the block i, n is:

$$\Psi_{1,n} = A_{1,n} W_{1,n} + B_{1,n} W_{1,n-1} + E_{1,n} W_{2,n} - F_{1,n} \quad (4.5.12)$$

in which the coefficients are:

$$A_{1,n} = -\theta \left[\overline{\Delta z}_{D_2} + f_{x_{1,n}} f_{r_1} \overline{\Delta z}_{D_1} + \frac{k_v}{k_{x_{2,n}} cos\beta_{2,n}} \frac{A_{1_1}}{\Delta z_{D_1}} + \frac{k_h}{k_{x_{2,n}} cos\beta_{2,n}} \frac{A_{1_1} \Delta z_{D_1}}{\theta \Delta t_D cos\overline{\beta}_{1,n}} c_{tD} \right] \quad (4.5.13)$$

$$B_{1,n} = \frac{\theta k_v A_{1_1}}{k_{x_{2,n}} cos\beta_{2,n} \Delta z_{D_1}} \quad (4.5.14)$$

$$E_{1,n} = \theta \overline{\Delta z}_{D_2} \quad (4.5.15)$$

$$F_{1,n} = -\frac{k_h}{k_{x_{2,n}} cos\beta_{2,n}} \frac{A_{1_1} \Delta z_{D_1}}{\Delta t_D cos\bar{\beta}_{1,n}} c_{t_D} W_{1,n}^k - \theta f_{x_{1,n}} f_{r_1} \overline{\Delta z}_{D_1} W_{w_n}$$

$$- (1-\theta) \left\{ \overline{\Delta z}_{D_2} \left[W_{2,n}^k - W_{1,n}^k \right] - f_{x_{1,n}} f_{r_1} \overline{\Delta z}_{D_1} \left[W_{1,n}^k - W_{w_n}^k \right] \right.$$

$$\left. + \frac{k_v}{k_{x_{2,n}} cos\beta_{2,n}} \frac{A_{1_1}}{\Delta z_{D_1}} \left[W_{1,n-1}^k - W_{1,n}^k \right] \right\} \quad (4.5.16)$$

Find the Jacobian matrix elements for the block $1,n$ using a Newton-Raphson procedure.

Differentiating **Eq.** 4.5.12 with respect to each variable W:

$$DA_{1,n} = \frac{\partial \Psi_{1,n}}{\partial W_{1,n}} = A_{1,n} - \frac{\partial F_{1,n}}{\partial W_{1,n}} = A_{1,n} + \theta f_{x_{1,n}} f_{r_1} \overline{\Delta z}_{D_1} \frac{\partial W_{w_n}}{\partial W_{1,n}} \quad (4.5.17)$$

$$DB_{1,n} = \frac{\partial \Psi_{1,n}}{\partial W_{1,n-1}} = B_{1,n} + \theta f_{x_{1,n}} f_{r_1} \overline{\Delta z}_{D_1} \frac{\partial W_{w_n}}{\partial W_{1,n-1}} \quad (4.5.18)$$

$$DC_{1,n} = 0 \quad (4.5.19)$$

$$DD_{1,n} = 0 \quad (4.5.20)$$

$$DE_{1,n} = \frac{\partial \Psi_{1,n}}{\partial W_{2,n}} = E_{1,n} \quad (4.5.21)$$

The partial differentiations of the inner boundary potentials (see App. A.1), calculated separately may be substituted above.

4.5.3 Lower Outer Boundary Equation

The residue in the block m,n is:

$$\Psi_{m,n} = A_{m,n} W_{m,n} + B_{m,n} W_{m,n-1} + D_{m,n} W_{m-1,n} - F_{m,n} \quad \textbf{(4.5.22)}$$

in which the coefficients are:

$$A_{m,n} = -\theta \left[\overline{\Delta z}_{D_{m+1}} + f_{x_{m,n}} f_{r_m} \overline{\Delta z}_{D_m} + \frac{k_v}{k_h} \frac{A_{1_m}}{\Delta z_{D_m}} + \frac{A_{1_m} \Delta z_{D_m}}{\theta \, \Delta t_D \, cos\overline{\beta}_{m,n}} c_{t_D} \right] \quad \textbf{(4.5.23)}$$

$$B_{m,n} = \frac{\theta \, k_v \, A_{1_m}}{k_h \, \Delta z_{D_m}} \quad \textbf{(4.5.24)}$$

$$D_{m,n} = \theta \, f_{x_{m,n}} \, f_{r_m} \, \overline{\Delta z}_{D_m} \quad (4.5.25)$$

$$\begin{aligned} F_{m,n} = & -\frac{A_{1_m} \Delta z_{D_m}}{\Delta t_D \, cos\overline{\beta}_{m,n}} c_{t_D} W^k_{m,n} - \Delta z_{D_{m+1}} \\ & - (1-\theta) \left\{ -\overline{\Delta z}_{D_{m+1}} W^k_{m,n} - f_{x_{m,n}} f_{r_m} \overline{\Delta z}_{D_m} \left[W^k_{m,n} - W^k_{m-1,n} \right] \right. \\ & \left. + \frac{k_v}{k_h} \frac{A_{1_m}}{\Delta z_{D_m}} \left[W^k_{m,n-1} - W^k_{m,n} \right] \right\} \end{aligned} \quad \textbf{(4.5.26)}$$

Determine Jacobian matrix elements for the block m,n using a Newton-Raphson procedure.

Differentiating **Eq. 4.5.22** with respect to each variable W:

$$DA_{m,n} = \frac{\partial \Psi_{m,n}}{\partial W_{m,n}} = A_{m,n} \quad (4.5.27)$$

$$DB_{m,n} = \frac{\partial \Psi_{m,n}}{\partial W_{m,n-1}} = B_{m,n} \quad (4.5.28)$$

$$DC_{m,n} = 0 \quad (4.5.29)$$

$$DD_{m,n} = \frac{\partial \Psi_{m,n}}{\partial W_{m-1,n}} = D_{m,n} \quad (4.5.30)$$

$$DE_{m,n} = 0 \quad (4.5.31)$$

4.6 Second Layer Region Blocks

The second layer, the one immediately below the free surface layer, is a saturated block. However, the vertical component of the discretized equation contains a variable corresponding to the thickness of the free surface layer block above it. For that reason, the equations are summarized below.

4.6.1 Second Layer Equations

The residue in the block $i, 2$ $(1 < i < m)$ is:

$$\Psi_{i,2} = A_{i,2} W_{i,2} + B_{i,2} W_{i,1} + C_{i,2} W_{i,3} + D_{i,2} W_{i-1,2} + E_{i,2} W_{i+1,2} - F_{i,1} \quad (4.6.1)$$

in which the coefficients are:

$$A_{i,2} = -\theta \left[\overline{\Delta z}_{D_{i+1}} + f_{x_{i,2}} f_{r_i} \overline{\Delta z}_{D_i} + \frac{k_v A_{1_i}}{k_{x_{i+1,2}} cos\beta_{i+1,2}} \left(\frac{1}{\Delta z_{D_i}} + \frac{2}{\Delta z_{D_i} + \Delta h_{D_i}} \right) + \frac{k_h}{k_{x_{i+1,2}} cos\beta_{i+1,2}} \frac{A_{1_i} \Delta z_{D_i}}{\theta \, \Delta t_D \, cos\overline{\beta}_{i,2}} c_{t_D} \right] \quad (4.6.2)$$

$$B_{i,2} = + \frac{2\theta \, k_v \, A_{1_i}}{k_{x_{i+1,2}} \, cos\beta_{i+1,2} \, (\Delta z_{D_i} + \Delta h_{D_i})} \quad (4.6.3)$$

$$C_{i,2} = + \frac{\theta \, k_v \, A_{1_i}}{k_{x_{i+1,2}} \, cos\beta_{i+1,2} \, \Delta z_{D_i}} \quad (4.6.4)$$

$$D_{i,2} = + \theta \, f_{x_{i,2}} \, f_{r_i} \, \overline{\Delta z}_{D_i} \quad (4.6.5)$$

$$E_{i,2} = + \theta \, \overline{\Delta z}_{D_{i+1}} \quad (4.6.6)$$

$$F_{i,2} = -\frac{k_h}{k_{x_{i+1,2}} \, cos\beta_{i+1,2}} \frac{A_{1_i} \, \Delta z_{D_i}}{\Delta t_D \, cos\overline{\beta}_{i,2}} c_{t_D} \, W_{i,2}^k - (1-\theta) \left\{ \overline{\Delta z}_{D_{i+1}} \left[W_{i+1,2}^k - W_{i,2}^k \right] - f_{x_{i,2}} f_{r_i} \overline{\Delta z}_{D_i} \left[W_{i,2}^k - W_{i-1,2}^k \right] + \frac{2k_v \, A_{1_i}}{k_{x_{i+1,2}} cos\beta_{i+1,2} \left(\Delta z_{D_i} + \Delta h_{D_i}^k \right)} \left[W_{i,1}^k - W_{i,2}^k \right] - \frac{k_v \, A_{1_i}}{k_{x_{i+1,2}} \, cos\beta_{i+1,2} \, \Delta z_{D_i}} \left[W_{i,2}^k - W_{i,3}^k \right] \right\} \quad (4.6.7)$$

Find the Jacobian matrix elements for the block $i, 2$ using a Newton-Raphson procedure.

Differentiating **Eq.** 4.6.1 with respect to each variable W:

$$DA_{i,2} = \frac{\partial \Psi_{i,2}}{\partial W_{i,2}} = A_{i,2} \quad (4.6.8)$$

$$DB_{i,2} = \frac{\partial \Psi_{i,2}}{\partial W_{i,1}} = B_{i,2}\left[1 - \frac{W_{i,1} - W_{i,2}}{(\Delta z_{D_i} + \Delta h_{D_i})\,\overline{\gamma}_i}\right] \quad (4.6.9)$$

$$DC_{i,2} = \frac{\partial \Psi_{i,2}}{\partial W_{i,3}} = C_{i,2} \quad \textbf{(4.6.10)}$$

$$DD_{i,2} = \frac{\partial \Psi_{i,2}}{\partial W_{i-1,2}} = D_{i,2} \quad \textbf{(4.6.11)}$$

$$DE_{i,2} = \frac{\partial \Psi_{i,2}}{\partial W_{i+1,2}} = E_{i,2} \quad \textbf{(4.6.12)}$$

4.6.2 Second Layer Inner Boundary Equation

The residue in the block 1,2 is:

$$\Psi_{1,2} = A_{1,2}\,W_{1,2} + B_{1,2}\,W_{1,1} + C_{1,2}\,W_{1,3} + E_{1,2}\,W_{2,2} - F_{1,2} \quad (4.6.13)$$

in which the coefficients are:

$$A_{1,2} = -\theta\left[\overline{\Delta z}_{D_2} + f_{x_{1,2}}\,f_{r_1}\overline{\Delta z}_{D_1} + \frac{k_v\,A_{1_1}}{k_{x_{2,2}}\,cos\beta_{2,2}}\left(\frac{1}{\Delta z_{D_1}} + \frac{2}{\Delta z_{D_1} + \Delta h_{D_1}}\right) + \frac{k_h}{k_{x_{2,2}}\,cos\beta_{2,2}}\,\frac{A_{1_1}\,\Delta z_{D_1}}{\theta\,\Delta t_D\,cos\overline{\beta}_{1,2}}\,c_{t_D}\right] \quad \textbf{(4.6.14)}$$

$$B_{1,2} = +\frac{2\theta\,k_v\,A_{1_1}}{k_{x_{2,2}}\,cos\beta_{2,2}\,(\Delta z_{D_1} + \Delta h_{D_1})} \quad \textbf{(4.6.15)}$$

$$C_{1,2} = +\frac{\theta\,k_v\,A_{1_1}}{k_{x_{2,2}}\,cos\beta_{2,2}\,\Delta z_{D_1}} \quad \textbf{(4.6.16)}$$

$$E_{1,2} = +\theta\,\overline{\Delta z}_{D_2} \tag{4.6.17}$$

$$F_{1,2} = -\theta\, f_{x_{1,2}}\, f_{r_1}\overline{\Delta z}_{D_1} W_{w_2} - \frac{k_h}{k_{x_{2,2}}\cos\beta_{2,2}} \frac{A_{1_1}\,\Delta z_{D_1}}{\Delta t_D \cos\overline{\beta}_{1,2}}\, c_{t_D}\, W^k_{1,2}$$

$$-(1-\theta)\left\{\overline{\Delta z}_{D_2}\left[W^k_{2,2} - W^k_{1,2}\right] - f_{x_{1,2}}\, f_{r_1}\,\overline{\Delta z}_{D_1}\left[W^k_{1,2} - W^k_{w_2}\right]\right.$$

$$\left.\frac{2\,k_v\,A_{1_1}}{k_{x_{2,2}}\cos\beta_{2,2}}\left[\frac{2\left(W^k_{2,2} - W^k_{1,2}\right)}{\Delta z_{D_1} + \Delta h^k_{D_1}} - \frac{W^k_{1,2} - W^k_{1,3}}{\Delta z_{D_1}}\right]\right\} \tag{4.6.18}$$

Find the Jacobian matrix elements for the block $i, 2$ using a Newton-Raphson procedure.

Differentiating **Eq.** 4.6.18 with respect to each variable W:

$$DA_{1,2} = \frac{\partial\Psi_{1,2}}{\partial W_{1,2}} = A_{1,2} - \frac{\partial F_{1,2}}{\partial W_{1,2}} = A_{1,2} + \theta\, f_{x_{1,2}}\, f_{r_1}\,\overline{\Delta z}_{D_1}\frac{\partial W_{w_2}}{\partial W_{1,2}} \tag{4.6.19}$$

$$DB_{1,2} = \frac{\partial\Psi_{1,2}}{\partial W_{1,1}} = B_{1,2}\left[1 - \frac{W_{1,1} - W_{1,2}}{(\Delta z_{D_1} + \Delta h_{D_1})\,\overline{\gamma}_1}\right] + \theta\, f_{x_{1,2}}\, f_{r_1}\,\overline{\Delta z}_{D_1}\frac{\partial W_{w_2}}{\partial W_{1,1}} \tag{4.6.20}$$

$$DC_{1,2} = \frac{\partial\Psi_{1,2}}{\partial W_{1,3}} = C_{1,2} + \theta\, f_{x_{1,2}}\, f_{r_1}\,\overline{\Delta z}_{D_1}\frac{\partial W_{w_2}}{\partial W_{1,3}} \tag{4.6.21}$$

$$DD_{1,2} = 0 \tag{4.6.22}$$

$$DE_{1,2} = \frac{\partial\Psi_{1,2}}{\partial W_{2,2}} = E_{1,2} \tag{4.6.23}$$

The partial differentiations of the inner boundary potentials (see App.A), calculated individually, may be substituted above.

4.6.3 Second Layer Outer Boundary Equation

The residue in **the block** $m,2$ is:

$$\Psi_{m,2} = A_{m,2}\,W_{m,2} + B_{m,2}\,W_{m,1} + C_{m,2}\,W_{m,3} + D_{m,2}\,W_{m-1,2} - F_{m,2} \quad (4.6.24)$$

where the coefficients are:

$$A_{m,2} = -\theta\left[\overline{\Delta z}_{D_{m+1}} + f_{x_{m,2}}\,f_{r_m}\,\overline{\Delta z}_{D_m} + \frac{k_v\,A_{1_m}}{k_h}\left(\frac{1}{\Delta z_{D_m}} + \frac{2}{\Delta z_{D_m} + \Delta h_{D_m}}\right) + \frac{A_{1_m}\,\Delta z_{D_m}}{\Delta t_D\,cos\overline{\beta}_{m,2}}\,c_{t_D}\right] \quad (4.6.25)$$

$$B_{m,2} = +\frac{2\theta\,k_v\,A_{1_m}}{k_h\,(\Delta z_{D_m} + \Delta h_{D_m})} \quad (4.6.26)$$

$$C_{m,2} = +\frac{\theta\,k_v\,A_{1_m}}{k_h \Delta z_{D_m}} \quad (4.6.27)$$

$$D_{m,2} = +\theta\,f_{x_{m,2}}\,f_{r_m}\overline{\Delta z}_{D_m} \quad (4.6.28)$$

$$F_{m,2} = -\frac{A_{1_m}\,\Delta z_{D_m}}{\Delta t_D\,cos\overline{\beta}_{m,2}}\,c_{t_D}\,W^{k}_{m,2} - \theta\,\overline{\Delta z}_{D_{m+1}} - (1-\theta)\left\{\overline{\Delta z}_{D_{m+1}}\left[1 - W^{k}_{m,2}\right] - f_{x_{m,2}}\,f_{r_m}\overline{\Delta z}_{D_m}\left[W^{k}_{m,2} - W^{k}_{m-1,2}\right] + \frac{2k_v\,A_{1_m}}{k_h\left(\Delta z_{D_m} + \Delta h^{k}_{D_m}\right)}\left[W^{k}_{m,1} - W^{k}_{m,2}\right] - \frac{k_v\,A_{1_m}}{k_h \Delta z_{D_m}}\left[W^{k}_{m,2} - W^{k}_{m,3}\right]\right\} \quad (4.6.29)$$

Find the Jacobian matrix elements for the block $m,2$ using **a Newton-Raphson procedure.**

Differentiating **Eq. 4.6.24** with respect to each variable ***W:***

$$DA_{m,2} = \frac{\partial \Psi_{m,2}}{\partial W_{m,2}} = A_{m,2} \quad \textbf{(4.6.30)}$$

$$DB_{m,2} = \frac{\partial \Psi_{m,2}}{\partial W_{m,1}} = B_{m,2}\left[1 - \frac{W_{m,1} - W_{m,2}}{(\Delta z_{D_m} + \Delta h_{D_m})\overline{\gamma}_m}\right] \quad (4.6.31)$$

$$DC_{m,2} = \frac{\partial \Psi_{m,2}}{\partial W_{m,1}} = C_{m,2} \quad \textbf{(4.6.32)}$$

$$DD_{m,2} = \frac{\partial \Psi_{m,2}}{\partial W_{m-1,2}} = D_{m,2} \quad \textbf{(4.6.33)}$$

$$DE_{m,2} = 0 \quad \textbf{(4.6.34)}$$

4.7 Capillary Fringe

So far in this chapter, the existence of the capillary fringe in the model has been neglected. The importance of the capillary fringe appears to be a matter of scale, because in most field cases, the capillary layer is negligible compared to the total liquid height. To verify the model against sandbox experiments, however, it is necessary to introduce capillary effects. Due to this modification, the free surface concept must be reconsidered. Thus, we will use the terminology of groundwater literature to denote as phreatic surface the interface domain corresponding to atmospheric pressure in the saturated region below the capillary fringe.

The capillary fringe is a layer immediately above the phreatic surface, partially or completely saturated, possessing the particular characteristic of pressures below atmospheric as a function of the capillary pressure. The uniformity of thickness and saturation is essentially dependent on the uniformity of grain and pore throat size distributions, and on the surface tension of the gas-liquid-rock system. At rest, the

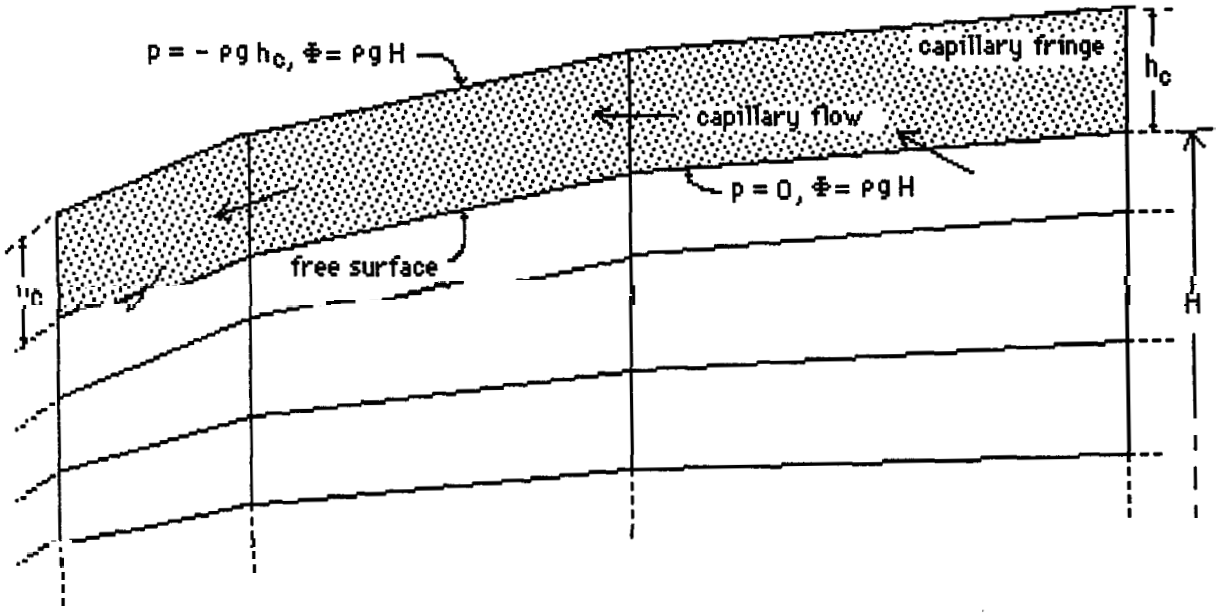

Figure 4.5: Representation of the capillary fringe layer.

potentials in the fringe have the same value as in the saturated region, but at dynamic conditions, the potentials have the same value as in the phreatic line. According to the *Wyckoff et al.* (1932) and ***Hull*** (1955) sandbox experiments, the capillary fringe is not a dead region, and downward movement of the phreatic surface causes liquid to flow by the potential reduction generating pressure gradients. In the radial model sandbox experiments, it is possible to observe the tracks of the stream lines in the capillary fringe leaving the outer boundary in an upward direction, then following the pheatic surface, and bending downward in the vicinity of the wellbore.

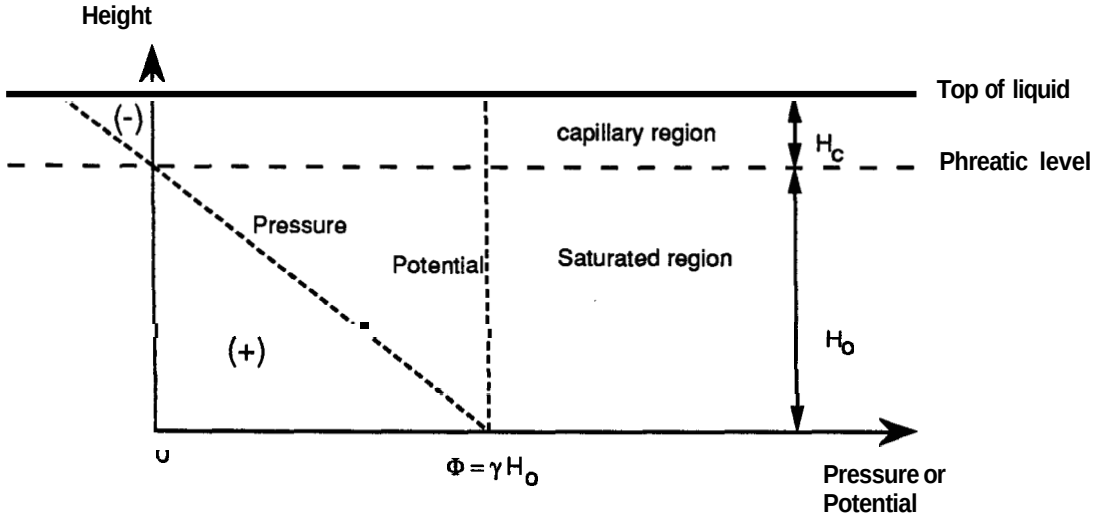

Figure **4.6:** Potential and pressure profiles at a radial position r, under static conditions.

4.7.1 Description of the Physical Mechanism of the Capillary Flow

A description of the physical behavior and the causes of the capillary flow is presented next, with the purpose of creating a mathematical representation to be added to the Stream Layer Model. We start by assuming an anisotropic formation saturated with a single liquid, presenting a uniform capillary layer of thickness h_c at rest, above the original static level H_o. The potential and pressure distributions at any radial position in the formation is represented by Fig. 4.6. The pressures above H_o are negative due to the capillary pressure γh_c, which pulls the gas-liquid contact out, normal to the surface. The phreatic line at rest corresponds to atmospheric pressure.

When pumping starts, the potentials below the phreatic surface decrease, and the surface travels downward producing a pressure reduction in the capillary layer.

Because there is a variable potential distribution along the phreatic surface, an equivalent distribution should exist above it. The liquid in the fringe starts moving accordingly. In the gas liquid contact, the pressure reduction forces a movement of the meniscus and gas entry in a typical two-phase flow leaving a decreasing liquid saturation above the gas-liquid contact decreasing to the irreducible value S_{w_r}. The capillary fringe tends to maintain the thickness h_c, but, in a transient flow it may be possible that h_c will become variable due to the resistence to the air entry by the lower relative permeability to gas at high liquid saturations in the desaturating region. Yet, it is also possible that the capillary fringe presents a residual gas saturation in cases of sandbox experiments, and two-phase flow should be considered in this region. It is reasonable to expect expansion of the capillary fringe mainly around the wellbore at early times where the vertical velocities of the free surface drawdown are higher than those of the air entry before reaching steady conditions.

The potential variation in the capillary layer generates flow in that region, which, neglecting the temporary expansion described before, may be considered of constant storativity. So, the capillary fringe acts as an aditional source of flow into the phreatic surface, close to the well. However, due to the constant storativity, the liquid change through the phreatic interface varies in direction and intensity. It was observed experimentally that there were stream lines moving upward across the phreatic surface feeding the capillary layer. ***Hull*** (1955) pointed out that "the phreatic *line* is not a *flow* line in a case where a capillary layer exists." Hence, there must be a flux profile along the radial direction showing maximum absolute values at the inner and outer boundaries, though with different directions. Somewhere in between the flux is zero.

4.7.2 Mathematical Representation of the Capillary Layer Boundary

Based on the preceeding flow concept, we could rewrite the free surface layer equation incorporating a source term, which is the contribution of the capillary layer. Some simplifications are often made in the capillary flow such as to consider constant dynamic vertical gradient approaching the static gradient in the capillary fringe, as well as neglecting the transient behavior of delayed air entry. The following mathematical relationships are valid in the capillary layer where the pressures are negative ($H_o \leq z \leq H_o + h_c$):

$$\Phi_c(r,t) = \Phi_{ph}(r,t) \tag{4.7.1}$$

$$\Phi_{ph}(r,t) = \left(\rho \frac{g}{g_c}\right) h(r,t) \tag{4.7.2}$$

$$\Phi(r, h + h_c, t) = \left(\rho \frac{g}{g_c}\right) h(r,t) \tag{4.7.3}$$

where the subscripts c and ph refer to the capillary layer and to the phreatic surface, and h represents the phreatic level. Equation **4.7.3** is a consequence of Eq. **4.7.1** and **Eq.** 4.7.2, and does not constitute an additional condition. Eq. **4.7.3** limits the upper geometric boundary of the system. **A** material balance for an incompressible system is translated by the Laplace equation if we think of the capillary layer changing its position in space, but not the mean pressure:

$$\nabla^2 \Phi_c = 0 \tag{4.7.4}$$

Assuming the discretization principles used before, Eq. **4.7.4** could be represented in the following way, considering the entire capillary fringe integrated into a single layer:

$$(q_{in} - q_{out})|_x + (q_{in} - q_{out})|_v = 0 \qquad (4.7.5)$$

For convenience, Eq. **4.7.5** can be expressed as function of the potential in the phreatic layer (the one immediately below the capillary layer). The notation used here is the same as for the free surface layer developed in the previous chapter. In fact, it is only a matter of nomenclature.

$$q_{in_x} = \frac{2\pi}{\mu} k^c_{x_{i+1,1}} \cos\beta_{i+1,1} h_c \frac{\Phi_{i+1,1} - \Phi_{i,1}}{\ln\left(\frac{\bar{r}_{i+1}}{\bar{r}_i}\right)} \qquad (4.7.6)$$

and

$$q_{out_x} = \frac{2\pi}{\mu} k^c_{x_{i,1}} \cos\beta_{i,1} h_c \frac{\Phi_{i,1} - \Phi_{i-1,1}}{\ln\left(\frac{\bar{r}_i}{\bar{r}_{i-1}}\right)} \qquad (4.7.7)$$

In the vertical flow direction, the downward movement of the entire liquid column leaves behind a volume equivalent to an average liquid saturation in the desaturated region. We may consider that the liquid volume going out of the capillary layer through the top boundary must be the same as the equivalent volume of liquid going into the capillary layer through the lower boundary. This means that the capillary layer has no role on the liquid balance. Hence, the only vertical capillary layer in or out flow to be considered, named q_c, is the net flow through the lower boundary, feeding the top of the phreatic surface. Since there is no cross flow between stream lines, flow is not produced by potential differentials between layers, but merely added to the top of the phreatic layer. Following the same sign convention for flow direction, Eq. 4.7.5 becomes:

$$(q_{in} - q_{out})|_x - q_c = 0 \qquad (4.7.8)$$

After substitutions, we may express q_c for a discrete capillary layer block i:

$$q_{c_i} = \frac{2\pi h_c}{\mu}\left[k^c_{x_{i+1,1}} \cos\beta_{i+1,1}\frac{\Phi_{i+1,1} - \Phi_{i,1}}{\ln\left(\frac{\bar{r}_{i+1}}{\bar{r}_i}\right)} - k^c_{x_{i,1}} \cos\beta_{i,1}\frac{\Phi_{i,1} - \Phi_{i-1,1}}{\ln\left(\frac{\bar{r}_i}{\bar{r}_{i-1}}\right)}\right] \qquad (4.7.9)$$

4.7.3 Mathematical Representation of the Phreatic Layer

The discretization of the phreatic layer will be handled the same way as the free surface layer was handled previously. The differencein the material balance equation is that the flow in is the source term q_c. The same principle of variable thickness will be employed to the phreatic layer as well, and the **Eq. 4.1.3** becomes:

$$\Delta_x(T_x\Delta_x\Phi) + \Delta_v(T_v\Delta_v\Phi) + q_{c_i} = \frac{1}{\Delta t}\Delta_t(\phi V) \qquad (4.7.10)$$

Discretization of a block i, **1,** $(M > i > 1)$**:**

Following the same exact procedures as in section **4.4,** the equivalent residue equation coefficients are:

$$A_{i,1} = -\theta\left[h_{c_D}k^o_r + \overline{\Delta h}_{D_{i+1}} + f_{x_{i,1}}f_{r_i}\left(h_{c_D}k^o_r + \overline{\Delta h}_{D_i}\right) + \frac{2k_v A_{1_i}}{k_{x_{i+1,1}}\cos\beta_{i+1,1}(\Delta h_{D_i} + \Delta z_{D_i})} + \frac{k_h A_{1_i}}{k_{x_{i+1,1}}\cos\beta_{i+1,1}}\frac{\Delta h_{D_i} + \Delta h^k_{D_i}}{2\theta\,\Delta t_D\cos\bar{\beta}_{i,1}}c_{t_D}\right] \qquad (4.7.11)$$

$$C_{i,1} = \frac{2\,\theta\,k_v\,A_{1_i}}{k_{x_{i+1,1}}\cos\beta_{i+1,1}\,(\Delta h_{D_i} + \Delta z_{D_i})} \tag{4.7.12}$$

$$D_{i,1} = +\,\theta\,f_{x_{i,1}}\,f_{r_i}\,\left(h_{c_D}\,k_r^o + \overline{\Delta h}_{D_i}\right) \tag{4.7.13}$$

$$E_{i,1} = \theta\left(h_{c_D}\,k_r^o + \overline{\Delta h}_{D_{i+1}}\right) \tag{4.7.14}$$

$$\begin{aligned} F_{i,1} = {} & \frac{k_h}{k_{x_{i+1,1}}\cos\beta_{i+1,1}\cos\overline{\beta}_{i,1}}\,\frac{A_{1_i}}{\Delta t_D}\,\left[\left(\Delta h_{D_i} - \Delta h_{D_i}^k\right) S_g - \right. \\ & \left.\left(\frac{\Delta h_{D_i} + \Delta h_{D_i}^k}{2}\right) c_{t_D}\,W_{i,1}^k\right] - (1-\theta)\left\{\left(h_{c_D}\,k_r^o + \overline{\Delta h}_{D_i}^k\right)\left[W_{i+1,1}^k - W_{i,1}^k\right]\right. \\ & + f_{x_{i,1}}\,f_{r_i}\left(h_{c_D}\,k_r^o + \overline{\Delta h}_{D_i}^k\right)\left[W_{i-1,1}^k - W_{i,1}^k\right] \\ & \left. + \frac{2\,k_v\,A_{1_i}\,\left[W_{i,2}^k - W_{i,1}^k\right]}{k_{x_{i+1,1}}\cos\beta_{i+1,1}\left(\Delta h_{D_i}^k + \Delta z_{D_i}\right)}\right\} \end{aligned} \tag{4.7.15}$$

where $k_r^o = k_{x_{i+1,1}}^c/k_{x_{i+1,1}} = k_{x_{i,1}}^c/k_{x_{i,1}}$ is the relative permeability of the liquid in the capillary fringe, at an assumed residual gas saturation.

We find the Jacobian matrix elements for the block $i, 1$ using a Newton-Raphson **pro**cedure. The coefficients determined for the Jacobian matrix are those of Eqs. **4.4.14** through **4.4.18,** because all the parameters related to the capillary fringe are constant in the present work.

4.7.4 Inner Boundary Phreatic Layer Equation

The capillary layer above the free surface does not produce to the wellbore because of the capillary forces in the sandface. In terms of a discretized block, the equation for the inner boundary blocks is developed using the same concept described in the previous sections for the capillary layer. Skipping the tedious algebraic manipulations, and by analogy with the procedures in section **4.3.2,** the resulting residue equation coefficients:

$$A_{1,1} = -\theta \left[h_{c_D} k_r^o + \overline{\Delta h}_{D_2} + f_{x_{1,1}} f_{r_1} \overline{\Delta h}_{D_1} + \frac{2\, k_v\, A_{1_1}}{K_{x_{2,1}} \left(\Delta h_{D_1} + \Delta z_{D_1}\right)} \right.$$

$$\left. \frac{k_h\, A_{1_1}}{k_{x_{2,1}} \cos\beta_{2,1} \cos\overline{\beta_1}} \frac{\Delta h_{D_1} + \Delta h_{D_1}^k}{2\theta\, \Delta t_D} c_{t_D} \right] \qquad \textbf{(4.7.16)}$$

$$C_{1,1} = \frac{2\theta\, k_v\, A_{1_1}}{K_{x_{2,1}} \cos\beta_{2,1} \left(\Delta h_{D_1} + \Delta z_{D_1}\right)} \qquad \textbf{(4.7.17)}$$

$$E_{1,1} = \theta \left(h_{c_D} k_r^o + \overline{\Delta h}_{D_2} \right) \qquad (4.7.18)$$

$$F_{1,1} = -\theta\, f_{x_{1,1}} f_{r_1} \overline{\Delta h}_{D_1} W_{w_1} +$$

$$\frac{k_h}{k_{x_{2,1}} \cos\beta_{2,1} \cos\overline{\beta_1}} \frac{A_{1_1}}{\Delta t_D} \left[\left(\Delta h_{D_1} - \Delta h_{D_1}^k \right) S_g - \left(\frac{\Delta h_{D_1} + \Delta h_{D_1}^k}{2} \right) c_{t_D} W_{1,1}^k \right]$$

$$- (1-\theta) \left\{ \left(h_{c_D} k_r^o + \overline{\Delta h}_{D_2}^k \right) \left[W_{2,1}^k - W_{1,1}^k \right] \right.$$

$$+ f_{x_{1,1}} f_{r_1} \left[\overline{\Delta h}_{D_1}^k W_{w_1}^k - \left(h_{c_D} k_r^o + \overline{\Delta h}_{D_1}^k \right) W_{1,1}^k \right]$$

$$\left. + \frac{2\, k_v\, A_{1_1}}{k_{x_{2,1}} \cos\beta_{2,1} \left(\Delta h_{D_1}^k + \Delta z_{D_1} \right)} \left[W_{1,2}^k - W_{1,1}^k \right] \right\} \qquad \textbf{(4.7.19)}$$

We find the Jacobian matrix elements for the block $i, 1$ using a Newton-Raphson **pro-**

cedure. The coefficients determined for the Jacobian matrix are those of Eqs. **4.4.38** through **4.4.42,** because the parameters related to the capillary fringe are constant in the present work.

4.7.5 Outer Boundary Phreatic Layer Equation

At the outer boundary, the capillary layer is passive, and does not have an external source feeding the capillary layer throughout. All liquid feeding the capillary layer comes vertically from the free surface due to capillary forces. If the impermeable top of the formation allows for the existence of the capillary fringe at that position, that is the origin of the uppermost stream flow lines. In terms of discretized block, the equation for the outer boundary blocks is developed using the same concept described in the previous sections for the capillary layer. Skipping again the tedious algebraic manipulations, by analogy with the procedures in section **4.4.3,** the resulting dimensionless equation coefficients are:

$$A_{m,1} = -\theta \left[\overline{\Delta h}_{m+1} + f_{x_{m,1}} f_{r_m} \left(h_{c_D} k_r^o + \overline{\Delta h}_{D_m} \right) + \frac{2 k_h A_{1_m}}{k_h \left(\Delta h_m + \Delta z_{D_m} \right)} + \frac{A_{1_m} \left(\Delta h_{D_m} + \Delta h_{D_m}^k \right)}{2 \theta \, \Delta t_D \cos \overline{\beta}_{m,1}} c_{t_D} \right] \tag{4.7.20}$$

$$C_{m,1} = \frac{2 k_h A_{1_m}}{k_h \left(\Delta h_m + \Delta z_{D_m} \right)} \tag{4.7.21}$$

$$D_{m,1} = \theta \, f_{x_{m,1}} f_{r_m} \left(h_{c_D} k_r^o + \overline{\Delta h}_{D_m} \right) \tag{4.7.22}$$

$$F_{m,1} = \frac{A_{1_m}}{\Delta t_D \cos\overline{\beta}_{m,1}} \left[\left(\Delta h_{D_m} - \Delta h^k_{D_m} \right) S_g - \frac{\Delta h_{D_m} - \Delta h^k_{D_m}}{2} c_{t_D} W^k_{m,1} \right] - \Delta h^k_{D_m}$$

$$-\theta \left\{ - \left[\overline{\Delta h}^k_{D_{m+1}} + f_{x_{m,1}} f_{r_m} \left(h_{c_D} k^o_r + \overline{\Delta h}^k_{D_m} \right) + \frac{2\, k_h A_{1_m}}{k_h \left(\Delta z_{D_m} + \Delta h^k_{D_m} \right)} \right] W^k_{m,1} \right.$$

$$\left. + \frac{2\, k_h\, A_{1_m}}{k_h \left(\Delta z_{D_m} + \Delta h^k_{D_m} \right)} W^k_{m,2} + f_{x_{m,1}} f_{r_m} \left(h_{c_D} k^o_r + \overline{\Delta h}^k_{D_m} \right) W^k_{m-1} \right\} \qquad (4.7.23)$$

Again, the Jacobian coefficientsare obtained from the partial derivatives. Because the capillary height was the only additional term in **Eqs. 4.7.20 - 4.7.23,** and because capillary height is considered constant in this study, the results for the derivatives are the same as presented by Eqs. **4.4.50** to **4.4.56.**

4.8 Sandface and Wellbore Conditions

The inner boundary conditions of the gravity drive problem are difficult to handle due to the changes occurring on the free surface and stream-lines entering the wellbore. **A** basic condition presented is the potential along the sandface in a position r_{w+} which depends on the vertical location of the liquid level in the wellbore:

$$\Phi_w = H_w \rho \, (g/g_c) \qquad \Rightarrow \qquad z_{r_{w+}} \leq H_w \qquad (4.8.1)$$

$$\Phi_w = z_{r_{w+}} \rho \, (g/g_c) \qquad \Rightarrow \qquad H_w < z_{r_{w+}} \leq H_s \qquad (4.8.2)$$

Using dimensionless parameters, the conditions are:

$$W_w = \gamma_o H_{w_D} \qquad \Rightarrow \qquad z_{w_D} \leq H_{w_D} \qquad \textbf{(4.8.3)}$$

$$W_w = \gamma_o z_{w_D} \quad \Rightarrow \quad H_{w_D} < z_{w_D} \leq H_{s_D} \tag{4.8.4}$$

In App. **A.l,** a discretization in dimensionless form of the preceeding conditions is developed, considering all possible relative positions of the liquid level in the wellbore and the grid blocks adjacent to it.

A second relevant condition is given by a material balance on the well. Considering the instantaneous mass flow rate of liquid measured at stock tank conditions as the result of the mass of liquid flowing across the sandface minus the change of mass in the wellbore due to storage, a general equation may be written:

$$q\, B_{w_b} = -\frac{\pi r_w^2\, \mathbf{A}\mathbf{H},}{\mathbf{A}t} + \frac{2\pi\, r_w}{\mu} \int_0^{H_s} k_x \frac{\partial p}{\partial r}\, dz \tag{4.8.5}$$

where k_x is the permeability in the direction tangent to a stream-line at the sandface, and B_{w_b} is the volume-formation factor corresponding to the average pressure of the liquid column in the wellbore. Next, the material balance analytical equation Eq. **4.8.5** is converted into dimensionless form. Multiplying both sides of **Eq. 4.8.5** by $\frac{\mu}{2\pi\, r_w\, k_h\, h_o \rho\, (g/g_c)}$, yields:

$$\frac{q\, \mu\, B_{wb}}{2\pi\, r_w\, k_h\, h_o \rho\, (g/g_c)} = -\frac{\mu r_w}{2k_h\, h_o \rho\, (g/g_c)} \frac{\Delta H_w}{\Delta t} + \frac{r_w}{r_w} \int_0^{H_s} \frac{k_x}{k_h} \frac{\partial \left[\frac{p}{h_o \rho\, (g/g_c)}\right]}{\partial r}\, dz \tag{4.8.6}$$

Using dimensionless parameters defined previously:

$$q_D\, B_{w_b} = -\frac{\Delta H_{w_D}}{2\phi\, \Delta t_D} + r_{D_1} \int_0^{H_{s_D}} \frac{k_x}{k_h} \frac{\partial p_D}{\partial r_D}\, dz_D \tag{4.8.7}$$

Equation **4.8.7** is discretized using a time-relaxation parameter θ. This process

follows the geometric characteristics of the stream-layer model. The integral representing flow through the sandface is replaced by a summation of radial steady-state flow through each layer cylindrical region from the geometric center to the sandface.

$$q_D\, B_{w_b} = -\frac{\Delta H_{w_D}}{2\,\phi\,\Delta t_D} + \frac{\Delta \overline{z}_{D_1}}{\ln(\overline{r}_1)}\left\{\frac{k_{x1,1}}{k_h}\,(1-\theta)\left(W^k_{1,1} - W^k_{w_1}\right) + \sum_{j=2}^{n}\frac{k_{x_{1,j}}}{k_h}\left[\theta\left(W_{1,j} - W_{w_j}\right) + (1-\theta)\left(W^k_{1,j} - W^k_{w_j}\right)\right]\right\} + \frac{\Delta \overline{h}_{D_1}}{\ln(\overline{r}_1)}\,\frac{k_{x_{1,1}}}{k_h}\,\theta\,(W_{1,1} - W_{w1})\,. \tag{4.8.8}$$

It is necessary to define some parameters introduced above. First, the formation-volume factor is calculated based on a time average wellbore pressure taken at half the distance from the top to the bottom of the liquid column:

$$B_{w_b} = \frac{V_{w_b}}{V_{std}} = \frac{1}{1 + \frac{H^*_w}{2}\rho\,(g/g_c)\,c_L} = \frac{2}{2 + \gamma_o\, H^*_{w_D}\, c_{L_D}} = \frac{4}{4 + \gamma_o\left(H_{w_D} + H^k_{w_D}\right) c_{L_D}} \tag{4.8.9}$$

Most of the time, $B_w b$ may be considered 1 due to the low liquid compressibilities. However, $B_w b$ is considered here for complete theorectical formulation. The asterisk superscript in Eq. **4.8.9** represents a time average liquid height. The average block thickness at the wellbore may be taken as the mean of the block thickness **at** the center (Δh_{D_1}) and the extrapolated thickness at the sandface (Δh_{D_w}):

$$\Delta \overline{h}_{D_1} = \frac{\Delta h_{D_1} + \Delta h_{D_w}}{2}\,, \qquad \text{and} \qquad \Delta \overline{z}_{D_1} = \frac{\Delta z_{D_1} + \Delta z_{D_w}}{2} \tag{4.8.10}$$

Also, the dimensionless radial distance $\overline{r}_{D_1}$ from the inner block geometric center to the sandface is used. The drop of the liquid column in the wellbore is:

$$\mathbf{AH_{,,}} = H_{w_D} - H^k_{w_D} \tag{4.8.11}$$

The superscript k stands for the value at the beginning of the time-step.

The discretization of the inner boundary potentials requires previous knowledge of the liquid position in the wellbore. Figure **4.1** shows that the base position of each block is an extrapolation of the coordinates expressed in dimensionless form as:

$$z_{w_{D_j}} = (n-j)\ \Delta z_{D_w} \tag{4.8.12}$$

where the extrapolated thickness is obtained by:

$$\Delta z_{D_w} = \alpha_w\ \Delta z_{D_1} + (1-\alpha_w)\ \Delta z_{D_2} \tag{4.8.13}$$

and:

$$\alpha_w = \frac{\ln(\bar{r}_2)}{\ln(\bar{r}_2/\bar{r}_1)} \tag{4.8.14}$$

A similar extrapolation is done to the layer containing the free surface:

$$\Delta h_{D_w} = \alpha_w\ \Delta h_{D_1} + (1-\alpha_w)\ \Delta h_{D_2} \tag{4.8.15}$$

Let j_1 be the position of the inner block adjacent to the liquid surface in the wellbore. The j_1 value is initially unknown, and must be estimated before the calculations. Fortunately, the variation of the liquid level in the wellbore is easy to follow, and this procedure becomes a minor iterative problem. Due to the dependence of the potentials at the sandface on the liquid level in the wellbore, there is a particular way to calculate the average potential at the sandface of each inner block according to the respective stream-layer position. Every case is detailed in App. **A.1.** It is possible to evaluate the liquid level H_{w_D} in the material balance equation by the appropriate substitution of the sandface potentials using an iterative method, or a direct method by solving a quadratic equation.

The partial derivatives of the sandface potentials must be determined in order to be substituted into the Jacobian equations required by the Newton-Raphson method. In view of the changes in the inner boundary condition along the sandface, there is a need for evaluating each case individually. In other words, due to the fact that in the material balance equation all the inner block potentials and sandface potentials are present, a variety of criteria must be considered in the differentiations. These procedures are summarized in App. A.l.

4.9 Computer Model

A general description of approximation of the numerical model described in the preceeding is presented in this section. The non-linear nature of the problem of gravity flow into a wellbore requires an iterative procedure to compute the potentials and the free surface positions in the reservoir, as well as the wellbore potential. Some criteria used in the simulator for a typical time-step calculation are described next:

1. At the beginning of a time-step, the model assumes the dimensionless free surface distribution as being the same as that at the end of the previous time-step. At each radial position i, the same number N of vertical blocks is allocated which have an initial uniform thickness calculated by dividing the total height by the constant number of blocks N:

$$\Delta z_{D_i} = \frac{H_{D_i}}{N} . \tag{4.9.1}$$

As an intial guess, the thickness of a block containing the free surface, Δh_{D_i}, takes the same value as Δz_{D_i}:

$$\Delta h_{D_i} = \Delta h^k_{D_i}. \tag{4.9.2}$$

2. During a time-step, the variation of the liquid column H_{D_i} will be the same as the free surface displacement in the correspondent block in the first layer **($j = 1$).** All other blocks in the saturated region will not have a change in thickness during this period. In other words, during the time-step loop calculations, Δz_{D_i} remains constant while Δh_{D_i} varies.

3. The wellbore liquid height H_{w_D} is initially estimated from the wellbore material balance equation developed in Appendix **A.2,** considering the initial potential distribution around the wellbore for the present time-step. The quadratic equation approach was the one preferred for accuracy and speed in the calculations.

4. After calculating H_{w_D} the sandface potentials W_{w_j} are determined according to the inner boundary condition.

5. The equation and Jacobian matrix coefficients are calculated.

6. The matrix system is solved for the dimensionless normalized potential $w_{i,j}^{v+1}$. The matrix solver used in the model was developed by *Brand et al.* **(1992)** at Stanford Univeristy. The iterative method of solution of the matrix allowed for a maximum of **30** iterations.

7. Convergence is verified for every i,j dimensionless potential and the wellbore liquid height normalized by the initial height:

$$\left| W_{i,j}^{v+1} - W_{i,j}^{v} \right| \leq \varepsilon, \qquad \text{and} \qquad \frac{\left| H_{w_D}^{v+1} - H_{w_D}^{v} \right|}{H_{o_D}} \leq \varepsilon \qquad (4.9.3)$$

where ε is an arbitrary small number that may be choosen as **an** input in the program.

8. If convergenceis not acchieved, H_{D_i} is recalculated based on potential calculated in the free surface layer:

$$H_{D_i} = W_{i,1} \times H_{o_D} \qquad (4.9.4)$$

In this case, the liquid gradient is assumed to be static.

9. The wellbore liquid level H_{w_D} and the dimensionless potential at the sandface W_{w_j} are updated and all other matrix and Jacobian coefficients are recalculated.

10. The procedures from **2** to **9** are repeated untill convergence is obtained. If convergence is not achieved within a given maximum number of iterations, or if the matrix calculation algorithm requires more than the prescribed number of iterations, the program reduces the time-step size and the calculations restart using the values calculated in the previous time-step.

11. After convergence, new block thicknesses are calculated as follows:

$$\Delta z_{D_i} = \frac{H_{D_i}}{n} . \qquad \textbf{(4.9.5)}$$

12. Interpolate the potential distribution for the new blocks, and update the geometrically dependent parameters such as permeabilities in the direction of flow, average thicknesses, geometrical factors based on the slope corrections for transmissivity and inter-layer distances.

13. The radial number of blocks included in the computation is checked for the necessity of incorporating one more column of blocks. The blocks located at the last column considered in that time step are verified to have a potential drop greater than an arbitrary small number. An additional column of blocks is added if at least one outer boundary block starts to be sensitive to the potential drops.

14. Restart a new time step following the procedures from **1.**

In App. E, a detailed description of the computer program is presented, as well as the code list. We turn now to operation of the *Stream Layer Model* and verification of results in Chapter **5.**

Chapter 5

Verification of the Numerical Model

The Stream Layer Model was compared with classical solutions in the groundwater literature, and the results were consistent with available data and traditional methods found in the literature. The best way to verify the wellbore response was to compare the simulator results with steady-state experimental model results performed by *Wyckoff et al.* **(1932)** and ***Hull*** **(1955).** The transient response at observation wells far from the producing wellbore were checked by comparing the simulator results with a classical groundwater method by *Neuman* **(1972,** 1974), and a numerical solution by Cooley **(1971).** Also, simulator results were compared with the *Theis* **(1935)** compressible flow line source solution and the p^2 transient solution derived by **Barney** *et al.* **(1989)** to approximate the gravity drainage problem with a free surface. The analyses were done for an isotropic reservoir $(k_h = k_v)$ using original data from the references above.

5.1 Verification with Wyckoff, Botset and Muskat Experiments

Wyckoff et al. **(1932)** investigated the *Dupuit* solution for steady-state gravity drainage flow into a well by means of an experimental sandbox apparatus which is briefly described in Ch. **2.** The experiments consisted of several runs at different steady state flow conditions, in which measurements of the head potentials used manometers at the bottom of the sand, and visual inspections of the liquid levels. In the experiments where the sand levels were much above the original liquid levels at the outer boundary, the free surface position was masked by the presence of the capillary fringe. The flow in the capillary fringe was detected by tracing streamlines with ink.

When the capillary fringe was absent, the experimental results verified the *Dupuit* equation to approximate the head distribution at the bottom of the sand, although there were some errors involved in the following assumptions: (a) the liquid moves towards the well in cylindrical shells, and (b) the slope of the free surface was so small that the square of dh/dr could be neglected. Those errors seemed to compensate each other in such a way that Eq. 5.1.1, intended to give the free surface position distribution, was shown to approximate the liquid head at the bottom of the sand:

$$h_o^2 - h^2 = \left(\frac{q}{\pi k \rho \frac{g}{g_c}} \right) \ln \frac{r}{r_e} \qquad (5.1.1)$$

To compare with the *Wyckoff et al.* results, the Stream Layer Model was run from an undisturbed initial condition until reaching steady-state. The permeability for Run No. 11 was determined using Eq. 5.1.1 and a plot of $(h_o^2 - h_n^2)$ versus $\ln r/r_e$. To avoid capillary fringe effects in Run No. 11, the top of the liquid was set at the top of the sand level in the sandbox, and the pumping flow rate was kept small enough to avoid a large cone of depression above the free surface. Based on the *Wyckoff et*

point	r (cm)	well head (cm)	A
well	6.4	32.50	0.0700
r_1	10.2	33.50	0.0691
r_2	15.3	34.20	0.0663
r_3	20.3	34.80	0.0654
r_4	25.3	35.30	0.0651
r_5	30.5	35.85	0.0674
r_6	35.6	36.20	0.0676
r_7	40.6	36.60	0.0703
r_8	45.7	36.80	0.0691
r_9	50.8	37.00	0.0684
r_{10}	55.8	37.20	0.0685
r_{11}	66.0	37.60	0.0704
r_{12}	76.2	37.80	0.0663
r_{13}	86.4	38.10	0.0681
r_{14}	96.5	38.30	0.0662
r_{15}	106.7	38.40	0.0581
r_{16}	116.8	38.70	0.0662
r_{17}	127.0	39.10	0.1403
r_{18}	137.2	39.10	0.0876
r_{19}	147.3	39.30	
r_{20}	156.0	39.30	

Table 5.1: Determination of the average constant **"A"** from the experimental Run No. 11, using the Dupuit approach.

al. observations, the *Dupuit* approach may be used to calculate the permeability by averaging the values of a constant **"A"** (see Tab. 5.1) defined as:

$$A = \frac{q \ln\left(\frac{r_e}{r_n}\right)}{h_o^2 - h_n^2} \tag{5.1.2}$$

from which the permeability k was calculated in mD with respect to the 15" sector ($1/24^{th}$ of a complete 360" cylinder):

$$k = \frac{(1000)\,(24)\,\mu}{\pi\,\rho\,\frac{g}{g_c}}\,A \tag{5.1.3}$$

For the units used in the experiments, and assuming a liquid viscosity of 1 cp in view of the lack of information about the temperature of the system, Eq. 5.1.3 simplifies to $k(mD) = 7,875,709A$. From the average computations of Tab. 5.1, a permeability of approximately 530,000 mD was calculated for the experiment of run No. 11.

To match Run No. 11, no capillary fringe ($h_c = 0$) was considered in the *SLM*. The results presented in Tab. 5.2 show good agreement of the liquid heads measured at the base of the sand at a steady-state condition with the head potentials calculated by the simulator.

Runs No. 18 and No. 19 were selected to further verify the *SLM*, because of the conditions of flow, where both capillary effects and high vertical velocities were present. The permeability used in the calculations was the same obtained from the experiment Run No. 11. In addition, the only informations available in the paper about the liquid levels observed in the sandbox were those correspondent to Runs No. 18 and No. 19, shown in Fig. 3 in *Wyckoff et al.*. There was no information about the free surface position in *Wyckoff et al.*, but only about the liquid top level (including the capillary fringe) and the liquid heads at the sand bottom. Table **5.2** shows the results of the experiments compared to the results of the simulator. There are acceptable differences of no more of 8 % in the worst case. **A** plot in Fig. 5.1 shows the observed liquid top position measured directly from Fig. **3** in *Wyckoff et al.* paper, compared with the results from *SLM*.

In the runs presented in Table 5.2, the grid dimensions were those that provided the best fit with the experiments within a reasonable computing time. Also, a no-flow sandface region estimated at about 1 cm, located at the free surface intersection, was considered, due to surface tension effects theoretically expected and confirmed by the *Hull* (1955) work. This restriction in the upper region of the seepage face becomes important when the vertical scale is reduced, as in Run No. 19. In Run No. 19, the no-flow region could represent 10% of the well liquid level in the reservoir at the sandface.

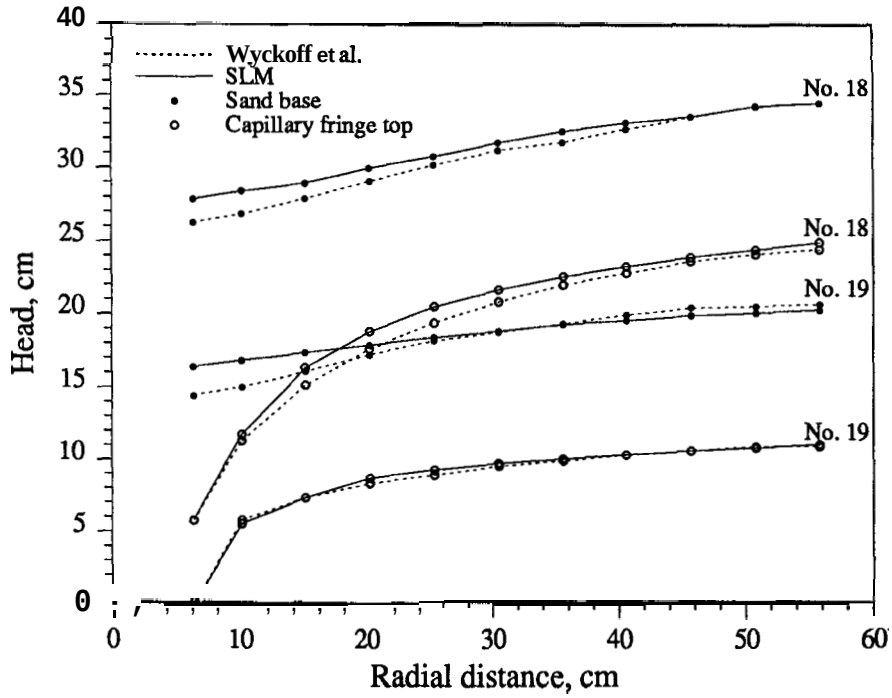

Figure 5.1: Liquid levels and heads in the sand model by *Wyckoff* **et** *al.* compared to the SLMresults of runs 18 and 19.

5.2 Verification with the Cooley and Neurnan Solutions

Cooley (1971) solved a problem of gravity drainage dedicated to interference testing numerically neglecting wellbore effects. He applied a finite difference method to solve an integral of the non-linear partial differential equation obtained by the divergence theorem. Also, the **Cooley** model considered the influence of capillary pressure in the unsaturated region in the capillary fringe. His results, compared with the *Boulton* (1963) convolution integral solution, show that the influence of the capillary fringe is negligible at field scale. The **Cooley** results used in the present comparison were obtained directly from the figures in the paper.

		Run No. 11			Run No. 18			Run No. 19		
Point	r (cm)	Wyc.	SLM	%	wyc.	SLM	%	wyc.	SLM	%
well	6.4	32.50	32.50	+0.00	5.80	5.80	+0.00	+0.00	0.00	0.00
1	10.2	33.50	33.58	+0.24	11.30	11.75	$0.40	5.80	5.53	-4.65
2	15.2	34.20	34.50	+0.88	15.10	16.29	+7.88	**7.30**	**7.30**	+6.71
3	20.3	34.80	35.13	+0.95	17.60	18.78	+6.70	8.30	8.68	+4.58
4	25.4	35.30	35.62	+0.91	19.40	20.47	$5.51	8.90	9.26	+4.04
5	30.5	35.85	36.02	+0.47	20.80	21.64	+4.03	9.50	9.70	+2.10
6	35.6	36.20	36.35	+0.41	22.00	22.56	+2.54	9.90	10.04	+1.41
7	40.6	36.60	36.62	+0.05	22.80	23.26	+2.02	10.30	10.33	+0.29
8	45.7	36.80	36.87	+0.19	23.60	23.88	+1.19	10.60	10.59	-0.09
9	50.8	37.00	37.27	+0.73	24.10	24.41	+1.29	10.90	10.82	-0.73
10	55.8	37.20	37.26	+0.16	24.40	24.87	$1.92	10.90	11.02	$1.01
q (bbl/D)		139.6	136.10	-2.48	284.3	283.9	-0.14	75.5	75.4	-0.13

Table 5.2: Heads (cm) at sand base from *Wyckoff et al.* experimental results compared with the *Stream Layer Model.*

Neuman (1972) used the same synthetic data as *Cooley* to verify his analytical approach not considering the influence of the unsaturated region, and concluded that capillarity "... has very little influence on the time-drawdown response of unconfined aquifers during gravitational drainage". Later, *Neurnan* (1974) extended his work to partially penetrating wells. A computer program related to the prior solution, kindly furnished to us by *Neurnan,* was applied to generate the present results for comparison. The *Cooley* data, summarized in the following, were used to calculate the head drawdown response at two different radial positions far from the wellbore center. In the example, the two observation points were selected at radial distances of 44.9 and 101.1 ft respectively, to avoid wellbore storage effects, not considered in the Cooley, *Boulton* and *Neuman* solutions.

The reservoir parameters were estimated from this data - see App. B:

(a) Reservoir porosity ϕ:

$$S_y \cong \phi_e \quad \Rightarrow \quad S_y = 0.23 \quad \Rightarrow \quad \phi = \phi_e = 0.23, \quad \text{for} \quad S_{w_r} = 0$$

constant pumping rate, q	**302** gpm **(10,354** BPD)
original height, H_o	**59.5** ft
pumping wellbore radius, r_w	**0.53** ft
storage coefficient, S	**0.034** (dimensionless)
transmissivity, T	**89,250** gpd/ft
specific yield, S_y	**0.23** (dimensionless)

Table **5.3:** Data from **Cooley (1971)**

(b) Total Compressibility c_t:

$$S_s = \rho g \phi (c_w + c_f) = \rho g \phi c_t \quad \text{[Cooley (1971), Eq.2]}$$

$$S_s = \frac{S}{h_o} = \frac{\mathbf{0.034}}{\mathbf{59.5}} = 0.0006\ \text{ft}^{-1}$$

Using appropriate units: $c_t = 0.006\ \text{psi}^{-1}$

(c) Reservoir permeability $k_h = k_v = \mathbf{k}$ (single phase isotropic reservoir):

$$T = \frac{kh_o}{\mu}\left(\rho\frac{g}{g_c}\right) = \mathbf{89{,}250}\ \text{gpd/ft} \quad \Rightarrow \quad \boldsymbol{k = 73\ \text{D}}$$

The Stream Layer model (SLM) was run using the above set of data translated from groundwater parameters to equivalent reservoir properties used in petroleum engineering. The mean radial drawdown $\bar{s}(r)$ was computed by averaging the head potentials along the the entire thickness at each radial position of the observation wells, while $s_b(r)$ and $s_h(r)$ were the head drawdowns at the lower boundary and free surface, respectively. The results presented good fit and coherence as observed in the figures below. Also, the applications of the **Ramey** *et al.* simplified analytical solution showed about the same results as the *Theis* line source solutions at early times, but

became closer to the Stream Layer Model as time increased. At late times, a log-log plot correlates the points closely such that it is difficult for one to observe any difference between all these methods. See Fig. **5.2** and **5.4.** behavior. The semilog graphs in Figs. **5.3** and **5.5** are better for an accurate view of the late time potentials.

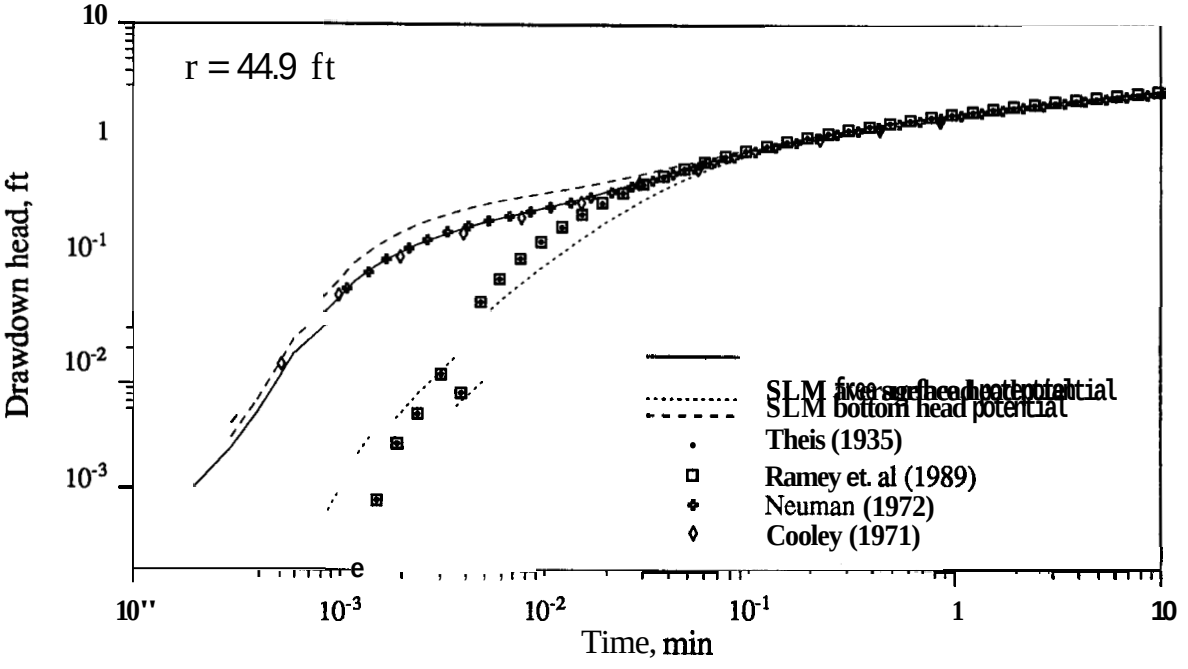

Figure **5.2:** Stream Layer Model compared to *Cooley, Theis* , *Ramey et ak.* and *Neuman.* Observation well at **44.9** ft. Log-log plot.

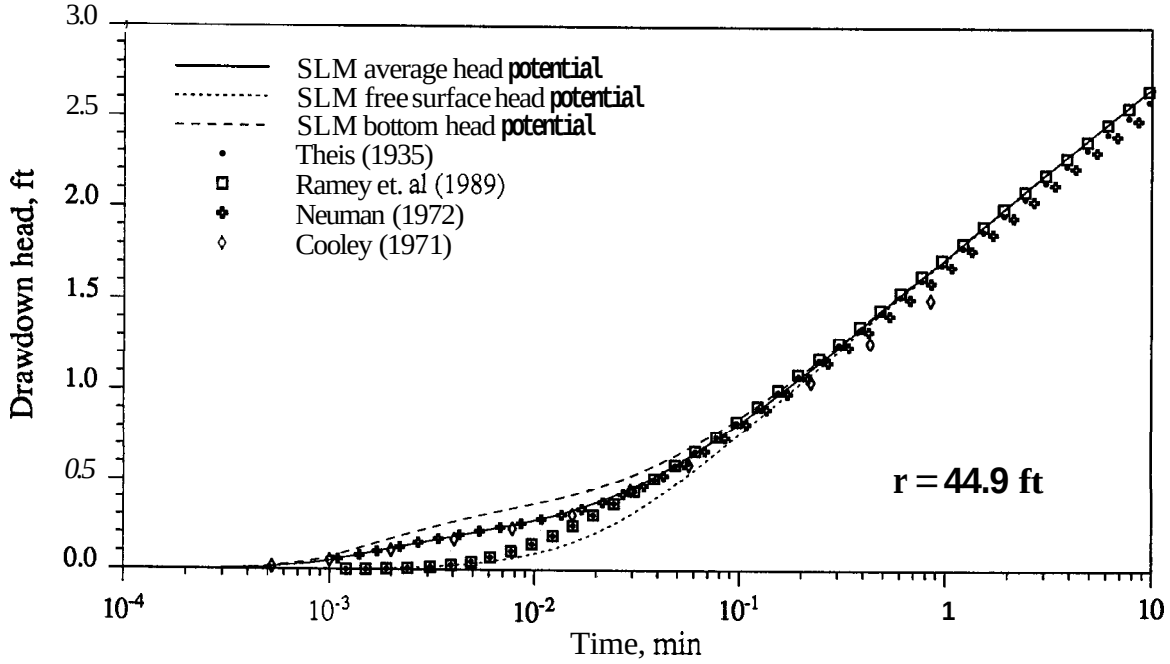

Figure **5.3:** Stream Layer Model compared to *Cooley, Theis* **,** *Barney et al.* and *Neuman.* Observation well at 44.9 ft. Semilog plot.

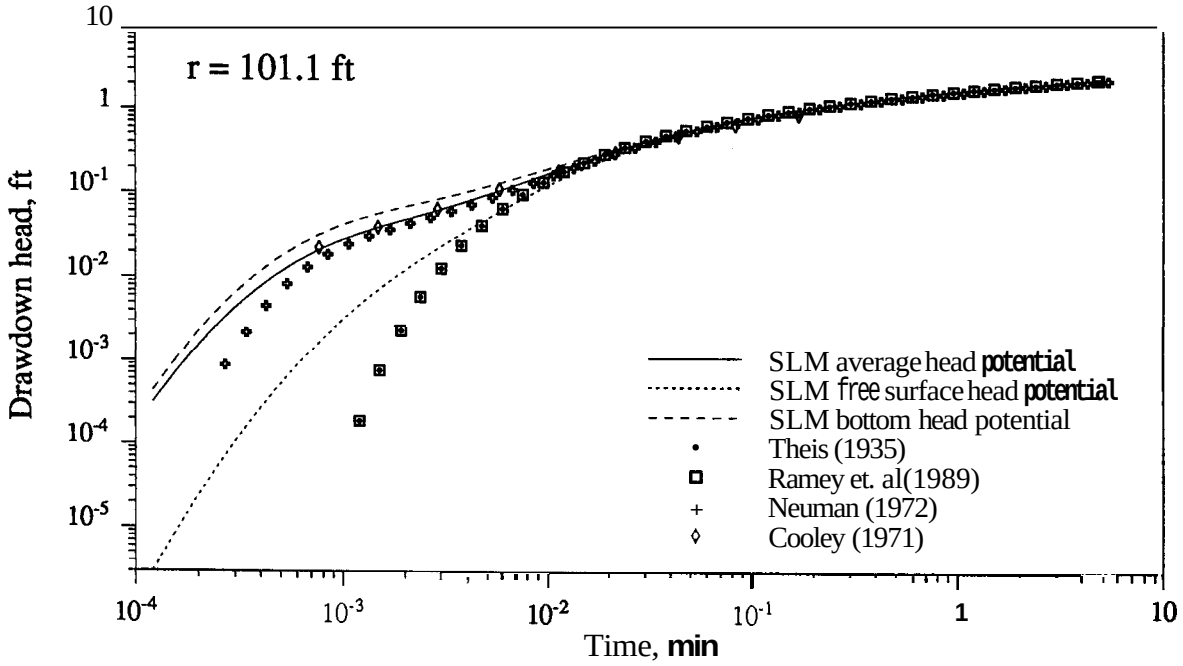

Figure **5.4:** Stream Layer Model compared to *Cooley, Theis* **,** *Barney et al.* and *Neurnan.* Observation well at 101.1 ft. Log-log plot.

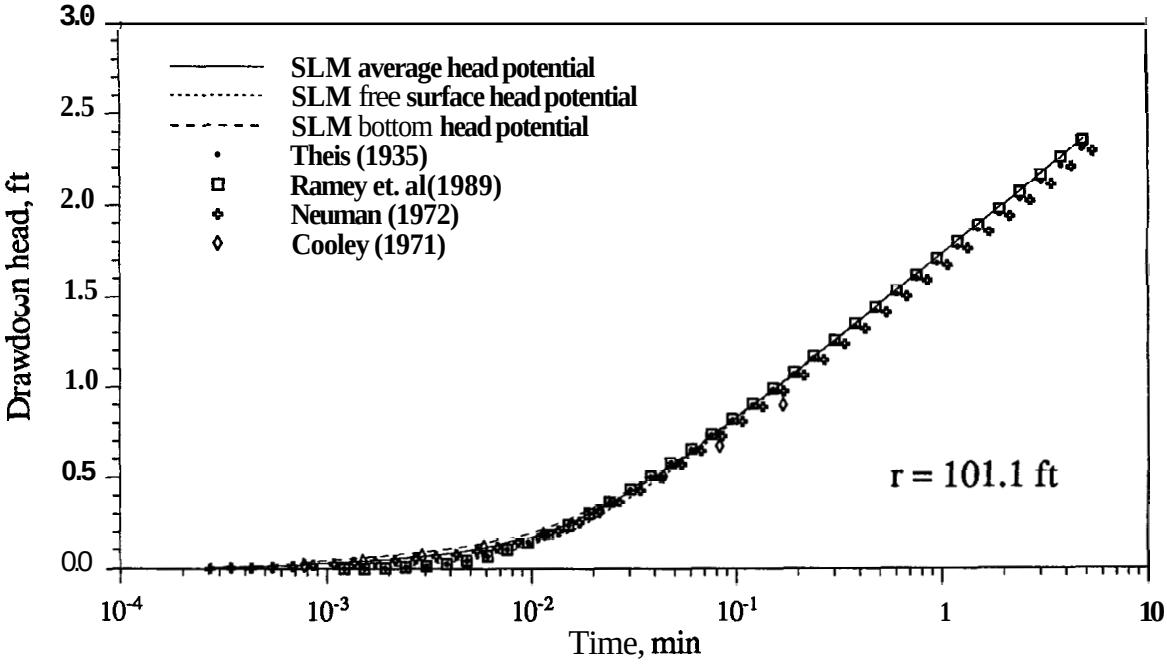

Figure 5.5: Stream Layer Model compared to Cooley, *Theis*, Ramey et *al.* and *Neuman.* Observation well at 101.1 ft. Semilog plot.

5.3 Verification with Hall Sandbox Experiments

Another verification compared the *SLM* with the experiments by ***Hall*** (1955). He performed measurements using a specially designed sandbox apparatus according to Fig. 2.1 in the Literature Review chapter reproduced from the *Hull* (1955) paper. As referenced in Ch. 2, there were four series of tests executed under different conditions, summarized below:

- Series A:

  Greatest degree of saturation, close to an ideal condition; increasing flow rate, steady-state steps.

- Series B:

  Non-uniform distribution of air voids in the sand by natural re-saturation; decreasing flow rates at each steady-state step.

- Series C:

  Tests executed in reverse order of series B; better saturation conditions.

- Series D:

  Same conditions as in series C, but using reduced surface tension water by chemical treatment.

The experiments of series **A** were selected to be compared with the *SLM*. The basic data were:

(a) Permeability from direct measurements:

$$k = 0.460 \text{ cm/s} \Rightarrow 453,000\text{mD}$$

(b) Water viscosity [1] at the experiment conditions:

Test No.	Temperature ("C)	Viscosity (cp)
1	26.8	0.86
2	28.5	0.82
3	29.0	0.81
4	29.1	0.81
5	29.5	0.81
6	29.2	0.81
7	29.5	0.81
8	29.6	0.80

(c) External radius: $r_e = 197.6$ cm

(d) Wellbore radius: $r_w = 12.2$ cm

(e) Porosity: $\phi = 0.40$

(f) Constant external liquid head: $H_o = 122$ cm

[1] Calculated by interpolation in Table **6-4** from ***Amyx et. al* (1960)**

	A-1	A-2	A-3	**A-4**	A-5	A-6	A-7	**A-8**
grid N	10	12	14	16	20	24	31	34
H_w *(Hull)*, cm	106.4	91.2	76.0	60.8	45.6	30.4	15.2	0
H_w (SLIM), cm	107.3	93.3	77.2	61.2	45.6	30.8	15.2	0
% Diff.	+0.85	+2.30	+1.58	+0.66	0	+1.18	0	0
Q *(Hull)*, BPD	1082	2100	2960	3613	4160	4500	4773	-
Q (*SLM*), BPD	1082	2100	2960	3613	4141	4500	4764	4849
% Diff.	0	0	0	0	–0.46	0	–0.19	-
H_s *(Hull)*, cm	110.7	104.3	94.5	90.2	86.4	84.8	83.3	83.3
H_s *(SLIM)*, cm	112.8	104.0	95.7	90.2	86.5	84.3	83.0	82.6
% Diff.	+1.90	–0.29	+1.27	0	+0.12	–0.58	–0.36	–0.84

Table 5.4: SLMresults compared to the ***Hull*** series A experiments.

(g) Capillary fringe thickness: $h_c = 8.9$ cm

(h) Residual liquid saturation (assumed): 20%

The *SLM* steady-state runs were obtained by establishing both a constant rate, and the corresponding measured wellbore liquid height. The vertical blocks were sized according to the gradient developed in the sand, looking always for the best fit to the data, and keeping the number of radial cylindrical blocks constant at 12. Each run started from **a** rest (flat liquid table) condition and produced at a constant rate until reaching a steady-state. Eventually, the wellbore pressure reached the value in the experiment, then that pressure was fixed and the simulator switched to a constant pressure inner boundary condition, re-calculating the flow rates at the wellbore. See cases A-5, **A-7,** and A-8 in Tab. 5.4.

Series A-6		Bottom			Free Surface		
Node	Dist., (cm)	Hall	SLM	Diff.,(%)	Hall	SLM	Diff.,(%)
w	11.68	30.48	30.84	+1.18	84.8	84.31	–0.58
1	14.02	38.10	36.74	–3.55	86.9	84.59	–2.66
2	19.20	52.83	49.83	–5.68	90.0	85.11	–5.43
3	26.52	66.29	63.04	–4.90	93.5	87.06	–6.89
4	36.58	78.74	75.60	–3.99	97.3	90.19	–7.31
5	51.51	89.92	87.59	–2.54	101.4	95.49	–5.83
6	71.63	99.06	97.76	–1.31	105.8	101.51	–4.06
7	96.62	106.43	105.91	–0.49	110.7	107.47	–2.92
8	121.92	111.76	111.61	–0.13	114.2	112.24	–1.72
9	146.61	115.57	115.80	+0.20	116.7	116.03	–0.57
10	171.6	119.13	119.20	$0.06	120.1	119.18	–0.77

Table 5.5: Comparison of potential heads between the ***Hall*** sandbox experiments and *SLM* $(M = 12, N = 24)$, series A, Test No.6

From the results of Tab. 5.4, good agreement was found between the numerical and the experimental methods. All the compared heads and flow rates were fitted with less than 3% error in the worst case. The greatest differences were observed in calculated and measured free surface positions along the radial distance, **as** shown in Tab. 5.5, for the series A-6 experiment. As a conclusion, since the discrepancies were within acceptable errors, the Stream Layer Model can be considered verified with the results contained in the present chapter.

In the next chapter, the sensitivity of the *Stream Layer Model* to the grid and time-step dimensions are studied.

Chapter 6

Sensitivity

In this chapter, some practical aspects of the *SLM* program regarding the simulation approach in wellbore drawdown or buildup pressure behavior will be analyzed, specially the model dimensioning of grid blocks and time-steps. The major difficulty is to handle non-linearities that occur throughout the reservoir, but are stronger around and at the inner boundary sandface. In some previous models, simplifications were made to avoid this difficulty which limited applications to regions sufficiently far from the well, or to small flow rates to assure compatibility with some assumptions.

The *SLM* is a finite-difference model that is able to simulate both pumping and observation wells, even those cases that generate large free surface drops. Nevertheless, widely-known restrictions of radial numerical models are still present and amplified by the non-linear characteristic of the mathematical problem. Stability, convergence and accuracy criteria follow characteristics similar to those of standard confined two-dimensional radial numerical models, tempered by difficulties introduced by the seepage face boundary condition.

6.1 Grid Block Dimensioning

The effects of grid sizing were determined by runs of several configurations of grid dimensions, fixing one direction, and varying the other. A large number of runs was performed from 20 to 60 radial blocks, and 60 to 100 vertical blocks, some results of which are presented in Figs. 6.1 and 6.2. The reservoir and production characteristics were kept constant throughout, and were selected for the present investigation from a field example summarized in Table 6.1. For the radial grid spacing, the *MULTIMODAL* method (*Terán* and *de la Garza* - 1988) was adopted, using a ratio of $4x10^5$ between the first and last radial block dimensions. This ratio was obtained by successive experimental runs in order to get large storage for the first column of blocks (containing the sandface) and keep a logarithmic spacing. An infinite reservoir was simulated by setting the external radius far enough that drawdown effects were not evident.

External dimensionless radius, r_e/r_w	10^6
Initial liquid level at rest	189 ft
Isotropic permeability (single phase)	80 mD
Liquid viscosity	1 cp
Liquid compressibility	$3x10^{-6}psi^{-1}$
Skin	0
Formation compressibility	0
Liquid density	**62.4** lb/ft^3
Formation volume factor	1.0 res vol/std vol
Production flow rate	250 bbl/day
Porosity	0.25
Residual saturation in the desaturated region	0

Table 6.1: Basic input data for the sensitivity runs

The numerical treatment of the partial differential equations in the gravity flow

problem introduces discretization errors in the potential solutions that normally tend to decrease with grid refinement. Grid dimensions affected the potential response immediately after the wellbore storage period when unconfined flow behavior became effective. In the examples of Fig. 6.1 and Fig. 6.2, the potentials in the wellbore show a considerable displacement at the beginning of the desaturating period, while at late times, the solutions tend to approach each other.

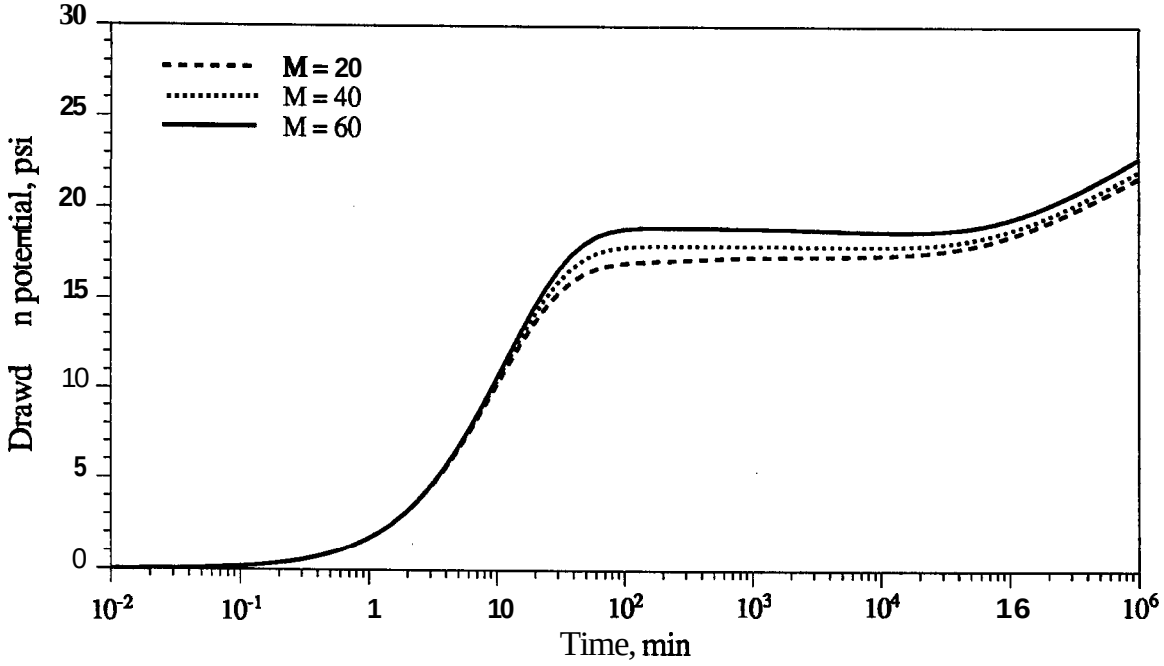

Figure 6.1: Radial mesh variation, 100 vertical grid blocks

Figures 6.1 and 6.2 show semilog plots of the wellbore pressure drawdown comparing the effect of grid size on the simulator response for a range of grid sizes which produced acceptable computing times. The results produced larger sensitivity of the model to the vertical mesh size than to the horizontal mesh size, because pressure gradients were larger in the vertical direction. The most important deviations were observed during the formation of the desaturating cone demonstrating that gross vertical block dimensions sensibly modify the numerical results of the vertical flow around the wellbore in this period.

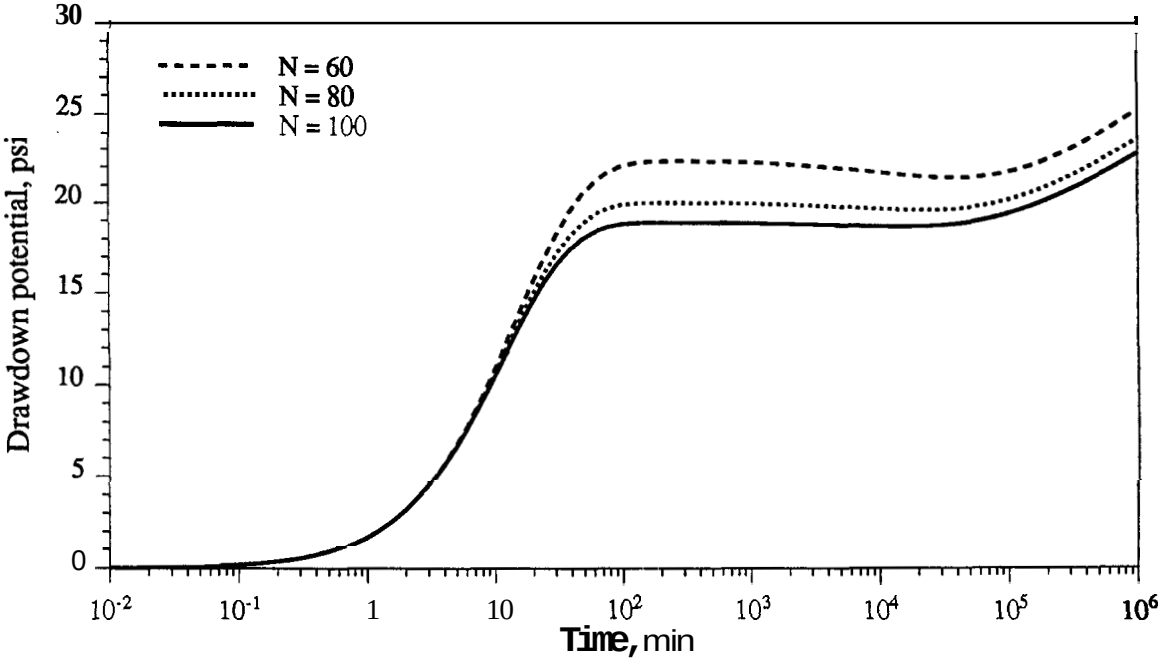

Figure 6.2: Vertical mesh variation, 60 radial grid blocks

An obvious but important limitation to grid refinement is computing time. For a very fine grid mesh, the CPU time becomes prohibitive to reach long drawdown or buildup times. Since we are concerned with the wellbore response, **an** additional difficulty is the fact that the desaturating period is sometimes long requiring that wells reach pseudo-confined behavior after months or years of pumping.

Some reservoir property relationships in the groundwater literature, mainly the *Boulton* parameter $\beta = k_v/k_h(r/h_o)^2$, are related to the time when the unconfined period is followed by the pseudo-confined period, as observed from the *Boulton* (1963) and *Neuman* (1975-a) type curves. According to these approaches, when the potential drawdown starts following a pseudo-radial solution, the dimensionless time increases as β decreases. In the wellbore ($r = r_w$) for example, practical values of β are much smaller than 0.001, the lowest value shown in the type-curves. As a consequence of the delay of the pseudo-radial response, simulation of the flowing period requires long production time, sometimes taking months of producing time. However, at late

times when the potentials near the well have large changes, computations require long computing time for the reduced time-step required by the numerical solution. Since the grid blocks around the well start having large variations in the potentials, the combined effects of geometry and time-step sizes influence computation performance.

To recall some calculation procedures of the program, the Jacobian matrix is solved iteratively in the Newton method. Only part of the blocks are included in the simulation at the beginning. Those located in the reservoir region affected by the production are included. Since the potential perturbation far from the wellbore is less than an arbitrarily small value, it is not necessary to include distant grid blocks in the calculations, thus saving computing time. The matrix solver requires approximately 80 to 93% of the computing time to calculate a complete iteration loop depending on the number of vertical and horizontal grid blocks. The number of vertical grid blocks is the most important factor due to the correspondence with the bandwidth of the matrix, according to the formulation of the matrix solver.

To give an idea of computing times, let us consider the examples in Fig. 6.2. For a fixed number of 60 horizontal grid blocks, a total of 184 CPU minutes were required for a complete run with a 60-vertical block mesh, and 318 CPU minutes were required for a 100-vertical block mesh to reach a total production period of 10^6 minutes. This was the pumping time required to get about one complete log-cycle of pseudo-radial drawdown behavior. The total number of matrix calculations was 25,338 for the 60-vertical block case, and 20,816 calculations for the 100-vertical block mesh. In this example, these numbers show that although the number of blocks is increased the number of iterations is reduced, the total computing time is still increased. These results were obtained with a DEC SYSTEM 5000/240 computer.

6.2 Time Weighting and Time Step Length

A strong reason for errors in the numerical model is the linearization imposed on the non-linear problem. As a consequence, accuracy is related to the time-step size and the time-interpolating parameter, besides the grid mesh size. The time-interpolating parameter is important, and gives the degree of implicitness of the unknowns. In the mathematical formulation of the present numerical approach, the potential variation during a time-step is assumed linear, and the calculation of the material balance for an element considers a constant time weighting factor θ:

$$\theta\left[q_{in} - q_{out}\right] + (1-\theta)\left[q_{in}^{k} - q_{out}^{k}\right] = \frac{\Delta V}{\Delta t} \qquad (6.2.1)$$

where k refers to the previous time-step.

Figure **6.3** shows the flux in or out of a grid block element during a time-step from t_k to $t_k + 1$. Depending on the shape of the curve and the time-step size, the flux approximated by linear interpolation may be under or over-estimated. For example, since during the drainage process the difference $q_{in} - q_{out}$ is almost zero (low compressibility systems - saturated region) or negative (free surface region), the material balance error introduced by the linearization may gradually increase when the flux through a block boundary is accelerating, and decrease when the flux is decelerating, as seen in Fig 6.3. At long times, the errors in both directions may compensate or attenuate the apparent deviations from the correct solution.

In the validation runs of the sandbox experiments, as steady-state conditions were reached, the Crank-Nicolson method ($\theta = 0.5$) developed oscillating problems, and a very large number of time-steps was required to avoid oscillations and a large number of low convergence iterations. The fully-implicit scheme in time calculations ($\theta = 1$) was then tested, and after reaching steady-state conditions, stability and convergence were obtained with any time-step size. The drawdown results were a little underestimated, compared with the Crank-Nicolson scheme. Figure 6.4 shows

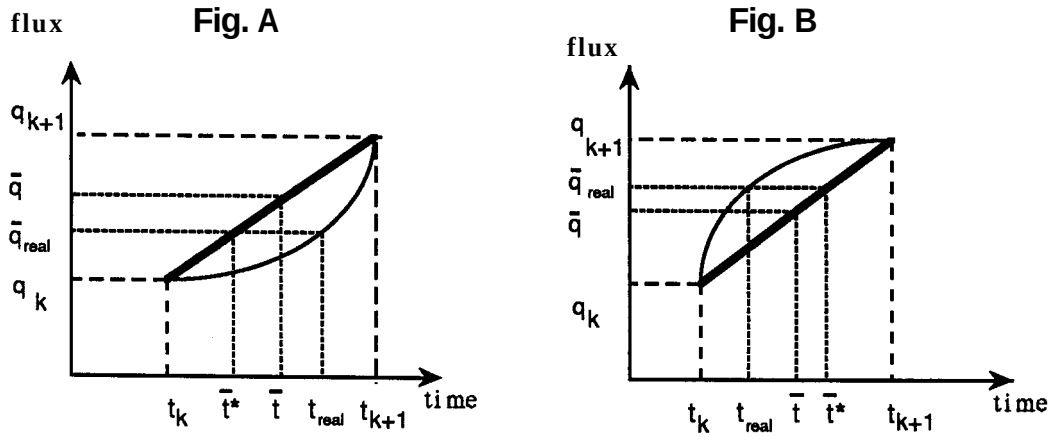

Figure **6.3:** Non-linear flux variation during a time-step. Acceleration and deceleration periods.

a graph containing the same data input run with different interpolation parameters 6. For $6 = 0.5$, the computing CPU time was as high as 900 minutes to reach 10^6 minutes of production time due to the exaggerated number of iterations generated by the oscillation in the results. These oscillations were avoided automatically by reducing the time-step sizes as necessary.

Based on the observations reported in the preceding, practical conclusions are that time-step dimensioning is important for convergence and accuracy, and that the interpolation parameter 6 may vary from 0.50 to 1. However, for improving the computing time, the Crank-Nicolson scheme should sometimes be avoided.

Bearing in mind that at a given time each particular region of the reservoir behaves according to one of three possible flow regimes, namely wellbore storage, desaturating cone, and pseudo-confined, the time-step sizes are dimensioned based on the most unfavorable conditions caused by the rate of potential changes with time. Since small time-steps make the computations long and expensive, some criteria were adopted in

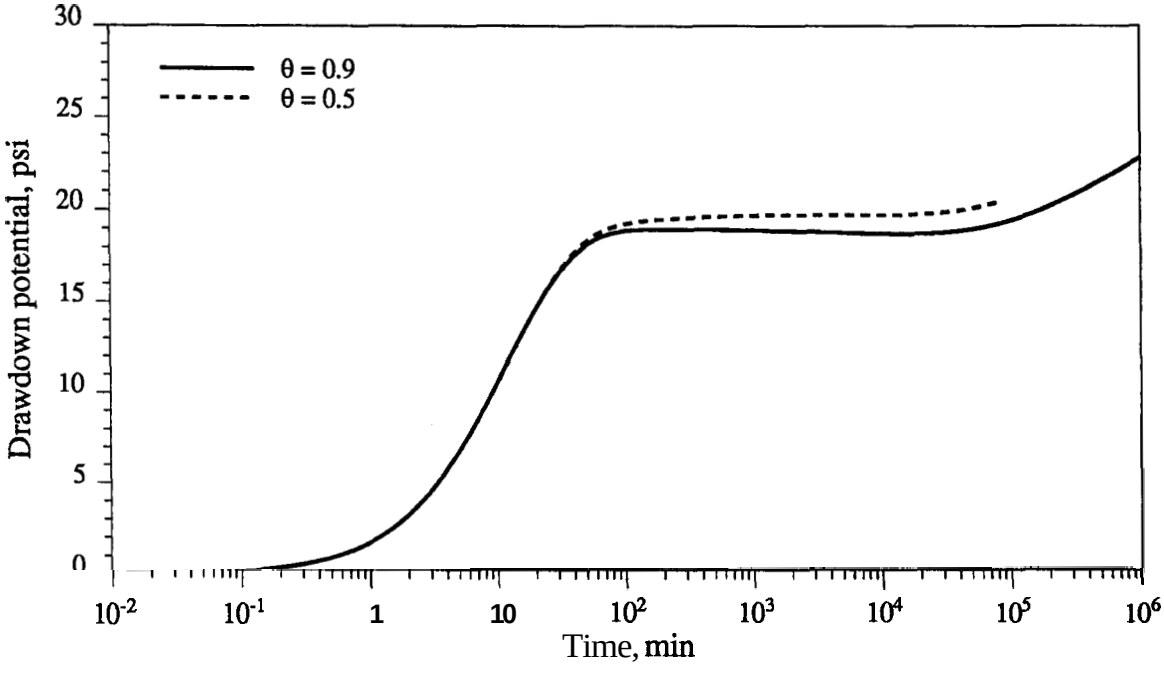

Figure 6.4: Effects of time interpolation parameter in the SLM results

the program to set time step sizes in a range such that time steps were maximum under an accuracy point of view, and minimum to achieve a reasonable computing time.

At early time, during the wellbore storage dominated period, the flow rate variation through the blocks and into the wellbore were similar to that represented in Fig. **6.3-A.** That is, the linearization over-estimates the fluxes in the boundaries $(\bar{q} > \bar{q}_{real})$. Noticeably q_{out} is affected more than q_{in}. **As** a consequence, the calculated drawdown pressures have a tendency to increase further, due to a material balance error. **As** time increases, if the deceleration process (Fig. **6.3-B)** takes over, or a less non-linear behavior starts, the error is reduced. Inside the reservoir, as we go far from the wellbore, the process explained before is repeated at different times and places, but it is really near the well where this phenomenon is most important.

Figure **6.5** is a graph showing the effects of the time-step size in the results during

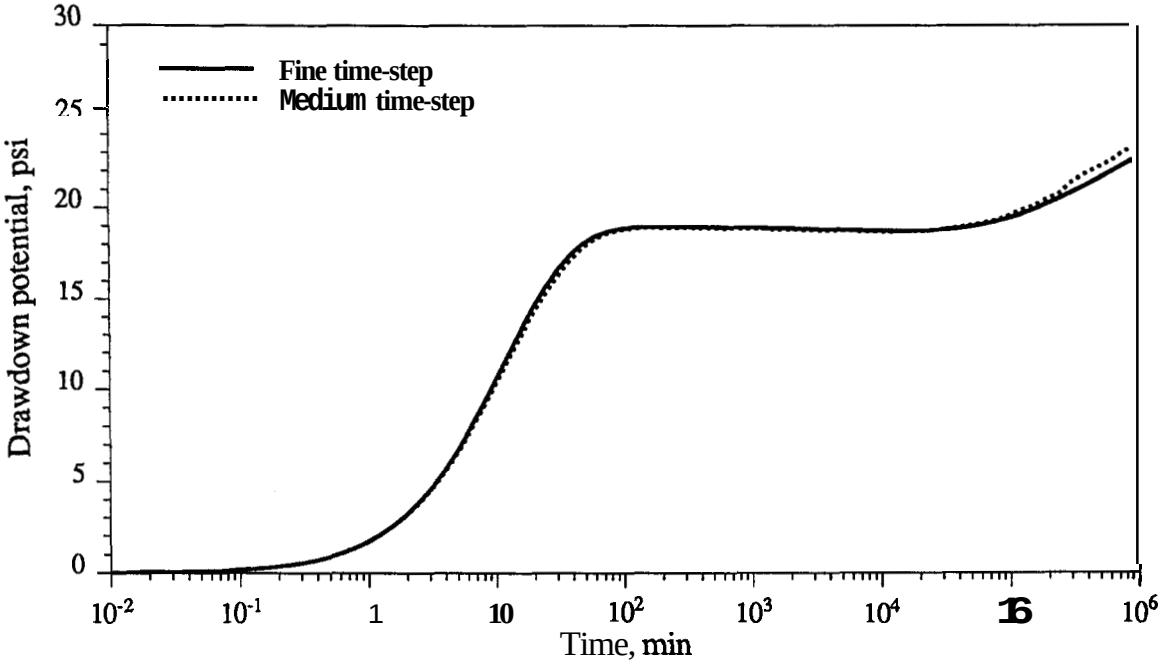

Figure *6.5:* Effects of time-step size in the wellbore potential drawdown

the drawdown period. Three different time-step sizes were compared, and the analytical approach of *Ramey et al.* (1989) was used as a reference. A very large time-step size case did not converge after $t_D = 100$ (not on Fig. **6.5)** when the wellbore storage period had finished and the desaturating surface (free-surface downward movement) started to accelerate. A medium time-step size was used in a second run, and a fine time-step size was used as a reference. The results observed in the plots of Fig. *6.5* were consistent with expectations.

The most critical problem with time-step dimensioning in the given examples starts in the transition between the desaturating and the "pseudo-confined" periods. We define "pseudo-confined" as the drawdown behavior that follows the period in which the free surface downward movement becomes approximately uniform, after the formation of the desaturating cone around the wellbore. In that transition, the pressure drawdown curve inflects upward, and the linearization tends to over-estimate the fluxes (see Fig. 6.3), increasing the pressure drawdown by material balance error

accumulation as observed in Fig. 6.5. Conservative time-steps are recommended during the pseudo-confined period during drawdown or buildup because of the grid block sizes related to the rate of potential change.

An empirical rule of thumb derived from an extensive number of runs is to start runs with a $t_D = 0.01$ for simulating field cases, and $t_D = 0.0001$ for lab experiments, and to increase the number of time-steps per log cycle by 10 or 100 at each new time log-cycle. A key for this choice was to observe the sharpness of the vertical potential gradient in the formation, near the well, and the dimensionless block sizes compared to the fluxes. The lower the mobility k/μ, or the higher the production flow rate, the smaller the required time-step sizes may be.

The time-step size can not be separated from the block sizes since large increases in the time interval may cause problems in stability. The blocks located around the wellbore are those of concern, because they have low storage capacity. The *SLM* simulator has an auto time-step control that helps to guarantee a time-step size reduction at any time when it is necessary. In other words, after a maximum number of iterations, because of problems with matrix solver convergence, lack of convergence in the wellbore pressure calculation, or exaggerated free surface movement, the time-step size control algorithm changes time step sizes gradually until acceptable values dictated by the built-in convergence criteria result. The maximum number of iterations, *itermx*, is generally input data, but can also be a variable in the program. A variable number departing from 3 and increasing by 1 at each new time log cycling has proven to be efficient, avoiding exaggerated reductions in the time-step sizes.

In terms of convergence, buildup behavior is poorer than drawdown behavior. As seen in Ch. 7, the late time potential buildup behavior is more non-linear than drawdown behavior. Thus, the time-steps must be reduced. Computing time for 10^6 minutes of real buildup, as in Fig. 7.9, takes more than 1000 CPU minutes in an IBM RISC 6000/550, most of them consumed in the late time computations.

In the next chapter, a discussion of the effects of some reservoir properties in production in a gravity drainage well test is presented.

Chapter 7

Discussion

In attempts to analyze drawdown and buildup behavior for a low-pressure production well, it became evident that free surface gravity drainage was a major factor, *Ramey et al.* (1989). A literature review indicated no pertinent interpretative methods in the petroleum literature, and contradictory methods for pumping well data interpretation in hydrology, *Boulton* (1963) and *Neuman* (1975-a,b). There even appeared to be problems with interference data interpretation. Although interference data matched the *Theis* (1935) line source solution, the apparent storativity (or compressibility) from type curve matching was hundreds of times larger than the known compressibility of water. This led some authors to speculate that trapped gas increased apparent compressibility. It appeared to *Ramey et al.* (1989) that using a confined system model was simply incorrect for free surface drainage of *an* essentially incompressible flow system. It is easy to compute that maximum production of water by expansion from a low pressure (100 psi) aquifer is less than 0.1% of the water in place.

It appeared to *Ramey et al.* (1989) that a solution of the Dupuit-Forchheimer equation similar to an early natural gas flow problem by *Jenkins* and *Aronofsky* (1953) could aid understanding. This study showed an incompressible liquid could match the line source solution exactly. However the parameter which appeared in

dimensionless times was not compressibility, but the reciprocal initial head, which is much larger than the compressibility of water for a low pressure system.

During analysis of the Dupuit-Forchheimer problem, review of the *Wyckoff et al.* (1932) study convinced *Ramey et al.* (1989) that the Dupuit-Forchheimer model violated physical principles and could not match the free surface behavior, or the existence of a seepage face in a producing well. **As** *Muskat* (1937) clearly stated, analytical solution of free surface problem was essentially hopeless. Thus it was decided to produce a finite-difference computer model which could be used for investigation behavior of both producing and observation wells. The report concerns construction of a program capable of solving this formidable non-linear problem.

To explore the characteristics of the *Stream Layer Model* to simulate a gravity drainage well, drawdown and buildup pressure behaviors are presented in this chapter. Also, influences of some parameters were investigated. Skin effect, permeability, flow rate, permeability ratio (anisotropy) and the initial position of the liquid level at rest have been considered in the following sections. A basic set of data used during this study is presented in Table 7.1.

The *Stream Layer Model* (SLM), unlike the available analytical methods in the literature, is able to represent the wellbore and formation pressure (head) behaviors during drawdown and buildup periods, since the most important limitations of this single-phase simulator is the discretization of a numerical solution, regardless of the consideration of unsaturated two-phase flow. Other classical approaches, such as *Theis* **(1935)** and *Ramey et al.* (1989), have been used in this chapter for comparison at late times. Two auxiliary programs, namely *FLIGRAM* and *PDE* were used in some cases to consider the wellbore storage and skin effects in the *Ramey et al.* and *Theis* solutions (see Appendix C). These modifications were not intended to represent the desaturating period, since both *Theis* and *Ramey et al.* neglected the vertical flow in the reservoir.

Dimension for horizontal grid (mdim)	**60**
Dimension for vertical grid (ndim)	100
Initial number of time-steps per cycle (ntd)	10
Initial dimensionless time (tdi)	10^{-4}
Dimensionless external radius (r_{e_D})	10^6
Liquid compressibility (c_L)	$3 \times 10^{-6} psi^{-1}$
Total compressibility (c_t)	$3 \times 10^{-6} psi^{-1}$
Original height of the free surface (H_o)	189 ft
Initial pressure (p_i)	81.9 psi
Well bore radius (r_w)	3.18 in.
Porosity - fraction (ϕ)	**0.25**
Liquid viscosity (μ):	1 cp
Liquid density $(\rho g/g_c)$	**62.4** lbf/ft^3
Formation volume factor (B_o)	1
Skin effect parameter (s)	**0**
Horizontal permeability (k_h)	120 mD
Vertical permeability (k_v)	120 mD
Constant production rate (q)	**100** bbl/d
Time-relaxation parameter $(1 \geq \theta \geq 0)$	0.9
Residual saturation in the desaturating region (S_{r_L})	0
Capillary fringe thickness *(h,)*	0
Error tolerance (ϵ)	10^{-6}

Table 7.1: Basic data used as input to the *SLM*. Equivalent variables used in the program are shown between parentheses.

7.1 Transient Wellbore Pressure Analysis

Using results of the *SLM* simulator, general observations of transient gravity drainage flow into a well are considered in this section, including drawdown and buildup behaviors of a typical oil field well. The basic reservoir properties are shown in Table 7.1. **A** complete run of the *SLM* is described and analyzed in the next subsections.

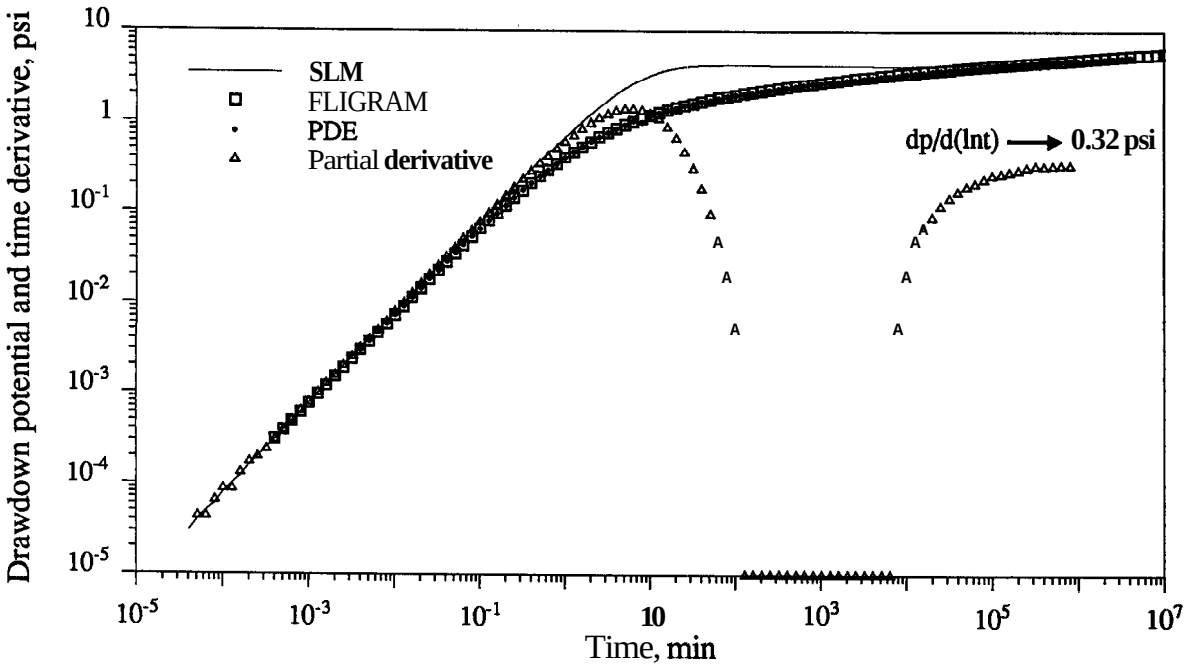

Figure **7.1:** Wellbore flowing pressure and pressure derivative log-log plot.

7.1.1 Drawdown

Figures from **7.2** to **7.7** present the results from the SLM simulator for a flow period of 10^6 minutes (278 days) of a single well located in an infinitely large reservoir. **As** described in several papers in the Groundwater literature, the SLMresults show the same three flow regimes during the flow period, namely wellbore storage, the desaturating and the pseudo-confined or pseudo-radial periods, as observed in Figs. **7.1** and **7.2.**

At the beginning of the flow period, wellbore storage completely dominates during the first minute, according to the log-log plot of wellbore potential vs. time in Fig. 7.1. The potential derivative $\frac{\partial \Delta p_w}{\partial \ln t}$ is also shown in the same graph. From the definition of the dimensionless wellbore storage coefficient in the Petroleum Engineering literature (see *van Everdingen* and *Hurst,* 1949), we present a similar definition based on the liquid level variation in the well:

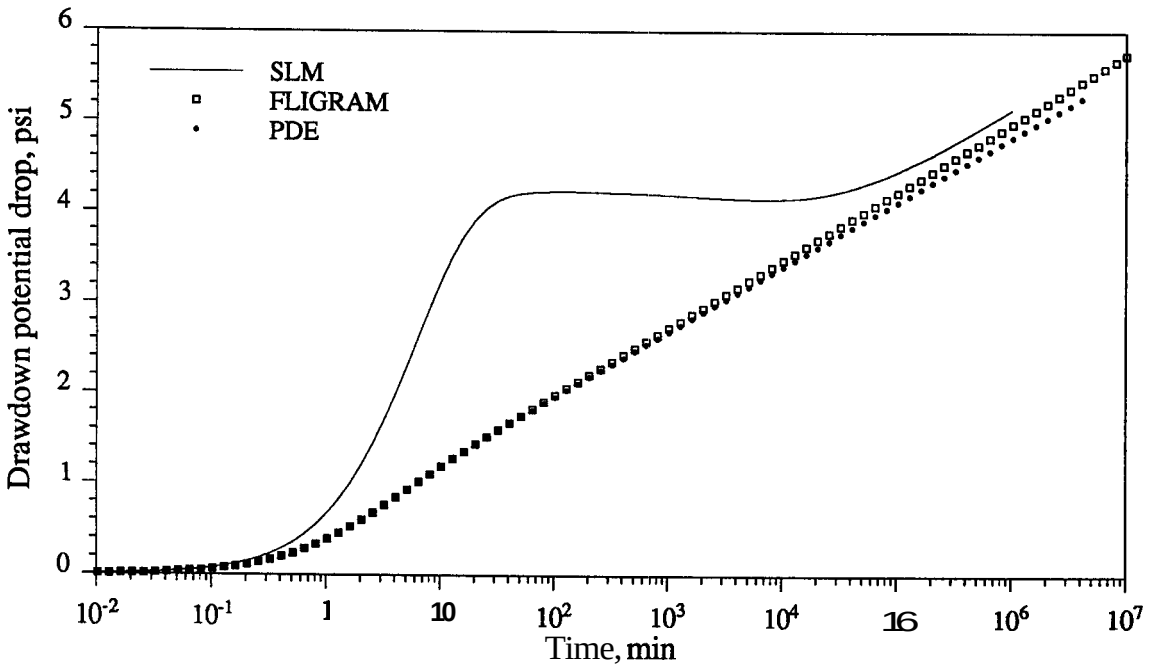

Figure 7.2: Wellbore flowing pressure semi-log graph

$$C_D = \frac{C}{\frac{2\pi\phi r_w^2}{\rho g/g_c}} = \frac{\frac{\pi r_w^2}{\rho g/g_c}}{\frac{2\pi\phi r_w^2}{\rho g/g_c}} = \frac{1}{2\phi} \tag{7.1.1}$$

According to *Agarwal et al.* (1970), the early time dimensionless pressure in the wellbore storage period is:

$$p_{w_D} = \frac{t_D}{C_D} \tag{7.1.2}$$

In the following, we define **a** non-normalized p_{w_D} and re-write the definition of t_D in the Ch. **3** in petroleum field English units:

$$p_{w_D} = \frac{k\,H_o}{(141.2)\,q\,B\,\mu}\,\Delta p_w \tag{7.1.3}$$

and:

$$t_D = \frac{(0.0002637)\, k\, t}{\phi\, \mu\, (1/p_i)\, r_w^2}. \tag{7.1.4}$$

Using time in minutes instead of days, and defining the liquid gradient $\gamma = \frac{p_i}{H_o}$, we combine Eqs. 7.1.3, 7.1.4 and 7.1.2:

$$C_D = \frac{(0.0002637)(141.2)}{(60)} \frac{\gamma\, q}{\phi\, r_w^2} \frac{t'(\text{min})}{\Delta p}. \tag{7.1.5}$$

In the log-log plot of p_w vs. time in Fig. 7.1, we identified a straight line at early times with a unit slope as expected for a pure wellbore storage period. **A** given point at 0.1021 minute corresponds to a pressure drop of 0.0766 psi (values read on the output list of the program). Using the input data of Table 7.1, the resulting dimensionless wellbore storage coefficient was calculated as 0.51, from **Eq.** 7.1.5. This value is very close to the theoretical value of 0.50. We see, then, that due to the wellbore storage effects, the early time line source solution used by *Boulton* (1954-b, 1963) can not be applied here.

As the wellbore storage effects are replaced by the formation response to pumping the well, the potential in the wellbore becomes almost constant, as verified in Figs. 7.2 and 7.1. This is the period during which the desaturating cone is intensely developed around the well, called the "delayed yield" period in the Groundwater literature. **A** first qualitative observation is that the duration of the unit slope straight line corresponding to pure wellbore storage effects in the log-log plot in Fig. 7.1 is greater in the *SLM* solution than in either the *FLIGRAM* or *PDE* solutions. It seems that the formation response is somewhat retarded in the gravity drainage flow into a well, and a very small increase in the wellbore pressure is observed in this example during the desturating period. **A** possible reason for this delayed reservoir response may be a slow development of the velocity gradients after start of pumping. The velocities of the uppermost stream flow lines are dependent on the development of potential differentials caused by the cone of depression around the wellbore. This is different

from the confined elastic system where the stream lines are straight in a vertical cross-sectional view. The pressure derivative goes to negative small values when this phenomenon is observed in this period.

After the desaturating period, the semilog graph in Fig. **7.2** shows a potential behavior in the wellbore similar to the *Ramey et al.* **(1989)** and *Theis* **(1935)** solutions obtained from FLIGRAM and *PDE* programs. This is the pseudo-radial flow or pseudo-confined radial flow period. This behavior occurs when the formation **of** the desaturating cone is stabilized and the flow regime becomes dominated by regions of the reservoir distant from the well where the streamlines are almost horizontal. For a quantitative evaluation of the late time potential response, and for a comparison of the SLMresults with the *Ramey et al.* **(1989)** method, a p-squared vs. semilog time drawdown graph on Fig. **7.3** is presented. In this figure, a late time m-permeability slope value of **114** psi^2/log-cycle was obtained graphically. From the analytical approach, the difference was only **3%:**

$$m = \mathbf{325.2}\ \frac{q B \mu}{k(h/p)} = \mathbf{117.4}\ \text{psi}^2/\text{cycle}.$$

In the traditional semilog *Theis* **(1935)** analysis, the late time pressure drawdown slope in Fig. **7.2** of an apparent straight-line was **0.672** psi/log-cycle, **6.6%** smaller than in the theory:

$$m = \mathbf{(162.6)}\ \frac{q B \mu}{k h} = 0.716\ \text{psi/cycle}.$$

Another quantitative verification was done by calculating the derivative of dimensionless pressure obtained from the dimensional asymptotic value in the graph of **0.32** psi. Based on the input data, the conversion factor for the dimensionless pressure in **Eq. 7.1.3** was **1.606** psi^{-1}. The resulting partial derivative $\frac{\partial p_{wD}}{\partial \ln t_D}$ was **0.51,** very close to the **0.50** in the theory. In fact, it is known that the p-squared solution produces a slightly higher slope than the log approximation of the line source solution.

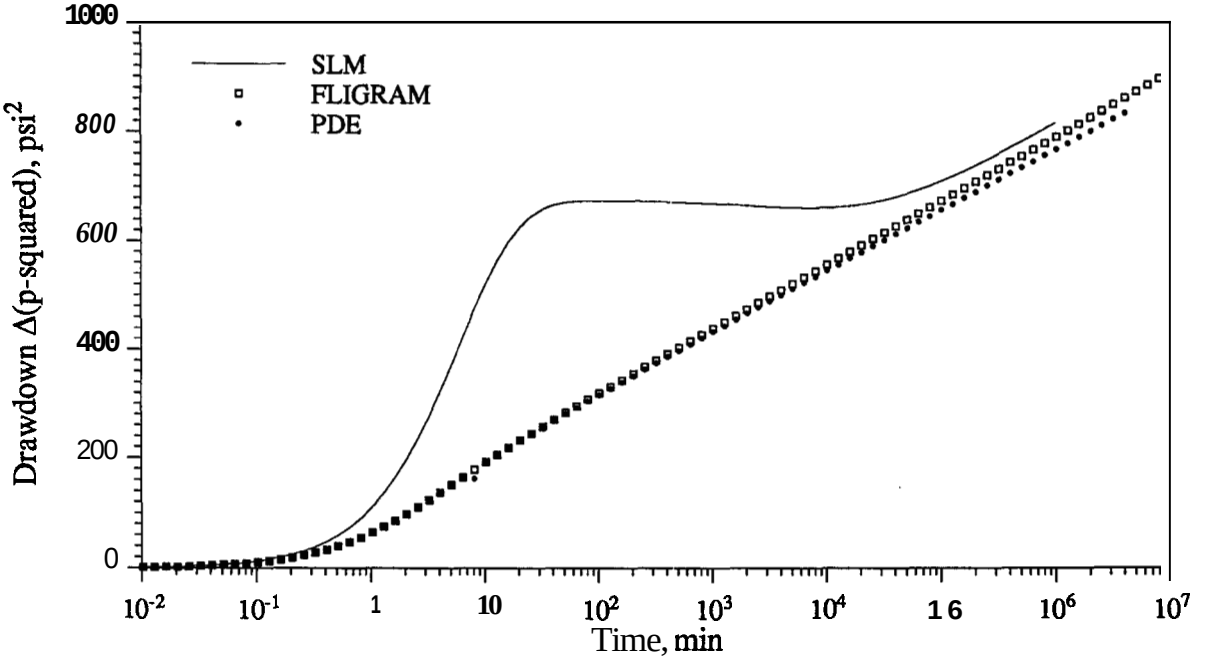

Figure **7.3:** Wellbore flowing pressure-squared semi-log plot

Closer results between the numerical model and the *Barney* ***et al.*** **(1989)** approaches has been found consistently in the present study compared to the *Theis* **(1935)** approach. The agreement, however, is only related to the late time slope of the apparent semilog straight lines. Further considerations about absolute differences are discussed in Section **7.2** in this chapter.

A graph in Fig. **7.4** shows the flow rate distribution along the sandface blocks of the *SLM* for the flow period. Relative flow rate profiles are shown for both the desaturating and the pseudo-confined periods. It may be observed that there is always a concentration of flow in the vicinity of the liquid level in the well indicating high velocities of streamlines in that region. In addition, the flow distribution is more uniform at late times. In all observations, the contribution of the seepage face gradually increases from zero at the free surface position to a maximum value at the wellbore liquid level. The flux variations are small below the liquid level in the wellbore, mainly at late times, as we go far from the liquid level in the well.

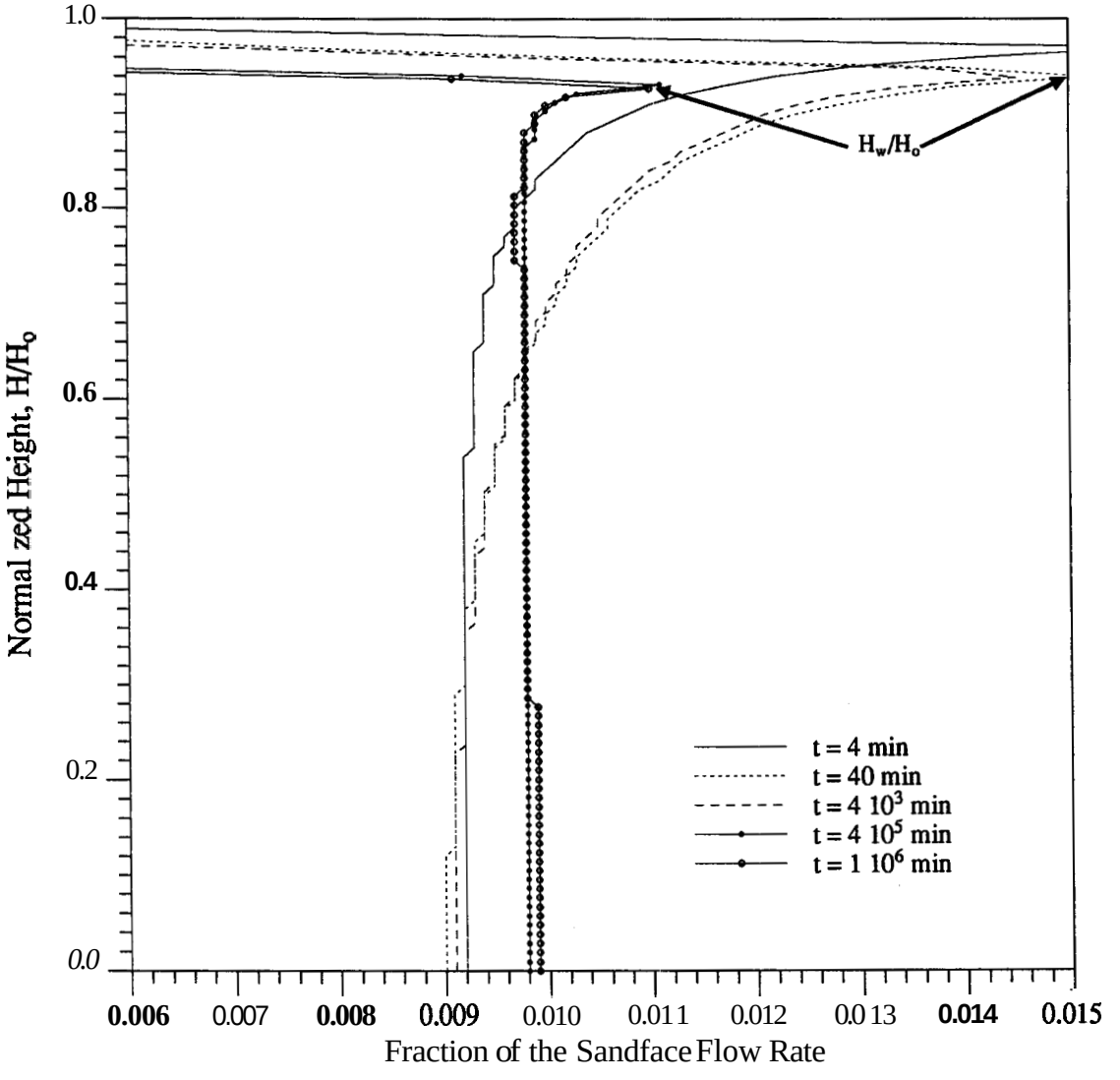

Figure 7.4: Sandface flow rate distribution. The liquid levels in the well coincid whith the higher flow rate values. See examples indicated by arrows in the figure.

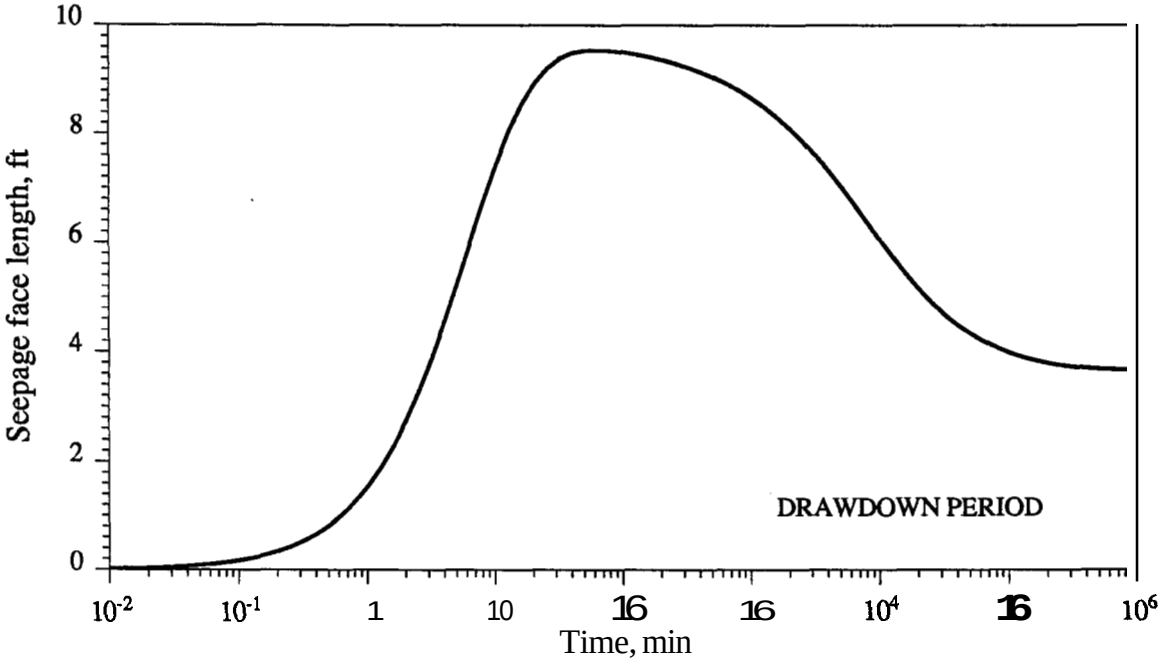

Figure 7.5: Seepage height vs. cumulative time for drawdown period

Figure 7.5 shows the seepage face behavior with the time. This is an important result from the present study which has not been found in any of the published papers in the surveyed literature. The seepage face presents an interesting transient behavior, following the three distinct periods of flow in a gravity drainage well. In this example, the seepage face starts developing after the pumping starts and reaches a maximum value of 9.5 ft at the end of wellbore storage effects. During the desaturating period, the seepage face length reduces while the free surface moves downward. This shrinkage seems to stabilize at about **3.2** ft as the pseudo-confined behavior takes place.

An illustration of radial potential distribution, seepage length and free surface radial profile is presented in Fig. 7.6. In this figure, the head potential in the bottom of the formation and the free surface position were normalized with respect to the original liquid height, H_o. Different flow regime periods are presented, starting at the end of the dominating wellbore storage effect period. The wellbore liquid level is also shown, and the seepage length may be identified by the difference between the liquid

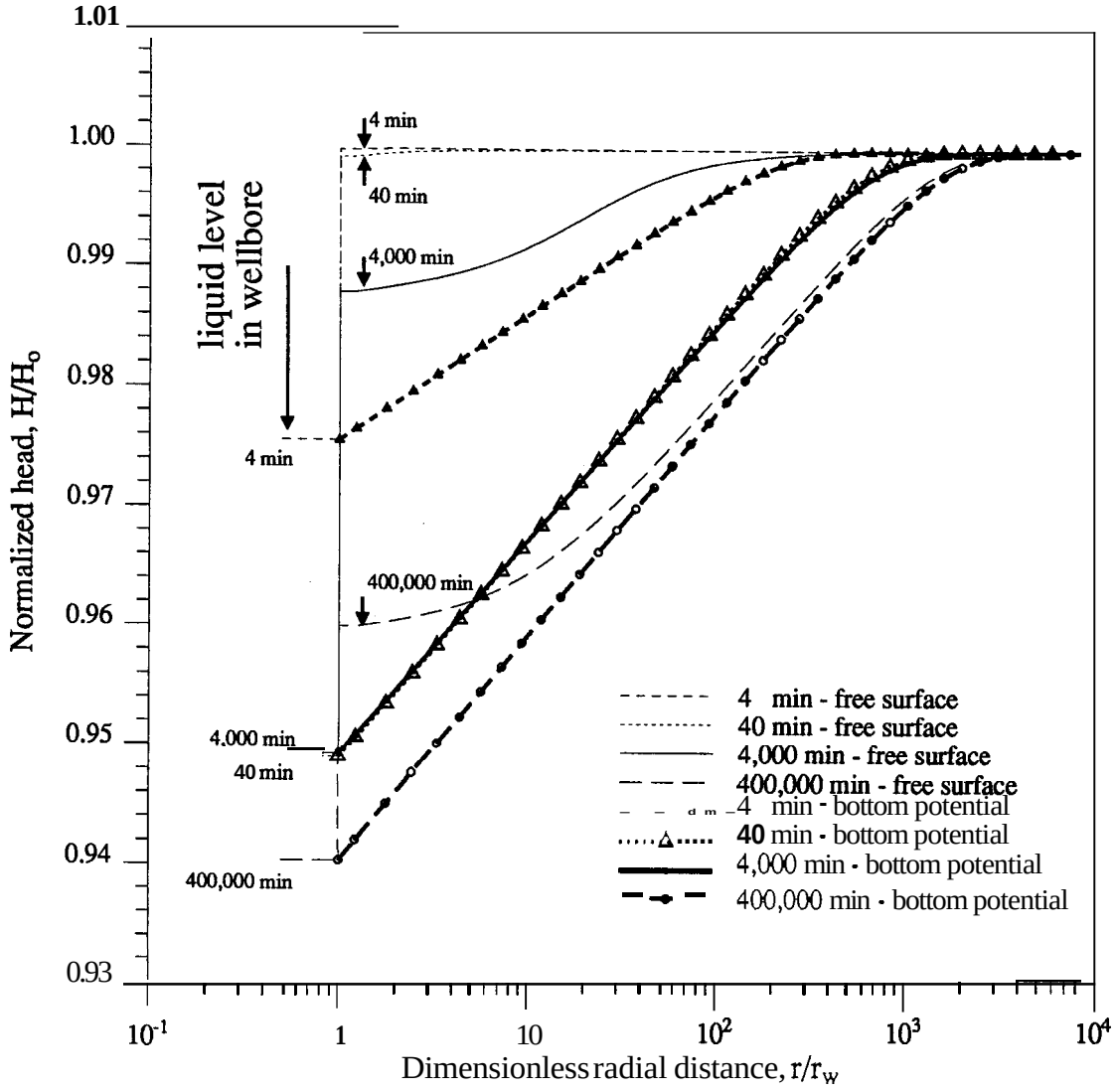

Figure 7.6: Dimensionless radial head profile during drawdown period. The sandface position corresponds to $r_D = 1$.

level in the wellbore and the free surface level at a dimensionless radius of 1.

Figure 7.6 gives important information about transient gravity drive flow into a well. The formation of the desaturating cone at different times can be seen. In the profiles in Fig. 7.6 corresponding to 40 and 4,000 minutes of pumping, the bottom head potential distribution presented the same values in this example as well as the liquid level in the wellbore, and the only apparent difference was the free surface position. After the stabilization of the seepage face length, the profile at 400,000 minutes shows the free surface head becoming uniformly closer to the bottom potential head close to the wellbore. This is when the vertical flow, given by the difference between the heads at the same radial location become stabilized. Based on the information obtained from Fig. 7.4 about the flow rate distribution along the sandface and in an iso-potential mapping given in Fig. 7.7, we infer that there is a region immediatly below the free surface where the potential gradients are steep near the wellbore. In Fig. 7.7, a representation of streamlines normal to the iso-potential curves was drawn by hand.

7.1.2 Buildup

Contrary to the conclusion found in the Groundwater literature that buildup behavior is similar to production behavior, the *SLM* has shown that the pressure buildup process is completely different from drawdown in the case of a single well located in the center of an infinitely large reservoir. To analyze the buildup period, we will use the same set of data as in the drawdown run. The results are shown in Figs. 7.8 to 7.12.

A log-log graph of buildup pressure drop vs time in Fig. 7.8 may be compared with Fig. 7.1 for an analogy between the flow regimes with the flow period. In this figure, the pressure derivative $\frac{\partial p_w}{\partial \ln t}$ was graphed versus time, as well as the pressure difference between the buildup and the flowing pressure at shutin time. In neither

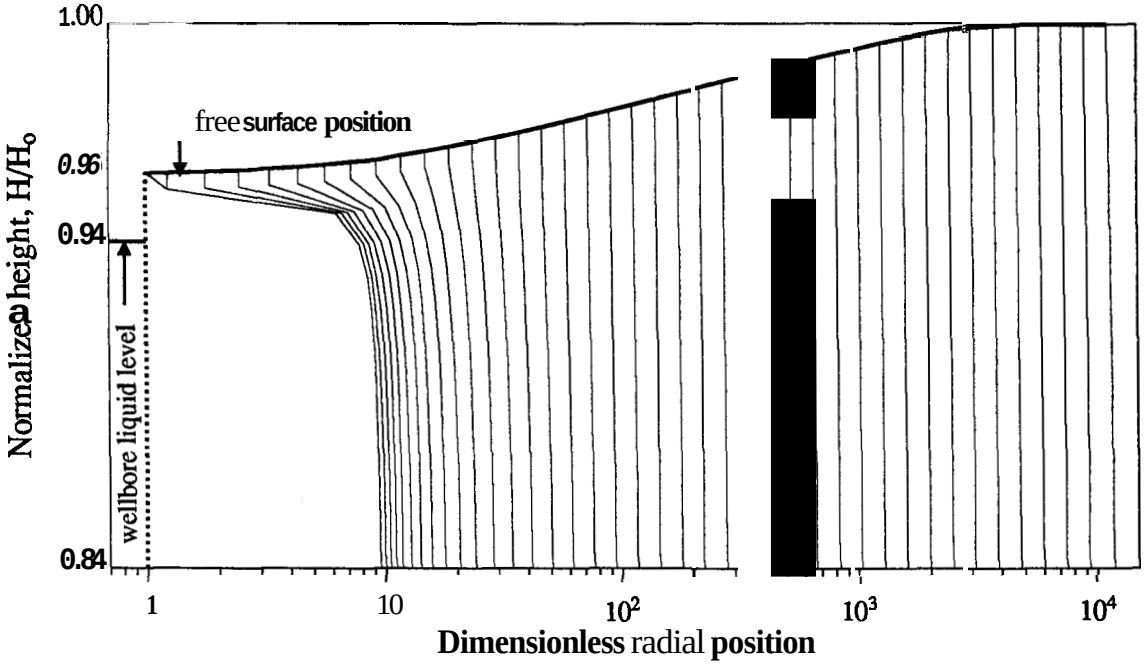

Figure 7.7: Iso-potential map and representation of a streamline at a production time of 10^6 minutes.

curve do we identify a pure unit slope wellbore storage effect. At early time, the wellbore buildup pressure seems to respond directly to the formation production, and since there are no confining and no compressing system involved, there is no apparent wellbore storage effect domination. The liquid level rises in the well responding directly to the formation flow capacity. There is no unit-slope evidenced in log-log graph in Fig. 7.8. The upward movement continues until both the liquid level in the well and in the sandface equilibrate. As the liquid level in the wellbore reaches the free surface level at the sandface, a different behavior in the log-log graph is evidenced by a discontinuity in the derivative curve. In the intermediate period in the pressure vs. time log-log graph in Fig 7.8 and also in the semilog graph of Fig. 7.9, an attenuated buildup behavior occurs for about four logarithmic cycles of time. The pressure derivative curve increases in this period, apparently with a constant slope, disregarding imprecisions. The waving observed in the pressure derivative curve in Fig. 7.8 may be due to numerical effects in the calculations.

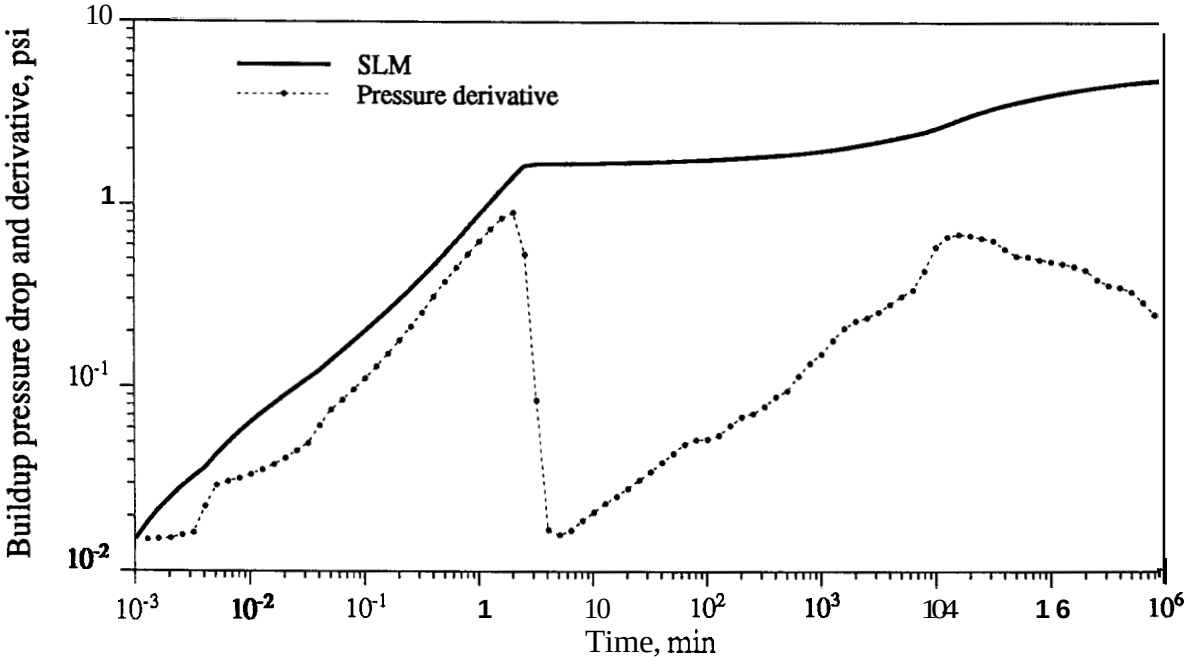

Figure 7.8: Wellbore buildup pressure and derivative - log-log plot

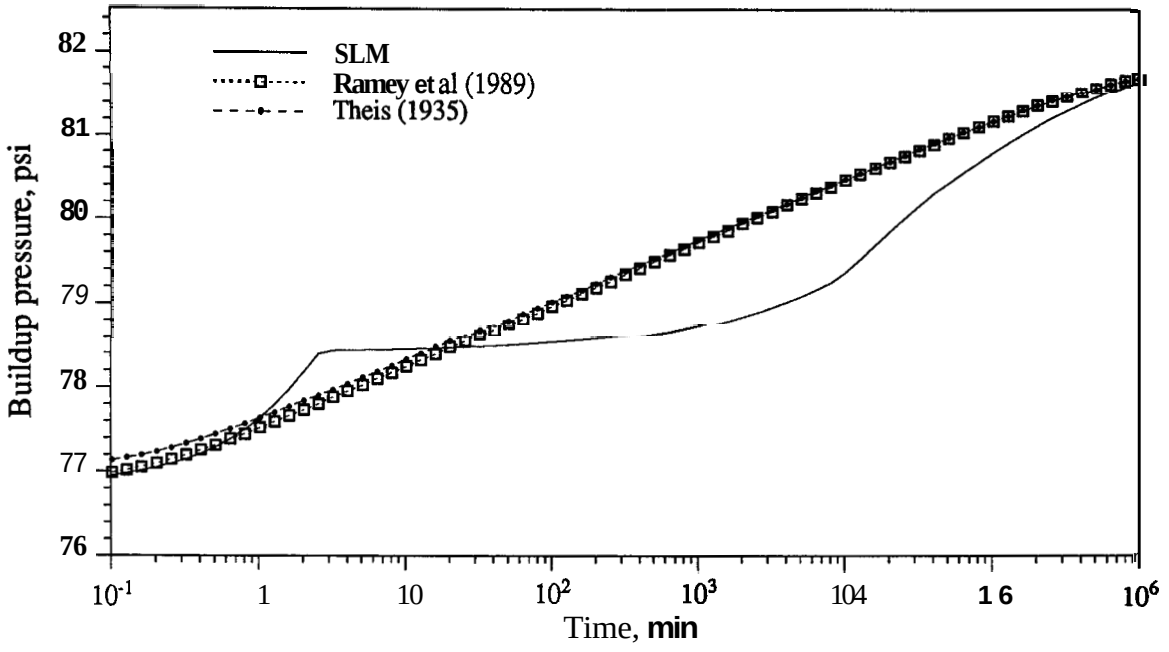

Figure 7.9: Wellbore buildup pressure - semilog plot

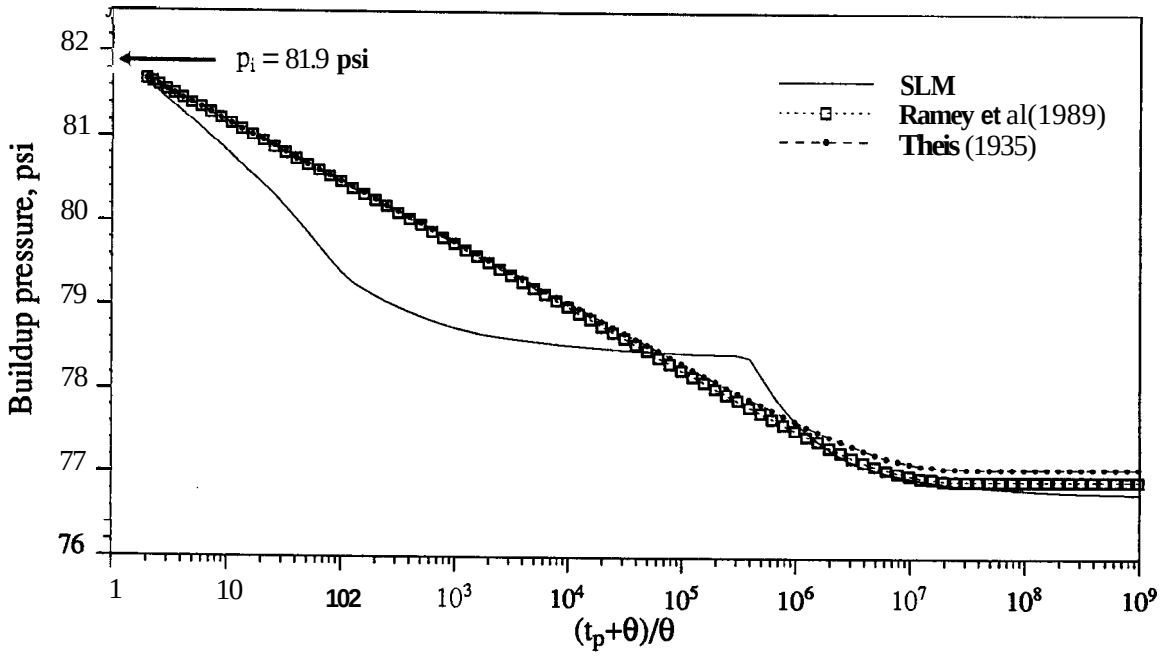

Figure 7.10: Wellbore buildup pressure - Horner plot

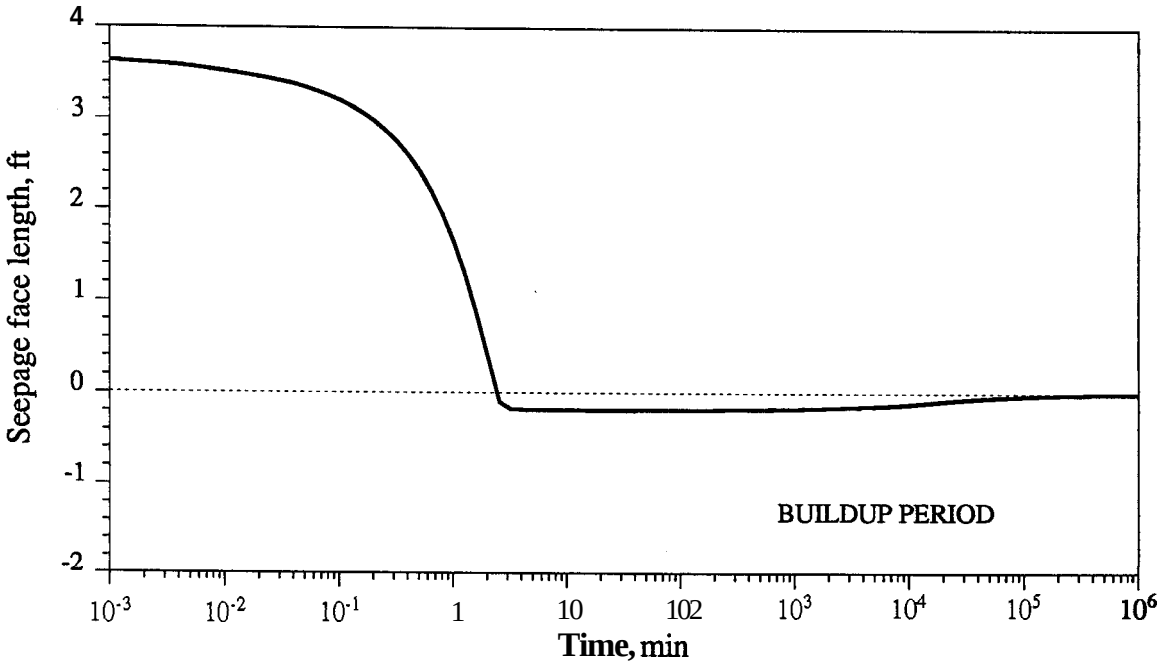

Figure 7.11: Seepage height vs. cumulative time for buildup period

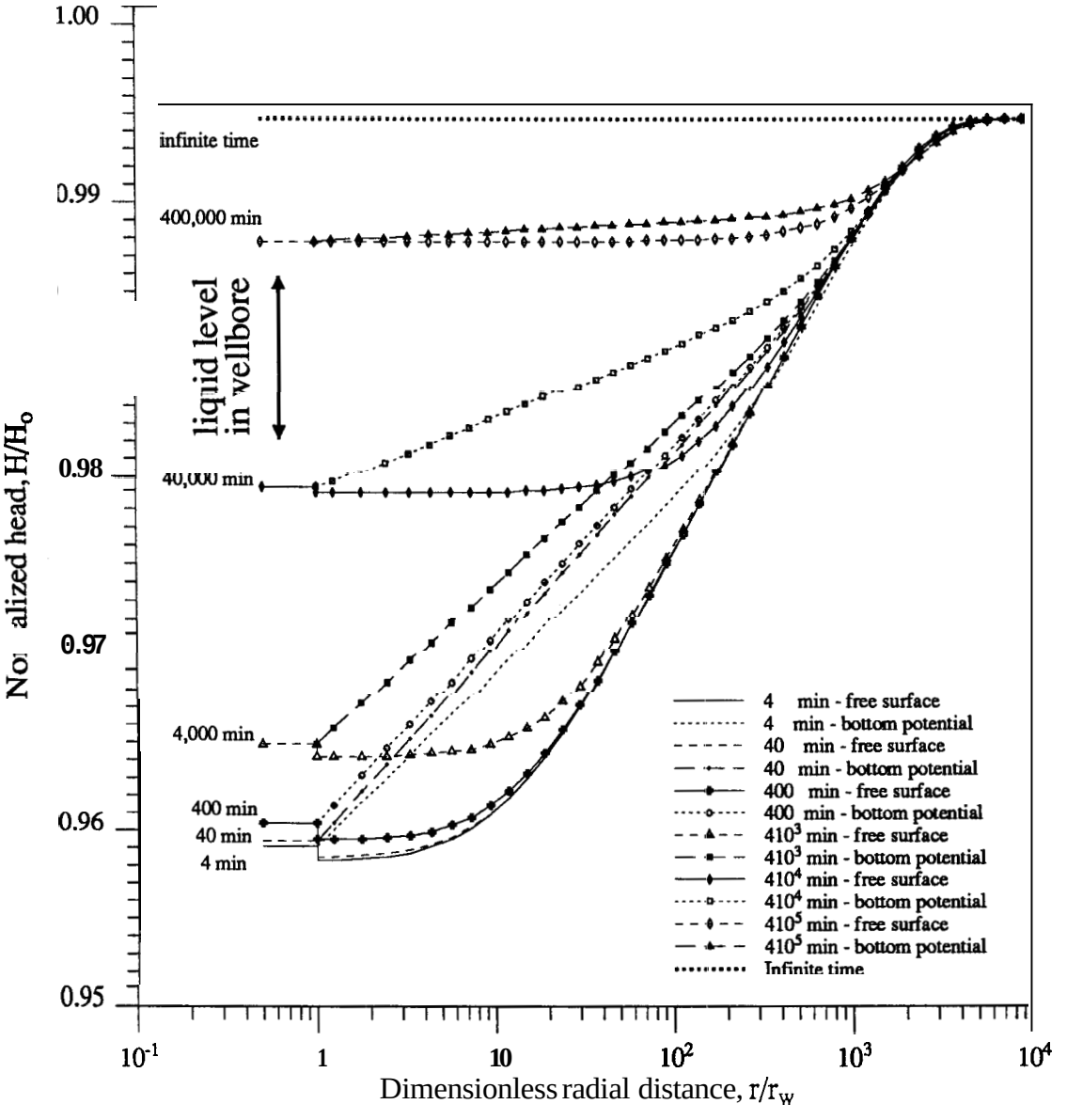

Figure 7.12: Dimensionless radial head profiles during buildup period. The sandface position corresponds to $r_D = 1$.

At late times, the buildup behavior becomes asymptotic to the confined flow solutions of both *Theis* (1935) and *Ramey et al.* (1989). But a slope similar to that of analytical approaches is only feasable at extremely long time.

A semilog *Horner* (1951) graph of the same data in Fig. 7.10 did not add further insight in the buildup pressure analysis. A conclusion, however, is that one could be mislead by trying to extrapolate pressures or to obtain a permeability slope from the buildup data. The simulator results do not indicate pseudo-radial behavior until very long times.

Another investigation of the pressure buildup behavior was done by observing the seepage face length vs. time semilog graph in Fig. 7.11. Comparing Figs. 7.11 with the seepage face in Fig. 7.5 it is clearly evident that drawdown and buildup behaviors are completely different. As can be seen, the seepage face height drops to essentially zero within a few minutes after shut in. This appears to be an original and unique finding of this study. Actually the free surface height at the sandface appears to be negative 0.2 ft lower than the liquid level in the wellbore during most of the buildup. Similar behavior was found for other buildup cases.

A better understanding of the physical phenomenon of the pressure buildup mechanism in the gravity drainage well is obtained by inspection of the potential at the bottom of the formation and the free surface head distributions along the radial distance at several times in Fig. 7.12. The free surface profile indicates that the re-saturation of the depressed cone is done uniformly. A flat liquid surface around the wellbore is progressively grown upwards, while the free surface at long distances remains almost stable. The radial extension of the flat free surface is increased with time as the liquid is replenished, and the liquid level rises. It appears that the depression cone fills like a tank of incompressible liquid. At the same time, the head potential in the wellbore is shown to be slighly higher than the free surface head potential at the sandface. This difference may be related to a viscous resistance of flow in the vertical direction. This negative seepage face is gradually reduced as the

vertical velocity of the free surface is reduced at long times, becoming negligible. The results shown in Fig. 7.12 also brought some explanation for the excessive time step cuts resulting in very long CPU times to simulate the buildup period. A possible reason may be found in steep potential gradient development far from the wellbore, where the discretization is much less refined than close to the well.

As a conclusion, the approximate methods employed to analyze the drawdown period in a gravity drive well problem appear useless for buildup analysis. This observation contradicts *Neuman* (1975-a). According to *Neuman*, no hysteresis would be expected between drawdown and recovery processes, and the same analytical equations and interpretation methods should apply to both periods. *Neuman* based this assertion on the idea that no flow from the unsaturated region was considered in his method, and the unconfined aquifer was treated as a compressible system. However, as pointed out by *Ramey* (personal communication - 1989) and *Ramey et al.* (1989), the semilog plots in the *Neuman* paper show different times for the beginning of the apparent straight line behavior of drawdown and recovery periods from well test data. Also, *Ramey et al.* compared drawdown and buildup field data and concluded that there were "different physical mechanisms between drawdown and buildup". However, *Ramey et al.* (1989) did believe they identified a semilog straight line immediatly after wellbore storage during buildup. It is significant that a semilog straight line was not clearly evident in *SLM* buildup runs. It appears that no thorough inspection of free surface recovery has been presented prior to this study.

7.2 Permeability

The effects of isotropic permeabilities in the pressure response from *SLM* are presented in two sets of drawdown curves for different formation permeabilities, Figs. 7.13 and 7.14. The permeability, as well as the flow rate, is a major factor driving the potential distribution in the formation because of the streamline shapes, and the consequent dynamic vertical pressure gradient development.

We define two sets of permeability range concerning the input data in Table 7.1. A low permeability range varying from 30 mD to 120 mD, and a high permeability range varying from 120 mD to 480 mD. In the low permeability range, Fig. 7.13 shows the same classical gravity drive curves, with the same late time trend, following the *Ramey et al.* (1989) slope. A shift in the drawdown potentials is observed for low permeability results. On the other hand, high permeability formation drawdown curves tend to approximate to the p-squared solution. Numerical model errors may explain some deviations. Another possible justification for the above observations is the accentuated slopes of the streamlines in low permeability formations. Bented streamlines cause enlongations of the liquid path into the wellbore introducing an equivalent viscous pressure drop. This influence of the vertical flow near the well was verified during the development of the numerical model which in early versions did not permit a correction in the stream layer slopes' resulting in potential drawdowns close to the *Ramey et al.* (1989) solution. Sandbox experiments also gave support to this analysis. In the *Hall* (1955) experiments, the time required for a particle located on a streamline to reach the inner boundary was observed to increase when approaching the free surface level (see Fig. 2.2 in the Literature Review Ch. 2). In addition, the runs of the simulator for the case of a true skin effect described in the Section 7.4 shows that the long time drawdown potential solutions are the same for the *SLM* and the *Ramey et al.* approaches. A possible explanation for this match

[1]The distances between blocks nodes were the horizontal projections and not the true distances corrected by the slopes.

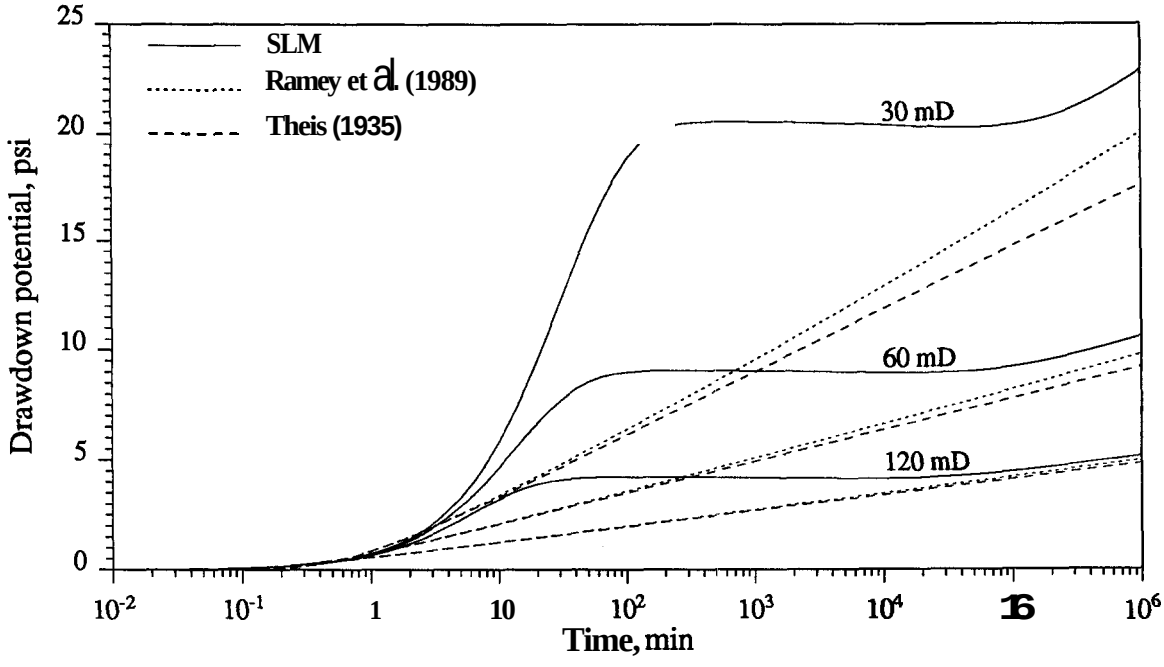

Figure 7.13: Wellbore pressure drawdown of intermediate to low permeability reservoirs under gravity drainage

is the reduction in the slopes of the streamlines as a consequence of flow restriction near the wellbore, under a skin effect.

7.3 The Seepage Surface

In the process of gravity drainage through a porous medium, it is generally recognized that a thin curtain of liquid falls along the inner production face, whatever the geometry of the flow. This surface, called the seepage face, reflects the difference between the maximum potential inside and outside the porous medium, and, in the case of water or oil wells, the seepage face is not easily measurable in the field. The analytical methods used so far have neglected the existence of the seepage face phenomenon. This is a major reason that the analytical models do not reproduce the well pressure (or head) behavior accurately.

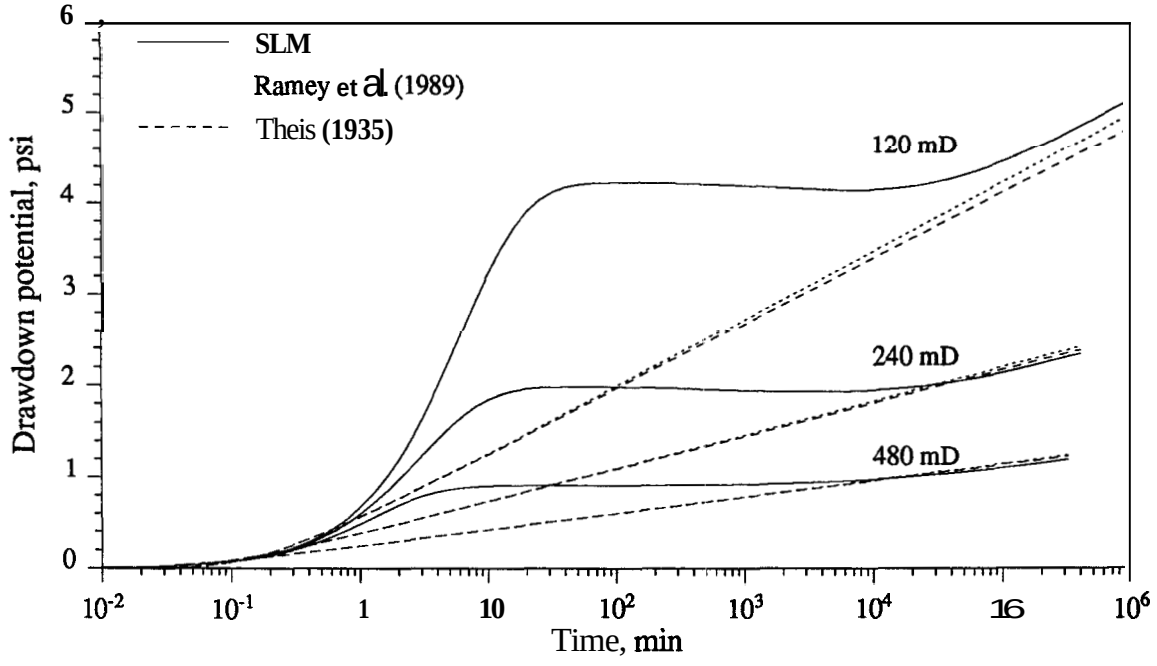

Figure 7.14: Wellbore pressure drawdown of intermediate to high permeability reservoirs under gravity drainage

The *SLM* simulator used the same classical inner boundary condition as in most formulations in the Groundwater literature. The *SLM* results consistently reproduced the seepage phenomenon with a clear visualization of the physics of the problem. No surface tension effect was necessary to cause the existence of the seepage face, which can be explained entirely by viscous flow theory, and verified by the numerical model.

The seepage height must be related to the formation permeability at the wellbore, the pumping rate and the original liquid height in the formation, because the seepage height represents a difference between the maximum and the minimum potential at the inner boundary. Skin effect should also be a contributing factor to the seepage face development. Figures 7.15 and 7.16 illustrate how the seepage face height changes with permeability, and Figs. 7.5 and 7.11 illustrate the seepage face behavior during drawdown and buildup tests, already discussed in Section 7.1. The observed trend in Figs. 7.15 and 7.16 for different sets of permeability is to reduce the seepage face

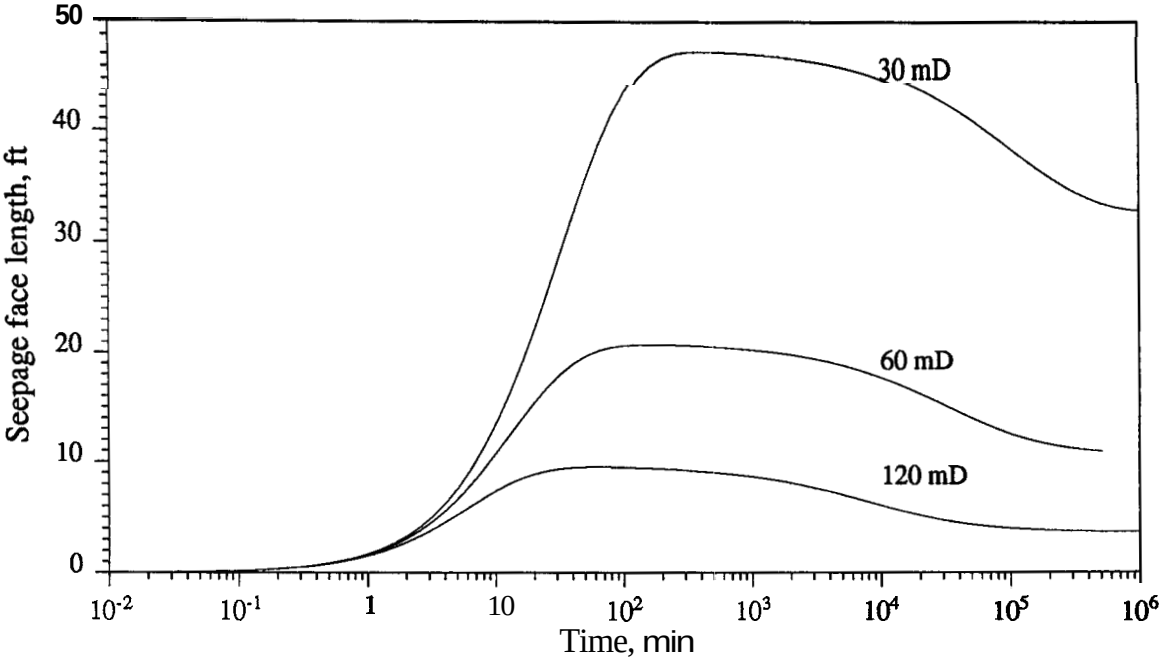

Figure 7.15: Semilog plot of the seepage height: low permeability range

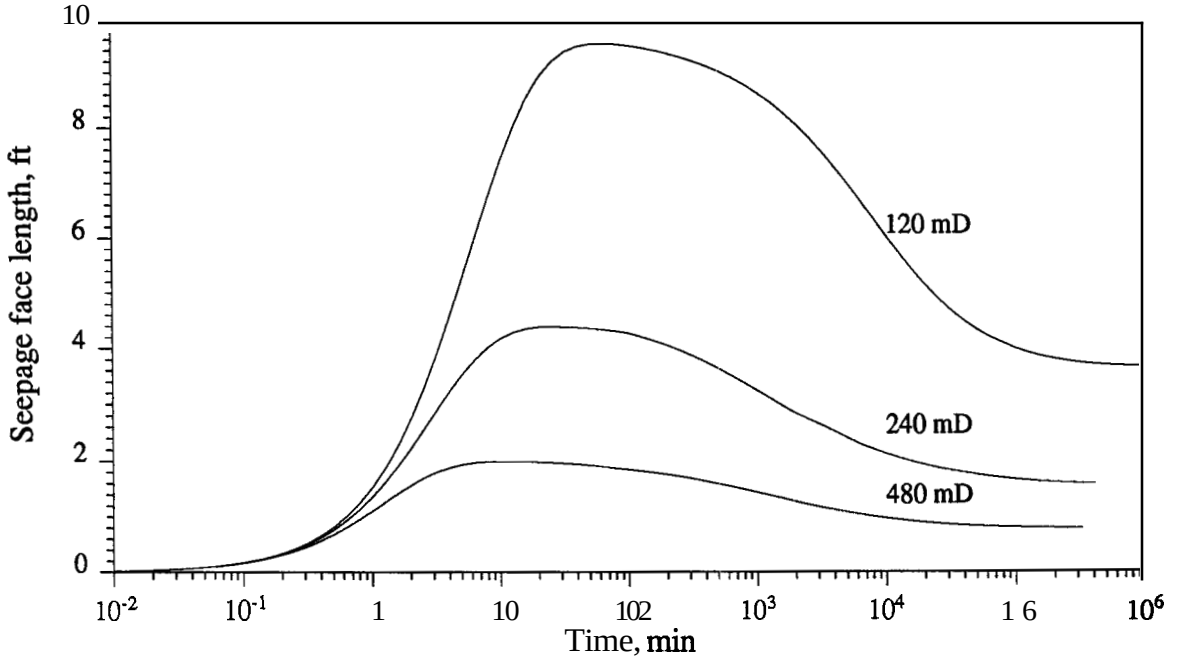

Figure 7.16: Semilog plot of the seepage height: high permeability range

height as the permeability increases.

The existence of the seepage face is a consequence of the free surface position, which is a function of the liquid velocity. When two streamlines converge while moving toward the sink (well), the resulting streamline velocity increases to preserve a material balance. Since there is enough voided pore space above the free surface, a fraction of that dynamic energy may be used by increasing the liquid column. Figure 7.6 shows an almost flat free surface profile in a log radial scale in the vicinity of the well after a long drawdown period.

This natural phenomenon may be described by the following implicit equation, Eq. D.1 in App. D, representing the free surface height at a location r from the well center, according to *Wyckoff et al.* **(1932):**

$$h(r) = \frac{\Phi_b(r)}{\rho \frac{g}{g_c}} + \frac{\overline{v}_v(r)\,\mu}{k_v\,\rho \frac{g}{g_c}}\,h(r)\,, \qquad \textbf{(Eq. D.1)}$$

The relationship between the free surface position and the head potential is verified in App. D.

There is little general information on the seepage face height for a free surface gravity drainage well. One conclusion in the Groundwater literature is that the seepage face height is about half the drawdown for cases where the drawdown is less than 10 percent of the initial head. Some of the figures presented in this chapter show that the seepage face height increased during the drawdown period, then declined and became reasonably constant near the end of the drawdown period. Comparison of the drawdown head and the seepage face height shows that the seepage face height is rarely half the drawdown. No obvious relationship for seepage face height was found in this study.

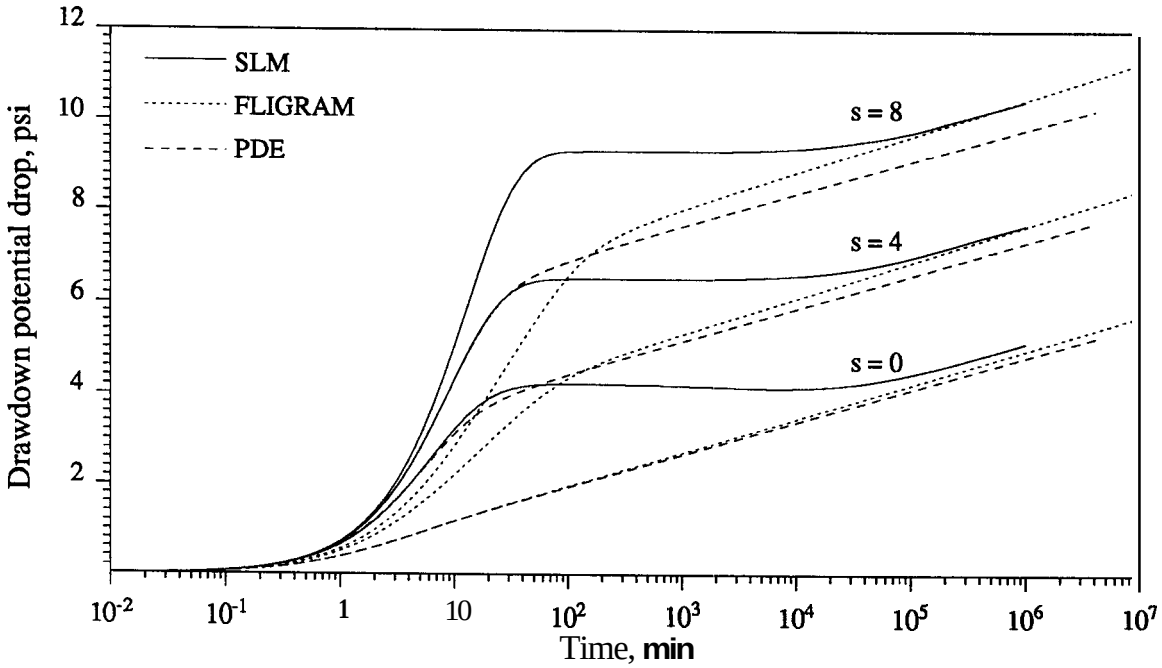

Figure 7.17: Pressure drawdown vs. time for different skin parameters.

7.4 Skin Effect

To complement the preceeding analysis of the influence of permeability on the well pressure response, the effects of a damaged annular region are now considered. Figure 7.17 contains a set of time-drawdown curves for skin parameters of **0, 4** and 8. The same basic reservoir properties in Table 7.1 were used in this analysis. The analytical solutions by *Theis* (1935) and *Ramey et al.* (1989) were evaluated by numerical solutions using *FLIGRAM* and *PDE* programs which include wellbore storage effects.

A thin region of reduced permeability around the wellbore keeps the liquid level high in the sandface vicinity, and the free surface location and the potential distribution along the reservoir become different. **A** change in the seepage face is another consequence, because the seepage face length increases as skin increases. Figure 7.18

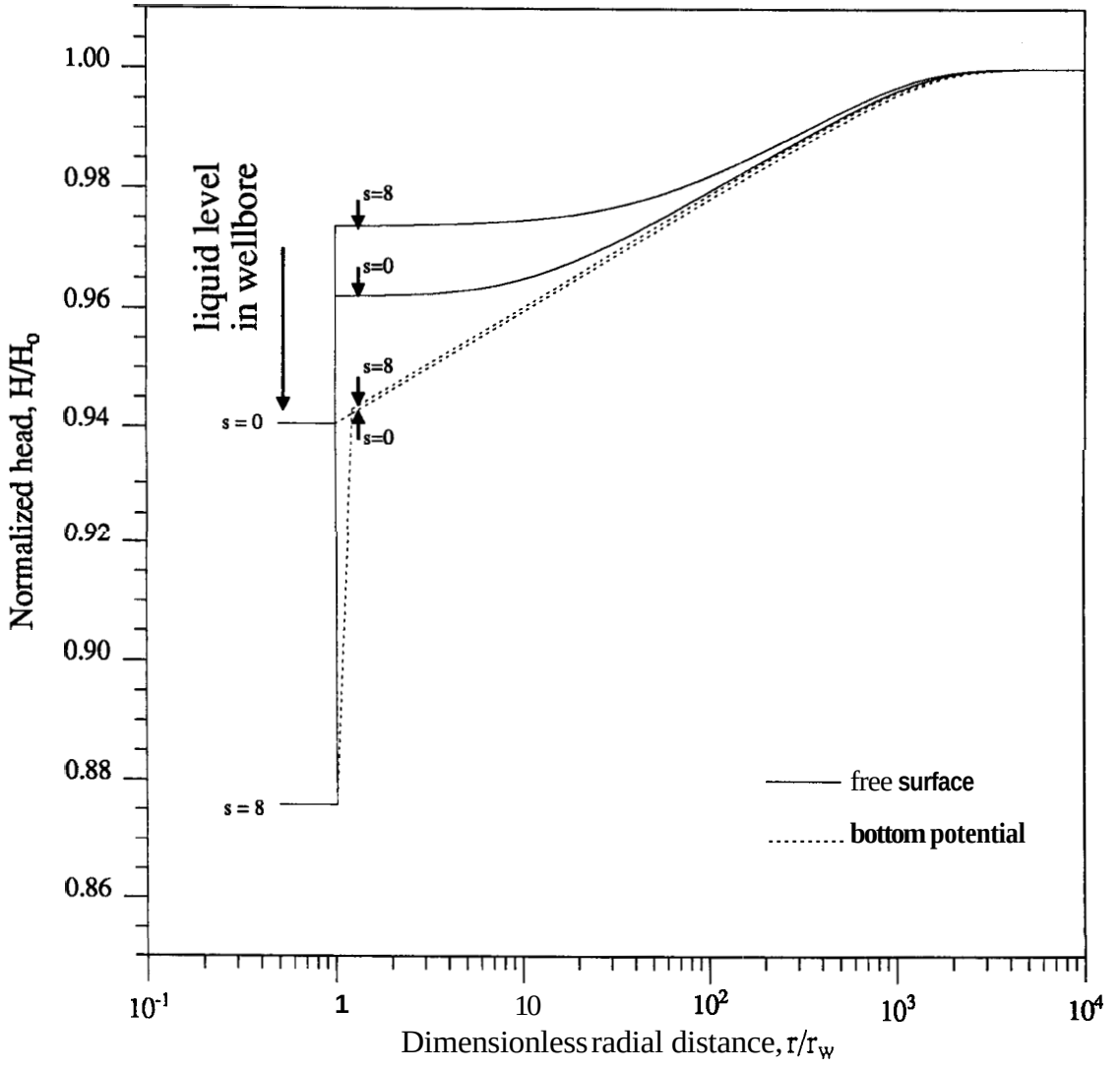

Figure 7.18: Radial head potential profile of a damaged well after a flowing time of 400,000 minutes. The sandface position corresponds to $r_D = 1$.

presents a radial profile of the potential head around a damaged well, compared with a non-damaged well. An increase in skin effect does not appear to affect the bottom potential. The free surface is higher around the wellbore in a damaged formation than in a non-damaged formation. However, at long distances from the wellbore, this situation is inversed, since the material balance is preserved. In the graph of Fig. 7.18 it is not possible to see a small difference between the free surface positions due to the scale. From these results, we infer that the presence of the damaged region reduces the slope of the stream-lines behind the damaged annulus, the vertical head gradients are reduced, and the flow becomes proportional to the liquid height, as idealized by *Dupuit* (1863). The time-drawdown curve of Fig. 7.17 also supports this explanation.

7.5 Anisotropy

The free surface gravity drainage problem depends greatly on vertical permeability. A set of different permeability factors f_k ($f_k = k_v/k_h$) ranging from 1 to 120 was chosen to analyze the effects of anisotropy on producing well pressure. Results of *SLM* runs were graphed together in Fig. 7.19 to make qualitative comparisons with isotropic reservoirs. From the results, we observe that high degree of formation anisotropy causes a strong influence on the wellbore potential, since vertical flow gradients near the well are steeper than in other regions.

In Fig. 7.19, the influence of vertical permeability is shown for several examples. In a case where k_h of 120 mD is a fairly high permeability for a flow rate of 100 BPD, the streamlines do not bend shajply, even near the well, as inferred from the profile in Fig. 7.18. However, when the vertical permeability decreases to 1 mD, the wellbore liquid level drops rapidly to zero at late times.

The effects of anisotropy are most important during the desaturating period. On the other hand, there is an observed trend of late time potentials to approximate the isotropic solution for the horizontal permeability. This observation may be an

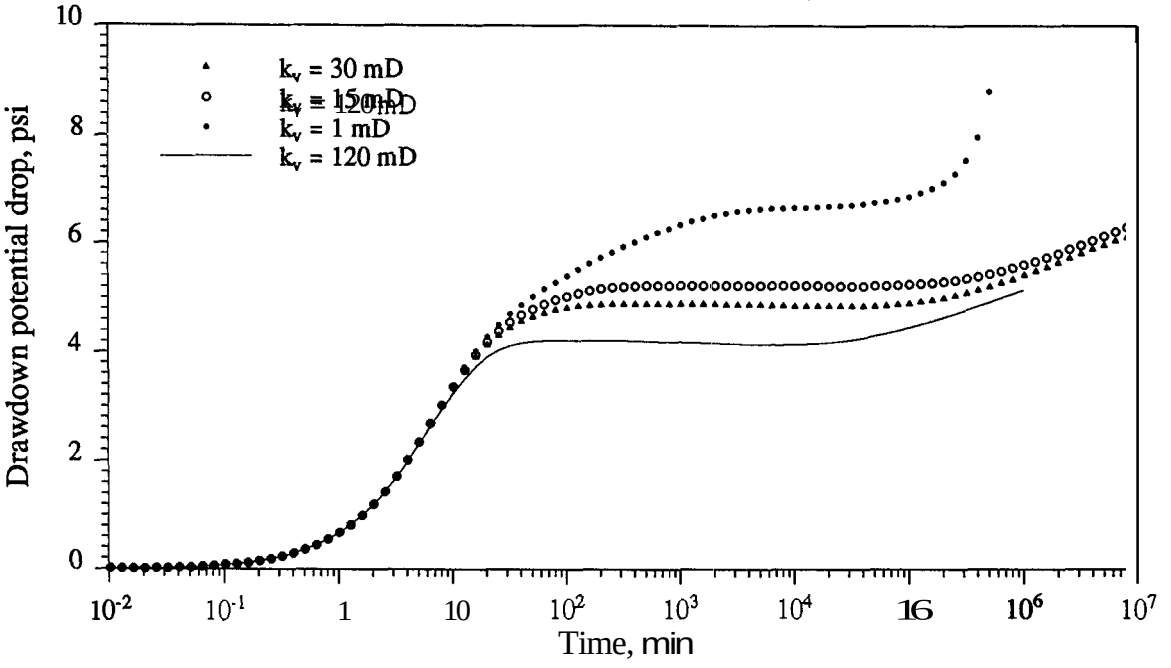

Figure 7.19: Results from *SLM* for a 120 mD horizontal permeability and different vertical permeabilities

important key for future study of a method to obtain the vertical permeability.

7.6 Production Flow Rate

Figure 7.20 presents a pressure drawdown graph for four different production flow rates ranging from 50 BPD to 400 BPD. The non-linearity of the potential near the wellbore and the flow rate variation is evident. For a flow rate variation from 50 to 400 BPD (8-fold increase) produced an increase from 1.94 to 20.42 psi (10.5-fold increase) in the drawdown during the flat desaturating potential period. A possible reason for the disproportional drawdown is that the high flow rate causes the uppermost streamlines to reach the inner boundary late, causing an additional potential drop. Figure 7.21 is a graph of the *SLM* results for the 400 BPD flow rate case compared

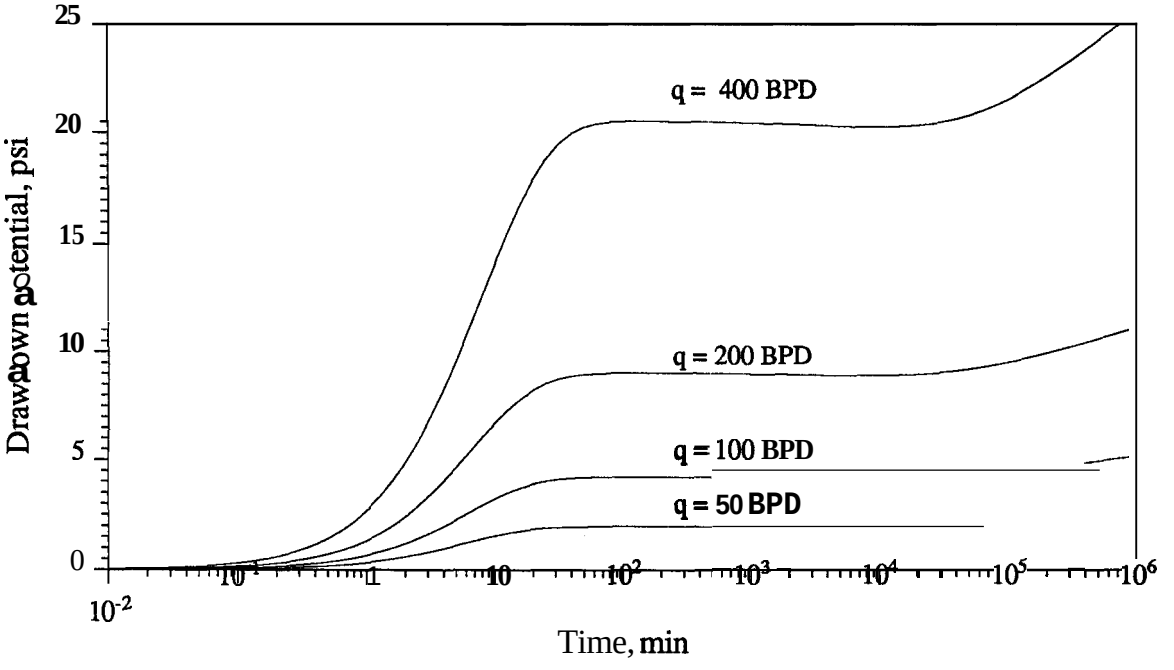

Figure 7.20: SLM results for different production flow rates

with the Ramey et *al.* (1989) approach. The late time pseudo-confined behavior shows the same slope for both solutions. The absolute values of the drawdonw at long times are different in the p-squared and the *SLM* numerical approaches.

A more interesting result is presented in Fig. 7.22 where two different runs for a constant q/k ratio of 0.6 are compared. The theory explains the shift in time observed in that figure. From the Ramey et *al.* (1989) solution,,the following equation **(Eq. 11** in Ramey et *al.* paper) applies at late times:

$$p_i^2 - p_w^2 = m\left\{\log_{10} t' + \log_{10}\left[\frac{k}{\phi\,\mu\,\left(p_i^{-1}\right)\,r_w^2}\right] - 3.23 + 0.87S\right\} \qquad (7.6.1)$$

We observe in Eq. 7.6.1 that the argument in the logarithmic term is only a function of the permeability k and not of the production flow rate. As a consequence, a change in permeability should produce a shift in the time proportional to

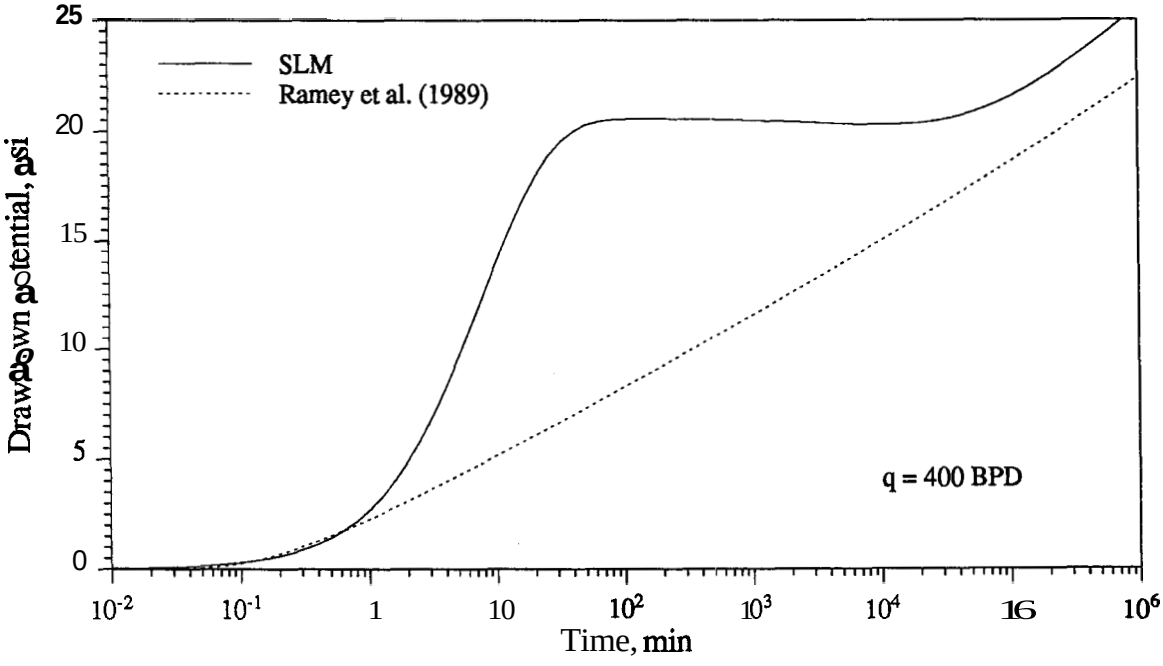

Figure 7.21: *SLM* result compared with *Ramey et al.* (1989) solution for a high flow rate case

the permeability-m. In the runs shown in Fig. 7.22, m is constant for both cases, according to the following expression also from *Ramey et al.* paper:

$$m = 325.2 \frac{q B \mu}{k(h/p)} = 234.9 \text{ psi}^2/\text{cycle}.$$

As a conclusion, both permeability and production flow rate produce the same non-linear effects in the problem. We learn from this result that for a same q/k ratio, the potential drawdown will present similar behavior, displaced in time by a constant logarithmic factor.

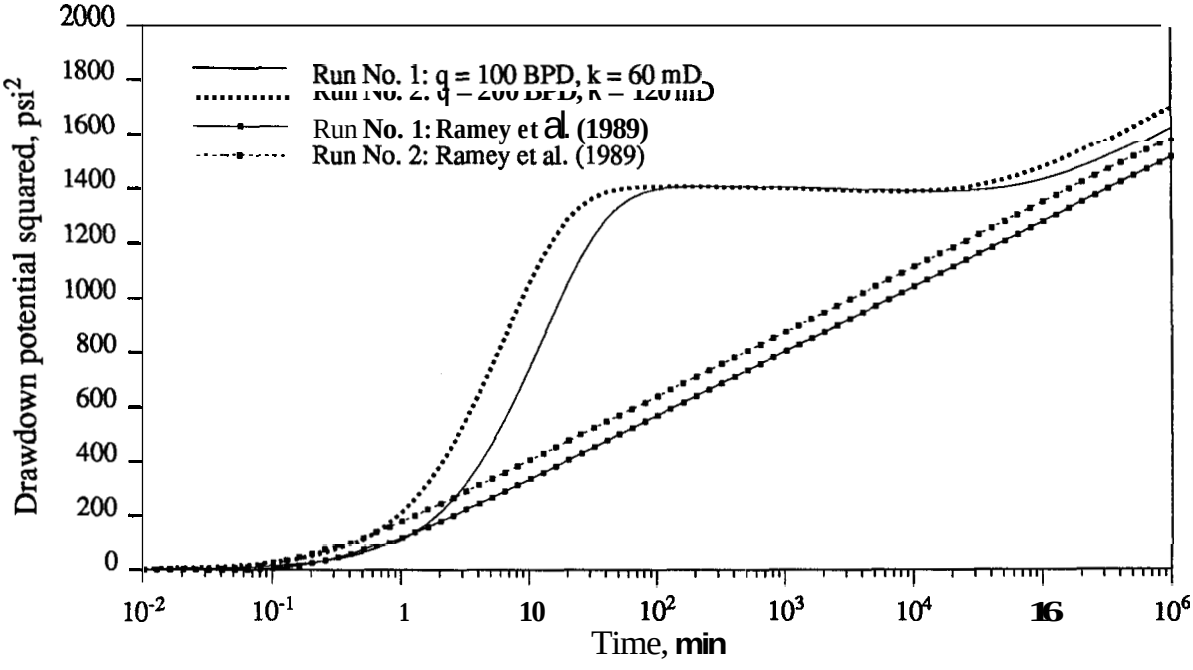

Figure **7.22:** Comparison between SLM runs of two tests in formations with the same q/k ratio

7.7 Original Liquid Height and Transmissivity

The influence of original height of the liquid column on the wellbore potential drawdown is verified in the following. Five different original heights were selected to run the examples in Fig. **7.23.** Using the same set of basic data in Table **7.1,** values of the liquid original height started from **63** ft, and were increased to **252** ft. The graph in Fig. **7.23** shows that the linearity does not exist in the potential drawdown behavior. The run for $H_o = 63 ft$ dropped the liquid level in the well abruptly during the wellbore storage period, reaching the bottom. However, increasing H_o by a factor of **2** the potential drop during the desaturating period was only approximately **6** psi.

Another verification was done comparing two runs with the same transmissivity $k H_o/\mu$ but different permeabilities and original liquid heights. A **120** mD reservoir with an original liquid height of **126** ft and an 80 mD reservoir with an original liquid

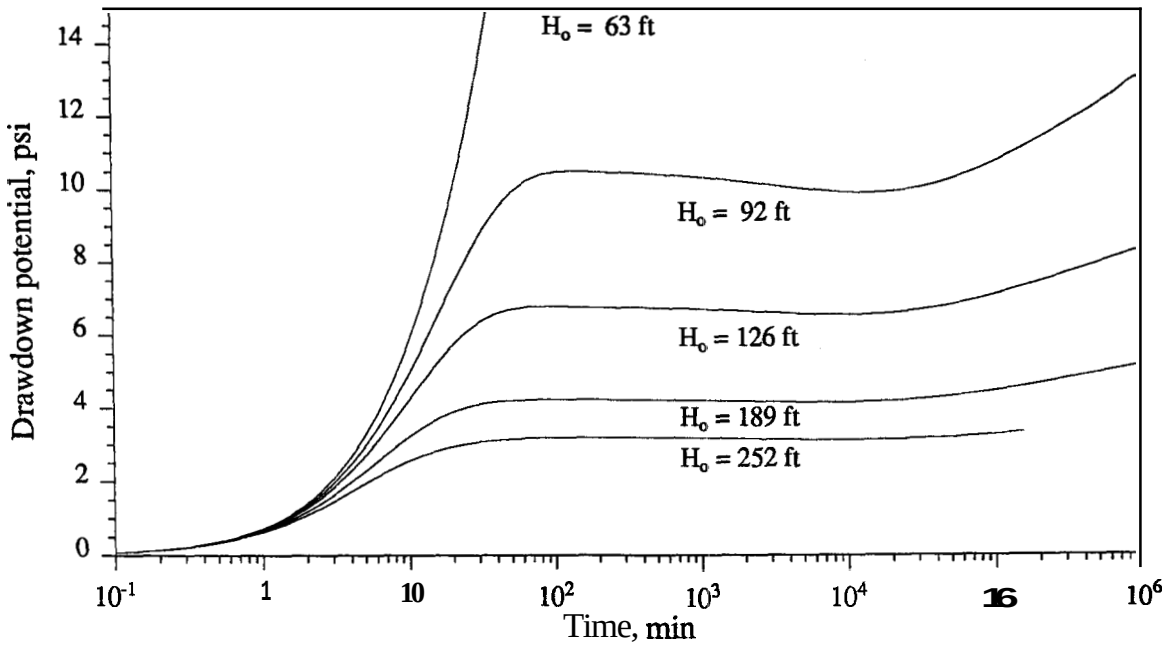

Figure **7.23:** *SLM* results for different original static liquid level

height of 189 ft were selected for this analysis. The transmissivity in both cases was **15,120** mD-ft/cp. The results presented in Fig. **7.24:** indicated that there was not a superposition of the curves during the desaturating period. However, at late times, the drawdown potential drops produced very close results with consistent slopes m, as compared with the *Ramey et al.* (1989) solution. The desaturating period presented a smaller potential in the wellbore (higher potential drop) in the case of smaller permeability.

An expected shift between the late time solutions was observed due to different initial pressures, in the p-squared plot of the same data, as seen in Fig. 7.25. In this example, the effect of retarded development of velocity gradients in the formation at the beginning of pumping is more pronounced in the lower permeability case. During the desaturating period characterized by the flat shape in the time-drawdown graph, the velocity gradients become larger and the drawdown potential in the well gradually reduces before the pseudo-confined behavior.

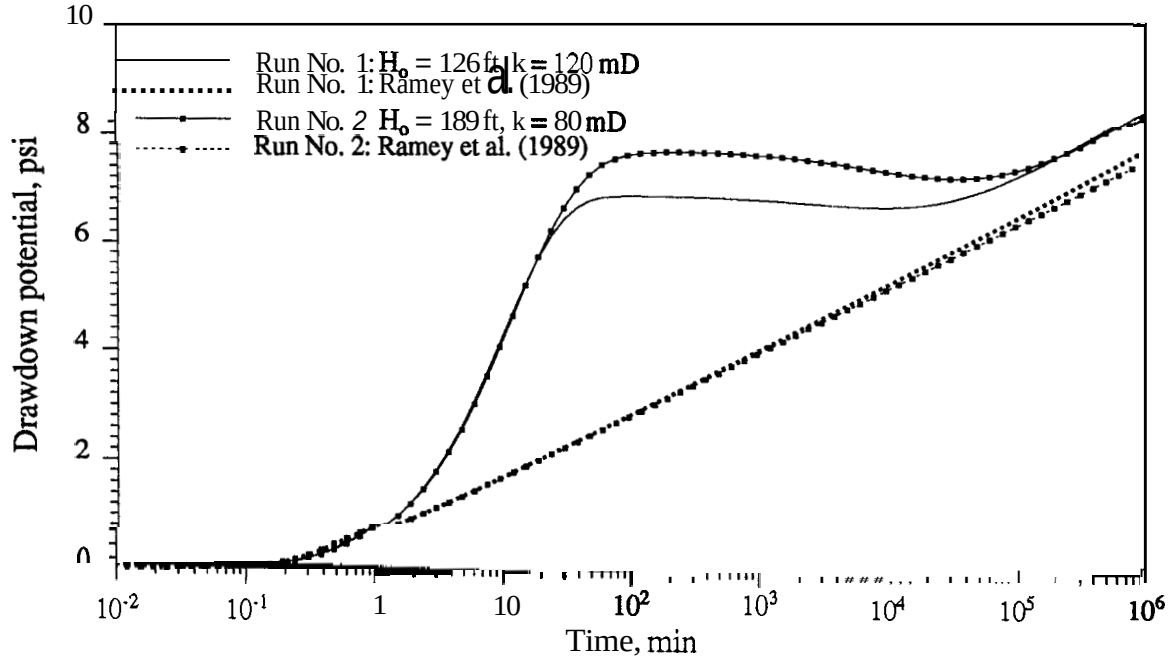

Figure 7.24: Potential drawdown results for the same transmissivity and different permeabilities

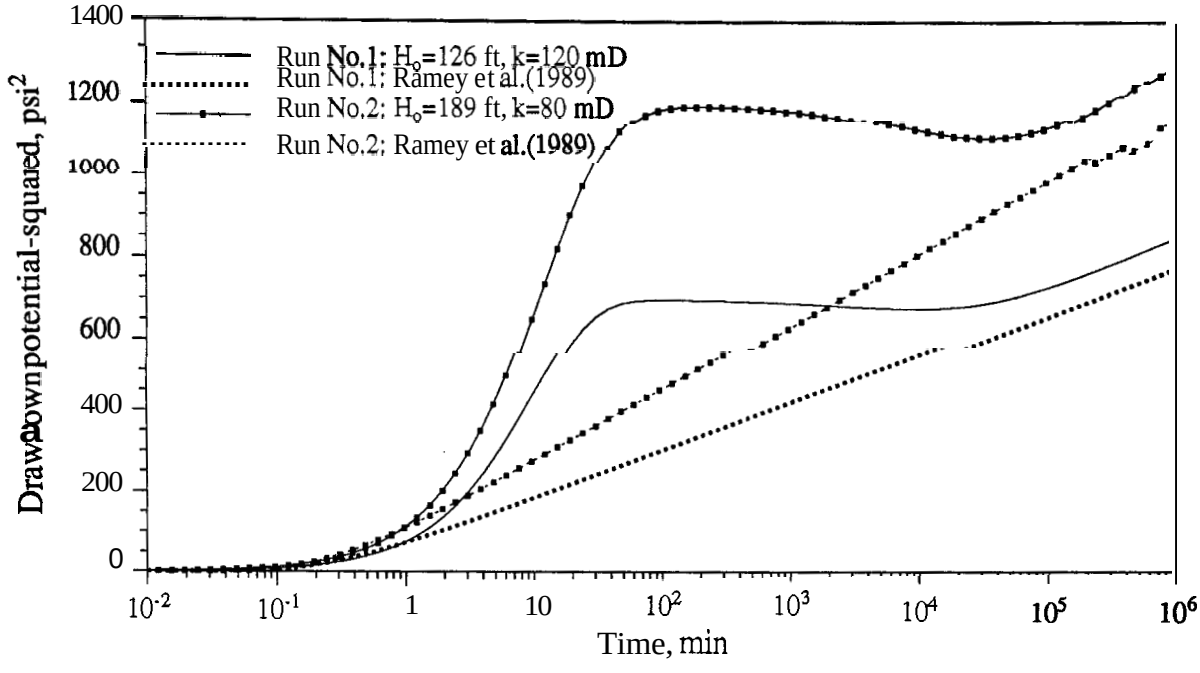

Figure 7.25: Potential squared drawdown results for the same transmissivity and different permeabilities

7.8 Considerations About Well Test Project

From the preceeding analysis, a consistent understanding of the physics of the problem allows us to reach further conclusions about the use of the ***Stream Layer Model*** in planning a gravity drainage well test. We have seen the effects of the main variables that determine the wellbore potential drop during drawdown and buildup periods. We have also seen that for different combinations of those variables, the producing time required to start pseudo-confined behavior was longer than one or two months of producing time. In addition, a full log-cycle in the time drawdown graph necessary to define the m-permeability from the slope of a straight line in a p-squared plot would require one or two years of production at a constant pumping rate in the given examples. The preceeding investigation did not include a full range of possible variations of the parameters, but parameter ranges were within practical field value ranges.

To briefly extend the investigations, the *SLM* was run to simulate a short well test of 24 hours of pumping followed by a buildup period. The buildup period was set long enough for the liquid level in the wellbore to equalize the liquid level in the sandface, shrinking the seepage face to a minimum, and starting the re-saturating period. Considering that in a gravity drainage well the major unknowns are the permeability, the permeability ratio and the skin parameters, sets of different values of permeability and skin were tested. We did not consider the effect of anisotropy in this study. In addition, other reservoir properties such as porosity, residual saturation in the desaturating region, wellbore radius, original liquid height at static condition, liquid viscosity and liquid density were known. The basic data in Table 7.1.1 were used.

Figures 7.26 to 7.28 show several sets of tests with skin effect parameters of 0, 4 and 8. Permeability ranged from 30 mD to 150 mD. A consolidation of the results is presented in Fig. 7.29 where only a few limiting permeability values were included.

The drawdown potential drop and the buildup potential drop vs time plots were placed side-by-side to characterize the differences between drawdown and buildup behaviors.

Important conclusions may be reached from the results shown in Figs. 7.26 to 7.29. Some discoveries were identified in previous sections of this chapter such as the degree of non-linearity of the formation permeability and the differences between the drawdown and buildup process. What is remarkable in the results presented in this section is the information about the free surface position at the sandface during the buildup period. The inflexion point in the buildup curve where the liquid level in the well reaches the same position as the free surface at the sandface varies only a few feet for formation permeabilities ranging from 30 mD to 150 mD. For usual field test accuracy, this information is not useful. The time in which the liquid levels equalize, however, increases as the permeability decreases with a large change as observed in Fig. 7.30.

In Fig. 7.31 the potential drops during the drawdown period are plotted for two different pumping times. The times when the re-saturating period starts in both cases are very close, different only by **4** minutes for production times of 1 day and 10 days.

Figure 7.32 gives important information about the free surface at the sandface while the liquid level travels in the wellbore during the 24-hour drawdown and buildup periods. This example was run for a **30** mD formation permeability and no skin effect. The free surface during the early buildup period remains immobile until the liquid level in the wellbore reaches the same position. Then, the free surface at the sandface start gently moving upwards during the re-saturating period.

Based on the results of the series of runs described in this subsection, the graph of Fig. 7.33 is presented. This is an example of a correlation obtained from the *SLM* for a typical set of data as in Table 7.1.1, and for the short well tests.

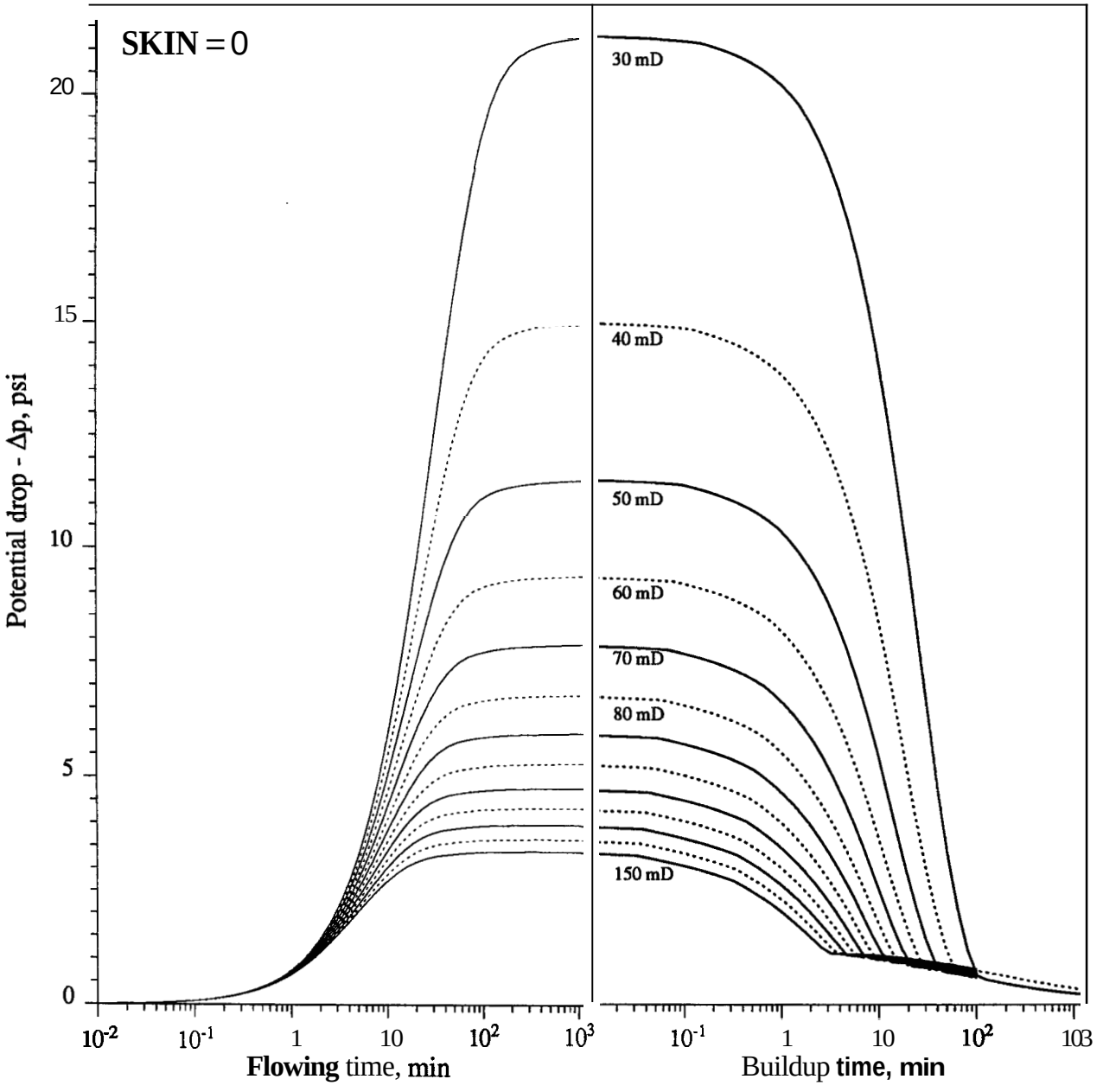

Figure 7.26: Combined 24-hour flowing and buildup test for a set of different permeabilities. Skin = 0.

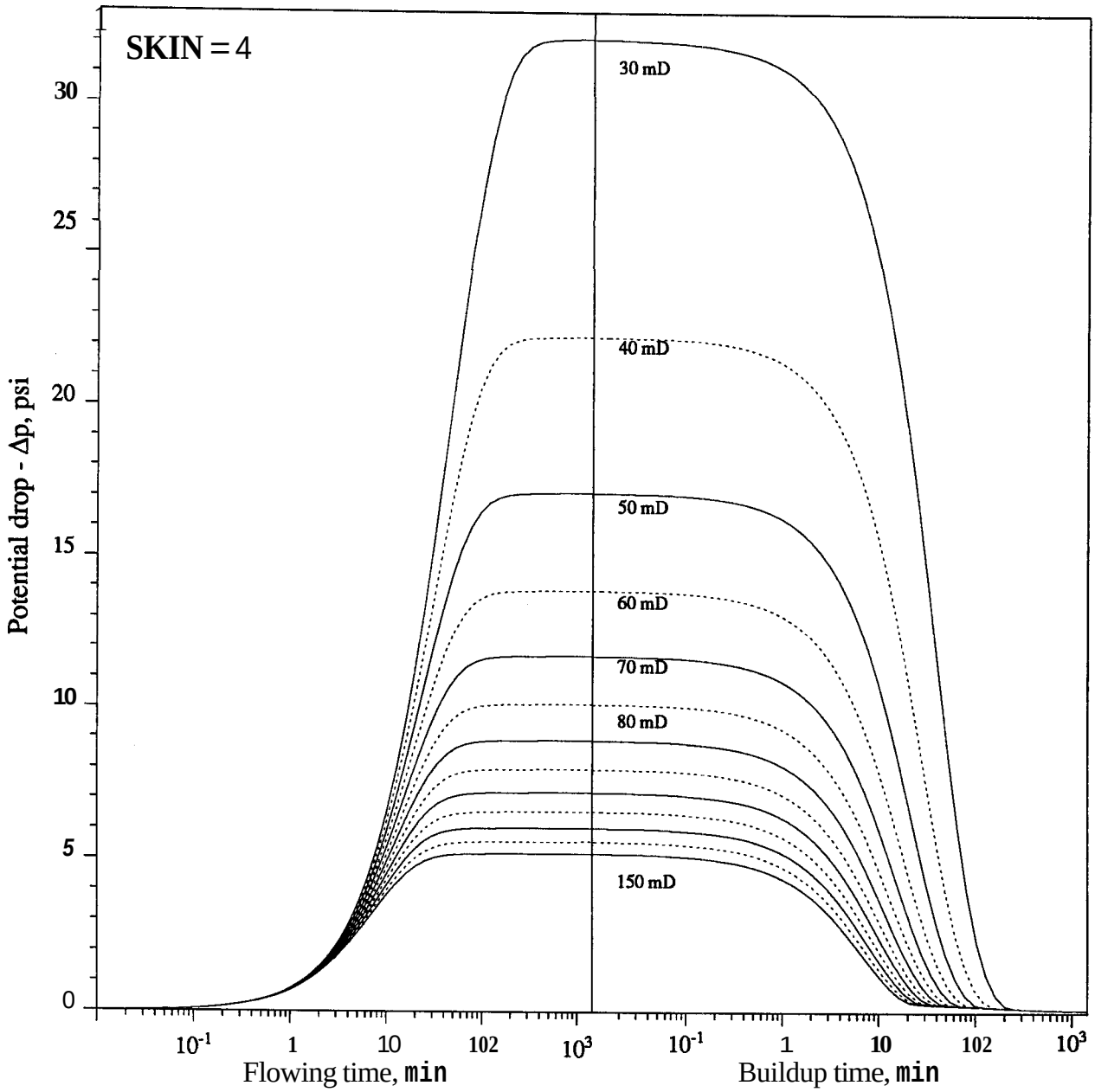

Figure 7.27: Combined 24-hour flowing and buildup test for a set of different permeabilities. Skin = 4.

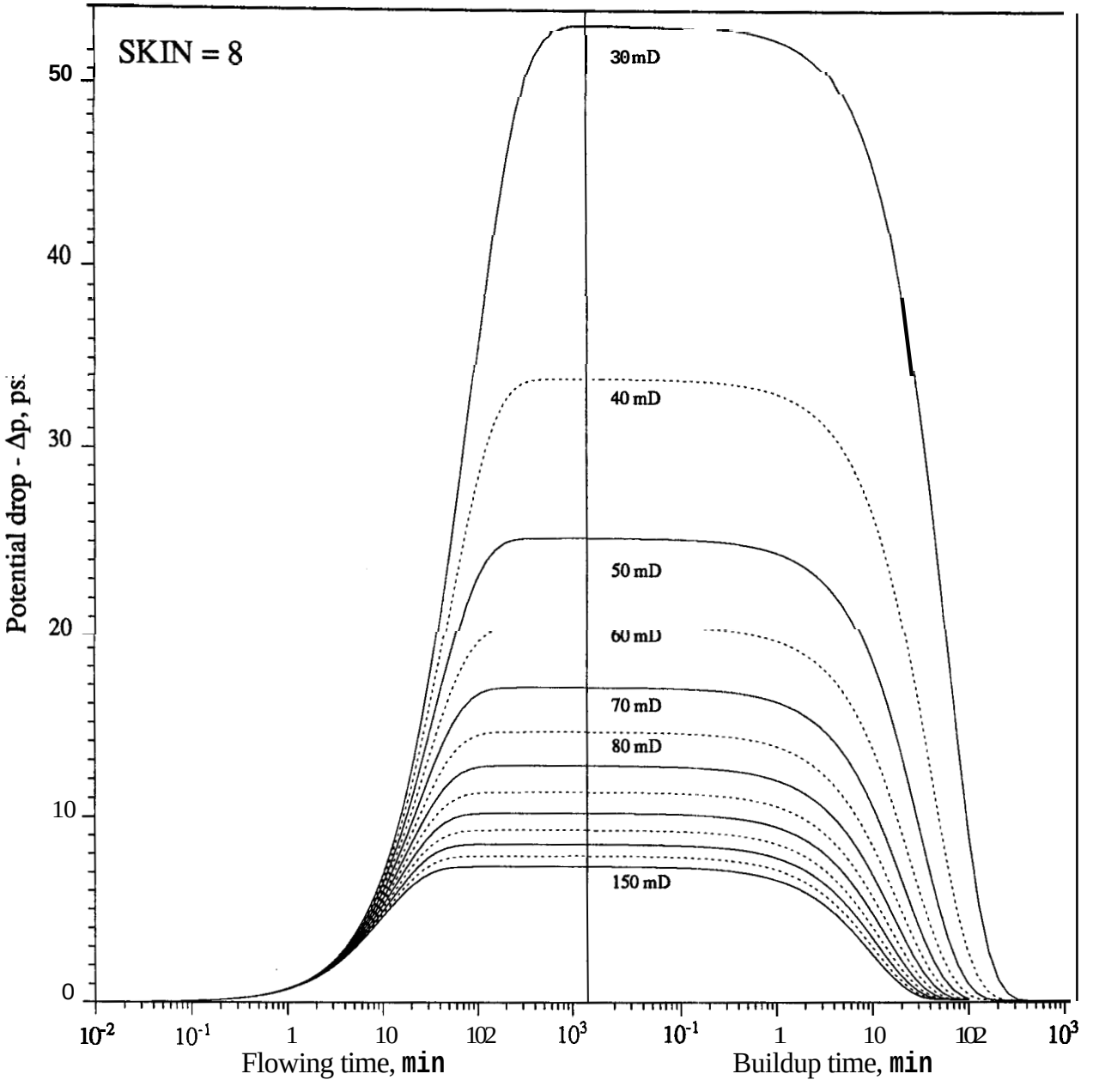

Figure 7.28: Combined 24-hour flowing and buildup test for a set of different permeabilities. Skin = 8.

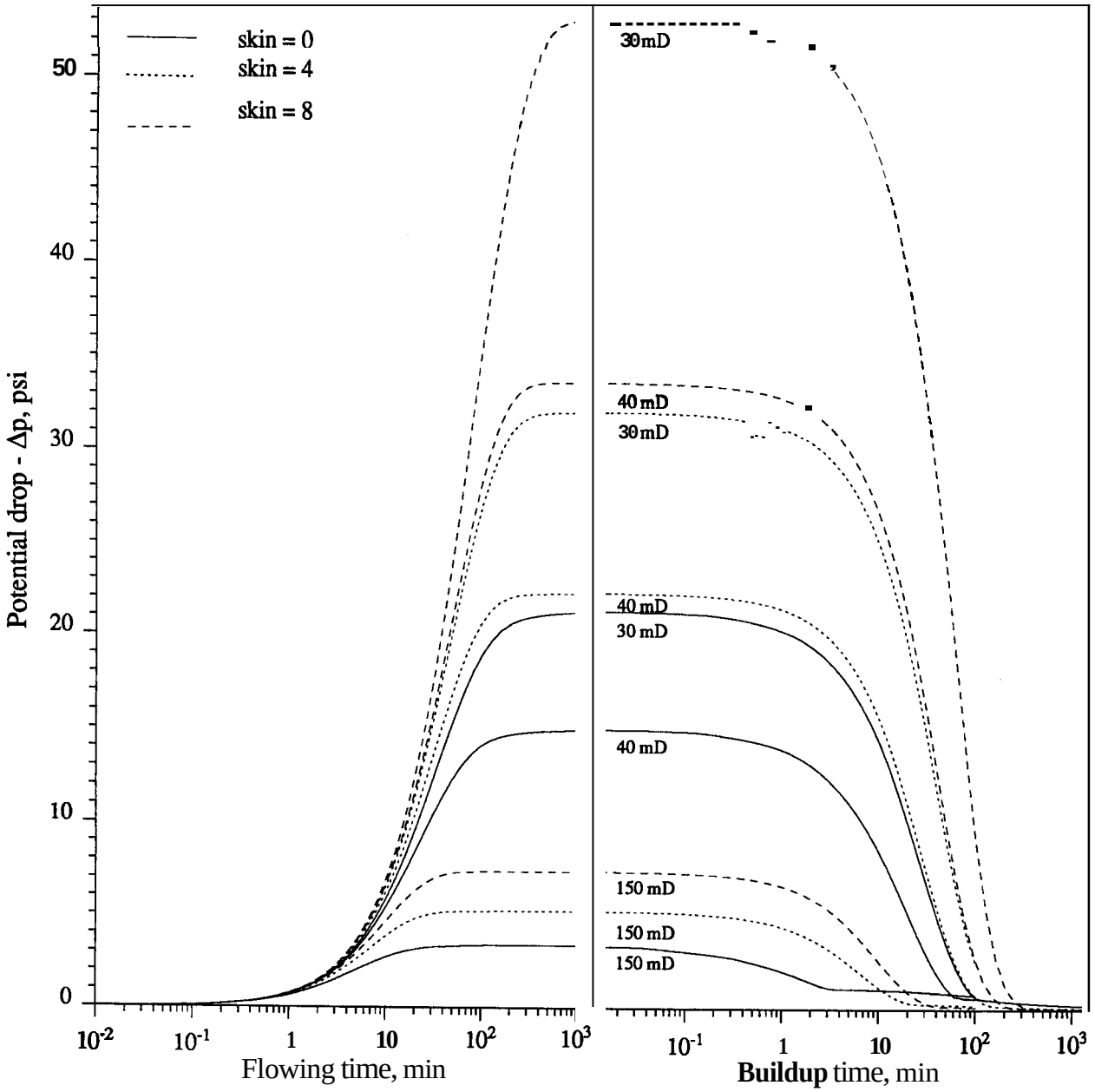

Figure 7.29: Combined 24-hour flowing and buildup test for a set of permeabilities and **skin** parameters.

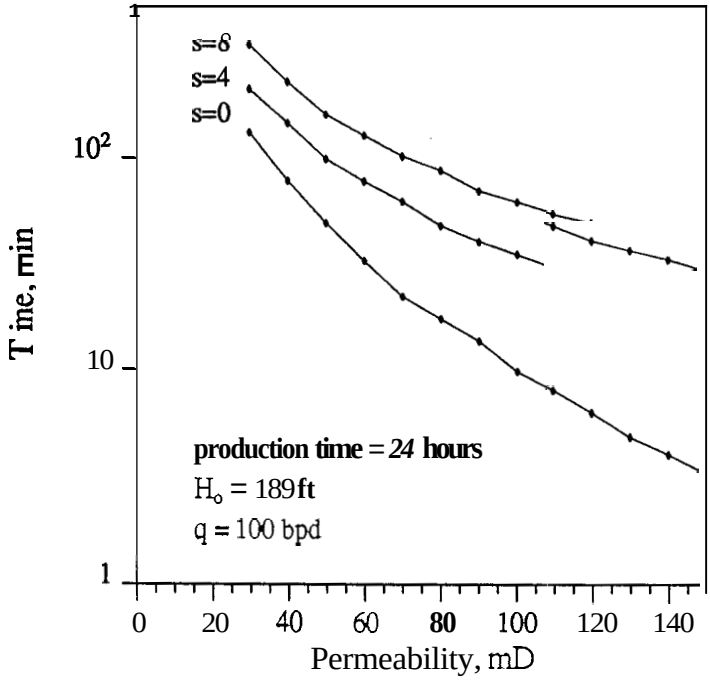

Figure 7.30: Time in which the liquid level in the well reaches the free surface level in the sandface during buildup.

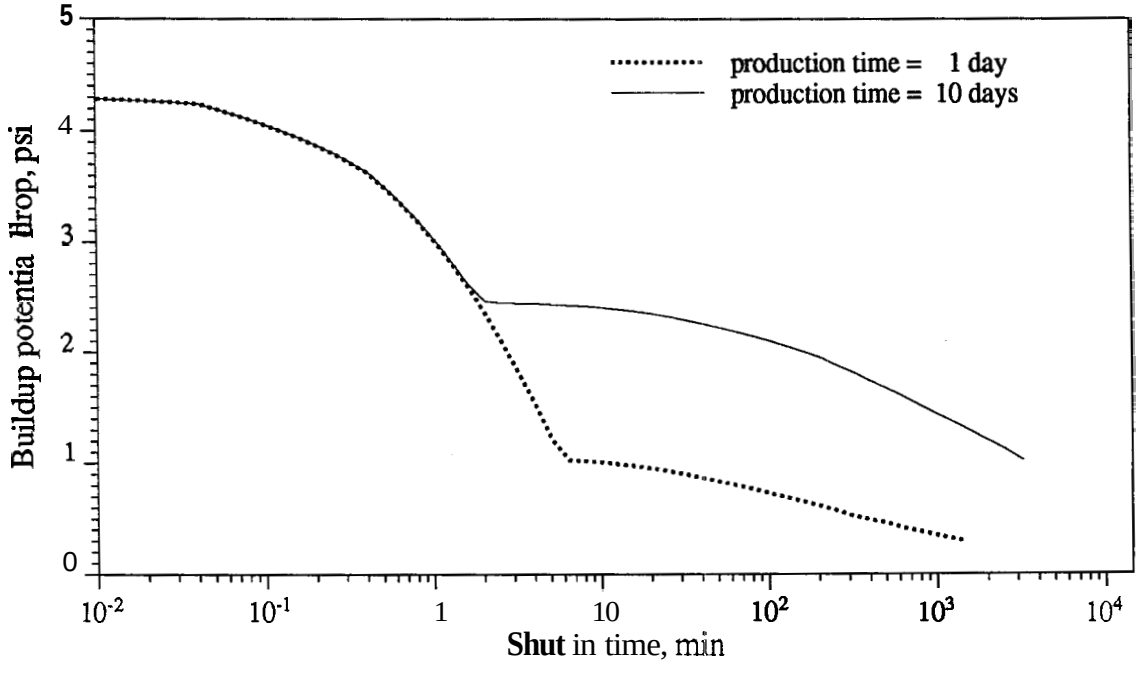

Figure 7.31: Buildup pressure drop behaviors for different production times

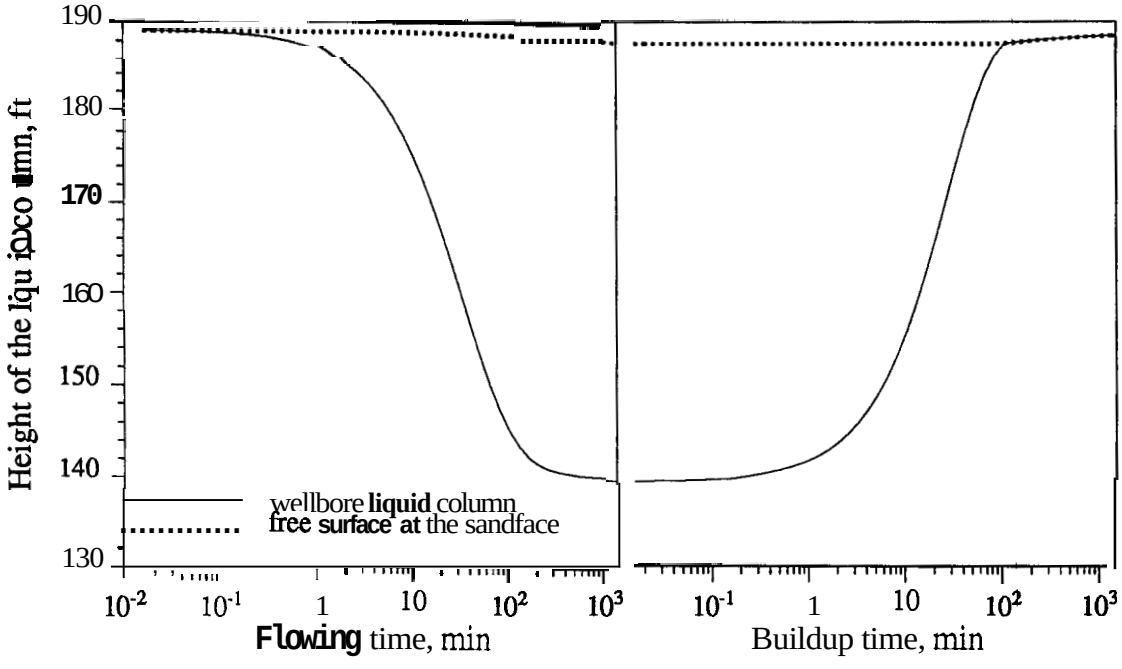

Figure **7.32:** Liquid levels in the wellbore and at the sandface during drawdown and buildup periods

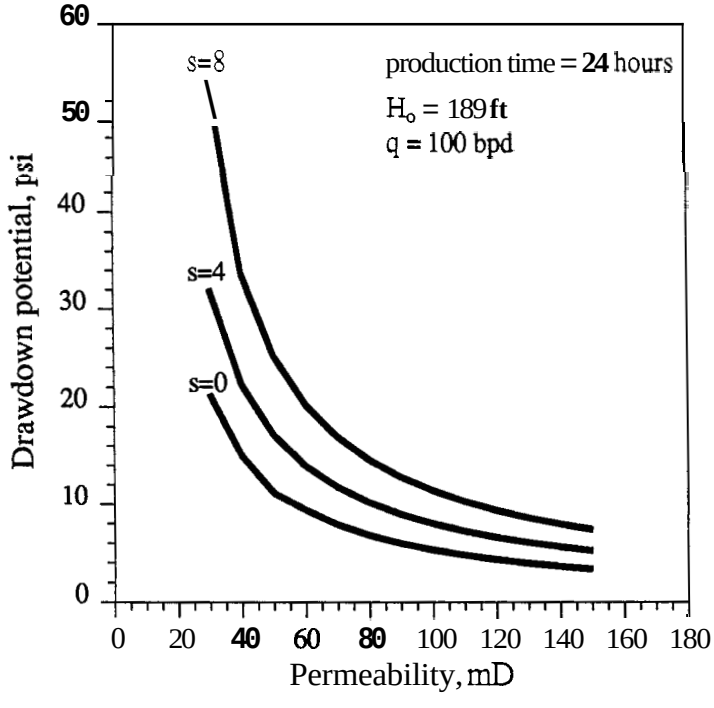

Figure **7.33:** Potential in the well after a 24-hour production period.

In the next chapter, a summary of the most important conclusions from the results of the *SLM* are presented, as well as some recommendations for future work.

Chapter 8

Conclusions and Recommendations

8.1 Conclusions

- The Stream Layer Model is able to reproduce free surface gravity flow well pressure behavior and the formation response with accuracy, depending on the finite-difference discretization in time and space. All three recognized transient flow periods in a constant flow rate test, namely wellbore storage, growth of the desaturating cone, and the pseudo-radial flow periods, are reproduced by the model.

- Steady-state flow was verified with the classical sandbox model experiments of *Wyckoff et al.* (1932), and *Hull* (1955). The seepage face phenomenon was reproduced with acceptable accuracy. Also, verification runs compared interference test results for observation wells located far from the wellbore with the *Neuman* (1972) analytical approach and Cooley (1971) numerical solution.

- Capillary fringe effects, though negligible on field scales, were important in the laboratory experiment verifications of *SLM*.

- The delayed yield period of a flat pressure-time response following wellbore

storage was evident in all computer runs, with or without a capillary fringe. It is clear that a capillary fringe is not necessary to generate a delayed yield effect. The major cause of deleayed yield is vertical, viscous drainage. Analytical solutions without a vertical flow component do not exhibit delayed yield.

- The strong non-linearities in the mathematical problem require **a** careful dimensioning of the grid parameters and time step sizes to obtain accuracy from the Stream Layer Model. Also, concerning the time interpolation parameter 8, the Crank-Nicolson method $(8 = 0.5)$ should be avoided because of number of iterations required for convergence.

- During the transient drawdown period, the seepage face length reaches a maximum value at the end of wellbore storage which frequently masked the confined system-like behavior reported in the Groundwater literature in the initial phase of production. After that, the liquid level in the formation adjacent to the wellbore starts to drop, as the potential gradients begin to increase. The pseudo-confined behavior is characterized by near stabilization of the potential gradients and free surface movement.

- The petroleum formation and liquid properties and well parameters tested by the *Stream Layer Model* caused the transient pressure drawdown behavior to persist longer than two or three log-cycles during the desaturating period. The pseudo-confined flow behavior generally required weeks or months of production to be graphically represented in a logarithimic cycle. **As** a consequence, to use a logarithmic approximation such as in the *Ramey et al.* **(1989)** p-square approach, a long term drawdown test should be planned to assure correct application of the method.

- As an approximate solution at late time, the method of *Ramey et al.* **(1989)** presented slopes closer to the Stream Layer Model results than the *Theis* **(1932)** line source solution. Low permeability reservoirs tend to present upward shifts from the p-squared approach at late times, keeping the same slope of the time-drawdown curve as in the *Ramey et al.* solution.

- Computer runs for pressure buildup also showed delayed yield. However the seepage face disappeared within a few minutes, and it appeared the free surface desaturated region refilled by radial flow, unlike the vertical drainage during production.

- Contrary to the drawdown results, the buildup pressures in the producing well generally require a short time to reach the resaturating period (equivalent to the desaturating period in the drawdown). Late time buildup pressures, however, could not be approximated by radial flow interpretation methods. The potential profiles in the radial direction taken at increasing buildup times show the distribution of the potential at the base with different slopes each time, tending to continuously reduce the radial potential gradient. The free surface profile shows uniform height from the wellbore into the reservoir during the buildup. This flat potential profile becomes extended with the shut-in time. The present study has shown that the buildup potential behavior in the producing well is not the reverse process of drawdown.

8.2 Recommendations

- The *Stream Layer* ***Model*** can be used for experimentation to aid developing a parametric correlation of dimensionless time and pressure drawdown in well test analysis, similar to the *Boulton* (1963) and *Neuman* (1972) correlations developed for observation wells. The use of the simulator is recommended for planning well tests for gravity drainage wells.

- The *SLM* simulator can be used to solve the semi-confined reservoir well problem. This simulator could be a useful tool to investigate the behavior of low pressure or low permeability pumping wells with dynamic liquid level reaching positions below the top of the formation and developing a free moving surface in the formation near the well. The computer program requires small modifications for this application.

- Wellbore pressure buildup analysis is a challenging matter remaining to be investigated, and an interpretation method should be studied using the simulator response for a physical understanding of the phenomenon. It is likely that computer aided interpretation with regression will be necessary.

- The observed anisotropic effects in the wellbore potential drawdown behavior by the *Stream Layer Model* may be used to produce an evaluation method to find vertical permeability of anisotropic reservoirs.

Nomenclature

A = area
A_1 = areal dimensionless factor
A_v = cross-sectional area of the vertical flow
$A_{i,j}$ = discretized equation coefficients
B_{wb} = formation volume factor of the wellbore liquid
$B_{i,j}$ = discretized equation coefficient
c_t = total compressibility
c_L = liquid compressibility
$C_{i,j}$ = discretized equation coefficient
$DA_{i,j}$ = Jacobian matrix coefficient
$DB_{i,j}$ = Jacobian matrix coefficient
$DC_{i,j}$ = Jacobian matrix coefficient
$DD_{i,j}$ = Jacobian matrix coefficient
$DE_{i,j}$ = Jacobian matrix coefficient
$DF_{i,j}$ = Jacobian matrix coefficient
$DG_{i,j}$ = Jacobian matrix coefficient
$D_{i,j}$ = discretized equation coefficient
$E_i(x)$ = exponential integral
$E_{i,j}$ = discretized equation coefficients
$F_{i,j}$ = discretized equation coefficients
f_r = ratio of logarithms of radial distances
f_x = ratio of axial permeabilities
g = acceleration constant of the gravity force
g_c = dimensional conversion factor
$G_{i,j}$ = wellbore discretized equation coefficients

H = vertical position of the free surface
H_o = original thickness at rest
H_s = vertical position of the liquid at the sandface
H_w = vertical position of the liquid at the wellbore
j_1 = vertical location of the liquid level in the well
k = formation permeability
k_x = permeability in the flow direction
M = number of grid blocks in the radial direction
N = number of grid blocks in the vertical direction
p = pressure
q = flow rate
q_x = flow rate in the stream layer direction
q_{in} = flow rate into a grid block element
q_{out} = flow rate out of a grid block element
r = radial distance
r_w = wellbore radius
$\bar{r}$ = radial distance of the gravity center of a 'block
s = skin effect parameter
S_g = gas saturation above the free surface
S_L = liquid saturation
S_w = water saturation
S_y = specific yield
T = transmissivity or transmissibility
t = time
V_{std} = volume of produced liquid at standard condition
V_{wb} = volume of produced liquid at wellbore condition
W = dimensionless potential
x_j = fraction of the inner block j_1 thickness above H_w
z = vertical coordinate
$z_{r_{w+}}$ = vertical coordinate at the sandface

SUBSCRIPT

D = dimensionless
h = horizontal direction
i = horizontal position of a discretized block;
j = vertical position of a discretized block
nw = non-wet or seepage region of sandface

o = initial condition
t = total
v = vertical direction
w = wellbore
wet = wet or drowned region of the sandface

SUPERSCRIPT

k = old time step
ν = level of iteration

GREEK

α = thickness interpolation parameter
δ = Dirac delta
δ_k = parameter: $delta_k = 1$ if $k = 1$, otherwise, $delta_k = 0$
δ_{j_1} = parameter: $\delta_{j_1} = 1$ if $j_1 = 1$; otherwise, $\delta_{j_1} = 0$
Δ = finite difference operator
Δh = free surface block thickness at its gravity center
Δh_w = thickness of a free surface block at the sandface
$\overline{\Delta} h$ = Free surface block boundary thickness
Δz = thickness of a saturated block at its gravity center
Δz_w = thickness of a saturated block at the sandface
$\overline{\Delta} h$ = saturated region block boundary thickness
ϵ = small residual number
Φ = potential
ϕ = porosity
γ = dimensionless liquid gradient
μ = liquid viscosity
θ = time relaxation parameter

ρ = density of the liquid
Ψ = residual equations

Bibliography

[1] Agarwal, R. G., Al-Hussainy, R., and Ramey, H. J. Jr.: "An Investigation of Wellbore Storage and Skin Effect in Unsteady Liquid Flow: I. Analytical Treatment", *Soc. Pet. Eng.* **J., (1970) 249, 279.**

[2] Amyx, J.W., Bass, D.M.,Jr., and Whiting, R.W.: *Petroleum Reservoir Engineering,* McGraw Hill, Inc., New York **(1960).**

[3] Aronofsky, J.S. and Jenkins, R.: "Unsteady Radial Flow of Gas Through Porous Media", *Jour. Appl. Mech.* **(1953) 20,** 210.

[4] Aziz, K. and Settari, **A.:** *Petroleum Reservoir Simulation,* Applied Science Publishers, London **(1979).**

[5] Babbit, H.E. and Caldwell, D.H.: "The Free Surface Around, and Interface between, Gravity Wells", *Engineering Experiment Station,* **(1948)** Bulletin Series, No. **374,** University of Illinois.

[6] Barenblatt, G. I., Zheltov Iu. P., and Kochina, I.F.: "Basic Concepts in the Theory of Seepage of Homogeneous Liquids in Fissured Rocks", *Jour. Appl. Math.* (1960), **24**(5), **1286.**

[7] Brand, C., Girard, P., Nacul E. C., and Aziz, K.: "Efficient Solvers for Reservoir Simulation", 8th Stanford Reservoir Simulation Workshop, May **16, 1992.**

[8] Boulton, N. S.: "The Flow Pattern near a Gravity Well in a Uniform Water Bearing Medium", *J. Instn. Civ. Engrs* (London - **1951) 36, 534.**

[9] Boulton, N. S.: "The Drawdown of the Water-Table under Non-Steady Conditions near a Pumped Well in an Unconfined Formation", *Proc. Instn. Civ. Engrs.* **(1954,** a) **3,** Part 111, **564.**

[10] Boulton, N. S.: "Unsteady Radial Flow to a Pumped Well Allowing for Delayed Yield from Storage", *Publication* No. **37** de l'Association Internationale d'Hydrologie, Assemblae Generale de Rome **(1954,** b) Tome **11, 472.**

[11] Boulton, N. S.: "Analysis of Data from Non-Equilibrium Pumping Tests Allowing for Delayed Yield from Storage", *Proc. Instn. Civ. Engrs.* (London - **1963) 26, 469.**

[12] Boulton, N. S.: "Analysis of Data from Pumping Tests in Unconfined Anisotropic Aquifers", *J.* Hydrology (1970), **10, 369.**

[13] Boulton, N. S., and Pontin, J. M. A.: "The Influence of Delayed Drainage on Data from Pumping Tests in Unconfined Anisotropic Aquifers", *J. Hydrology* (1971), **19**(1), **157.**

[14] Bouwer, H.: "Soil Water Hysteresis as a Cause of Delayed Yield from Unconfined Aquifers", *Groundwater* (1979), **15**(4), **965.**

[15] Bouwer, H., and Rice, R. C.: "A Slug Test for Determining Hydraulic Conductivity of Unconfined Aquifers with Completely or Partially Penetrating Wells", *Water Resources Res.* (1976), **12**(3), **423.**

[16] Bouwer, H., and Rice, R. C.: "Delayed Aquifer Yield as a Phenomenon of Delayed Air Entry", *Water Resources Res.* (1978), **14**(6), **1068.**

[17] Carslaw, H. S. and J. C. Jaeger: *Conduction of Heat in Solids,* Oxford University Press **(1959).**

[18] Cooper, H. H. Jr., Bredehoeft, J.D., and Papadopulos, I.S.: "Response of a Finite Diameter Well to an Instantaneous Charge of Water", *Water Resour. Res.* (1967), **3, 263-269.**

[19] Cooley, R. L.: "A Finite Difference method for Unsteady Flow in Variably Saturated Porous Media: Application to a single Pumping Well", *Water Resour. Res.* (1971), **7**(6), 1607.

[20] Cooley, R. L., and Donohue, D. A. T.: "Numerical Simulation of Unconfined Flow into a Single Pumping Water-well Using Two-phase Flow Theory", Technical Completion Report, Inst. for Res. on Land and Water Resour., Pa. State Univ., State College, 1969.

[21] Dagan, G.: "Second Order Linearized Theory of Free-Surface Flow in Porous Media", *Houille Blanche* (1964), ***8,*** 901.

[22] Dagan, G.: "A Method of Determining the Permeability and Effective Porosity of Unconfined Anisotropic Aquifers", *Water Resour. Res.* (1967), **3**(4), 1059.

[23] Dagan, G.: "A Note on Packer, Slug, and Recovery Tests in Unconfined Aquifer", *Water Resour. Res.* (1978), **14**(5), 929.

[24] Dieleman, P. J.; Riedder N. A. and Wesseling, J.: "Drainage Principles and Applications", *Int'l Inst. for Land Reclamation and Improvement,* Wageningen The Netherlands (1972) **1,** 153.

[25] Dupuit, J.: *Etudes Theoriques et Pratiques sur le Mouvement des Eaux dans l Couverts et a Travers les Terrains Permeables,* 2nd edn, Dunod, Paris (1863).

[26] Earlougher, R. C., Jr.: *Advances in Well Test Analysis,* SPE Monograph, Henry L. Doherty Series, v. 5, New York, 1977.

[27] Forchheimer, P.: *Zeits. Arch. Ing. Ver.,* Hannover (1886).

[28] Fligelman, H.: "Drawdown and Interference Test Analysis for Gas Wells with Wellbore Storage, Damage, and Nonlaminar Flow Effects", PhD dissert., Stanford Univ. (1980).

[29] Gambolati, G.: "Transient Free Surface Flow to a Well: An Analysis of Theoretical Solutions", *Water Resour. Res.* (1976) **12**(1), 27.

[30] Green, D. W., Dabiri, H., Weinaug, C. F. and Prill, R. : "Numerical Modeling of Unsaturated Groundwater Flow and Comparison of the Model to a Field Experiment", *Water Resour. Res.* **(1970) 6(3), 862.**

[31] Hall, H.P.: "An Investigation of Steady Flow toward a Gravity Well", ***La Houille Blanche*** **(1955) 25, 8-35.**

[32] Hantush, M. S.: "Hydraulics of Wells", *Advances in Hydroscience,* **1,** edited by V .T. Chow, Academic Press, NY **(1964).**

[33] Hawkins, M. F.: "A Note on the Skin Effect", *Trans.,* AIME (1956), ***207,*** **356-357.**

[34] Hornberger, G. M., and Remson, I.: "A moving boundary model of a One-dimensional Saturated-unsaturated, Transient Porous Flow System", *Water Resour. Res.* **(1970) 6(3), 898.**

[35] Horner, D. R.: "Pressure Buildup in Wells", Proc. 3rd. World Pet. Cong., E. J. Brice, London, Heiden, Neth. **(1951)** Sect II, Preprint **7.**

[36] Hurst, W.: "Establishment of the Skin Effect and its Impediment to Fluid-Flow Into a Well Bore", *Pet. Eng.* **(1953) 25,** B-6.

[37] Kipp, K. L.: "Unsteady Flow to a Partially Penetrating Finite Radius Well in an Unconfined Aquifer", *Water Resour. Res.* **(1973) 9(2), 448.**

[38] Kroszynski, U. I., and Dagan, G.: "Well Pumping in Unconfined Aquifers: The Influence of the Unsaturated Zone", *Water Resour. Res.* **(1975) 11(3), 479.**

[39] Matthews, C. S., and Lefkovits, H. C.: "Gravity Drainage Performance of Depletion-Type Reservoirs in the Stripper Stage", *Tmns.,* AIME (1956), ***207,*** 263-274.

[40] Moore, T. V., Shilthuis, R. J. and Hurst, W.: "The Determination of Permeability from Field Data", ***Proc.,*** API Meeting, Tulsa, Okla. (May **17-19, 1933) 4.**

[41] Muskat, M.: "The Seepage of Water Through Dams with Vertical Faces", *Physics* **(1935) 6, 402.**

[42] Muskat, M.: Flow of *Homogeneous Fluids Through Porous Media,* I.H.R.D.C., Boston **(1937-1982).**

[43] Muskat, M.: *Physical Principles of Oil Production,* McGraw Hill **Book** Company, Inc., New York **(1949).**

[44] Narasimhan, T.N. and Zhu, M.: "Transient Radial Flow to a Well in an Unconfined Aquifer, **1.** Applicability of Some Conceptual Models", *Water Resour. Res.*, in press.

[45] Neuman, S. P., and Witherspoon, P. A.: "Finite Element Method of Analyzing Steady Seepage with a Free Surface", *Water Resour. Res.* (1970-a) 6(5), **889.**

[46] Neuman, S. P., and Witherspoon, P. A.: "Variational Principles for Confined and Unconfined Flow of Ground Water", *Water Resour. Res.* **(1970-b)** 6(5), **1376.**

[47] Neuman, S. P., and Witherspoon, P. A.: "Analysis of Nonsteady Flow with a Free Surface Using the Finite Element Method", *Water Resour. Res.* **(1971) 7(3), 611.**

[48] Neuman, S. P.: "Theory of Flow in Unconfined Aquifers Considering Delayed Response of the Water Table", *Water Resour. Res.* **(1972)** 8(4), **1031.**

[49] Neuman, S. P.: "Supplementary Comments on 'Theory of Flow in Unconfined Aquifers Considering Delayed Response of the Water Table"', *Water Resour. Res.* **(1973)** 9(4), **1102.**

[50] Neuman, S. P.: "Effect of Partial Penetration on Flow in Unconfined Aquifers Considering Delayed Gravity Response", *Water Resour. Res.* **(1974)** 10(2), **303.**

[51] Neuman, S. P., Feedes, R. E., and Bresler, E.: "Finite Element Simulation of Flow in Saturated-Unsaturated Soils Considering Water Uptake by Plants" completion rep., Proj. ALO-SWC-77 (1974), Hydrodyn. and Hydraul. Eng. Lab., Haifa, Israel.

[52] Neuman, S. P.: "Analysis of Pumping Test Data From Anisotropic Unconfined Aquifers Considering Delayed Response", *Water Resour. Res.* (1975-a) **11**(2), 329.

[53] Neuman, S. P.: "Galerkin Approach to Saturated-Unsaturated Flow in Porous Media", *Finite Element in Fluids*, vol. **1**, edited by R. H. Gallagher, J. T. Oden, C. Taylor, and O. C. Zienkiewicz, John Wiley, New York, 1975-b.

[54] Neuman, S. P.: Reply, *Water Resour. Res.* (1976) **12**(1), 115.

[55] Neuman, S. P.: "Perspective on Delayed Yield"', *Water Resour. Res.* (1979) **15**(4), 899.

[56] Neuman, S. P.: "On Methods of Determining Specific Yield", Groundwater (1987) **25**(6), 67.

[57] Nwankwor, G. I., Cherry J. A., and Gillham, R. W.: "A Comparative Study of Specific Yield Determinations for a Shallow Sand Aquifer", *Groundwater* (1984) **22**(6), 764.

[58] Peaceman, D. W.: *Fundamentals of Numerical Reservoir Simulation*, Elsevier Sci. Pub. Co., New York (1977).

[59] Papadopulos, I. S.: "Drawdown Distribution around a Large Diameter Well", *Proc. Symp. on Groundwater Hydrology*, San Francisco, Nov., *Proc.* Am. Water Resources Assoc. (1967) **4**, 157-168.

[60] Papadopulos, I. S. and Cooper, H. H., Jr.: "Drawdown in a Well of Large Diameter", *Water Resour. Res.* (1967) **3**(1), 241.

[61] Patel, S. C., and Mishra, G. C.: "Analysis of Flow to a Large-Diameter Well by a Discrete Kernel Approach", *Groundwater* (1983) 21 (5), 573.

[62] Polubarinova-Kochina, P.YA.: *Theory of Ground Water Movement*, Translated from the russian by J. M. Roger de Wiest, Princeton University Press, Princeton, NY (1962).

[63] Prickett T. A.: "Type Curve Solution to Aquifer Tests under Water-Table Conditions", *Groundwater* (1965) **3**(3), 5.

[64] Ramey, H. J., Lichtenberg, S., and Davitt, J.: "Well Testing Analysis for Gravity Drainage System", Paper SPE No. 890017, *Proceedings* of Petroleum Technology into the Second Century Meeting, Socorro, New Mexico, Oct.,1989.

[65] Rushton, K. R., and Holt, S. M.: "Estimating Aquifer Parameters for Large-Diameter Wells", *Groundwater* (1981) **19**(5), 505.

[66] Rushton, K. R., and Singh, V. S.: "Pumping Test Analysis in Large Diameter Wells with a Seepage Face by Kernel Function Technique", *Groundwater* (1987) **25**(1), 81.

[67] Shamsai, A. and Narasimhan, T. N.: **"A** Numerical Investigation of Free Surface-Seepage Face Relationship Under Steady State Flow Conditions", *Water Resour. Res.* (1991) **27**(3), 409.

[68] Stehfest, H.: "Algorithm 368: Numerical Inversion of the Laplace Transform", *Comunication of the* **A.** *C. M.*, **1** (13), (August 1970).

[69] Streltsova, T. D.: "Unconfined Aquifer and Slow Drainage", ***J.*** *Hydrology* (1972-a) 16, 117.

[70] Streltsova, T. D.: "Unsteady Radial Flow in an Unconfined Aquifer", *Water Resour. Res.* (1972-b) **8**(4), 1059.

[71] Streltsova, T. D.: "Flow near a Pumped Well in an Unconfined Aquifer under Nonsteady Conditions", *Water Resour. Res.* (1973) **9**(1), 227.

[72] Streltsova, T. D.: "Drawdown in a Compressible Unconfined Aquifer ", *Div.*, Amer. Soc. Civil Eng., **100**(HY11), 1974.

[73] Streltsova, T. D.: "Comments on 'Analysis of Pumping Test Data from Anisotropic Unconfined Aquifers Considering Delayed Gravity Response' by Shlomo P. Neuman", *Water Resour. Res.* (1976) **9**(1), 236.

[74] Streltsova, T. D. and Rushton, K. R.: "Water Table Drawdown due to a Pumped Well in an Unconfined Aquifer", Water Resour. *Res.*(1973) 9(1), 236.

[75] Szabo, B. A. and McCaig, I. W.: "A Mathematical Model for Transient Free Surface Flow in Nonhomogeneous Porous Media", Water Res. Bull. (1968), **4** part 3.

[76] Terán, M. A. and de la Garza, F. R.: "Efecto de la Geometria de la Malla sobre la Estabilidad de un Simulador Numerico", *Inginieria* Petrolera (1988) 28, 10.

[77] Theis, C. V: "The Relation between the Lowering of the Piezometric Surface and the rate of Duration of Discharge of a Well using Ground-Water Storage", *Trans*. Amer. Geophys. Un. (1935) 16, 519.

[78] Thomas, G. W.: Hydrocarbon Reservoir *Simulation,* Int. Human Res. Dev. Corp., Boston (1982).

[79] van Everdingen, A. F. and Hurst, W.: "The Application of the Laplace Transformation to Flow Problems in Reservoirs", *Trans.* AIME (1949) 186,305-324.

[80] van Everdingen, A. F.: "The Skin Effect and Its Influence on the Productive Capacity of a Well", *Trans.* AIME (1953) 198,171-176.

[81] Walton, W. C.: "Application and Limitations of Methods used to Analyse Pumping Test Data", part **2,** Water Well *J*. (1960) March, 45.

[82] Wyckoff, R. D., Botset, H. G., and Muskat, M.: "Flow of Liquids through Porous Media under the Action of Gravity", Physics (1932) **3,** 90-113.

Appendix A

Inner Boundary Condition

A.1 Partial Derivatives of the Sandface Potential

Potentials at the sandface are a function of the vertical coordinate and of the liquid level in the wellbore. The criteria used to define the inner boundary conditions are shown next in dimensionless form:

$$W_w = \gamma_o z_{w_D} \quad \Rightarrow \quad H_{w_D} < z_{w_D} \leq H_{s_D} \tag{A.1.1}$$

A finite difference form of the equation and grid definitions of the reservoir requires that the inner boundary be reordered into different regions, according to the position of the liquid level in the wellbore at each time-step. A vertical grid parameter j_1 was defined as the grid position at the sandface adjacent to the wellbore liquid level. The potentials were calculated:

$$W_{w_j} = \gamma_o H_{w_D} \qquad \Rightarrow \qquad j > j_1 \tag{A.1.2}$$

$$W_{w_j} = \gamma_o \left(z_{w_{D_j}} + \frac{\Delta h_{D_w}}{2} \right) \qquad \Rightarrow \qquad 1 = j < j_1 \tag{A.1.3}$$

$$W_{w_j} = \gamma_o \left(z_{w_{D_j}} + \frac{\Delta z_{D_w}}{2} \right) \qquad \Rightarrow \qquad 1 \neq j < j_1 \tag{A.1.4}$$

$$W_{w_j} = \frac{\gamma_o}{2} \left[(1 + x_{j_1}) H_{w_D} + (1 - x_{j_1}) \left(z_{w_{D_{j_1}}} + \Delta z_{D_w} \right) \right] \qquad \Rightarrow \qquad j = j_1 \neq 1 \tag{A.1.5}$$

where:

$$x_{j_1} = \frac{H_{w_D} - z_{w_{D_{j_1}}}}{\Delta z_{D_w}} \tag{A.1.6}$$

$$W_{w_j} = \frac{\gamma_o}{2} \left[(1 + x_{j_1}) H_{w_D} + (1 - x_{j_1}) \left(z_{w_{D_1}} + \Delta h_{D_w} \right) \right] \qquad \Rightarrow \qquad j = j_1 = 1 \tag{A.1.7}$$

where:

$$x_{j_1} = \frac{H_{w_D} - z_{w_{D_1}}}{\Delta h_{D_w}} \tag{A.1.8}$$

Partial differentials with respect to $W_{1,k}$ were calculated from the above definitions. Initially, k is set different from **1:**

(a) $j > j_1$:

$$\frac{\partial W_{w_j}}{\partial W_{1,k}} = \gamma_o \frac{\partial H_{w_D}}{\partial W_{1,k}} \tag{A.1.9}$$

(b) $j < j_1$

$$\frac{\partial W_{w_j}}{\partial W_{1,\kappa}} = 0 \qquad \text{(A.1.10)}$$

(c) $j = 1$ and $1 < j_1$

$$\frac{\partial W_{w_j}}{\partial W_{1,\kappa}} = 0 \qquad \text{(A.1.11)}$$

(d) $j = j_1$ and $j_1 \neq 1$

$$\frac{\partial W_{w_j}}{\partial W_{1,\kappa}} = x_{j_1}\gamma_o \frac{\partial H_{w_D}}{\partial W_{1,\kappa}} \qquad \text{(A.1.12)}$$

(e) $j = j_1 = 1$

$$\frac{\partial W_{w_j}}{\partial W_{1,\kappa}} = x_{j_1}\gamma_o \frac{\partial H_{w_D}}{\partial W_{1,\kappa}} \qquad \text{(A.1.13)}$$

Partial differentiations with respect to $W_{1,1}$ are particular cases in which there is a dependence of several paramaters on the potential:

(a) $j > j_1$

$$\frac{\partial W_{w_j}}{\partial W_{1,1}} = \gamma_o \frac{\partial H_{w_D}}{\partial W_{1,1}} \qquad \text{(A.1.14)}$$

(b) $j < j_1$

$$\frac{\partial W_{w_j}}{\partial W_{1,1}} = 0 \qquad \text{(A.1.15)}$$

(c) $j = 1$ and $1 < j_1$

$$\frac{\partial W_{w_j}}{\partial W_{1,1}} = \frac{\gamma_o\, \alpha_w}{2\, \overline{\gamma}_1} \qquad \text{(A.1.16)}$$

(d) $j = j_1$ and $j_1 \neq 1$

$$\frac{\partial W_{w_j}}{\partial W_{1,1}} = x_{j_1}\gamma_o \frac{\partial H_{w_D}}{\partial W_{1,1}} \qquad \text{(A.1.17)}$$

(e) $j = j_1 = 1$

$$\frac{\partial W_{w_j}}{\partial W_{1,1}} = \gamma_o \left[x_{j_1} \frac{\partial H_{w_D}}{\partial W_{1,1}} + \left(1 - x_{j_1}^2\right) \frac{\alpha_w}{2\,\overline{\gamma}_1} \right] \tag{A.1.18}$$

In the last case, Δh_{D_w} is also directly dependent on $W_{1,2}$. Thus, another condition must be considered when $j = 1$:

(a) $j = 1$ and $j_1 > 1$

$$\frac{\partial W_{w_j}}{\partial W_{2,1}} = \frac{\gamma_o\,(1 - \alpha_w)}{2\,\overline{\gamma}_2} \tag{A.1.19}$$

(b) $j = 1$ and $j_1 = 1$

$$\frac{\partial W_{w_j}}{\partial W_{2,1}} = \gamma_o \left[x_{j_1} \frac{\partial H_{w_D}}{\partial W_{2,1}} + \left(1 - x_{j_1}^2\right) \frac{1 - \alpha_w}{2\,\overline{\gamma}_2} \right] \tag{A.1.20}$$

A.2 Liquid level in the Wellbore from Material Balance Equation

From the material balance discretized equation and the substitution of the sand-face potentials, it is possible to determine the liquid level in the wellbore within a time-step. The possibility of guessing the position j_1 and a global iterative procedure enable one to estimate the value of H_{w_D}.

There are two ways to determine the liquid level in the well, starting from the material balance equation represented by Eq.3.2.5 in the Ch. **3,** presented below.

A.2.1 Quadratic Equation

A quadratic equation is obtained from the discretization of Eq. 3.2.5 starting from the introduction of a time interpolation parameter as follows:

$$q\,B_{wb} = -\frac{\pi\, r_w^2 \Delta H_w}{2\,\phi\,\Delta t} + \frac{2\,\pi}{\mu \ln(\bar{r}_1)}\left[\theta \int_0^{h_s} k_x\,\Delta\Phi|_{r=r_w}\,dz \;+\; (1-\theta)\int_0^{h_s} k_x \Delta\Phi^k\Big|_{r=r_w} dz\right] \tag{A.2.1.1}$$

Multiply by $\frac{\mu}{2\pi r_w\, k_h\, H_o \rho \frac{g}{g_c}}$ to obtain the dimensionless expression:

$$q_D\,B_{wb} = -\frac{H_{w_D} - H_{w_D}^k}{2\,\phi\,\Delta t_D} + \frac{1}{k_h \ln(\bar{r}_1)}\left[\theta \int_0^{H_s} k_x\,\Delta W|_{r_D=1}\,dz_D + (1-\theta)\int_0^{H_s} k_x\,\Delta W^k\Big|_{r_D=1} dz_D\right] \tag{A.2.1.2}$$

A quadratic equation can be obtained isolating H_{w_D}. The following parameter is introduced in order to handle all possible positions of the liquid level in the wellbore with a single equation:

$$\begin{cases} \mathbf{6 = 1} & \text{as} \quad j_1 = 1 \\ \delta = 0 & \textbf{as} \quad j_1 \neq 1 \end{cases}$$

Next, a proportionality factor x_j is introduced to average the potential at the sandface position adjacent to the liquid surface in the wellbore:

$$x_j = \frac{H_{w_D} - z_{D_{w_{j_1}}}}{\delta\,\Delta h_{D_w} + (1-\delta)\,\Delta z_{D_w}} \tag{A.2.1.3}$$

Using the parameters 6 and x_j, the integrals can be symplified by calculating average permeabilities and factoring the average permeability out of the the integrands:

$$\overline{k}_{x_w} = \frac{\left(x_j^{\kappa}\ k_{x_1,j_1^{\kappa}} + \sum_{j_1^{\kappa}+1}^{n}\left(k_{x_1,j}\right)\right)\overline{\Delta z}_{D_1}}{H_{w_D}^{k}} \tag{A.2.1.4}$$

$$\overline{k}_{x_{nw}}^{\kappa} = \frac{\left[\left(1-x_j^{\kappa}\right)\ k_{x_{1,j_1^k}} + \sum_{1}^{j_1^{\kappa}-1}\left(k_{x_1,j}\right)\right]\overline{\Delta z}_{D_1}}{H_s^{\kappa} - H_{w_D}^{\kappa}} \tag{A.2.1.5}$$

$$k_{x_{nw}} = \frac{x_j k_{x_1,j_1}\left[\delta\overline{\Delta h}_{D_1} + (1-\delta)\overline{\Delta z}_{D_1}\right] + \overline{\Delta z}_{D_1}\sum_{j_1+1}^{n}\left(k_{x_1,j}\right)}{H_{w_D}} \tag{A.2.1.6}$$

$$\overline{k}_{x_{nw}} = \frac{1}{H_s - H_{w_D}}\left\{(1-x_j)\ k_{x_1,j_1}\left[\delta\overline{\Delta h}_{D_1} + (1-\delta)\overline{\Delta z}_{D_1}\right] + \overline{\Delta z}_{D_1}\sum_{2}^{j_1-1}\left(k_{x_1,j}\right) + (1-\delta)\overline{\Delta h}_{D_1} + k_{x_{1,1}}\right\} \tag{A.2.1.7}$$

The superscript **k** means the begining of the time-step, and the subscripts nw and ***wet*** represent the seepage face *(non-wet)* and the liquid submerged ***(wet)*** wellbore regions, respectively. A first decomposition of the material balance equation at the wellbore gives the following:

$$q_D\, B_{wb} = -\frac{H_{w_D} - H_{w_D}^{k}}{2\,\phi\,\Delta t_D} + \frac{1}{k_h \ln(\overline{r}_1)}\left\{\theta\left[\overline{\Delta h}_{D_1} + k_{x_{1,1}} W_{1,1} + \Delta\overline{z}_{D_1}\sum_{2}^{n}\left(k_{x_1,j} W_{1,j}\right) - \frac{H_{w_D}^2}{H_{o_D}}\overline{k}_{x_{wet}} - \frac{H_s^2 - H_{w_D}^2}{2H_{o_D}}\overline{k}_{x_{nw}}\right] + (1-\theta)\left[\overline{\Delta z}_{D_1}\sum_{1}^{n} k_{x_1,j} W_{1,j}^{\kappa} - \frac{H_{w_D}^{k\,2}}{H_{o_D}}\overline{k}_{x_{wet}}^{k} - \frac{H_s^{\kappa 2} - H_{w_D}^{k\,2}}{2\,H_{o_D}}\overline{k}_{x_{nw}}^{k}\right]\right\} \tag{A.2.1.8}$$

Rearranging the terms in the above expression, a quadratic equation is obtained in the format:

$$A\,H_{w_D}^2 \;+\; B\,H_{w_D} \;+\; C \;=\; 0 \qquad \textbf{(A.2.1.9)}$$

in which the coefficients are easily identified. This equation gives two possible solutions. Negative values are always neglected, and if there are two positive roots, some logical criteria of analysis are introduced in the computer program.

$$\frac{\theta}{H_{o_D} k_h \ln(\bar{r}_1)}\left[\bar{k}_{x_w} - \frac{\bar{k}_{x_{nw}}}{2}\right] H_{w_D}^2 + \frac{1}{2\phi\,\Delta t_D} H_{w_D} - \frac{H_{w_D}^k}{2\phi\,\Delta t_D} + q_D\,B_{wb} -$$
$$\frac{1}{k_h \ln(\bar{r}_1)}\left\{\theta\left[\overline{\Delta h}_{D_1} k_{x_{1,1}} W_{1,1} + \overline{\Delta z}_{D_1}\sum_{2}^{n}\left(k_{x_{1,j}} W_{1,j}\right) - \frac{H_s^2}{2H_{o_D}}\bar{k}_{x_{nw}}\right] +\right.$$
$$\left.(1-\theta)\left[\overline{\Delta z}_{D_1}\sum_{1}^{n} k_{x_{1,j}} W_{1,j}^{\kappa} - \frac{H_{w_D}^{k\,2}}{H_{o_D}}\bar{k}_{x_{wet}}^{k} - \frac{H_s^{\kappa 2} - H_{w_D}^{k\,2}}{2\,H_{o_D}}\bar{k}_{x_{nw}}^{k}\right]\right\} = 0$$

(A.2.1.10)

A.2.2 Iterative Solution for the Wellbore Liquid Level

An optional way to solve the wellbore liquid level equation is to use **an** iterative process as the Newton-Raphson approach. This procedure gives only one of two roots for H_{w_D} from the quadratic equation, and the initial guess to start the iterative process is of fundamental importance for the usefulness of the result. The procedure starts from the discretized material balance equation below:

$$q_D B_{w_b} = -\frac{\Delta H_{w_D}}{2\phi \Delta t_D} + \frac{\overline{\Delta z}_{D_1}}{\ln(\bar{r}_1)} \left\{ \frac{k_{x_{1,1}}}{k_h} (1-\theta) \left[W^k_{1,1} - W^k_{w_1} \right] + \sum_{j=2}^{n} \frac{k_{x_{1,j}}}{k_h} \left[\theta \left[W_{1,j} - W_{w_j} \right] + (1-\theta) \left[W^k_{1,j} - W^k_{w_j} \right] \right] \right) + \frac{\overline{\Delta h}_{D_1}}{\ln(\bar{r}_1)} \frac{k_{x_{1,1}}}{k_h} \theta \left[W_{1,1} - W_{w_1} \right]$$

(A.2.2.1)

Call the function:

$$\mathcal{F}\left(H^v_{w_D}\right) = q_D B_{w_b} + \frac{H^v_{w_D} - H^k_{w_D}}{2\phi \Delta t_D} - \frac{\overline{\Delta z}_{D_1}}{\ln(\bar{r}_1)} \left\{ \frac{k_{x_{1,1}}}{k_h} (1-\theta) \left[W^k_{1,1} - W^k_{w_1} \right] + \sum_{j=2}^{n} \frac{k_{x_{1,j}}}{k_h} \left[\theta \left[W_{1,j} - W_{w_j} \right] + (1-\theta) \left[W^k_{1,j} - W^k_{w_j} \right] \right] \right\} - \frac{\overline{\Delta h}_{D_1}}{\ln(\bar{r}_1)} \frac{k_{x_{1,1}}}{k_h} \theta \left[W_{1,1} - W_{w_1} \right]$$

(A.2.2.2)

and its derivative:

$$\mathcal{F}'(H_{w_D}) = \frac{\partial \mathcal{F}(H_{w_D})}{\partial H_{w_D}} = q_D \frac{\partial B_{w_b}}{\partial H_{w_D}} + \frac{1}{2\phi \Delta t_D} + \frac{\theta}{k_h \ln(\bar{r}_1)} \times \left\{ \overline{\Delta z}_{D_1} \sum_{j_1+1}^{n} k_{x_{1,j}} \frac{\partial W_{w_j}}{\partial H_{w_D}} + \left[(1-\delta) \overline{\Delta z}_{D_1} + \delta \overline{\Delta h}_{D_1} \right] k_{x_{1,j_1}} \frac{\partial W_{w_{j_1}}}{\partial H_{w_D}} \right\}$$

(A.2.2.3)

where δ is defined by the grid position of the liquid level in the wellbore j_1:

$$S = 1 \quad \Rightarrow \quad j_1 = 1 \tag{A.2.2.4}$$

$$\delta = 0 \quad \Rightarrow \quad j_1 > 1 \tag{A.2.2.5}$$

and:

$$\frac{\partial B_{w_b}}{\partial H_{w_D}} = -\frac{\gamma_o c_{L_D} B_{w_b}}{4 + \left(H^v_{w_D} + H^k_{w_D}\right) \gamma_o c_{L_D}} \tag{A.2.2.6}$$

From the definition of the inner boundary potentials:

$$W_{w_{j_1}} = \gamma_o \left[\frac{1 + x_{j_1}}{2} H_{w_D} + \frac{\bar{x}_{j_1}}{2} \left(z_{w_{D_{j_1-1}}}\right)\right] \tag{A.2.2.7}$$

and:

$$\frac{\partial W_{w_{j_1}}}{\partial H_{w_D}} = \gamma_o \left[\frac{1 + x_{j_1}}{2} - \frac{1 - x_{j_1}}{2} \left[(1-\delta)\Delta z_{D_w} + \delta \Delta h_{D_w}\right] \frac{\partial x_{j_1}}{\partial H_{w_D}}\right]$$

$$= \gamma_o x_{j_1} \tag{A.2.2.8}$$

Thus:

$$\mathcal{F}'(H_{w_D}) = -\frac{q_D \gamma_o c_{L_D} B_{w_b}}{4 + \left(H^v_{w_D} + H^k_{w_D}\right) \gamma_o c_{L_D}} + \frac{1}{2\phi \Delta t_D} + \frac{\theta \gamma_o}{k_h \ln(\bar{r}_1)} \times$$

$$\left\{\overline{\Delta z}_{D_1} \left[x_{j_1} k_{x_1,j_1} (1 - \delta) + \sum_{j_1+1}^{n} k_{x_1,j}\right] + \delta x_{j_1} \overline{\Delta h}_{D_1} k_{x_1,j_1}\right\} \tag{A.2.2.9}$$

From the Newton-Raphson iteration aproach:

$$H^{v+1}_{w_D} = H^v_{w_D} - \frac{\mathcal{F}\left(H^v_{w_D}\right)}{\mathcal{F}'\left(H^v_{w_D}\right)} \tag{A.2.2.10}$$

where v is the iterative level. Convergence is achieved when the difference below becomes small, compared to a residue ϵ:

$$H_{w_D}^{v+1} - H_{w_D}^{v} \leq \epsilon \qquad \text{(A.2.2.11)}$$

A.3 Material Balance Equation Partial Derivatives

The discretized wellbore material balance equation in App. A.2 may be differentiated with respect to each inner block potential $W_{1,\kappa}$, to evaluate the partial differentials of the sandface potentials, which were written as functions of H_{w_D} and z_{w_D} in App. A.l. Thus $\partial H_{w_D}/\partial W_{1,\kappa}$ may be substituted into the equations presented in App. **A.l. A** step-by-step development of the Jacobian equations is presented next.

The discretized material balance equation in App. A.2 is:

$$q_D\, B_{w_b} = -\frac{\Delta H_{w_D}}{2\,\phi\,\Delta t_D} + \frac{\overline{\Delta z}_{D_1}}{\ln(\bar{r}_1)} \left\{ \frac{k_{x_{1,1}}}{k_h} (1-\theta) \left[W_{1,1}^{k} - W_{w_1}^{k} \right] + \right.$$

$$\left. \sum_{j=2}^{n} \frac{k_{x_{1,j}}}{k_h} \left[\theta \left[W_{1,j} - W_{w_j} \right] + (1-\theta) \left[W_{1,j}^{k} - W_{w_j}^{k} \right] \right] \right\} + \frac{\overline{\Delta h}_{D_1}}{\ln(\bar{r}_1)} \frac{k_{x_{1,1}}}{k_h} \theta \left[W_{1,1} - W_{w_1} \right] \qquad \text{(A.3.1)}$$

Differentiating Eq. A.3.1 with respect to $W_{1,\kappa}$:

$$q_D \frac{\partial B_{w_b}}{\partial W_{1,\kappa}} = -\frac{1}{2\phi\,\Delta t_D}\frac{\partial H_{w_D}}{\partial W_{1,\kappa}} + \frac{\theta}{k_h \ln(\overline{r}_1)}$$
$$\left\{\overline{\Delta z}_{D_1}\left[(1-\delta_\kappa)\,k_{x_{1,\kappa}} - \sum_{j_1+1}^{n} k_{x_{1,j}}\frac{\partial W_{w_j}}{\partial W_{1,\kappa}} - \delta_{j_1}\,k_{x_{1,j_1}}\frac{\partial W_{w_{j_1}}}{\partial W_{1,\kappa}}\right]\right.$$
$$\left. + \overline{\Delta h}_{D_1}\,k_{x_{1,1}}\left[\delta_\kappa - \frac{\partial W_{w_1}}{\partial W_{1,\kappa}}\right] + k_{x_{1,1}}\,(W_{1,1} - W_{w_1})\,\frac{\partial \overline{\Delta h}_{D_1}}{\partial W_{1,\kappa}}\right\} \qquad \text{(A.3.2)}$$

Also:

$$\alpha_1 = \frac{1 + Q_w}{2} \qquad \text{(A.3.3)}$$

and:

$$\frac{\partial \overline{\Delta h}_{D_1}}{\partial W_{1,\kappa}} = \delta_\kappa\,\alpha_1\,\frac{\partial \Delta h_1}{\partial W_{1,\kappa}} = \frac{\delta_\kappa\,\alpha_1}{\overline{\gamma}_1} \qquad \text{(A.3.4)}$$

From the derivatives in App. **A.l:**

$$\frac{\partial W_{w_1}}{\partial W_{1,\kappa}} = (1-\delta_{j_1})\,x_{j_1}\gamma_o\,\frac{\partial H_{w_D}}{\partial W_{1,1}} + \delta_k\frac{\gamma_o\,\alpha_w}{2\overline{\gamma}_1}\left[\delta_{j_1} + (1-\delta_{j_1})\left(1-x_{j_1}^2\right)\right] \qquad \text{(A.3.5)}$$

The parameters δ_κ and δ_{j_1} are:

$$\begin{cases}\delta_\kappa = 1 & \rightarrow \kappa = 1\\ \delta_\kappa = 0 & \rightarrow \kappa \neq 1\end{cases} \qquad \begin{cases}\delta_{j_1} = 1 & \rightarrow j_1 \neq 1\\ \delta_{j_1} = 0 & \rightarrow j_1 = 1\end{cases} \qquad \text{(A.3.6)}$$

Equation A.3.5 can be written as a function of H_{w_D} as the only unknown by differenting B_{w_b} and by using the relationships defined in App. A.l for the potential differentiations:

$$-\frac{q_D B_{w_b} \gamma_o c_{L_D}}{4 + \gamma_o \left(H_{w_D} + H^k_{w_D}\right) c_{L_D}} \frac{\partial H_{w_D}}{\partial W_{1,\kappa}} = -\frac{1}{2\phi \Delta t_D} \frac{\partial H_{w_D}}{\partial W_{1,\kappa}} + \frac{\theta}{k_h \ln(\overline{r}_1)} \times$$

$$\left\{ \overline{\Delta z}_{D_1} \left[(1 - \delta_\kappa) k_{x_{1,\kappa}} - \gamma_o \frac{\partial H_{w_D}}{\partial W_{1,\kappa}} \sum_{j_1+1}^{n} k_{x_{1,j}} - \delta_{j_1} k_{x_{1,j_1}} \gamma_o x_{j_1} \frac{\partial H_{w_D}}{\partial W_{1,\kappa}} \right] \right.$$

$$+ \Delta \overline{h}_{D_1} k_{x_{1,1}} \left[\delta_\kappa - (1 - \delta_{j_1}) x_{j_1} \gamma_o \frac{\partial H_{w_D}}{\partial W_{1,\kappa}} + \right.$$

$$\delta_k \frac{\gamma_o \alpha_w}{2\overline{\gamma}_1} \left[\delta_{j_1} + (1 - \delta_{j_1}) \left(1 - x^2_{j_1}\right) \right] \Big] +$$

$$\left. k_{x_{1,1}} (W_{1,1} - W_{w_1}) \frac{\delta_\kappa \alpha_1}{\overline{\gamma}_1} \right\} \qquad \text{(A.3.7)}$$

where x_{j_1} is the fraction defined in App. A.1. The general partial differentiation of H_{w_D} is:

$$\frac{\partial H_{w_D}}{\partial W_{1,\kappa}} = \frac{\frac{\theta k_{x_{1,\kappa}}}{k_h \ln(\overline{r}_1)} \left[F_1(j_1, x_{j_1}) + (W_{1,1} - W_{w_1}) \frac{\delta_\kappa \alpha_1}{\overline{\gamma}_1} \right]}{-\frac{q_D B_{w_b} \gamma_o c_{L_D}}{4 + \gamma_o \left(H_{w_D} + H^k_{w_D}\right) c_{L_D}} + \frac{1}{2\phi \Delta t_D} + \frac{\theta \gamma_o}{k_h \ln(\overline{r}_1)} F_2\left(j_1, x_{j_1}, \overline{k}_1\right)}$$

(A.3.8)

where:

$$F_1(j_1, x_{j_1}) = (1 - \delta_\kappa) \Delta \overline{z}_{D_1} + \delta_\kappa \overline{\Delta h}_{D_1} \left[1 - \frac{\gamma_o \alpha_w}{2\overline{\gamma}_1} \left[\delta_{j_1} + (1 - \delta_{j_1}) \left(1 - x^2_{j_1}\right) \right] \right]$$

(A.3.9)

and:

$$F_2\left(j_1, x_{j_1}, \overline{k}_1\right) = \Delta \overline{z}_{D_1} \left[\sum_{j_1+1}^{n} k_{x_{1,j}} + \delta_{j_1} k_{x_{1,j_1}} x_{j_1} \right] + \Delta \overline{h}_{D_1} k_{x_{1,1}} (1 - \delta_{j_1}) x_{j_1}$$

(A.3.10)

Next, differentiate the same expression with respect to $W_{2,1}$:

$$q_D \frac{\partial B_{w_b}}{\partial W_{2,1}} = -\frac{1}{2\phi \Delta t_D} \frac{\partial H_{w_D}}{\partial W_{2,1}} - \frac{\theta}{k_h \ln(\bar{r}_1)} \times \left\{ \overline{\Delta z}_{D_1} \left[\sum_{j_1+1}^{n} k_{x_{1,j}} \frac{\partial W_{w_j}}{\partial W_{2,1}} + \delta_{j_1} k_{x_{1,j_1}} \frac{\partial W_{w_{j_1}}}{\partial W_{2,1}} \right] + \overline{\Delta h}_{D_1} k_{x_{1,1}} \frac{\partial W_{w_1}}{\partial W_{2,1}} - k_{x_{1,1}} (W_{1,1} - W_{w_1}) \frac{\partial \overline{\Delta h}_{D_1}}{\partial W_{2,1}} \right\} \quad \text{(A.3.11)}$$

Also:

$$\frac{\partial \overline{\Delta h}_{D_1}}{\partial W_{2,1}} = (1-\alpha_1) \frac{\partial \Delta h_2}{\partial W_{2,1}} = \frac{1-\alpha_1}{\bar{\gamma}_2} = \frac{1-\alpha_w}{2\bar{\gamma}_2} \quad \text{(A.3.12)}$$

$$\frac{\partial W_{w_j}}{\partial W_{2,1}} = \gamma_o \frac{\partial H_{w_D}}{\partial W_{2,1}} \quad \Rightarrow \quad j < j_1 \quad \text{(A.3.13)}$$

$$\frac{\partial W_{w_{j_1}}}{\partial W_{2,1}} = x_{j_1} \gamma_o \frac{\partial H_{w_D}}{\partial W_{2,1}} \quad \Rightarrow \quad j = j_1 \neq 1 \quad \text{(A.3.14)}$$

$$\frac{\partial W_{w_{j_1}}}{\partial W_{2,1}} = \gamma_o \left\{ (1-\delta_{j_1}) x_{j_1} \frac{\partial H_{w_D}}{\partial W_{2,1}} + \frac{1-\alpha_w}{2\bar{\gamma}_2} \left[(1-\delta_{j_1}) \left(1 - x_{j_1}^2\right) + \delta_{j_1} \right] \right\} \Rightarrow \quad j = j_1 = 1 \quad \text{(A.3.15)}$$

Substituting the partial differentials and considering optional positions for the liquid level in the wellbore by taking j_1:

A.3 Material Balance Equation Partial Derivatives

$$\frac{-q_D\, B_{w_b}\, \gamma_o\, c_{L_D}}{4 + \gamma_o \left(H_{w_D} + H^k_{w_D}\right) c_{L_D}} \frac{\partial H_{w_D}}{\partial W_{2,1}} = -\frac{1}{2\,\phi\,\Delta t_D} \frac{\partial H_{w_D}}{\partial W_{2,1}} - \frac{\theta}{k_h \ln(\overline{r}_1)} \times$$

$$\left\{ \overline{\Delta z}_{D_1} \left[\sum_{j_1+1}^{n} k_{x_{1,j}} + \delta_{j_1}\, x_{j_1}\, k_{x_{1,j_1}} \right] \gamma_o \frac{\partial H_{w_D}}{\partial W_{2,1}} \right.$$

$$+ \gamma_o \overline{\Delta h}_{D_1}\, k_{x_{1,1}} \left[(1-\delta_{j_1}) \left(x_{j_1} \frac{\partial H_{w_D}}{\partial W_{2,1}} + \left(1 - x^2_{j_1}\right) \frac{(1-\alpha_w)}{2\,\overline{\gamma}_2} \right) + \delta_{j_1} \frac{(1-\alpha_w)}{2\,\overline{\gamma}_2} \right]$$

$$\left. - k_{x_{1,1}}\, (W_{1,1} - W_{w_1}) \frac{1-\alpha_w}{2\,\overline{\gamma}_2} \right\} \qquad \textbf{(A.3.16)}$$

After rearrangement:

$$\frac{\partial H_{w_D}}{\partial W_{2,1}} = \frac{-\frac{\theta\,\gamma_o\, k_{x_{1,1}}}{k_h \ln(\overline{r}_1)} \frac{(1-\alpha_w)}{2\,\overline{\gamma}_2} \left\{ \Delta \overline{h}_{D_1} \left[(1-\delta_{j_1}) \left(1 - x^2_{j_1}\right) + \delta_{j_1} \right] - \frac{W_{1,1} - W_{w_1}}{\gamma_o} \right\}}{-\frac{q_D\, B_{w_b}\, \gamma_o\, c_{L_D}}{4 + \gamma_o \left(H_{w_D} + H^k_{w_D}\right) c_{L_D}} + \frac{1}{2\,\phi\,\Delta t_D} + \frac{\theta\,\gamma_o}{k_h \ln(\overline{r}_1)} F_2\left(j_1, x_{j_1}, \overline{k}_1\right)}$$

(A.3.17)

Appendix B

Groundwater and Petroleum Engineering Units

Although dealing with similar properties of fluids and rocks and the same mathematical description of the physical phenomena, the Hydrology and Petroleum Engineering literatures use different symbols. **As** an example, the Groundwater transmis*sivity* does not have the same units as the *transmissivity* in Petroleum Engineering. **A** good reference to have in mind regarding symbols is App. A in ***Earlougher*** (1977).

A short conversion set follows to help understanding and comparisons of units with those in the Groundwater references used in this dissertation. Most of the Petroleum Engineering parameters can be directly measured in laboratories or in situ. Conversely, the hydrologic terminology frequently uses lumped properties related to the diffusivity equation. Thus, terms like *storage coefficient, specific yield, specific storage, transmissivity, coefficient of permeability,* etc. are not familiar to many petroleum engineers.

The following partial differential equation is used in Hydrology to represent the **r-z** flow of liquid (water) in a porous medium in a cylindrical model:

$$K_r \frac{\partial^2 s}{\partial r^2} + \frac{K_r}{r} \frac{\partial s}{\partial r} + K_z \frac{\partial^2 s}{\partial z^2} = S_s \frac{\partial s}{\partial t} \qquad \text{(B.1)}$$

where:

K_r, K_z - coefficient of permeability in both r and z directions, LT^{-1}

s - head drawdown, L

S_s - specific (elastic) storage, L^{-1}

t - time, T

r, z - radial and vertical coordinates, L

The same **Eq.** B.1 in petroleum engineering symbols is:

$$\frac{k_r}{\mu}\frac{\partial^2 p}{\partial r^2} + \frac{k_r}{\mu}\frac{\partial p}{\partial r} + \frac{k_z}{\mu}\frac{\partial^2 p}{\partial z^2} = \phi c_t \frac{\partial p}{\partial t} \qquad \text{(B.2)}$$

where:

k_r, k_z - permeability in r and z directions, L^2

p - pressure, $L^{-1}MT^{-2}$

μ - viscosity, $L^{-1}MT^{-1}$

ϕ - porosity, fraction

c_t - total system compressibility, $LM^{-1}T^2$

t - time, T

r, z - radial and vertical coordinates, L

Correspondence may be established by a dimensional analysis. **Usual** conversion of units into field units follows for a water saturated system ($\mu = 1$ cp):

Coefficient of permeability and permeability:

$$K = \frac{k}{\mu}\left(\rho\frac{g}{g_c}\right) \tag{B.3}$$

Field units:

$$\left(K,\ gal/D/ft^2\right) = 0.047339\ \frac{(k,\ \mathrm{mD})}{(\mu,\ \mathrm{cp})}\ \left(\rho\frac{g}{g_c}\ ,\ \mathrm{psi/ft}\right) \tag{B.4}$$

Specific storage and diffusivity:

$$S_s = \phi\, c_t \left(\rho\frac{g}{g_c}\right) \tag{B.5}$$

Field units:

$$\left(S_s,\ ft^{-1}\right) = (\phi)\left(c_t\ ,\ psi^{-1}\right)\left(\rho\frac{g}{g_c}\ ,\ \mathrm{psi/ft}\right) \tag{B.6}$$

Head drawdown and pressure drawdown:

$$s = \frac{p_o - p}{\rho\frac{g}{g_c}} \tag{B.7}$$

Field units:

$$s\ ,\ ft = \frac{(p_o - p\ ,\ \mathrm{psi})}{\left(\rho\frac{g}{g_c}\ ,\ \mathrm{psi/ft}\right)} \tag{B.8}$$

There are other important variables. Storage coefficient, transmissivity and specific yield are:

Storage coefficient, S (dimensionless):

$$S = S_s\, h = \phi\, c_t\, h \left(\rho \frac{g}{g_c}\right) = \phi\, c_t\, p \tag{B.9}$$

where h is the thickness of the formation in consistent units. In the unconfined flow theory, h is the liquid height, and the pressure p may replace $h(\rho g/g_c)$. Some theories of unconfined aquifers consider a constant S_s, neglecting the unsaturated flow *(Neuman* (1972), *Streltsova* (1972), and others). In this case, h should be the original liquid level at rest.

Transmissivity (L^2T^{-1})

$$T = K_r\, h \tag{B.lO}$$

Field units:

$$(T,\ \text{gal/D/ft}) = 0.047339\, \frac{(k,\ \text{mD})\,(h,\ \text{ft})}{(\mu,\ \text{cp})} \left(\rho \frac{g}{g_c},\ \text{psi/ft}\right) \tag{B.ll}$$

From the unconfined **flow** theory

Specific yield, S_y (dimensionless):
This variable was introduced in the free surface boundary equation (see *Neuman,* (1972), (1974), among others):

$$K_r \frac{\partial s}{\partial r} n_r + K_z \frac{\partial s}{\partial z} n_z = \left(S_y \frac{\partial \xi}{\partial t} - I\right) n_z, \qquad \text{at} \qquad z = \xi \tag{B.12}$$

where:

n_r, n_z - component of unit normal in r and z directions

ξ - free surface elevation from the aquifer bottom, L

I - recharge source rate at the free surface, LT^{-1}

Equation **B.12** may be related to the free surface boundary condition in the Chapter **3.** S_y is related to the effective porosity:

$$S_y = \phi\,(1 - S_{w_r}) \qquad \textbf{(B.13)}$$

where S_{w_r} is the residual water saturation in the unsaturated region. The term **I** may be considered a net flow liquid left behind by the water table moving boundary as an effect of capillarity. Generally, S_y has been considered constant and **I** takes care of the recharge, but in the *Neuman* **(1972, 1974)** studies the recharge **I** was neglected.

Usual dimensionless parameters

Dimensionless permeability:

$$K_D = \frac{\left(K_z,\ \text{gal/D/ft}^2\right)}{\left(K_r,\ \text{gal/D/ft}^2\right)} = \frac{(k_z,\ \text{mD})}{(k_r\ \text{mD})} \qquad \textbf{(B.14)}$$

Dimensionless drawdown, constant producing flow rate - see *Neuman* **(1972):**

$$s_D = \frac{4\pi\,(T,\ \text{gal/D/ft})}{(Q,\ gal/D)}\ (s,\ \text{ft})$$

$$= 0.014164\frac{(k,\ \text{mD})\,(h_o,\ \text{ft})}{(\mu,\ \text{cp})\,(Q,\ bbl/D)}\ (p,\ \text{psi}) \qquad \textbf{(B.15)}$$

Dimensionless time with respect to the specific storage S:

$$t_S = 5.57 \times 10^{-3} \frac{(T,\ \text{gal/D/ft})}{S\ \left(r^2,\ \text{ft}^2\right)}\ (t,\ \text{hr})$$

$$= 2.637 \times 10^{-4} \frac{(k_r,\ \text{mD})\ (t,\ \text{hr})}{\phi\,(\mu,\ \text{cp})\left(c_t\ ,\ \text{psi}^{-1}\right)\ \left(r^2,\ \text{ft}^2\right)} \tag{B.16}$$

Dimensionless time with respect to the specific yield S_y:

$$t_y = 5.57 \times 10^{-3} \frac{(T,\ \text{gal/D/ft})}{S_y\ \left(r^2,\ \text{ft}^2\right)}\ (t,\text{hr})$$

$$= 2.637 \times 10^{-4} \frac{(k_r,\ \text{mD})\,(h_o,\ \text{ft})\ (t,\ \text{hr})}{\phi\,(1 - S_{w_r})\,(\mu,\ \text{cp})\ \left(r^2,\ \text{ft}^2\right)} \tag{B.17}$$

β-parameter:

$$\beta = K_D \frac{(r^2,\ ft^2)}{(h_o^2,\ ft^2)} = \frac{(k_z,\ mD)}{(k_r,\ mD)} \frac{(r^2,\ ft^2)}{(h_o^2,\ ft^2)} \tag{B.18}$$

σ-parameter:

$$\sigma = \frac{S}{S_y} = \frac{(c_t\ ,\ psi^{-1})\,(p_o\ ,\ psi)}{(1 - S_{wr})} \tag{B.19}$$

Appendix C

Symplified Approaches

The analytical approximations of *Theis* **(1935)** and *Ramey et al.* **(1989)** used to give late time approaches for the gravity well problem do not consider the vertical velocity component in the reservoir, as well as wellbore storage effects. **A** need to incorporate wellbore storage effects in those solutions required additional formulation, and two computer programs were developed. This improvement in the approaches were not intended to reproduce the unconfined flow behavior at early times, but only to reproduce a better transient flow behavior, mainly when skin effects were considered. In this appendix, a brief description of each program is presented.

The *Theis* **(1935)** method has been used by hydrologists as a late time reference solution for the unconfined flow of liquid in a gravity drainage well. The derivation of the *Theis* solution did not consider either a skin effect nor a wellbore storage effect in the inner boundary condition. *Theis* used a partial differential equation developed for heat transfer to approximate the unconfined flow problem, but his solution is mainly applicable to confined compressible flow. To incorporate wellbore storage and skin effects, a computer program called *PDE* was developed. Details of this approach are described in App. **C.l.**

Recently, *Ramey et al.* **(1989)** developed **an** approximate method in which the flow

was proportional to the column of liquid, and considered skin effects. The transient p^2 solution of the gravity problem proposed by *Ramey et al.* **(1989)** was an improvement to the *Theis* **(1935)** solution, because the variable height of the liquid column in the reservoir was considered in a partial differential equation. As a result, a non-linear Forchheimer-type equation in dimensionless form was obtained similar to the non-linear partial differential equation in the ideal gas problem studied by *Jenkins* and *Aronofsky* **(1953).** *Jenkins* and *Aronofsky* correlated their numerical solutions with the *van Ewerdingen* and *Hurst* **(1949)** liquid solutions to conclude that the later could be reasonably applied to solve for the transient pressure at the wellbore, if an appropriate dimensionless pressure (in terms of p^2) were used. Using a late time logarithmic approximation, *Ramey et al.* included the *van Ewerdingen* and *Hurst* skin effect, but not wellbore storage effects. To consider storage effects in the wellbore, a numerical model for ideal and real gas radial flow developed by *Fligelman* **(1980)** was adapted to the liquid gravity drainage well problem, since the non-linear partial differential equations for ideal gas flow and the Dupuit-Forchheimer approach are exactly the same when appropriate dimensionless parameters are used (see App **C.2).** This program was named *FLIGRAM*.

C.1 Wellbore Effects in the Theis Solution

Appropriate boundary conditions were applied to the diffusivity equation for wellbore storage and skin effects for an infinitely large reservoir. Some results were compared to the *Theis* **(1935)** line source solution.

The basic diffusivity equation for radial flow in Darcy units is:

$$\frac{\partial^2 p}{\partial r^2} + \frac{1}{r}\frac{\partial p}{\partial r} = \frac{\phi \mu c_t}{k}\frac{\partial p}{dt} . \qquad \text{(C.1.1)}$$

Theis applied Eq. **C.1.1** for a constant rate well to obtain the pressure response at any

radial distance r and time t, for both a confined and an unconfined aquifer. Wellbore effects were not considered. Based on the simplified assumption of a line-sink, the *Theis* approach had no valid response close to the wellbore, where the storage effects are important. Eventually, at late time, the pressure response approaches that of a confined reservoir, and the line source solution becomes accurate enough. In terms of Petroleum Engineering nomenclature, the *Theis* approach was expressed by:

$$p(r,t) = \frac{q\,B\,\mu}{2\pi\,k\,h}\; p_D(r_D,t_D)\;, \tag{C.1.2}$$

where:

$$p_D(r_D,t_D) = -\frac{1}{2}\; E_i\left(-\frac{\phi\,\mu\,c_t\,r^2}{4\,k\,t}\right), \tag{C.1.3}$$

For a small argument, the integral function $E_i(-x)$ may be approximated by:

$$E_i(-x) = -\int_x^\infty \frac{e^{-u}}{u}\,du = \left[\ln x - \frac{x}{1!} + \frac{x^2}{2 \times 2!} - \frac{x^3}{3 \times 3!} + \cdots\right]_x^\infty$$

$$\approx \frac{1}{2}\left[\ln\left(\frac{k\,t}{\phi\,\mu\,c_t\,r^2}\right) + 0.80907\right]. \tag{C.1.4}$$

Wellbore storage and skin effects were added to the solution of the partial differential equation, Eq. C.1.1. The inner boundary condition was:

$$q = C\,\frac{\partial p_w}{\partial t} - \frac{2\pi\,k\,h}{\mu}\left(r\frac{\partial p}{\partial r}\right)_{r=r_w} \tag{C.1.5}$$

and:

$$p_w = \left[p - s\left(r\frac{\partial p}{\partial r}\right)\right]_{r=r_w}, \tag{C.1.6}$$

where C is the wellbore storage parameter. The initial condition was:

$$p(r,0) = p_i \,. \tag{C.1.7}$$

As an infinite reservoir, the pressure approaches the initial value, as the distance from the wellbore center becomes large:

$$\lim_{r\to\infty} p(r,t) = p_i \,. \tag{C.1.8}$$

It was convenient to introduce dimensionless variables as defined below. Both Darcy and field units are given.

	Darcy units:	**Field units:**	
	$r_D = \dfrac{r}{r_w}$	$r_D = \dfrac{r}{r_w}$	(C.1.9)
	$t_D = \dfrac{k\,t}{\phi\,\mu\,c_t\,r_w^2}$	$t_D = \dfrac{(0.0002637)\,k\,t}{\phi\,\mu\,c_t\,r_w^2}$	(C.1.10)
$p_D =$	$\dfrac{2\pi\,k\,h\,(p_i - p)}{q\,\mu}$	$p_D = \dfrac{k\,h\,(p_i - p)}{141.2\,q\,B\,\mu}$	(C.1.11)
	$C_D = \dfrac{1}{2\,p_i\,c_t}$	$C_D = \dfrac{1}{2\,p_i\,c_t}$	(C.1.12)

Substituting the dimensionless parameters into the diffusivity equation:

$$\frac{\partial^2 p_D}{\partial r_D^2} + \frac{1}{r_D}\frac{\partial p_D}{\partial r_D} = \frac{\partial p_D}{\partial t_D} \,. \tag{C.1.13}$$

Initial Condition:

$$p_D(r_D, 0) = 0 . \tag{C.1.14}$$

Outer Boundary Condition:

$$\underset{r_D \to \infty}{p_D}(r_D, t_D) = 0 . \tag{C.1.15}$$

Combined Wellbore and Sandface Conditions:

$$1 = C_D \left[\frac{\partial p_D}{\partial t_D} - s r_D \frac{\partial}{\partial t_D} \left(\frac{\partial p_D}{\partial r_D} \right) \right]_{r_D = 1+} - \left(r_D \frac{\partial p_D}{\partial r_D} \right)_{r_D = 1+} \tag{C.1.16}$$

The solution for the dimensionless pressure in the wellbore in Laplace space is:

$$\bar{p}_{w_D} = \frac{K_o(\sqrt{z}) + s\sqrt{z} K_1(\sqrt{z})}{z^{3/2} [K_1(\sqrt{z}) + C_D \sqrt{z} K_o(\sqrt{z}) + z C_D s K_1(\sqrt{z})]} \tag{C.1.17}$$

A computer program was written to calculate the wellbore pressures using **Eq.** C.1.17. Inversion from the Laplace space was done numerically using the *Stehfest* (1970) algorithm. Early and late time approximate analytical solutions of Eq. C.1.17 were also derived. An early time approximation ($z \to \infty$) inverted to real space after simplification of the Bessel functions produced:

$$p_{w_D} = \frac{t_D}{C_D} \tag{C.1.18}$$

A late time approximation was similar to that expressed by Eq. C.1.4, including the skin parameter:

$$p_{w_D} = \frac{1}{2} [\ln(t_D) + 0.80907 + 2s] . \tag{C.1.19}$$

Figures C.1 and C.2 show the results in both semi-log and log-log plots of the solutions from the computer program PDE and the line source solution. **Also,** the buildup behavior is shown in Fig. C.3. **A** perfect match between the solutions when the wellbore effects were no longer important verify the results from the program PDE.

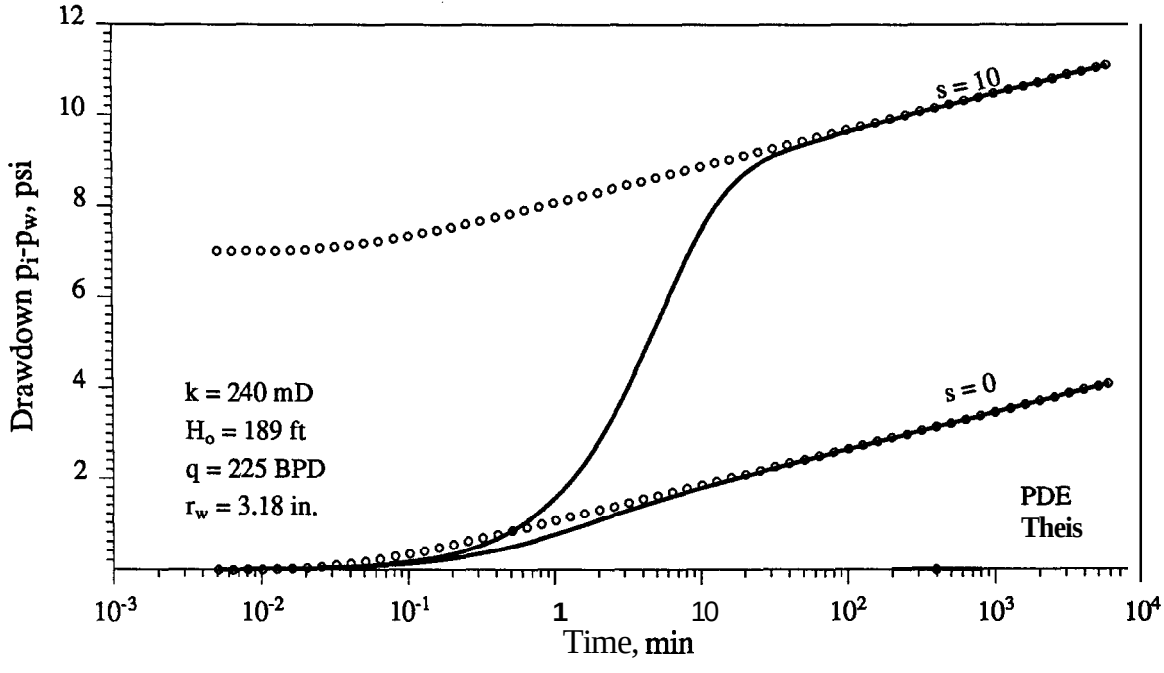

Figure C.1: *PDE* and analytical *Theis* (1935) solution. Semilog plot.

C.2 Wellbore Effects in the p^2 Solution

Wellbore storage effects were considered in the inner boundary condition for a constant production rate well in an infinitely large reservoir. The wellbore storage coefficient **was** coupled with a partial differential equation (Eq. C.2.1 in ***Ramey et al.***, 1989) for an approximate late time solution of a gravity drainage well. **A** resulting

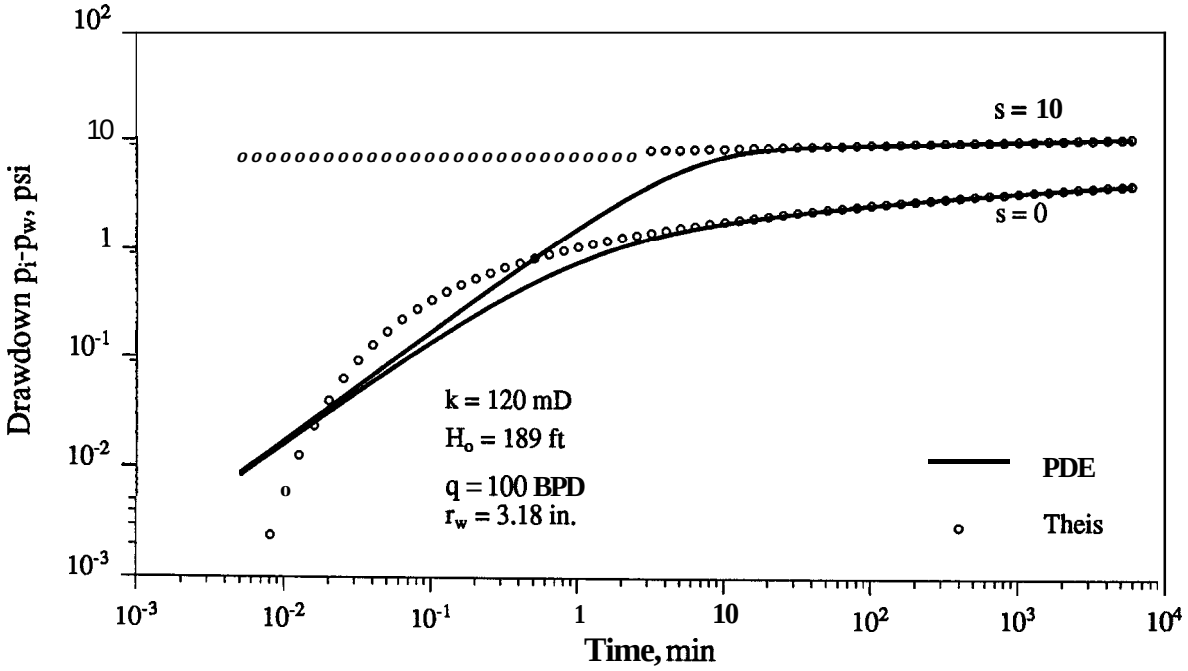

Figure **C.2:** *PDE* and the analytical *Theis* **(1935)** solution. Log-log plot.

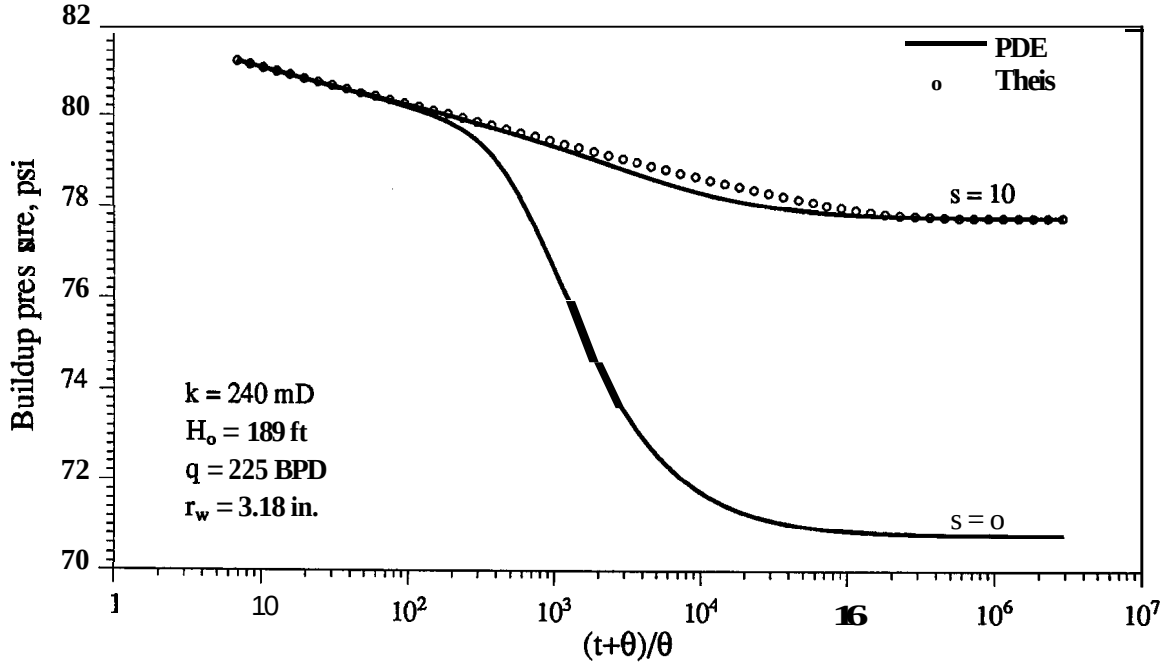

Figure **C.3:** *PDE* and analytical *Theis* **(1935)** solution. Buildup pressure semilog plot.

system of non-linear equations similar to the ideal gas problem numerically solved by *Fligelman* (1980) was adapted to a single phase liquid with a free surface. Transmissivity was taken proportional to the liquid column in the reservoir, and vertical velocities were neglected.

Ramey et al. (1989) re-introduced the p^2 approach for the free surface gravity drainage, re-writing the *Dupuit-Forchheimer* partial diferential equation in terms of a variable height $h(r,t)$ converted into pressure. The partial differential equation presented a pressure-factor in the diffusivity term, obtained for an incompressible system. Equation 1.2 in the Introduction Ch. 1, presented below as Eq. C.2.1, shows the proposed equation in terms of pressure. The similarity with the ideal gas equation studied by *Jenkins* and *Aronofsky* (1953) is perfect. Notice the pressure-dependent diffusivity coefficient.

$$\frac{\partial^2 p^2}{dr^2} + \frac{1}{r}\frac{\partial p^2}{dr} = \frac{\phi \mu (p^{-1})}{k}\frac{\partial p^2}{\partial t} . \qquad \text{(C.2.1)}$$

The fundamental assumption to obtain Eq. C.2.1 was that at given a time t and a radial position r the liquid pressure at the lower boundary was assumed to be proportional to the column of liquid. The assumption of incompressible flow requires that pressure is proportional to liquid height:

$$p(r,t) = h\rho\frac{g}{g_c} . \qquad \text{(C.2.2)}$$

Jenkins and *Aronofsky* correlated numerical solution of Eq. C.2.1 with the *van Everdingen* and *Hurst* (1949) solutions of the linear diffusivity problem. *Rarney et al.* adapted the *Jenkins* and *Aronofsky* correlations for a constant rate wellbore condition to write an approximate analytical solution, not valid at early times:

$$p_i^2 - p_w^2 = \frac{2.303}{4\pi}\frac{qB\rho}{k\rho\frac{g}{g_c}}\left\{\log_{10}\left(\frac{kt}{\phi\mu(p_i^{-1})r_w^2}\right) + 0.80907 + 2s\right\} . \qquad \text{(C.2.3)}$$

To consider wellbore storage effects, and to allow the *Fligelman* (1980) program to handle pressure buildup behavior as well as drawdown, a new simplified program was written and named *FLIGRAM*. The mathematical procedure is described next.

First, a gravity drainage pseudo-pressure was defined:

$$m_p = \frac{k}{\mu} p^2 \ . \qquad \text{(C.2.4)}$$

The inner and outer boundary conditions were the same as those described in App. C.1, as well as the initial condition. The dimensionless parameters were:

Darcy units:	**Field units:**	
$r_D = \frac{r}{r_w}$	$r_D = \frac{r}{r_w}$	(C.2.5)
$t_D = \frac{k p_i t}{\phi \mu r_w^2}$	$t_D = \frac{(0.0002637)\ k p_i t}{\phi \mu r_w^2}$	(C.2.6)
$m_D = \frac{m_{p_i} - m_p}{m_{p_i}} = \frac{p_i^2 - p^2}{p_i^2}$	$m_D = \frac{m_{p_i} - m_p}{m_{p_i}} = \frac{p_i^2 - p^2}{p_i^2}$	(C.2.7)
$C_D = \frac{1}{2\phi}$	$C_D = \frac{1}{2\phi}$	(C.2.8)
$\alpha_D = \frac{h_o}{h}$	$\alpha_D = \frac{h_o}{h}$	(C.2.9)
$q_D = \frac{q B \rho \frac{g}{g_c}}{\pi m_{p_i}}$	$q_D = \frac{282.41 q B \rho \frac{g}{g_c}}{m_{pi}}$	(C.2.10)

Substituting the dimensionless parameters into the diffusivity equation (Eq. C.2.1) and into the boundary conditions:

$$\frac{\partial^2 m_D}{\partial r_D^2} + \frac{1}{r_D}\frac{\partial m_D}{\partial r_D} = \alpha_D \frac{\partial m_D}{\partial t_D} . \qquad \text{(C.2.11)}$$

Initial Condition:

$$m_D(0, r_D) = 0 . \qquad \text{(C.2.12)}$$

Outer Boundary Condition:

$$\lim_{r_D \to \infty} m_D(t_D, r_D) = 0 . \qquad \text{(C.2.13)}$$

Wellbore Material Balance:

$$q_D = C_D \alpha_D \left.\frac{dm_{D_1}}{dt_D}\right|_{r_D=1+} - \frac{k_1}{k} r_D \left.\frac{dm_{D_1}}{dr_D}\right|_{r_D=1+} , \qquad \text{(C.2.14)}$$

where the subscript 1 stands for the damaged region around the wellbore. The skin effect was translated into an equivalent permeability using *Hawkins* (1956) method (see Eq. 4.1).

Results from the *FLIGRAM* program are presented next and verified with the late time *Ramey et al.* approach. Figures C.4 through C.6 are graphs of drawdown pressure vs. time for a typical set of data. Two skin values, 0 and **5** respectively, were used. At late times, when wellbore effects have no sensible influence on the pressure response, the numerical method matches the analytical approach. In a semilog graph in Fig. C.4, the late time behavior shows an approximate linear relationship between pressure drawdown and the logarithm of time. Fig. C.5 is a log-log graph where the wellbore storage effects can be clearly identified by the unit slope straight line at very early times. In the p-squared vs. time semilog graph in Fig. C.6, the slope of the

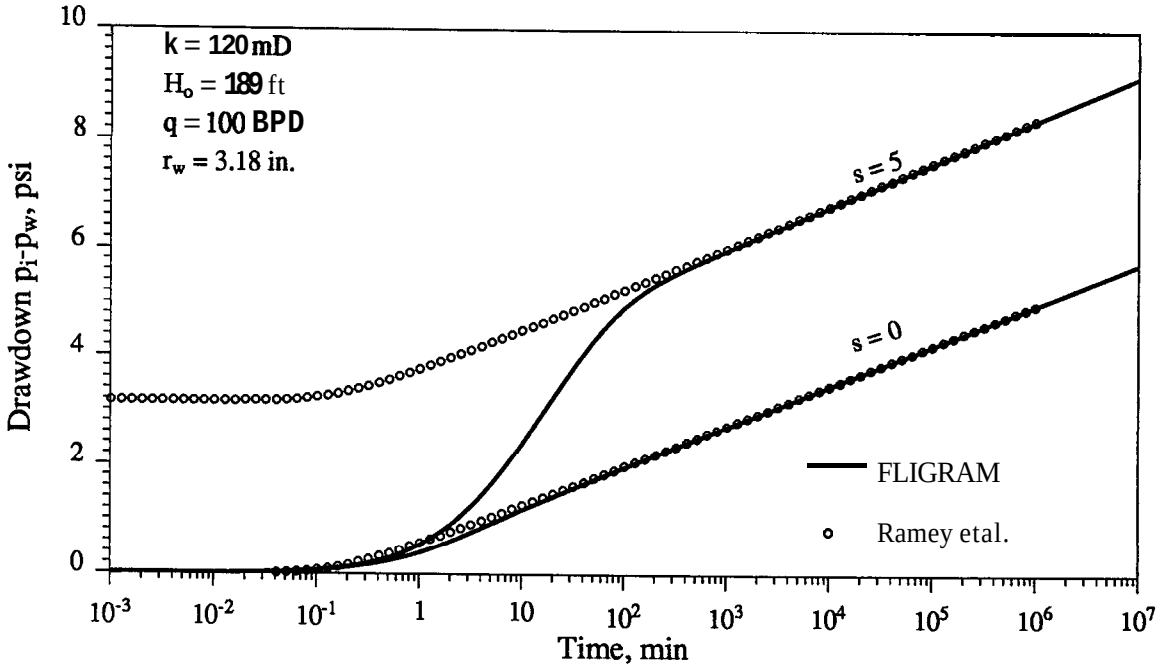

Figure **C.4:** FLIGRAM and *Ramey et al.* approaches for the drawdown period, semilog plot.

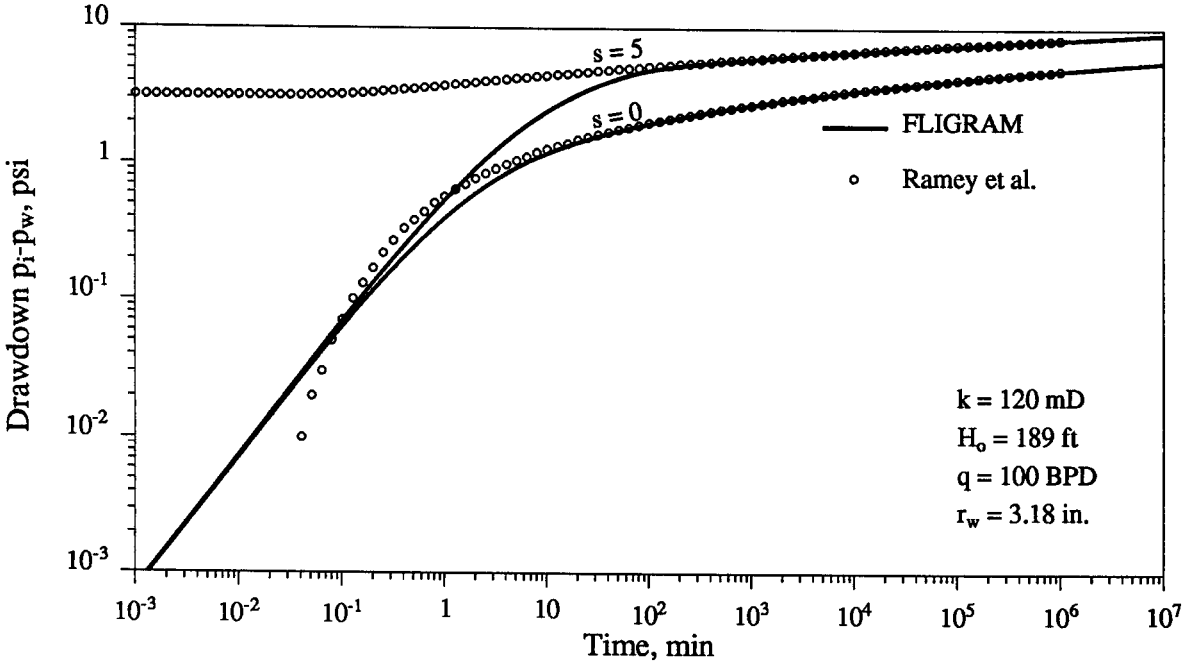

Figure C.5: *FLIGRAM* and *Ramey et al.* approaches for the drawdown period, log-log graph.

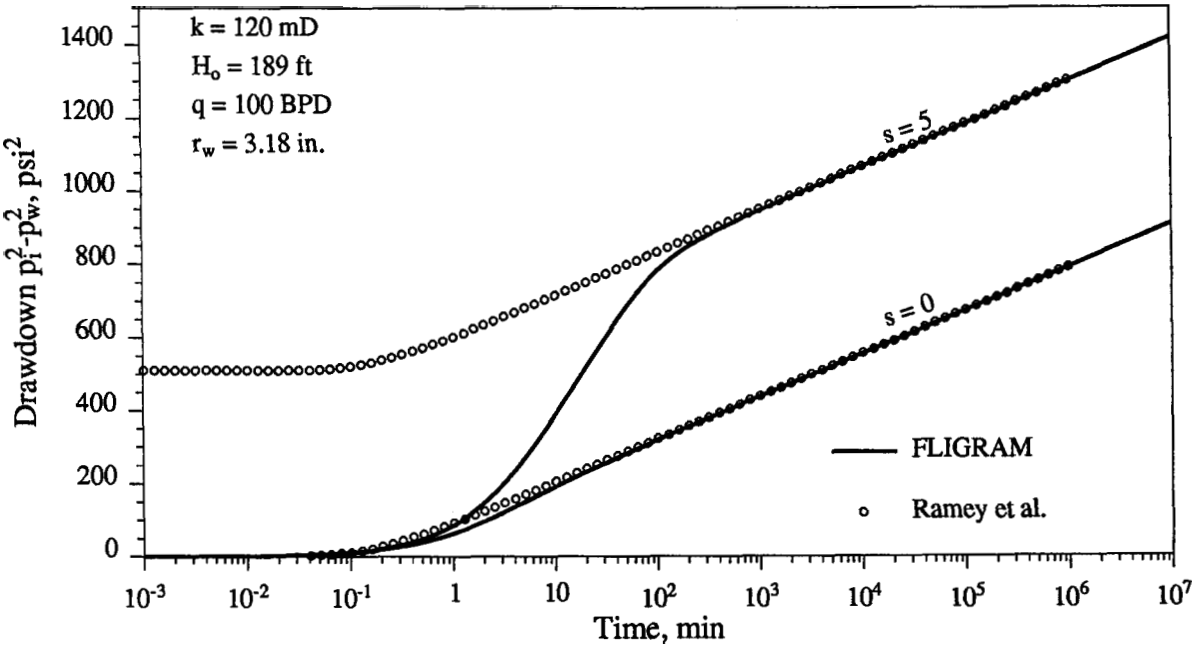

Figure C.6: *FLIGRAM* and *Ramey et al.* approaches for the drawdown period, p-squared semilog graph.

logarithmic behavior period calculated from **Eq.** 10 in the *Ramey et al.* (1989) paper, 132.1 psi^2/cycle, was matched.

Using the given example for a test, we calculated the m-permeability using an approximate late time semilog straight line obtained in Fig. C.4, and compared with the input data of 240 mD. The semilog straight line slope was 0.89 psi/cycle, corresponding to a permeability of 217 mD:

$$\text{Radial Flow:} \quad k = 162.6 \frac{q\,B\,\mu}{m\,h_o} = (162.6) \frac{(225)\,(1)\,(1)}{(0.89)\,(189)} = 217.4\,\text{mD}$$

This rough solution is less than 10% lower than the p-squared solution, for the given example.

Appendix D

Verification of the Free Surface Boundary Condition Relationship with the Average Vertical Velocity

An interesting way of representing a relationship between the free surface position and the vertical velocity can be found in the *Wyckoff et al.* **(1932)** work. Using the symbology employed in the present study:

$$h(r) = \frac{\Phi_b(r)}{\rho \frac{g}{g_c}} + \frac{\overline{v}_v(r)\,\mu}{k_v\,\rho \frac{g}{g_c}}\,h(r)\,, \tag{D.1}$$

where $h(r)$ is the free surface vertical position at a radial location r from the well center, $\Phi_b(r)$ is the potential in the base of the reservoir at the same r, $v_v(r)$ is the average vertical velocity of the liquid, μ is the liquid viscosity, k_v is the vertical permeability, and $\rho g/g_c$ is the liquid pressure gradient. If we define v_v as:

$$\overline{v}_v(r) = \frac{1}{h(r)} \int_0^{h(r)} \frac{k_v}{\mu} \left.\frac{\partial \Phi}{\partial z}\right|_r dz\,, \tag{D.2}$$

the integration produces:

$$\overline{v}_v(r) = \frac{k_v}{\mu} \frac{\Phi_{fs}(r) - \Phi_b(r)}{h(r)} \tag{D.3}$$

where f_s refers to the free surface vertical position. Direct substitution of **Eq. D.3** vertical velocity v_v into the *Wyckoff et al.* expression gives:

$$h(r) = \frac{\Phi_{fs}(r)}{\rho \frac{g}{g_c}} \tag{D.4}$$

which is the free surface boundary condition in the current study.

Appendix E

SLM Computer Program

In this Appendix, the SLM computer program is described in detail in Section E.1, and the program code is presented in Section E.5. The computer program was written in double precision FORTRAN. An exception was the subroutine that calculates the liquid level in the wellbore which gives an appropriate accuracy using extended precision on IBM machines. In that subroutine, when calculating the production flow rate for a constant-pressure inner boundary condition, a quadratic equation computes differences of squared large numbers and divisions which require a large number of significant digits in the operations. In Section **E.3,** an example of an input data file is given. Example of output file is given in Section ??.

E.1 Structure of the Program

The simulator is composed of a main program, **30** subroutines and 5 functions. A flow chart is presented next to aid understanding of the program. Some controls, such as the start of a buildup period or the start of constant flow rate in the well, were omitted in the diagram.

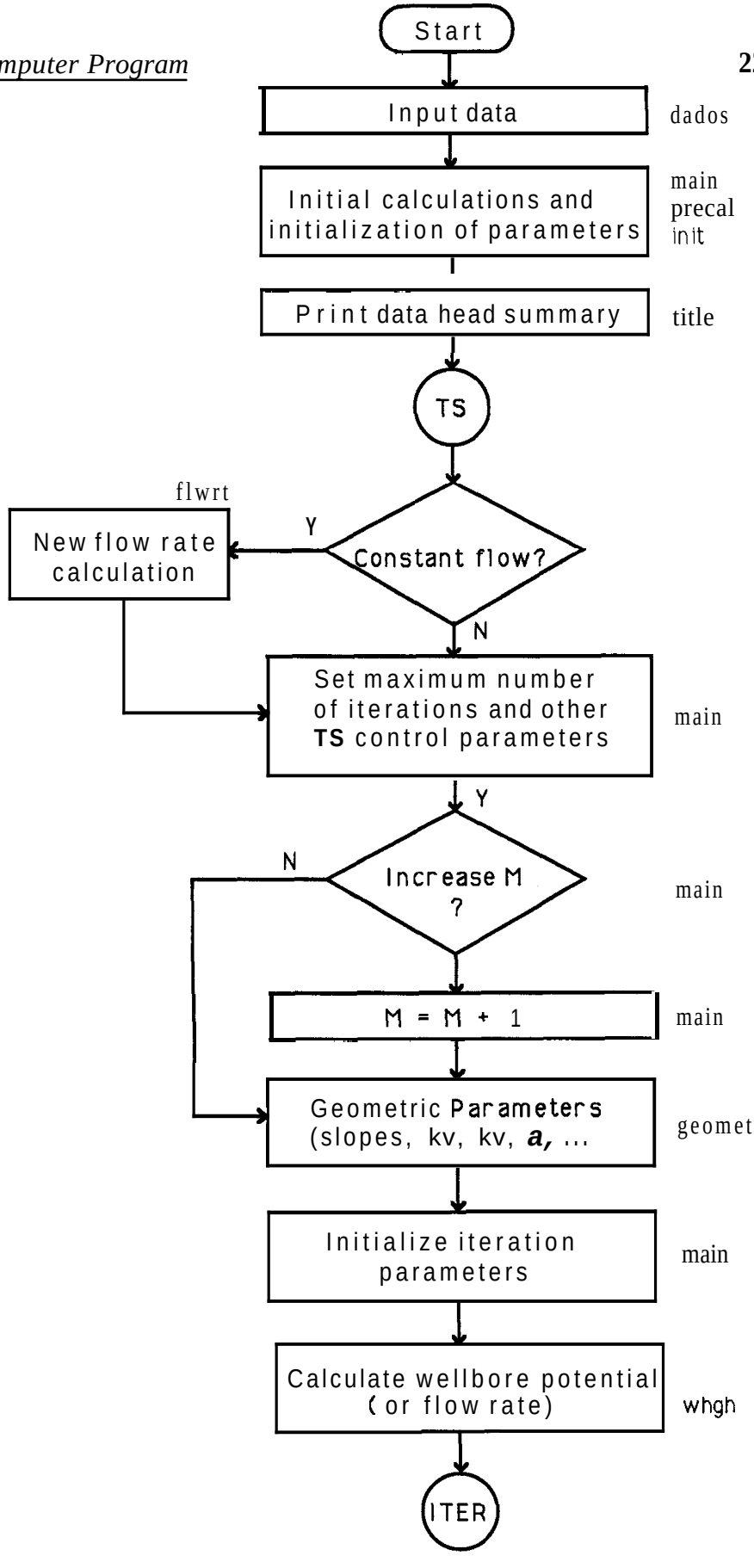
Start
Input data
dados
Initial calculations and initialization of parameters
main
precal
init
Print data head summary
title
TS
flwrt
New flow rate calculation
Y
Constant flow?
N
Set maximum number of iterations and other TS control parameters
main
Y
N
Increase M ?
main
M = M + 1
main
Geometric Parameters (slopes, kv, kv, a, ...
geomet
Initialize iteration parameters
main
Calculate wellbore potential (or flow rate)
whgh
ITER

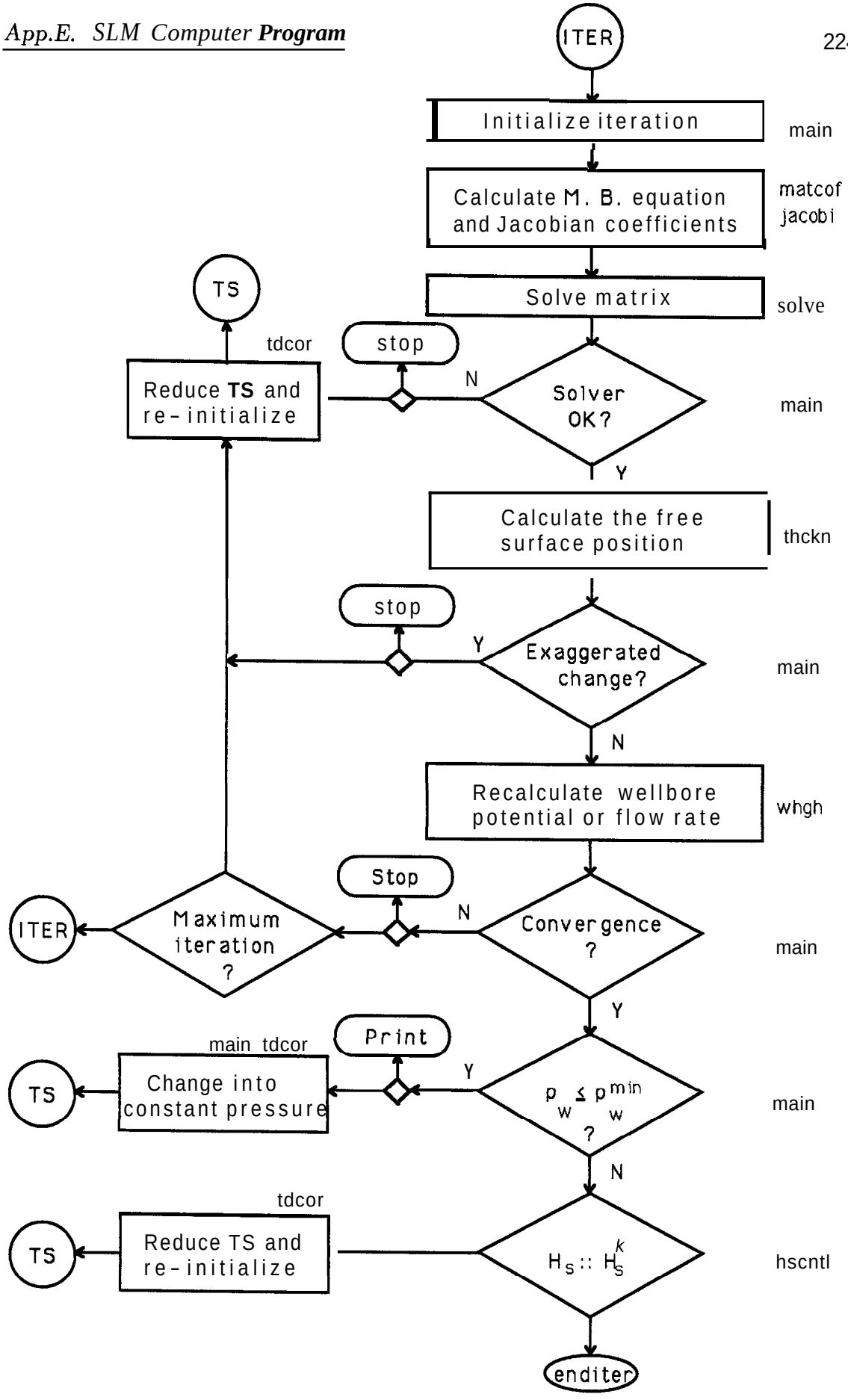
ITER
Initialize iteration
main
Calculate M. B. equation and Jacobian coefficients
matcof jacobi
Solve matrix
solve
TS
tdcor
stop
Reduce TS and re-initialize
N
Solver OK?
main
Y
Calculate the free surface position
thckn
stop
Y
Exaggerated change?
main
N
Recalculate wellbore potential or flow rate
whgh
Stop
ITER
Maximum iteration ?
N
Convergence ?
main
Y
Print
main tdcor
TS
Change into constant pressure
Y
$p_w \leq p_w^{min}$?
main
N
tdcor
TS
Reduce TS and re-initialize
$H_s :: H_s^k$
hscntl
enditer

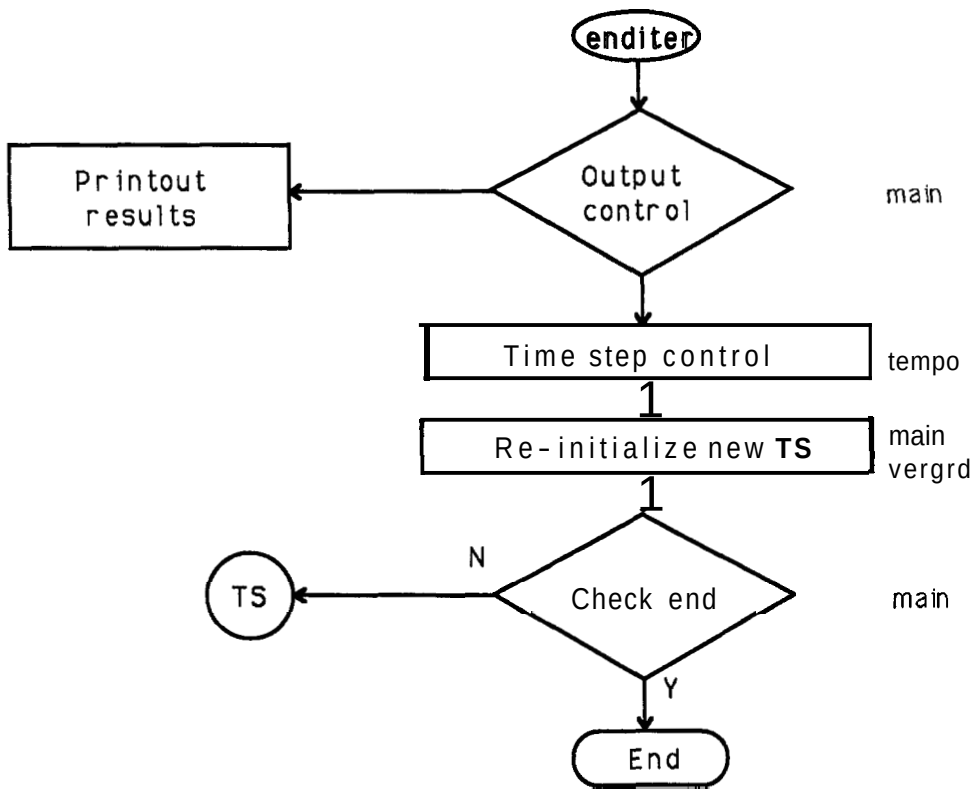
enditer
Output control
main
Printout results
Time step control
tempo
1
Re-initialize new TS
main vergrd
1
N
Check end
main
TS
Y
End

E.2 Description of some Characteristics

In this section, some important characteristics of the computer program are summarized.

E.2.1 Radial Block Distribution

The radial mesh distribution uses a block-centered scheme given by a progressive radial positioning of the block boundaries, according to the *MULTIMODAL* griding. See *Terán and de* ***la Garza*** (1988) for details of the algorithm. The log-spacing is a particular case of the *MULTIMODAL* method. The parameter necessary to define the ratio between the last and the first block radial size, $\frac{\Delta r_{mm}}{\Delta r_1}$, is an input data, as well as a flag integer that provides the selection of the *MULTIMODAL* of the standard logarithmic spacing.

Another important characteristic concerning the computer program is the progressive number of radial blocks considered in the matrix set-up. The remaining blocks, far from the inner boundary are added to the system as the external boundary is disturbed by a small dimensionless potential drop (10^{-9} in the program). After several runs, a number equal the half of the radial dimension ($MM/2$) was considered a good start.

E.2.2 Axial Permeability

The variable geometry of the problem required a calculation of directional permeability. The permeability tensor for an anisotropic case is defined by an elliptic

equation as:

$$k_x = \frac{k_h\, k_v}{\sqrt{k_h^2 \sin^2\beta + k_v^2 \cos^2\beta}} \qquad \text{(E.2.1)}$$

where β is the angle of the flow axis with the horizontal.

E.2.3 Sandface Block Transmissivity Control

The program contains a parameter $part(j)$ which is an input data for each sandface block. This parameter multiplies each transmissivity term of the inner boundary blocks and can be set from 0 for a no-flow block to **1** for a fully transmissive block. Thus, any block or set of blocks at any position in the wellbore can be partially or totally plugged or partially plugged by this transmissivity control parameter.

E.2.4 Skin Effect

The skin effect was simulated by calculating a modified permeability for the first block. Thus, both vertical and horizontal permeabilities should be affected. However, the method used to determine the skin parameter was the *Hawkins* **(1956)** approach which deals only with the horizontal permeability:

$$s = \left(\frac{k}{k_d} - 1\right) \ln\left(\frac{r_d}{r_w}\right) \qquad \text{(E.2.2)}$$

$$k_d = \frac{1}{1 + s \ln \bar{r}_{D_1}} k_h = f_s\, k_h \qquad \text{(E.2.3)}$$

where $\bar{r}_{D_1}$ is the first block radial mesh location.

We must understand this expression. First, Eq. E.2.2 expresses effects in the radial direction only, and there is nothing in the *Huwkins* approach relating to the vertical permeability, an important component of flow near wellbore. In the program, the vertical permeability is not affected by the skin effect defined this way.

Another problem concerns negative skins. Since we the damaged (or stimulated) region was set to be in the first block only, we are limited to a negative skin range defined by the denominator of Eq. E.2.3:

$$1 + s \ln \bar{r}_{D_1} > 0 \qquad \text{(E.2.4)}$$

$$s > -\frac{1}{\ln \bar{r}_{D_1}} . \qquad \text{(E.2.5)}$$

E.3 Input-Data File

A sample of the input-data file is presented next. The integer values are right justified at column 64, and the decimal numbers are left justified at column 60. The blank lines must be observed.

INPUT DATA - Exemple of input data	
Number of horizontal grid blocks (M):	60
Number of vertical grid blocks (N):	100
Use MULTINODAL radial spacing? (mult) (no=0, otherw,1)	1
Maximum number of iterations (itermx):	5
Maximum number of matrix calculations (matmax)	99999
Number of time-step per cycle (ntd)	10
Var. flowrate indx (iflow: 0=const, 1=cont.var, 2=step.var)	0

Boundary limit dimensionless external radius - (redf)	1000000.
First and last blck ratio - multimodal (Ratio)	400000.
Liquid compressibility - 1/psi:	0.000003
Total compressibility - 1/psi:	0.000003
Original heigth of the free surface - ft, (ho):	189.
Well bore radius - in, (rw):	3.18
Porosity - fraction, (poros):	0.25
Liquid viscosity - cp, (visc):	1.
Liquid density times g/gc - lbf/cuft, (rho):	62.4
Volume formation factor - (Bo)	1.
Skin effect parameter - (skin):	0.
Horizontal permeability - mD, (permh):	120.
Vertical permeability - mD, (permv):	120.
Constant Production rate - bbl/D, (q):	100.
Initial Pressure - psi, (presi)	81.9
Small number to be used as residue (eps)	0.000001
Over-relaxation parameter (1>=teta>=0)	0.9
Output control of wellbore dimless. press. (iprnt1)	1
Output control of head profile (iprnt2)	1

Output control of total pressure dist. (iprnt3) 1
Output control: 0=dimless., l=field units (iprnt4) 1

Initial dimensionless time - (tdi) 1.00e-02
Maximum buildup time for the shuttin period - min, (tmax) 0.00e+01
Time for Shutt-in (production time) - (tshut) 1.00e+06
Number of tdpr for pres. prof. line below - (nprof) 10
0.1 1. 10. 100. 1000. 10000. 1.e5 1.e6 1.e7 1.e8

Number of observation wells - (nprof) 2
Distance from wellbore center, ft (dist(i))
44.9 101.1

Partial penetration factor - part(j)
1. 1. 1. 1. 1. 1. 1. 1. 1. 1. 1. 1. 1. 1. 1.
I. 1. 1. 1. 1. 1. 1. 1. 1. 1. 1. 1. 1. 1.
1. 1. 1. 1. 1. 1. 1. 1. 1. 1. 1. 1. 1. 1.
1. 1. 1. 1. 1. 1. 1. 1. 1. 1. 1. 1. 1. 1.
1. 1. 1. 1. 1. 1. 1. 1. 1. 1. 1. 1. 1. 1.
1. 1. 1. 1. 1. 1. 1. 1. 1. 1. 1. 1. 1. 1.
1. 1. 1. 1. 1. 1. 1. 1. 1. 1. 1. 1. 1. 1.

Residual Saturation - (srw) 0.00

Flow rate table: time - tq(i) (min) and qvar(i) (bbl/d)
Number of variable flow rates - (nqv) 5

0.	214.
1230.	242.
2640.	218.
4080.	191.
5520.	183.

E.4 Example of the Program Output

The program has a main output file containing informations for each time step selected for output printing. There are also some output files for specific applications such as the sandface flow rate profile, the radial head distribution, observation wells, and others. The following labels generate corresponding outputs:

Label 2

Normalized head potentials: sand base, vertically averaged, and free surface.

Label 3

Isopotential xy distribution at prescribed times.

Label 11

Main output table: time, wellbore pressure or drawdown, number of iterations in the time step, cumulative number of matrix calculations, position J_1 of the block adjacent to the liquid level in the wellbore, seepage face length, result from Ramey *et al.* (1989) approach, result from *Theis* (1935) approach, cumulative CPU time in seconds.

Label 14

Sandface flow rate profile at prescribed times.

Label 21

Same as **label 11** for observation wells. Each label starting on 21 corresponds to a different locations or observation well.

Any output subroutine may be included by the user. If the user intends to have the same output time step control as in the program, just add the new subroutine call line next to the callings for *PRINTA* subroutine. A frequency of ten output data per logarithmic cycle of the dimensionless time was designed in the program, and

controlled by a variable *ntprt*. Another important information for the user is how the information are storaged. At the end of each time step, the following variables are updated. In the next time step, the vectors or scalar parameters are normally substituted by new values in the iterative process. The notation of the variables is the same as that used in the program, regardless capitalization.

H_{wD} = wellbore dimensionless liquid level
H_s = free surface dimensionless height at the sandface
$H(i)$ = free surface dimensionless height at position i
$dh(i)$ = free surface block dimensionless thickness
$dzd(i)$ = block dimensionless thickness
$W_w(j)$ = normalized sandface potential
$W(i,j)$ = normalized i,j block potential

An example of the main output run is presented next.

tmin= .4065E+00x td, Hc= .000ft, Red= 1000000., MULTIMODAL, Rmult= .4000E+0
MMF 60, n=100 Ho=189.000 ft, Skin= .0, Kh= 120., Kv= 120., visc=1.000
POROS= .25 Ct= .30E-05psi-1, C1= .30E-05psi-1, Q= 100.0 Swr= .000 Teta=1.00
.....

FIELD UNITS:

Time = minutes
Pw = psi
Iter = Number of iterations to complete the printed time-step
Matrix = Cumm. number of matrix calc. during the execution
J1 = Vertical grid position of the wellbore liquid level
Seepage = Seepage face length, ft
Ramey = Well pressure from Ramey et al. **(1989)** solution, psi
cpul = CPU time to calculate the matrix once, sec.
cpu2 = Fraction of time: matrix solver / entire interation loop
cpu3 = Cummulative CPU time, sec,

Time	Pw	Iter	Matrix	J1	Seepage	Ramey	Theis	cpu3
.4065E-04*	.00003*0*	1*	1*		.7182E-04*	NaNQ*	NaNQ*	.28
.5117E-04*	.00004*0*	2*	1*		.9042E-04*	NaNQ*	NaNQ*	.52
.6442E-04*	.00005*0*	3*	1*		.1138E-03*	NaNQ*	NaNQ*	.77
.8110E-04*	.00006*0*	4*	1*		.1433E-03*	NaNQ*	NaNQ*	1.02
.1021E-03*	.00008*0*	5*	1*		.1804E-03*	NaNQ*	NaNQ*	1.26
.1285E-03*	.00010*0*	6*	1*		.2271E-03*	NaNQ*	NaNQ*	1.51
.1618E-03*	.00012*0*	7*	1*		.2859E-03*	NaNQ*	NaNQ*	1.76
.2037E-03*	.00016*0*	8*	1*		.3599E-03*	NaNQ*	NaNQ*	2.00
.2565E-03*	.00020*0*	9*	1*		.4531E-03*	NaNQ*	NaNQ*	2.25
.3229E-03*	.00025*0*	10*	1*		.5704E-03*	NaNQ*	NaNQ*	2.49
.4065E-03*	.00031*0*	11*	1*		.7180E-03*	NaNQ*	NaNQ*	2.75
.5117E-03*	.00039*0*	22*	1*		.9039E-03*	NaNQ*	NaNQ*	5.42
.6442E-03*	.00049*0*	33*	1*		.1138E-02*	NaNQ*	NaNQ*	8.09

.8110E-03*	.00062*0*	44*	1*	.1432E-02*	NaNQ*	NaNQ*	10.76
.1021E-02*	.00078*0*	55*	1*	.1803E-02*	.0000E+00*	.0000E+00*	13.43
.1285E-02*	.00098*0*	66*	1*	.2270E-02*	.0000E+00*	.0000E+00*	16.10
.1618E-02*	.00124*0*	77*	1*	.2857E-02*	.0000E+00*	.0000E+00*	18.76
.2037E-02*	.00156*0*	88*	1*	.3597E-02*	.0000E+00*	.0000E+00*	21.43
.2565E-02*	.00196*0*	99*	1*	.4527E-02*	.0000E+00*	.0000E+00*	24.11
.3229E-02*	.00247*0*	110*	1*	.5698E-02*	.0000E+00*	.0000E+00*	26.79
.4065E-02*	.00311*0*	121*	1*	.7172E-02*	.0000E+00*	.0000E+00*	29.46
.5117E-02*	.00391*0*	142*	1*	.9027E-02*	.0000E+00*	.0000E+00*	34.57
.6442E-02*	.00492*0*	163*	1*	.1136E-01*	.0000E+00*	.0000E+00*	39.63
.8110E-02*	.00619*0*	184*	1*	.1430E-01*	.0000E+00*	.0000E+00*	44.73
.1021E-01*	.00779*0*	205*	1*	.1799E-01*	.0000E+00*	.0000E+00*	49.85
.1285E-01*	.00981*1*	244*	1*	.2263E-01*	.0000E+00*	.0000E+00*	57.00
.1618E-01*	.01234*1*	286*	1*	.2847E-01*	.7362E-04*	.7362E-04*	64.50
.2037E-01*	.01552*1*	328*	1*	.3581E-01*	.3673E-03*	.3673E-03*	72.02
.2565E-01*	.01952*1*	370*	1*	.4504E-01*	.1236E-02*	.1236E-02*	79.51
.3229E-01*	.02454*1*	412*	1*	.5662E-01*	.3376E-02*	.3375E-02*	87.01
.4065E-01*	.03084*1*	454*	1*	.7117E-01*	.7761E-02*	.7761E-02*	94.48
.5117E-01*	.03875*1*	516*	1*	.8943E-01*	.1553E-01*	.1553E-01*	105.54
.6442E-01*	.04867*1*	578*	1*	.1123E+00*	.2778E-01*	.2778E-01*	116.62
.8110E-01*	.06110*1*	640*	1*	.1410E+00*	.4538E-01*	.4537E-01*	127.70
.1021E+00*	.07665*1*	702*	1*	.1769E+00*	.6887E-01*	.6884E-01*	138.73
.1285E+00*	.09609*1*	764*	1*	.2217E+00*	.9842E-01*	.9836E-01*	149.78
.1618E+00*	.12034*1*	826*	1*	.2777E+00*	.1339E+00*	.1338E+00*	160.85
.2037E+00*	.15053*1*	888*	1*	.3474E+00*	.1749E+00*	.1747E+00*	172.09
.2565E+00*	.18804*1*	950*	1*	.4339E+00*	.2209E+00*	.2206E+00*	183.59
.3229E+00*	.23448*1*	1012*	1*	.5411E+00*	.2714E+00*	.2710E+00*	195.11
.4065E+00*	.29176*1*	1074*	1*	.6732E+00*	.3257E+00*	.3251E+00*	206.66
.5117E+00*	.36210*1*	1156*	1*	.8355E+00*	.3833E+00*	.3824E+00*	221.89
.6442E+00*	.44798*1*	1238*	1*	.1034E+01*	.4436E+00*	.4424E+00*	237.11
.8110E+00*	.55207*1*	1320*	1*	.1274E+01*	.5063E+00*	.5047E+00*	252.67

.1021E+01*	.67716*1*	1402* 1*	.1562E+01*	.5708E+00*	.5688E+00*	268.51
.1285E+01*	.82588*1*	1484* 2*	.1905E+01*	.6369E+00*	.6344E+00*	284.36
.1618E+01*	1.00130*1*	1566* 2*	.2310E+01*	.7042E+00*	.7012E+00*	300.20
.2037E+01*	1.20611*1*	1648* 2*	.2782E+01*	.7726E+00*	.7689E+00*	316.39
.2565E+01*	1.44132*1*	1730* 2*	.3324E+01*	.8418E+00*	.8375E+00*	332.91
.3229E+01*	1.70611*1*	1812* 3*	.3934E+01*	.9117E+00*	.9067E+00*	349.59
.4065E+01*	1.99719*1*	1894* 3*	.4605E+01*	.9823E+00*	.9764E+00*	366.63
.5117E+01*	2.30822*1*	1996* 3*	.5322E+01*	.1053E+01*	.1046E+01*	388.03
.6442E+01*	2.62923*1*	2098* 4*	.6061E+01*	.1125E+01*	.1117E+01*	410.14
.8110E+01*	2.94734*1*	2200* 4*	.6793E+01*	.1196E+01*	.1188E+01*	432.58
.1021E+02*	3.24784*1*	2302* 4*	.7484E+01*	.1268E+01*	.1258E+01*	455.11
.1285E+02*	3.51637*1*	2404* 5*	.8101E+01*	.1340E+01*	.1329E+01*	478.16
.1618E+02*	3.74154*1*	2506* 5*	.8616E+01*	.1413E+01*	.1401E+01*	501.28
.2037E+02*	3.91738*1*	2608* 5*	.9018E+01*	.1485E+01*	.1472E+01*	524.83
.2565E+02*	4.04446*1*	2710* 5*	.9305E+01*	.1558E+01*	.1543E+01*	548.50
.3229E+02*	4.12906*1*	2812* 6*	.9493E+01*	.1631E+01*	.1615E+01*	572.49
.4065E+02*	4.18080*1*	2914* 6*	.9604E+01*	.1704E+01*	.1686E+01*	596.60
.5117E+02*	4.20970*2*	3042* 6*	.9660E+01*	.1777E+01*	.1758E+01*	625.94
.6442E+02*	4.22378*2*	3225* 6*	.9679E+01*	.1850E+01*	.1829E+01*	659.59
.8110E+02*	4.22811*1*	3324* 6*	.9680E+01*	.1923E+01*	.1901E+01*	682.01
.1021E+03*	4.23038*0*	3415* 6*	.9675E+01*	.1997E+01*	.1972E+01*	703.60
.1285E+03*	4.23124*1*	3507* 6*	.9665E+01*	.2070E+01*	.2044E+01*	725.27
.1618E+03*	4.23100*0*	3598* 6*	.9649E+01*	.2144E+01*	.2116E+01*	746.85
.2037E+03*	4.22907*2*	3765* 6*	.9610E+01*	.2217E+01*	.2187E+01*	777.96
.2565E+03*	4.22601*2*	3948* 6*	.9559E+01*	.2291E+01*	.2259E+01*	811.10
.3229E+03*	4.22244*2*	4131* 6*	.9498E+01*	.2365E+01*	.2331E+01*	844.47
.4065E+03*	4.21838*2*	4314* 5*	.9426E+01*	.2439E+01*	.2402E+01*	878.32
.5117E+03*	4.21372*2*	4527* 5*	.9341E+01*	.2512E+01*	.2474E+01*	917.59
.6442E+03*	4.20854*2*	4740* 5*	.9242E+01*	.2586E+01*	.2546E+01*	957.14
.8110E+03*	4.20276*2*	4953* 5*	.9126E+01*	.2660E+01*	.2617E+01*	997.78
.1021E+04*	4.19642*2*	5166* 5*	.8992E+01*	.2735E+01*	.2689E+01*	1038.41

.1285E+04*	4.18955*2*	5379*	5*	.8837E+01*	.2809E+01*	.2761E+01*	1079.04
.1618E+04*	4.18191*2*	5600*	5*	.8659E+01*	.2883E+01*	.2832E+01*	1122.37
.2037E+04*	4.17432*2*	5823*	5*	.8458E+01*	.2957E+01*	.2904E+01*	1166.25
.2565E+04*	4.16660*2*	6046*	5*	.8233E+01*	.3032E+01*	.2976E+01*	1210.59
.3229E+04*	4.15941*2*	6266*	5*	.7984E+01*	.3106E+01*	.3047E+01*	1255.35
.4065E+04*	4.15280*2*	6481*	5*	.7711E+01*	.3181E+01*	.3119E+01*	1300.03
.5117E+04*	4.14731*2*	6725*	4*	.7417E+01*	.3255E+01*	.3191E+01*	1350.97
.6442E+04*	4.14368*2*	6968*	4*	.7106E+01*	.3330E+01*	.3262E+01*	1401.73
.8110E+04*	4.14260*2*	7211*	4*	.6785E+01*	.3405E+01*	.3334E+01*	1452.53
.1021E+05*	4.14482*2*	7454*	4*	.6461E+01*	.3480E+01*	.3406E+01*	1503.27
.1285E+05*	4.15147*2*	7701*	4*	.6143E+01*	.3554E+01*	.3477E+01*	1554.95
.1618E+05*	4.16300*2*	7944*	4*	.5840E+01*	.3629E+01*	.3549E+01*	1607.14
.2037E+05*	4.17957*2*	8187*	4*	.5556E+01*	.3704E+01*	.3621E+01*	1659.37
.2565E+05*	4.20171*2*	8430*	3*	.5299E+01*	.3780E+01*	.3692E+01*	1712.04
.3229E+05*	4.23087*2*	8673*	3*	.5074E+01*	.3855E+01*	.3764E+01*	1765.78
.4065E+05*	4.26524*2*	8916*	3*	.4878E+01*	.3930E+01*	.3836E+01*	1820.39
.5117E+05*	4.30577*2*	9192*	3*	.4711E+01*	.4005E+01*	.3907E+01*	1882.01
.6442E+05*	4.35193*3*	9492*	3*	.4570E+01*	.4081E+01*	.3979E+01*	1948.23
.8110E+05*	4.40394*3*	9856*	3*	.4453E+01*	.4156E+01*	.4051E+01*	2022.57
.1021E+06*	4.46034*3*	10220*	3*	.4355E+01*	.4232E+01*	.4122E+01*	2098.02
.1285E+06*	4.52060*3*	10584*	3*	.4274E+01*	.4307E+01*	.4194E+01*	2175.20
.1618E+06*	4.58549*3*	10956*	3*	.4211E+01*	.4383E+01*	.4266E+01*	2255.46
.2037E+06*	4.65297*3*	11320*	3*	.4158E+01*	.4459E+01*	.4337E+01*	2333.43
.2565E+06*	4.72390*3*	11701*	3*	.4120E+01*	.4535E+01*	.4409E+01*	2415.41
.3229E+06*	4.79253*4*	12189*	3*	.4089E+01*	.4611E+01*	.4481E+01*	2519.34
.4065E+06*	4.86499*3*	12678*	3*	.4067E+01*	.4687E+01*	.4552E+01*	2626.41
.5117E+06*	4.93985*4*	13232*	3*	.4049E+01*	.4763E+01*	.4624E+01*	2745.25
.6442E+06*	5.01430*6*	13863*	3*	.4038E+01*	.4839E+01*	.4696E+01*	2882.58
.8110E+06*	5.08842*4*	14498*	3*	.4027E+01*	.4915E+01*	.4767E+01*	3022.08
.1000E+07*	5.15839*4*	15084*	3*	.4022E+01*	.4984E+01*	.4833E+01*	3153.72

Buildup starting at **td=** .24601372E+07 CPU(MTRX CALC.)= **2061.710**

.4065E-04*	76.74164*2*	15087*	3* .4022E+01*	NaNQ*	NaNQ*	3154.89
.5117E-04*	76.74165*1*	15089*	3* .4022E+01*	NaNQ*	NaNQ*	3155.34
.6442E-04*	76.74167*1*	15091*	3* .4021E+01*	NaNQ*	NaNQ*	3155.80
.8110E-04*	76.74169*1*	15093*	3* .4021E+01*	NaNQ*	NaNQ*	3156.25
.1021E-03*	76.74171*1*	15095*	3* .4021E+01*	NaNQ*	NaNQ*	3156.70
.1285E-03*	76.74174*1*	15097*	3* .4021E+01*	NaNQ*	NaNQ*	3157.16
.1618E-03*	76.74177*1*	15099*	3* .4021E+01*	NaNQ*	NaNQ*	3157.61
.2037E-03*	76.74181*1*	15101*	3* .4021E+01*	NaNQ*	NaNQ*	3158.06
.2565E-03*	76.74186*1*	15103*	3* .4021E+01*	NaNQ*	NaNQ*	3158.52
.3229E-03*	76.74192*1*	15105*	3* .4021E+01*	NaNQ*	NaNQ*	3158.97
.4065E-03*	76.74199*1*	15107*	3* .4021E+01*	NaNQ*	NaNQ*	3159.43
.5117E-03*	76.74214*1*	15129*	3* .4020E+01*	NaNQ*	NaNQ*	3164.38
.6442E-03*	76.74232*1*	15151*	3* .4020E+01*	NaNQ*	NaNQ*	3169.33
.8110E-03*	76.74253*1*	15173*	3* .4020E+01*	NaNQ*	NaNQ*	3174.28
.1021E-02*	76.74278*1*	15195*	3* .4019E+01*	.7692E+02*	.7707E+02*	3179.24
.1285E-02*	76.74307*1*	15217*	3* .4018E+01*	.7692E+02*	.7707E+02*	3184.18
.1618E-02*	76.74341*1*	15239*	3* .4017E+01*	.7692E+02*	.7707E+02*	3189.12
.2037E-02*	76.74382*1*	15261*	3* .4017E+01*	.7692E+02*	.7707E+02*	3194.05
.2565E-02*	76.74431*1*	15283*	3* .4015E+01*	.7692E+02*	.7707E+02*	3199.01
.3229E-02*	76.74490*1*	15305*	3* .4014E+01*	.7692E+02*	.7707E+02*	3203.96
.4065E-02*	76.74563*1*	15327*	3* .4012E+01*	.7692E+02*	.7707E+02*	3208.91
.5117E-02*	76.74660*1*	15369*	3* .4010E+01*	.7692E+02*	.7707E+02*	3218.36
.6442E-02*	76.74777*1*	15411*	3* .4007E+01*	.7692E+02*	.7707E+02*	3227.81
.8110E-02*	76.74921*1*	15453*	3* .4004E+01*	.7692E+02*	.7707E+02*	3237.26
.1021E-01*	76.75098*1*	15495*	3* .4000E+01*	.7692E+02*	.7707E+02*	3246.72
.1285E-01*	76.75316*1*	15537*	3* .3995E+01*	.7692E+02*	.7707E+02*	3256.18
.1618E-01*	76.75586*1*	15579*	3* .3989E+01*	.7692E+02*	.7707E+02*	3265.61
.2037E-01*	76.75921*1*	15621*	3* .3981E+01*	.7692E+02*	.7707E+02*	3275.07
.2565E-01*	76.76338*1*	15663*	3* .3971E+01*	.7692E+02*	.7707E+02*	3284.52
.3229E-01*	76.76857*1*	15705*	3* .3959E+01*	.7692E+02*	.7707E+02*	3293.95
.4065E-01*	76.77505*1*	15747*	3* .3944E+01*	.7692E+02*	.7708E+02*	3303.36

.5117E-01*	76.78322*1*	15809*	3*	.3926E+01*	.7693E+02*	.7708E+02*	**3317.32**
.6442E-01*	76.79341*1*	15871*	3*	.3902E+01*	.7695E+02*	.7710E+02*	**3331.29**
.8110E-01*	76.80611*1*	15933*	3*	.3873E+01*	.7696E+02*	.7711E+02*	**3345.22**
.1021E+00*	76.82197*1*	15995*	3*	.3836E+01*	.7699E+02*	.7714E+02*	**3359.19**
.1285E+00*	76.84173*1*	16057*	3*	.3791E+01*	.7702E+02*	.7717E+02*	**3373.15**
.1618E+00*	76.86637*1*	16119*	3*	.3734E+01*	.7706E+02*	.7720E+02*	**3387.07**
.2037E+00*	76.89703*1*	16181*	3*	.3663E+01*	.7710E+02*	.7724E+02*	**3401.51**
.2565E+00*	76.93513*1*	16243*	2*	.3575E+01*	.7715E+02*	.7729E+02*	**3416.06**
.3229E+00*	76.98237*1*	16305*	2*	.3466E+01*	.7720E+02*	.7734E+02*	**3430.61**
.4065E+00*	77.04077*1*	16367*	2*	.3331E+01*	.7726E+02*	.7739E+02*	**3445.19**
.5117E+00*	77.11278*1*	16449*	2*	.3165E+01*	.7732E+02*	.7745E+02*	**3464.45**
.6442E+00*	77.20104*1*	16531*	2*	.2961E+01*	.7739E+02*	.7751E+02*	**3483.67**
.8110E+00*	77.30860*1*	16613*	2*	.2713E+01*	.7745E+02*	.7757E+02*	**3503.62**
.1021E+01*	77.43873*1*	16695*	2*	.2413E+01*	.7752E+02*	.7764E+02*	**3523.69**
.1285E+01*	77.59475*1*	16777*	2*	.2053E+01*	.7759E+02*	.7770E+02*	**3543.79**
.1618E+01*	77.77956*1*	16859*	1*	.1627E+01*	.7766E+02*	.7777E+02*	**3563.90**
.2037E+01*	77.99377*1*	16941*	1*	.1133E+01*	.7773E+02*	.7784E+02*	**3584.68**
.2565E+01*	78.23704*1*	17023*	1*	.5716E+00*	.7780E+02*	.7790E+02*	**3605.64**
.3229E+01*	78.50305*1*	17105*	1*-.4149E-01*		.7788E+02*	.7797E+02*	**3626.59**
.4065E+01*	78.55411*1*	17187*	1*-.1582E+00*		.7795E+02*	.7804E+02*	**3647.58**
.5117E+01*	78.55712*1*	17289*	1*-.1638E+00*		.7802E+02*	.7811E+02*	**3673.64**
.6442E+01*	78.55912*1*	17391*	1*-.1668E+00*		.7810E+02*	.7818E+02*	**3699.73**
.8110E+01*	78.56098*1*	17493*	1*-.1690E+00*		.7817E+02*	.7825E+02*	**3725.78**
.1021E+02*	78.56284*1*	17595*	1*-.1707E+00*		.7824E+02*	.7833E+02*	**3751.52**
.1285E+02*	78.56479*1*	17697*	1*-.1720E+00*		.7832E+02*	.7840E+02*	**3776.55**
.1618E+02*	78.56692*1*	17799*	1*-.1730E+00*		.7839E+02*	.7847E+02*	**3801.18**
.2037E+02*	78.56930*1*	17901*	1*-.1736E+00*		.7847E+02*	.7854E+02*	3824.98
.2565E+02*	78.57205*1*	18003*	1*-.1740E+00*		.7854E+02*	.7861E+02*	**3847.91**
.3229E+02*	78.57528*1*	18105*	1*-.1743E+00*		.7862E+02*	.7868E+02*	3870.84
.4065E+02*	78.57866*0*	18195*	1*-.1743E+00*		.7869E+02*	.7875E+02*	**3892.19**
.5117E+02*	78.58100*0*	18256*	1*-.1743E+00*		.7876E+02*	.7882E+02*	**3911.48**

.6442E+02*	78.58387*0*	18317*	1*-.1742E+00*	.7884E+02*	.7890E+02*	3930.80
.8110E+02*	78.58738*0*	18378*	1*-.1740E+00*	.7891E+02*	.7897E+02*	3950.15
.1021E+03*	78.59193*0*	18469*	1*-.1739E+00*	.7899E+02*	.7904E+02*	3974.73
.1285E+03*	78.59763*0*	18657*	1*-.1733E+00*	.7906E+02*	.7911E+02*	4016.17
.1618E+03*	78.60668*1*	19015*	1*-.1725E+00*	.7914E+02*	.7918E+02*	4097.48
.2037E+03*	78.61749*0*	19409*	1*-.1718E+00*	.7921E+02*	.7925E+02*	4184.46
.2565E+03*	78.62922*1*	19883*	1*-.1708E+00*	.7928E+02*	.7933E+02*	4290.67
.3229E+03*	78.64175*0*	20462*	1*-.1699E+00*	.7936E+02*	.7940E+02*	4419.01
.4065E+03*	78.65674*3*	21109*	1*-.1686E+00*	.7943E+02*	.7947E+02*	4561.35
.5117E+03*	78.67379*0*	21947*	1*-.1673E+00*	.7951E+02*	.7954E+02*	4744.36
.6442E+03*	78.69228*1*	23002*	1*-.1657E+00*	.7958E+02*	.7961E+02*	4977.22
.8110E+03*	78.71922*1*	24187*	1*-.1635E+00*	.7965E+02*	.7968E+02*	5244.94
.1021E+04*	78.74697*0*	25470*	1*-.1614E+00*	.7973E+02*	.7976E+02*	5556.63
.1285E+04*	78.78185*0*	26921*	1*-.1586E+00*	.7980E+02*	.7983E+02*	5910.92
.1618E+04*	78.81782*1*	28480*	1*-.1556E+00*	.7987E+02*	.7990E+02*	6305.51
.2037E+04*	78.86046*0*	30136*	1*-.1522E+00*	.7995E+02*	.7997E+02*	6756.93
.2565E+04*	78.90745*1*	31930*	1*-.1485E+00*	.8002E+02*	.8004E+02*	7257.74
.3229E+04*	78.96061*1*	33927*	1*-.1443E+00*	.8009E+02*	.8011E+02*	7815.56
.4065E+04*	79.02000*1*	36117*	1*-.1396E+00*	.8017E+02*	.8018E+02*	8406.25
.5117E+04*	79.08611*1*	38718*	1*-.1344E+00*	.8024E+02*	.8026E+02*	9092.54
.6442E+04*	79.15923*1*	41661*	1*-.1288E+00*	.8031E+02*	.8033E+02*	9863.95
.8110E+04*	79.23937*1*	44958*	1*-.1226E+00*	.8038E+02*	.8040E+02*	10728.41
.1021E+05*	79.39075*1*	50113*	1*-.1111E+00*	.8046E+02*	.8047E+02*	11994.20
.1285E+05*	79.56135*1*	56270*	1*-.9867E-01*	.8053E+02*	.8054E+02*	13482.53
.1618E+05*	79.72292*1*	62812*	1*-.8727E-01*	.8060E+02*	.8061E+02*	15072.10
.2037E+05*	79.87088*1*	69494*	1*-.7721E-01*	.8067E+02*	.8068E+02*	16741.85
.2565E+05*	79.98974*0*	75448*	1*-.6942E-01*	.8074E+02*	.8075E+02*	18395.98
.3229E+05*	80.08998*0*	80918*	1*-.6306E-01*	.8081E+02*	.8082E+02*	20071.73
.4065E+05*	80.19373*0*	86927*	1*-.5675E-01*	.8088E+02*	.8089E+02*	21922.98
.5117E+05*	80.29954*0*	93616*	1*-.5051E-01*	.8095E+02*	.8096E+02*	24002.54
.6442E+05*	80.40696*0*	100911*	1*-.4444E-01*	.8102E+02*	.8103E+02*	26281.09

.8110E+05* 80.51722*0* 108974* 1*-.3853E-01* .8109E+02* .8109E+02* **28807.23**
.1021E+06* 80.62913*0* 117855* 1*-.3286E-01* .8116E+02* .8116E+02* **31592.46**
.1285E+06* 80.74135*0* 127586* 1*-.2753E-01* .8122E+02* .8122E+02* **34650.95**
.1618E+06* 80.85273*0* 138262* 1*-.2264E-01* .8128E+02* .8129E+02* **38008.31**
.2037E+06* 80.95985*0* 149645* 1*-.1832E-01* .8135E+02* .8135E+02* **41588.24**
.2565E+06* 81.06714*0* 162429* l*-.1439E-01* .8140E+02* .8141E+02* **45525.17**
.3229E+06* 81.22254*1* 183762* 1*-.9439E-02* .8146E+02* .8146E+02* **50616.67**
.4065E+06* 81.34708*1* 204014* 1*-.6215E-02* .8151E+02* .8151E+02* **55422.03**
.5117E+06* 81.44751*1* 223220* 1*-.4101E-02* .8156E+02* .8156E+02* **60049.94**
.6442E+06* 81.52831*1* 241015* 1*-.2725E-02* .8161E+02* .8161E+02* **64321.11**
.8110E+06* 81.58149*0* 256457* 1*-.2037E-02* .8165E+02* .8165E+02* **68507.10**
.1000E+07* 81.61504*0* 269209* 1*-.1651E-02* .8168E+02* .8168E+02* **72342.23**

E.5 Computer Program Code Listing